

Thermal and calorimetric investigations of some phosphorus-modified polymeric materials

Miss Malavika Arun

A thesis submitted in fulfilment of the requirement for the degree of Doctor of Philosophy



Institute of Sustainable Industries and Liveable Cities (ISILC),

Victoria University, Melbourne

May 2020

Abstract:

The ease of ignition and associated combustion hazards of modern synthetic polymers are major concerns, and often limit their wider applicability, especially in construction and transport sectors. It is quite evident that many of the chain-growth polymers that are widely used as commodity plastics in the modern era need adequate flame resistance before they can be put in the market. Whilst there are many known and tried-out methods, to achieve acceptable levels of fire proofing of polymers that undergo extensive random chain scission and/or unzipping, like polymethyl methacrylate (PMMA) and polystyrene (PSt), can be still problematic. The main impetuses behind the chosen chain-growth polymers (PMMA and PSt) emanated from their known desirable properties, such as the ability of PMMA to form transparent plaques and thermal-insulation properties of foamed polystyrene. Furthermore, the use of certain condensation polymers as fire proofing coatings are also under explored.

Whilst there are a number of reports in the literature describing the use of phosphorus-containing compounds to flame retard PMMA and PSt, none of these have so far attempted a systematic and detailed investigation. In addition, the elucidation of mechanisms of flame retardance, operating in condensed and vapour phases, are also far from complete. Therefore, through the present work, an attempt to fill the current knowledge gap in this context is carried out.

The primary aim of the present project was to design different methods to modify some commercially important polymers with phosphorus-containing groups with a view to exploring their passive fire protection attributes. In this context, the thermal and calorimetric properties of polyaniline (PA), polypyrrole (PPE) and polydopamine (PDA) were also examined. The corresponding attributes of some modified styrenic- and acrylic-based systems were investigated, in detail, which also included their combustion behaviours. Furthermore, in the case of chain-growth polymers, both *additive* and *reactive* strategies were adopted, where the modifying species consisted of phosphorus- and/or phosphorus/nitrogen-containing compounds/groups.

Through the current programme, polymerizations of styrene- and methyl methacrylate-based systems were carried out through a host of polymerization routes, such as: solution, bulk, aqueous-slurry, suspension and emulsion. These processes, except the solution technique, are common practices in the industry owing to their environmentally benign features where monomer(s) are used as neat, or an aqueous-based heterogeneous medium is employed. The

structural characterization of both the low-molecular weight compounds (i.e. precursors, additives and monomers) and polymeric systems was achieved through some routine spectroscopic techniques. Furthermore, the products obtained through the bulk polymerization route were chosen for detailed investigations in terms of their thermal degradation behaviours and combustion characteristics.

Whilst the synthetic methodology employed to prepare step-growth polymers was found to be successful, and resulted in materials that exhibited superior thermal properties and combustion characteristics, all of them failed to produce uniform and coherent coatings onto mild steel and some common polymeric surfaces. It was also found that, generally with PMMA-based systems, the modifying groups only exhibited co-operative interaction during forced flaming combustion, whereas PSt-based systems also showed varying degrees of combustion inhibition in other tests (i.e. programmed heating: DSC, and forced non-flaming combustion: PCFC and ‘complete’ combustion: ‘bomb’ calorimetry). Some probable elements of mechanism(s) operating in the condensed- and gaseous-phases of the PMMA- and PSt-based systems were also formulated. In the case of PMMA-based systems, there is evidence that some of the P-bearing compounds/groups, upon thermal cracking during the early stages of flaming combustion, produce ‘phosphorus’ acid species. These acidic species can subsequently initiate the chemical pathway for producing char precursors. In the case of solid additives, it was found to be more likely that they produce phosphorus- and/or oxygenated phosphorus-containing volatiles that can act in the gaseous-phase. On the other hand, with PSt-based systems, a probable mechanistic pathway involving the phosphorylation of the phenyl rings leading to crosslinking and char formation is proposed.

Furthermore, preliminary investigations were conducted with a view to gauging the corrosion inhibiting attributes of some of the modified-acrylic systems. In addition, two software programs, primarily developed in-house, were successfully utilized to analyse the kinetic parameters from TGA thermograms, and to follow the extent of corrosion of mild steel substrates with time. A relatively straightforward analytical technique (inductively-coupled optical emission spectroscopy: ICP/OES) was also explored with a view to following the extents of corrosion on mild steel surfaces, both coated and uncoated, of various sizes and shapes. In conclusion, the current research programme opened up potential and commercially viable routes to adequately flame retard two of the most important thermoplastics.

Acknowledgements:

I greatly acknowledge my principal supervisor, Dr Paul Joseph, for his enduring guidance and constant encouragement, without which this thesis would not have been possible. I am also grateful to my associate supervisor, Professor Stephen Bigger, for his help and support throughout my PhD programme. Thanks are also due to Professor Andrew Smallridge for recording and helping to interpret the solution-state NMR spectra. I also greatly acknowledge the technical support from various people at Victoria University: Lyndon Mcindoe; Philip Dunn; Stephen Downing; Stacey Lloyd; Nishantha Illangantilaka; Larruceo Bautista; and Mary Marshall.

I register my deep sense of gratitude to Drs Luke O'Dell and Haijin Zhu for recording the solid-state NMR spectra; Joseph Pelle, Monash University, for giving me access to their analytical suite; Dr Svetlana Tretsiakova-McNally and Alosly Baby, Ulster University, UK, for the help with calorimetric tests; and Dr Doris Pospiech and Christina Harnisch, Leibniz-Institut für Polymerforschung, Dresden, Germany, for conducting the pyrolysis-GC/MS measurements.

I am greatly indebted to Victoria University for the provision of a Centenary Research Fellowship for my doctoral study. I also express my profound gratefulness to my teachers, past and present, especially to Professor Sabu Thomas, Vice Chancellor, Mahatma Gandhi University, Kottayam, India. Last but not the least, I deeply register my heartfelt gratitude towards my family for their unflinching love and support throughout my studies.

Declaration by author:

I, Malavika Arun, declare that the PhD thesis entitled, “Thermal and calorimetric investigations of some phosphorus-modified polymeric materials”, is no more than 100,000 words in length including quotes and exclusive of tables, figures, appendices, bibliography, references and footnotes. This thesis contains no material that has been submitted previously, in whole or in part, for the award of any other academic degree or diploma. Except where otherwise indicated, this thesis is my own work.



Signature

Date: 28 May 2020

Research outputs produced during the PhD candidature:

I. Peer-reviewed papers

1. Tretsiakova-McNally, S., Baby, A., Zhang, J., Arun, M. & Joseph, P. Reactive and additive modifications of styrenic polymers with phosphorus containing compounds and their effects on fire retardance. *Molecules* (manuscript in preparation).
2. Thomas, A., Arun, M., Moinuddin, K. & Joseph, P. Mechanistic aspects of condensed- and gaseous-phase activities of some phosphorus-containing fire retardants. *Polymers* (submitted).

II. Conference publications

1. Joseph, P., Arun, M., Bigger, S. & Zhu, H (2020, August). Thermal and calorimetric investigations of some phosphorus-modified polymeric materials. *American Chemical Society National Meeting*, San Francisco, USA (accepted).
2. Arun, M., Joseph, P., Bigger, S. & Zhu, H (2020, August). Mechanistic studies on the thermal, calorimetric and combustion properties of some chain-growth polymers modified with phosphorus. *American Chemical Society National Meeting*, San Francisco, USA (accepted).

List of abbreviations:

With a view to simplifying the main text, the following abbreviations are used:

1. ABS	Acrylonitrile-butadiene-styrene
2. ADEPMAE	Acrylic acid-2-[(diethoxyphosphoryl) methyl amino] ester
3. A-factor (A)	Arrhenius factor (min^{-1})
4. amu	Atomic mass unit
5. APS	Ammonium persulfate
6. AR	Analytical reagent
7. AS/NZ	Australia/New Zealand (ref. standards)
8. ASTM	American Society for Testing Materials
9. ATR	Attenuated Total Reflectance
10. BPO	Benzoyl peroxide
11. CP/MAS	Cross-polarization/magic angle spinning
12. CS	Coated substrates
13. D2	Two-dimensional diffusion model
14. DCM	Dichloromethane
15. DCP	Dicumyl peroxide
16. DEE	Diethyl ether
17. DE-1-AEP	Diethyl-1-(acryloyloxyethyl)phosphonate
18. DEAEPa	Diethyl-2-(acryloyloxy)ethylphosphate
19. DEBP	Diethylbenzylphosphonate
20. DECP	Diethylchlorophosphate
21. DEHEP	Diethyl(1-hydroxyethyl)phosphonate
22. DEHPi	Diethylphosphite
23. DEPP	Diethylpropylphosphonate
24. DEpVBP	Diethyl- <i>p</i> -vinylbenzylphosphonate
25. DIW	Deionized water
26. DOPO	9,10-Dihydro-9-oxa-10-phosphaphenanthrene-10-oxide
27. DSC	Differential scanning calorimetry
28. E_a	Activation energy (kJ mol^{-1})
29. EHC	Effective heat of combustion (also denoted as h_c) (kJ g^{-1})
30. EPS	Expanded polystyrene
31. EtAc	Ethyl acetate
32. F1	First order model
33. FR	Flame retardant

34. FT-IR	Fourier-transform infrared spectroscopy
35. GC	Gas chromatography
36. ΔH_{comb}	Heat of combustion (kJ g^{-1})
37. HEA	2-hydroxyethyl acrylate
38. ΔH_{pyro}	Heats of pyrolysis (mJ mg^{-1})
39. HRC	Heat release capacity ($\text{J g}^{-1} \text{K}^{-1}$)
40. ICP/OES	Inductively-coupled plasma/optical emission spectrometry
41. ISO	International Organization for Standardization
42. LOI	Limiting oxygen index
43. MCC	Microscale combustion calorimetry
44. MMA	Methyl methacrylate
45. MS	Mass spectrometry
46. MSD	Mass selective detector
47. MW_a	Molecular weight of additive/reactive
48. NBS	National Bureau of Standards
49. NIST	National Institute of Standards Technology
50. NMR	Nuclear Magnetic Resonance
51. NTU	Nephelometric turbidity unit
52. ORP	Oxidation-reduction potential
53. PA	Polyaniline
54. PAN	Polyacrylonitrile
55. PCFC	Pyrolysis combustion flow calorimetry
56. PDA	Polydopamine
57. PE	Polyethylene
58. pHRR	Peak heat release rate (W g^{-1})
59. PMMA	Polymethyl methacrylate
59. PP	Polypropylene
60. PPe	Polypyrrole
61. ppt	Parts per thousand
62. PSt	Polystyrene
63. PVC	Polyvinyl chloride
64. PVP	Polyvinyl pyrrolidone
65. R_a	Allyl benzene radical
66. R_p	Primary radical
67. R_{sb}	Secondary benzyl radical
68. SAN	Styrene-acrylonitrile
69. SBR	Styrene-butadiene-rubber

70. SDS	Sodium dodecyl sulfate
71. SMBS	Sodium metabisulfite
72. St	Styrene
73. SW	Seawater
74. TEA	Triethylamine
75. TEPa	Triethylphosphate
76. TEPi	Triethylphosphite
77. TGA	Thermogravimetric analysis
78. THF	Tetrahydrofuran
79. THR	Total heat release (kJ g^{-1})
80. TMG	Tetramethyl guanidine
81. TPP	Triphenylphosphine
82. TPPO	Triphenylphosphineoxide
83. US	Uncoated substrates
84. UV	Ultra-violet
85. XPS	Extruded polystyrene

Contents:

CHAPTER 1: INTRODUCTION	1
1.1 General background	2
1.2 Rationale behind the current programme	3
1.3 Condensation polymers as protective coatings for marine structures	4
1.4 Combustion and flammability of polymeric materials – general considerations	6
1.5 Specific mechanisms of thermal decomposition of chain-growth polymers	9
1.5.1 Polystyrene (PSt)	10
1.5.2 Polymethyl methacrylate (PMMA).....	13
1.6 Improving the flame retardancy of polymers – general considerations	16
1.6.1 Mode of action of halogen- and phosphorus-containing flame retardants	19
1.6.2 Passive fire protection of PSt and PMMA	21
1.7 Passive protection coatings for ferrous metals.....	23
1.8 Overall aim of the project	25
1.8.1 Individual objectives	25
CHAPTER 2: MATERIALS AND METHODS	27
2.1 Materials	28
2.2 Methods.....	28
2.2.1 Synthesis of step-growth polymers	28
2.2.2 Procedures for coating the step-growth polymers.....	30
2.3 Chain-growth polymers	31
2.3.1 Synthesis of the additive (diethylbenzylphosphonate).....	31
2.3.2 Synthesis of precursors to monomers	32
2.3.3 Synthesis of monomers	35
2.3.4 Chain-growth polymerization reactions (homo- and co-polymers)	39
2.3.5 Preparation of test solutions for determination of P and Fe(III) contents	48
2.4 Analytical instrumentation and techniques	53
2.4.1 Inductively-Coupled Plasma Optical Emission Spectroscopy (ICP/OES)	53
2.4.2 Morphological and structural analyses of the materials.....	54
2.4.3 Thermal and calorimetric analysis	56
2.4.4 Software used for data analysis and imaging	57
2.4.4.1 Thermogravimetric Analysis (TGA).....	57
2.4.4.2 Corrosion studies.....	63
CHAPTER 3: RESULTS AND DISCUSSION	65
3.1 Synthesis of step-growth polymers	66

3.2 Characterization of step-growth polymers	66
3.3 Synthesis of the additive, precursors and comonomers	77
3.4 Synthesis of chain-growth polymers	77
3.5 Bulk polymers	85
3.5.1 Thermal and calorimetric characterization.....	87
3.5.2 Kinetic analysis of the TGA thermograms.....	97
3.5.3 Differential Scanning Calorimetry	105
3.5.4 Pyrolysis Combustion Flow Calorimetry (PCFC)	110
3.5.5 ‘Bomb’ calorimetry.....	121
3.5.6 Some generalizations among the test parameters.....	124
3.5.7 Mechanisms of flame retardance- condensed phase	127
3.5.7.1 PMMA-based materials	128
3.5.7.2 PSt-based materials	138
3.5.7.3 Mechanisms of flame retardance – gaseous phase.....	145
3.6 Corrosion studies	163
3.6.1 Imaging software for analyzing the extent of surface corrosion on mild steel	166
CHAPTER 4: MAIN CONCLUSIONS AND SUGGESTIONS FOR FUTURE WORK	172
4.1 Main conclusions	173
4.2 Some suggestions for future work	176
LIST OF REFERENCES	178

Legends of figures:

Figure 1.1 A diagrammatic representation of polymer combustion cycle.	7
Figure 1.2 A Schematic representation of the elementary processes relating to the chain reactions in the flaming zone.....	8
Figure 1.3 A scheme showing the polymerization of styrene to form polystyrene	11
Figure 1.4 A schematic representation of mechanism of polystyrene decomposition.....	13
Figure 1.5 A scheme showing the polymerization of methyl methacrylate to form PMMA.....	14
Figure 1.6 A schematic representation of unzipping reaction of PMMA on decomposition.....	16
Figure 1.7 A diagrammatic representation of interruption of polymer combustion cycle	18
Figure 1.8 A schematic representation of the various elementary processes in the vapour phase relating to the activity of phosphoric acid.....	20
Figure 1.9 A schematic representation of the mechanism of corrosion reaction forming rust on ferrous metals	24
Figure 2.1 A schematic representation of step-growth polymers.....	29
Figure 2.2 A schematic representation of the synthesis of diethylbenzylphosphonate.....	32
Figure 2.3 A schematic representation of the synthesis of acryloyl chloride	32
Figure 2.4 A schematic representation of the synthesis of diethyl(1-hydroxyethyl)phosphonate (DEHEP).....	33
Figure 2.5 A schematic representation of the synthetic route to the precursor for hydroxyphosphorlaminoester.....	34
Figure 2.6 A schematic representation of the synthesis of diethyl-1-(acryloyloxyethyl) phosphonate (DE-1-AEP)	35
Figure 2.7 A schematic representation of the synthetic route to diethyl-p-vinylbenzyl phosphonate (DEpVBP).....	37
Figure 2.8 A schematic representation of the synthetic route to diethyl-2-(acryloyloxy)ethyl phosphate (DEAEPa)	38
Figure 2.9 A schematic representation of the synthetic route to acrylic acid-2-(diethoxyphosphoryl) methyl amino ethyl ester (ADEPMAE)	39
Figure 2.10 Calibration curve (Beer-Lambert plot) for phosphorus	49
Figure 2.11 Calibration curves (Beer-Lambert plot) for Fe(III)	50
Figure 2.12 Plot showing an increase in the degree of corrosion of the first set of test samples (iron nails) kept in sea water at specified intervals of time	51
Figure 2.13 Plot showing an increase in the extent of corrosion of the second set of iron samples (nails) in sea water at specified intervals of time	51

Figure 2. 14 A plot of $g(\alpha)$ vs. $p(x)$ obtained from the TGA software run of the PMMA bulk sample.	63
Figure 3.1 FT-IR spectrum of polyaniline	66
Figure 3.2 FT-IR spectrum of polypyrrole.....	67
Figure 3.3 FT-IR spectrum of polydopamine	68
Figure 3.4 Thermogram of polyaniline at a heating rate of $10^{\circ}\text{C min}^{-1}$	70
Figure 3.5 Thermogram of polyaniline at a heating rate of $60^{\circ}\text{C min}^{-1}$	70
Figure 3.6 Thermogram of polypyrrole at a heating rate of $10^{\circ}\text{C min}^{-1}$	71
Figure 3.7 Thermogram of polypyrrole at a heating rate of $60^{\circ}\text{C min}^{-1}$	71
Figure 3.8 Thermogram of polydopamine at a heating rate of $10^{\circ}\text{C min}^{-1}$	72
Figure 3.9 Thermogram of polydopamine at a heating rate of $60^{\circ}\text{C min}^{-1}$	72
Figure 3.10 DSC curve of polyaniline at a heating rate of $10^{\circ}\text{C min}^{-1}$	73
Figure 3.11 DSC curve of polypyrrole at $10^{\circ}\text{C min}^{-1}$	74
Figure 3.12 DSC curve of polydopamine at $10^{\circ}\text{C min}^{-1}$	74
Figure 3.13 A schematic representation of the initiating species from benzoyl peroxide and dicumyl peroxide	79
Figure 3.14 A schematic representation of the initiating species from ammoniumpersulfate/sodium metabisulfite redox pair	79
Figure 3.15 ^1H NMR spectrum of PMMA obtained through the aqueous-slurry route: region predominantly showing the syndiotactic placements of the $\beta\text{-CH}_2$ protons	80
Figure 3.16 ^1H NMR spectrum of PMMA obtained through the aqueous-slurry route: region predominantly showing syndiotactic placements of the $\alpha\text{-CH}_3$ protons	80
Figure 3.17 ^{13}C NMR spectrum of PSt obtained through the emulsion route: region of the ipso-carbons predominantly showing atactic placements	81
Figure 3.18 ^{13}C NMR spectrum of PSt obtained through the emulsion route: region of the methine and methylene carbons predominantly showing atactic placements	81
Figure 3.19 Structure of the copolymer of MMA and DEpVBP	83
Figure 3.20 An overlay of the TGA curves of the PMMA-based materials with solid additives, at $10^{\circ}\text{C min}^{-1}$	89
Figure 3.21 An overlay of the TGA curves of the PMMA-based materials with liquid additives, at $10^{\circ}\text{C min}^{-1}$	89
Figure 3.22 An overlay of the TGA curves of PMMA-based materials with reactives, at $10^{\circ}\text{C min}^{-1}$	90
Figure 3.23 An overlay of the TGA curves of PMMA and PMMA+aliphatic phosphonate materials	90
Figure 3.24 An overlay of the TGA curves of PMMA and PMMA+aromatic phosphonate materials	91

Figure 3.25 An overlay of the TGA curves of PMMA and PMMA+phosphate materials	91
Figure 3.26 An overlay of the TGA curves of the PSt-based materials with solid additives, at 10°C min ⁻¹	94
Figure 3.27 An overlay of the TGA curves of the PSt-based materials with liquid additives, at 10°C min ⁻¹	94
Figure 3.28 An overlay of TGA curves of the PSt-based materials with reactives, at 10°C min ⁻¹	95
Figure 3.29 An overlay of the TGA curves of PSt and PSt+aliphatic phosphonate materials, at 10°C min ⁻¹	95
Figure 3.30 An overlay of the TGA curves of PSt and PSt+aromatic phosphonate materials, at 10°C min ⁻¹	96
Figure 3.31 An overlay of the TGA curves of PSt and PSt+phosphate materials, at 10°C min ⁻¹	96
Figure 3.32 A plot of the apparent energy of activation (E_a) for the various PMMA-based materials	103
Figure 3.33 A plot of the apparent activation energy (E_a) for various PSt-based materials	104
Figure 3.34 An illustration showing the deduction of the values of ΔH_{pyro} from the DSC curves in the case of unmodified polymers: (A) PMMA and (B) PSt.....	106
Figure 3.35 A plot of heats of pyrolysis of various PMMA-based materials	108
Figure 3.36 A plot of heats of pyrolysis of PSt-based materials.....	109
Figure 3.37 A schematic diagram of the PCFC instrument	111
Figure 3.38 An overlay of the HRR curves obtained from the PCFC runs of all the PMMA-based systems with solid additives.....	114
Figure 3.39 An overlay of the first derivative of the TGA curves of all the PMMA- based systems with solid additives, at 60°C min ⁻¹	114
Figure 3.40 An overlay of the HRR curves obtained from PCFC runs of all the PMMA- based systems with liquid additives.....	115
Figure 3.41 An overly of the first derivative TGA curves of all the PMMA-based systems with liquid additives, at 60°C min ⁻¹	115
Figure 3.42 An overlay of the HRR curves obtained from the PCFC runs of all the PMMA-based systems with reactives.....	116
Figure 3.43 An overlay of the first derivative of TGA derivative curves of all the PMMA- based systems with reactives, at 60°C min ⁻¹	116
Figure 3.44 An overlay of the HRR curves obtained from the PCFC runs of all the PSt-based systems with solid additives	118
Figure 3.45 An overlay of the first derivative of TGA curves of all the PSt-based systems with solid additives, at 60°C min ⁻¹	118

Figure 3.46 An overlay of the HRR curves obtained from the PCFC runs of all the PSt- based systems with liquid additives.....	119
Figure 3.47 An overlay of the first derivative of TGA curves of all the PSt-based systems with liquid additives, at 60°C min ⁻¹	119
Figure 3.48 An overlay of the HRR values obtained from the PCFC runs of all the PSt-based systems with reactives	120
Figure 3.49 An overlay of the first derivative of TGA curves of all the PSt-based systems with reactives, at 60°C min ⁻¹	120
Figure 3.50 A plot of ΔH_{comb} of various PMMA-based materials.....	122
Figure 3.51 A plot of ΔH_{comb} of various PSt-based materials	123
Figure 3.52 A plot of wt.% of char residues from TGA runs and PCFC tests for the PMMA-based materials.....	125
Figure 3.53 A plot of wt.% of char residues from TGA runs and PCFC tests of PSt-based materials	125
Figure 3.54 A plot of the values of ΔH_{comb} from ‘bomb’ calorimetry and EHC from PCFC runs for the PMMA-based materials	126
Figure 3.55 A plot of the values of ΔH_{comb} from ‘bomb’ calorimetry and EHC from PCFC runs for the PSt-based materials.....	127
Figure 3.56 Solid-state ³¹ P-NMR spectrum of char obtained from PMMA+DOPO	130
Figure 3.57 Solid-state ³¹ P-NMR spectrum of char obtained from PMMA+TPP	130
Figure 3.58 Solid-state ³¹ P-NMR spectrum of char obtained from PMMA+TPPO	131
Figure 3.59 Solid-state ³¹ P-NMR spectrum of char obtained from PMMA+TEPi.....	131
Figure 3.60 Solid-state ³¹ P-NMR spectrum of char obtained from PMMA + TEPa	132
Figure 3.61 Solid-state ³¹ P-NMR spectrum of char obtained from PMMA+ADEPMAE.....	132
Figure 3.62 Solid-state ³¹ P-NMR spectrum of char obtained from PMMA+DE-1-AEP.....	133
Figure 3.63 Solid-state ¹³ C-NMR spectrum of char obtained from PMMA+DE-1-AEP	133
Figure 3.64 Solid-state ³¹ P-NMR spectrum of char obtained from PMMA+DEpVBP	134
Figure 3.65 FT-IR spectrum of PMMA (unburnt sample).....	136
Figure 3.66 FT-IR spectrum of PMMA+DEpVBP (partially burnt sample).....	136
Figure 3.67 FT-IR spectrum of PMMA+DE-1-AEP (partially burnt sample).....	137
Figure 3.68 A schematic representation of the formation of char residues in the PMMA-based polymers upon flaming combustion	137
Figure 3.69 Solid-state ³¹ P-NMR spectrum of char obtained from PSt+TPP.....	139
Figure 3.70 Solid-state ³¹ P-NMR spectrum of char obtained from PSt+TPPO	140
Figure 3.71 Solid-state ³¹ P-NMR spectrum of char obtained from PSt+DEHPi	140

Figure 3.72 Solid-state ^{31}P -NMR spectrum of char obtained from PSt+TEPa.....	141
Figure 3.73 Solid-state ^{31}P -NMR spectrum of char obtained from PSt+TEPi.....	141
Figure 3.74 Solid-state ^{31}P -NMR spectrum of char obtained from PSt+DEBP.....	142
Figure 3.75 Solid-state ^{31}P -NMR spectrum of char obtained from PSt+DE-1-AEP	142
Figure 3.76 Solid-state ^{31}P -NMR spectrum of char obtained from PSt+ADEPMAE.....	143
Figure 3.77 Solid-state ^{31}P -NMR spectrum of char obtained from PSt+DEpVBP.....	143
Figure 3.78 A schematic representation of the possible pathway leading to cross-linking and formation of polyphosphate linkages in modified PSt-based materials.....	145
Figure 3.79 A schematic representation of possible fragmentation pattern of DEHPi	148
Figure 3.80 A schematic representation of possible fragmentation pattern of TEPI	148
Figure 3.81 A schematic representation of possible fragmentation pattern of TEPa.....	149
Figure 3.82 A schematic representation of possible fragmentation pattern of DEPP	149
Figure 3.83 A schematic representation of possible fragmentation pattern of DEBP	150
Figure 3.84 A schematic representation of possible fragmentation pattern of DE-1-AEP	150
Figure 3.85 A schematic representation of possible fragmentation pattern of ADEPMAE	151
Figure 3.86 A schematic representation of possible fragmentation pattern of DEAEPA	151
Figure 3.87 A schematic representation of possible fragmentation pattern of DEpVBP.....	152
Figure 3.88 Thermogram and the corresponding first derivative of TPP in nitrogen under a heating rate of $10^\circ\text{C min}^{-1}$	152
Figure 3.89 GC/MS of TPP	153
Figure 3.90 Thermogram and the corresponding first derivative of TPPO in nitrogen under a heating rate of $10^\circ\text{C min}^{-1}$	153
Figure 3.91 GC/MS of TPPO.....	154
Figure 3.92 Thermogram and the corresponding first derivative of DOPO in nitrogen under a heating rate of $10^\circ\text{C min}^{-1}$	155
Figure 3.93 GC/MS of DOPO	155
Figure 3.94 A schematic diagram of production of phosphorus-centred species in the gaseous phase in the case of solid organophosphorus additives.....	157
Figure 3.95 A general schematic diagram of the production of phosphorus acidic species, in the condensed phase through the elimination of ethene from the ester side groups of the liquid additives	158
Figure 3.96 GC and MS of PMMA.....	159
Figure 3.97 Gas chromatogram of PMMA+TPP	160
Figure 3.98 Gas chromatogram of PMMA+TPPO	160
Figure 3.99 Gas chromatogram of PMMA+DOPO	161

Figure 3.100 Gas chromatogram of PSt.....	162
Figure 3.101 Gas chromatogram of PSt+TPP.....	162
Figure 3.102 Gas chromatogram of PSt+TPPO.....	163
Figure 3.103 Gas chromatogram of PSt+DOPO.....	163
Figure 3.104 A plot of black pixels (in percentage) vs. time (in days).....	167
Figure 3.105 Digital photographs and corresponding software outputs of the exposed surface of the test specimen at different time intervals	170

List of tables:

Table 2.1 Preparative data for step-growth polymers	30
Table 2.2 Preparative data for chain-growth solution polymerization reactions of PMMA-based polymers (feed ratio, 9:1).....	40
Table 2.3 Preparative data for chain-growth solution polymerization reactions of PSt-based polymers (feed ratio, 9:1).....	40
Table 2.4 Preparative data for aqueous-slurry polymerizations.....	41
Table 2.5 Preparative data for suspension polymerization reactions of homo- and co-polymers of styrene in the 9:1 ratio	42
Table 2.6 Preparative data for suspension polymerization reactions of co-polymers of styrene in the 8:2 ratio	42
Table 2.7 Preparative data for chain-growth emulsion polymerization reactions of St and MMA	43
Table 2.8 Various additives and reactives used for the bulk polymerization of styrene and MMA	44
Table 2.9 Details of the preparative data for MMA-based bulk polymers	47
Table 2.10 Details of the preparative data for St-based bulk polymer.....	48
Table 2.11 Preparative data of uncoated (US) mild steel substrates immersed in deionized (DIW) and sea water (SW) to different time intervals (days)	52
Table 2.12 Preparative data of coated mild steel substrates immersed in deionized (DIW) and sea water (SW) to different time intervals (22 days)	53
Table 3.1 TGA data of the step-growth samples at heating rates $10^{\circ}\text{C min}^{-1}$ and $60^{\circ}\text{C min}^{-1}$	69
Table 3.2 PCFC data of the step-growth polymers performed at a heating rate of $1^{\circ}\text{C sec}^{-1}$	75
Table 3.3 Preparation of PMMA via different polymerization routes	78
Table 3.4 Preparation of PSt via different polymerization routes.....	78
Table 3.5 Styrene and PMMA-based polymers via the solution route in the 9:1 (monomer:co-monomer) ratio; reaction time	84
Table 3.6 Styrene-based polymers via suspension route in the 8:2 (monomer:co-monomer) ratio; reaction time.....	85
Table 3.7 Some relevant parameters from the TGA analyses of PMMA-based systems	87
Table 3.8 Some relevant parameters from the TGA analyses of PSt-based systems.....	93
Table 3.9 Values of the apparent energy of activation (E_a) and other relevant parameters of PMMA-based samples obtained using the software.....	102
Table 3.10 Energy of activation (E_a) and other relevant parameters of PSt-based samples obtained using the software	104

Table 3.11 Heats of pyrolysis data of PMMA-based materials obtained from DSC tests	107
Table 3.12 Heats of pyrolysis data of PSt-based materials obtained from DSC tests.....	109
Table 3.13 PCFC data of PMMA-based materials.....	112
Table 3.14 PCFC data of PSt-based materials	117
Table 3.15 Heats of combustion data for PMMA-based samples from ‘bomb’ calorimetric measurements.....	121
Table 3.16 Heats of combustion data for PSt-based samples from bomb calorimetric measurements	123
Table 3.17 Phosphorus contents of the unburned samples and char residues of PMMA-based materials	128
Table 3.18 The ³¹ P chemical shift values (δ , in ppm) of the additives/reactives and char residues of PMMA-based materials	134
Table 3.19 Phosphorus contents of the unburned samples and char residues of PSt-based materials	138
Table 3.20 Chemical shift values (δ in ppm) of P nucleus in the additives/reactives and in the char residue obtained from PSt-based systems	144
Table 3.21 Retention times and fragmentation features of the various liquid additives	146
Table 3.22 Retention times and fragmentation features of the various solid additives.....	156
Table 3.23 The retention times and corresponding masses of the major fragments for PSt	162
Table 3.24 Different parameters relating to the aqueous media	164
Table 3.25 Fe(III) in the aqueous extracts of blank and uncoated substrates	165
Table 3.26 Fe(III) and P contents in the aqueous extracts of uncoated and coated substrates after 22 days	166

CHAPTER 1: INTRODUCTION

1.1 General background

Polymers are macromolecules formed by the chemical bonding of small repeating units, called monomers, *via* a process called polymerization (Cowie & Arrighi, 2007). Polymeric materials are present in every walk of life and can be seen almost everywhere in the world. They can be classified as either natural (cellulose, wool, silk, natural rubber, etc.), or synthetic (common man-made polymers such as polythene, polypropylene, polystyrene, acrylic resins, polycarbonates, polyesters, polyurethanes, epoxy resins, or elastomers like styrene butadiene rubber- SBR, nitrile rubbers, etc.). Generally, the common applications of synthetic polymers include: components for buildings and vehicles; moulded materials in electrical and mechanical fields; bio-materials for medical applications; finished products for general household applications; packaging materials in the food processing industry; etc. (Saunders, 1988).

Syntheses of polymers *via* polymerization reactions can be carried out with different initiation mechanisms, such as free radical, cationic, anionic, (Moad & Solomon, 2006), and also through condensation reactions involving appropriate functional groups (Odian, 2004). Generally, most of the standard techniques employed for the production of polymers can be classified into two main categories: chain-growth and step-growth processes, depending on the mechanism by which their corresponding monomers are reacted together to form the polymeric chains (Braun, *et al.*, 2012).

Over the past decades, several novel polymeric materials have made their distinct contributions to the advancement of the present-day technical era. Generally, polymers are comparatively light weight in nature, especially when matched against metals, ceramics, or wood. This coupled with their relatively high impact strength and other desirable physical properties have made them useful for many high-end applications (Van Krevelen & Te Nijenhuis, 2009). Amongst the step-growth polymers, the classic examples in the present context include polyaniline (PA), polypyrrole (PPE) and polydopamine (PDA). These materials, owing to their salient structural features are shown to have superior film-forming and thermal properties, and often exhibit significant level of fire-, corrosion- and biofouling-resistance. On the other hand, some of the most common polymers used today for buildings and other associated construction applications are based on commercially important chain-growth polymers (or thermoplastics) like, polymethyl methacrylate (PMMA) and polystyrene (PSt) (Akovaıı, 2005).

Whilst many of the synthetic commodity plastics have excellent properties, such as light weight, good weatherability, and can be easily manufactured and/or processed into a variety of products with useful applications, they also possess some obvious disadvantages (Joseph & Tretsiakova-McNally, 2011). Flammability is one such problem, and it often limits their wider applicability, especially as building materials and as components for use in the transport sector (Cullis & Hirschler, 1981). For instance, chain-growth polymers such as PMMA and PSt are relatively easy to ignite, and can also lead to uncontrolled fire spread. Therefore, it is highly desirable to improve the flame retardant properties of these materials to warrant safer and wider use, especially in the construction and transport industries.

1.2 Rationale behind the current programme

The preliminary plan of the present project was to develop corrosion-, biofouling- and fire-resistant polymeric coatings for structural components, especially those prevalent in a marine environment, based on some known step-growth polymers. In this context, the initial phase of the experimental programme was set out to synthesize some common step-growth polymers, such as PA, PPe and PDA (Carraher, *et al.*, 2002). The rationale behind the choice of these polymeric systems was multi-fold: all of them have condensed and conjugated aromatic units as the main structural feature, and therefore are endowed with relatively higher thermal stabilities; they exhibit varying levels of electronic conductance, primarily owing to their extended conjugated network, and therefore are expected to interfere and slow down the galvanic reactions pertaining to the corrosion of metallic elements that are disposed in a marine environment; anti-biofouling effects emanating from the water-repelling attributes of their chemical structures, thus preventing the proliferation of protein by the fouling organisms (both uni- and multi-cellular organisms); etc. (Cai, *et al.*, 2018; Nautiyal, *et al.*, 2018; Ou, *et al.*, 2010).

However during the course of the investigation, it was clearly identified that the step-growth polymers, in spite of their desirable attributes (such as anti-corrosion, anti-biofouling and temperature resistance), failed to form uniform and durable coatings onto the substrates of interest without resorting to specialized techniques, such as spray coating, or electrospinning. Hence, the exhaustive synthetic realm of chain-growth

polymers was explored in detail in the later stages of the research programme. Here, the natural choice was those systems based on styrenic and acrylic monomeric precursors owing to a number of reasons that included: 1) polystyrene and polymethyl methacrylate are evidently among the most widely used members of the thermoplastic family; 2) the monomeric precursors, i.e. styrene and methyl methacrylate are prominent among the typical examples of a donor and acceptor pair (Ebdon, *et al.*, 2000), and are easily polymerizable unsaturated compounds under free-radical initiation; 3) both types of monomers can be easily made to undergo addition reactions through a host of techniques (such as solution, bulk, suspension and emulsion- the latter two processes are common practices in the industry, due to their environmentally benign characteristics, where water is used as the medium); 4) the thermal degradation and combustion attributes of the base polymers and their chemically modified versions are well known (Joseph & Tretsiakova-McNally, 2011); 5) film-forming attributes of the acrylic based emulsions are well-established as a desirable property (Lovell, *et al.*, 1997); 6) suspension polymerization of styrene to form expandable beads are extensively used as an industrial technique for making insulation materials for built environments (Lynwood, 2014); 7) virgin and chemically modified versions, especially those bearing phosphorus-containing pendent groups, of acrylic polymers are known to prevent bio-fouling and corrosion (Pospiech *et al.*, 2017; Pospiech *et al.*, 2013); etc.

1.3 Condensation polymers as protective coatings for marine structures

The major issues concerning marine structures are, primarily, corrosion and bio-fouling. The marine industry is traditionally one of the major trade sectors worldwide, where a large number of goods, bulk materials, equipment, etc. are handled and transported on a regular basis (Tsinker, 2012). Therefore, it forms an important part of the economy of nations, especially those having significant sea-port activities. The need for modernization and restructuring of the existing ports and structures is increasing tremendously as newer technologies are being introduced and developed day-by-day (Soares, 2011; Tsinker, 2012). Generally, most of the marine structures are built with a life expectancy of around 30-50 years (Cook, 2005), and are constituted mainly of concrete and steel structures. However marine structures, both onshore and offshore, are always exposed to harsh and aggressive environmental conditions, such as climatic

variations, varying properties of the surrounding media, seasonal fluctuations, tide ranges, (Tsinker, 2012), etc., throughout their service life. In this context, both corrosion (Crawford, 1995) and biofouling (Cao, *et al.*, 2011) are considered to be the major issues encountered during the service life of such structures. It is also relevant to note here that often these two problems complement each other, and therefore are detrimental on each account.

In the above context, and during the initial stage of the work, three film-forming polymers such as PDA, PA and PPe were chosen. Generally, these polymers are synthesized by the oxidative polymerization of their respective monomers; for instance, dopamine hydrochloride reacts to form polydopamine (Coleman, 2019). Polydopamine, generally, exhibits excellent adhesion properties to almost all substrates, irrespective of the nature of the substrates (i.e. it adheres to both organic and inorganic surfaces including metals, glass, and polymeric substrates with different polarity) (Liebscher, *et al.*, 2013; Liu, *et al.*, 2014). It was also shown that PDA can form excellent fire-resistant films on surfaces (Cho, *et al.*, 2015). In addition, PDA was shown to have good corrosion-resistant attributes, and anti-bacterial properties which was explored in bio-medical applications such as bio-compatible implants for bone fixation, stents, etc. (Singer, 2015; Su, 2016). Polypyrrole and polyaniline, on the other hand, are prominent members amongst conducting polymers and are known to have good anti-corrosive properties (Liu & Oliveira, 2007; Valença, 2015; Fang, *et al.*, 2007; Peikertová, *et al.*, 2011). Furthermore, these polymers have been shown to exhibit a significant degree of resistance against bacterial proliferation, especially, against *Escherichia coli* (Varesano *et al.*, 2013; Boomi, Prabu, & Mathiyarasu, 2014).

The inability of the step-growth polymers to form uniform and durable coatings onto the substrates of interest led to an exploration in detail of some of the desirable properties, especially the passive fire proofing attributes (Ebdon, *et al.*, 2000) of some commercially important chain-growth polymers based on styrenic and acrylic monomers. Here, two simple and quick laboratory-scale techniques to gauge the extent of corrosion occurring on the surfaces of uncoated and coated mild steel substrates were also explored. These techniques involved, either the quantitative measurement of Fe(III) ions using inductively-coupled plasma/optical emission spectroscopy (ICP/OES), or through an imaging technique that utilized a bespoke software.

1.4 Combustion and flammability of polymeric materials – general considerations

Flammability is a general term commonly used to denote the susceptibility of a material to get ignited easily, burn sustainably and rapidly, and often with a visible flame. On the other hand, combustion is the scientific term used to describe burning of any type of material in the presence of oxygen (Horrocks & Price, 2001). An exothermic oxidation reaction releases energy predominantly as heat, and to some extent as light, to the surrounding environment and can result in the formation of residues (i.e. a carbonaceous residue/char). Even though polymeric chains exhibit similar types of intermolecular and intramolecular forces as seen in the case of low molecular weight compounds, they are quite susceptible to thermolysis (i.e. mainly pyrolysis). Hence, given sufficient heat input, a polymeric material can undergo extensive chain cleavages to produce volatiles. This is often exacerbated by the fact that most polymers have an organic backbone, and thus making them inherently highly flammable (Joseph & Ebdon, 2000).

Generally, polymer combustion processes can occur in three phases: condensed phase, interphase and gaseous phase (Cullis & Hirschler, 1981) (see Figure 1.1). The interphase can be considered as the region between condensed and gaseous phases, and often is not a very well defined zone. This phase can also incorporate the thermal decomposition products in all different physical states such as, liquids, solids and gases. Furthermore, the burning of solid fuels generally depends on other environmental parameters that include, pressure, temperature, extent of oxygen ingress, etc., as well as on the innate material properties associated with molecular, thermophysical, thermochemical and decomposition characteristics. Generally, combustion can be referred to as either flaming combustion, or non-flaming combustion. If combustion of a material occurs with the presence of flame in the vapour phase, it is called flaming combustion and that occurs without the presence of a flame, mostly in a condensed phase, is called as non-flaming combustion (Novozhilov, *et al.*, 2011).

The tendency of polymeric materials to melt and flow, forming a pool of flammable decomposition products as well as volatile matter, can constitute a very serious secondary hazard as it often can lead to further burning of surrounding fuel loads (Joseph & Tretsiakova-McNally, 2015). This tendency strongly depends on the class of the polymeric material (i.e., thermoplastic or thermoset) as well as on their chemical constitution. The flammability characteristics of different polymers depend also on their

chemical structure (Joseph & Ebdon, 2000). In addition, common polymers exhibit a wide range of propensities for ignition. Generally, they require a temperature range of around 270-470°C to undergo ignition. However, in the case of foamed products like flexible polyurethane, or polystyrene foams, the products are highly ignitable even in the presence of low-intensity sources for piloted ignition, and can initially go through a smouldering phase of combustion (Byard, 2018; Denecker, *et al.*, 2006; Dick, *et al.*, 2001; Morgan & Galaska, 2008). The main reason behind this relatively high ignitability/flammability can be attributed to their porous structure.

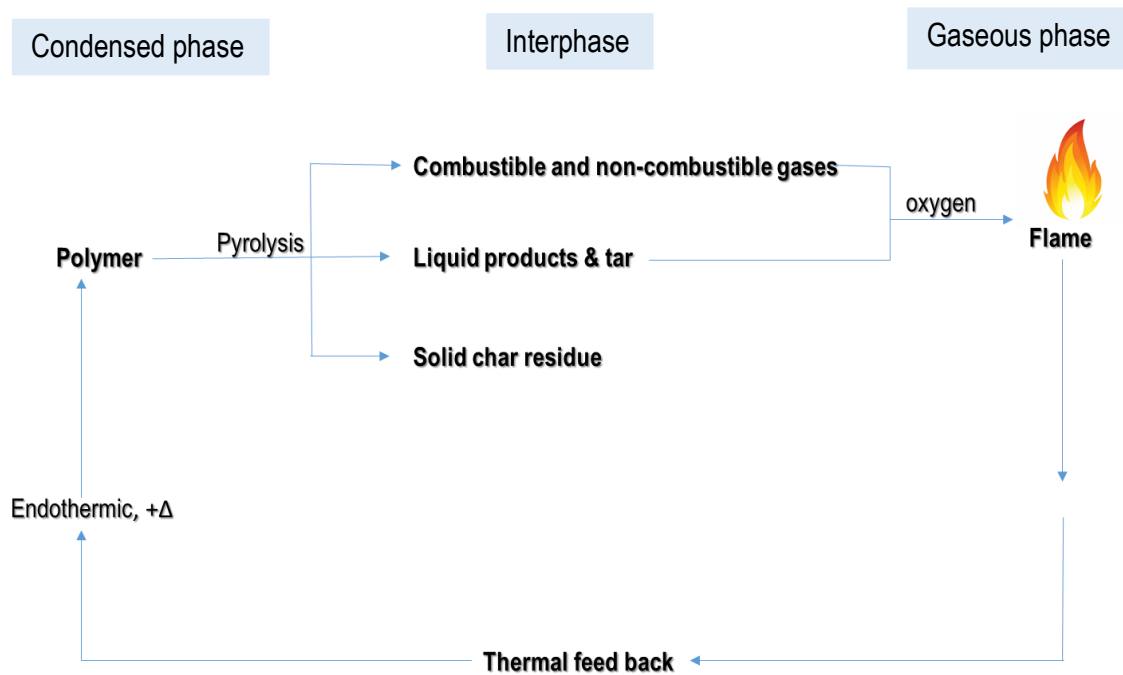


Figure 1.1 A diagrammatic representation of polymer combustion cycle (Joseph, *et al.*, 2016).

During burning, in the initial stages of decomposition of combustible solids low molecular weight volatile components are formed, which can then be mixed with air to form a flammable mixture. This mixture, if it happens to be within its flammability limit, can then proceed to flaming combustion provided a suitable pilot is present. The chemical reactions occurring in the gas phase can be considered as very fast chain reactions

primarily propagated by H[•] and HO[•] centred radicals (Joseph, *et al.*, 2016) (see Figures 1.1 and 1.2).

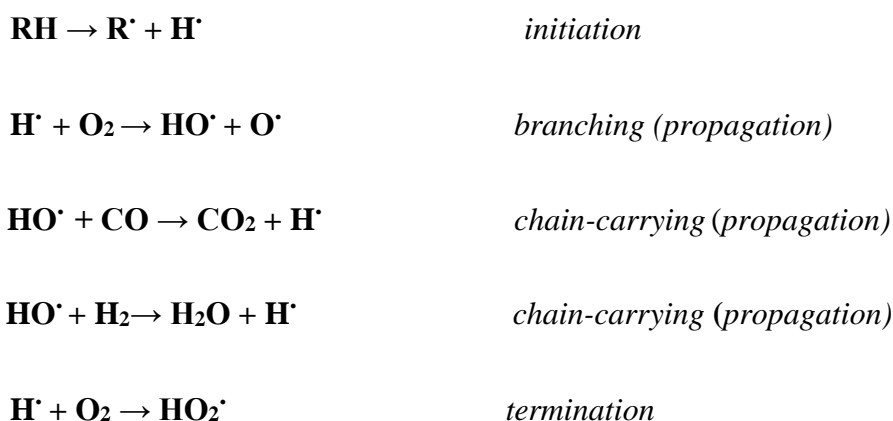


Figure 1.2 A Schematic representation of the elementary processes relating to the chain reactions in the flaming zone

The thermal decomposition pathways of individual polymers also largely depend on their chemical structures. Typical decomposition patterns involve: hydrogen transfer to α - or β -carbon atoms, oxygen or nitrogen; cyclization; side-chain reactions; molecular rearrangements; unzipping to monomer; elimination of small molecules such as carbon dioxide, sulfur dioxide, or sulfide; etc. (Ebdon, *et al.*, 2001). Aromatic backbone-containing polymers such as polycarbonate involve cross-linking and side-chain reactions leading to carbonaceous char residues. High carbon/hydrogen ratios can also facilitate crosslinking between carbon radicals, thus producing a char. On the other hand, low carbon/hydrogen ratios favour the termination process by hydrogen transfer, leading to the formation of low molecular weight species rather than char residues (Van Krevelen & Te Nijenhuis, 2009). Furthermore, heat transfer to the condensed phase and the rate at which the thermal energy is stored are important, as they determine the time to ignition and combustion rates of polymers (Drysedale, 2011).

1.5 Specific mechanisms of thermal decomposition of chain-growth polymers

As already mentioned, polymer decomposition can also result in substantial amounts of char residues, and these often prevent further decomposition, or burning, of the material. However, some polymers completely undergo decomposition leaving no solid residues behind. Polymethyl methacrylate (PMMA) is a classic example of such a polymer, which upon thermal decomposition produces a near quantitative yield of the monomer (MMA), through a chain ‘unzipping’ mechanism (Price, *et al.*, 2008). Furthermore, owing to its complete combustion at higher temperatures, PMMA leaves no char residue. Generally, the mechanisms of decomposition of various polymers can be classified into four categories (McNeill, 1970; Cullis & Hirschler, 1981):

- Random chain scission
- Chain-end scission (unzipping)
- Elimination of side groups without any backbone scission
- Crosslinking

In random chain scission, as the name indicates, the polymer chains break into small fragments. Commercial polymers such as polyethylene (PE) and polypropylene (PP) follow mostly this type of decomposition pattern. Chain-end scission involves mainly depolymerisation of the whole polymer from the chain ends, such as in the case of PMMA and poly- α -methylstyrene. Polyvinyl chloride (PVC) (Carty, *et al.*, 2002) and some polystyrene-based copolymers, primarily undergo elimination of side groups, whereas others like polyacrylonitrile (PAN) undergo intra-chain cyclization reactions (Crook, *et al.*, 2010). A small amount of cross-linking can also be seen in the case of PE (Banks, *et al.*, 1993).

Generally, polymers that tend to undergo cross-linking as well as the elimination of side groups, while burning, are likely to be less flammable than those undergoing random chain scission, or unzipping types of decomposition. This can be attributed to the fact that, when the chains start to cross link, the material forms more rigid structures leading to char formation (Van Krevelen & Te Nijenhuis, 2009). A layer of char, once formed on the surface of a burning solid fuel, can act as a barrier between the underlying material and oxygen supply, thereby facilitating the extinguishing of the fire and/or preventing further flame spread. The elimination of side groups may also result in cross-linking between chains (Cullis & Hirschler, 1981). Polymers containing aromatic structures

within the main chain may yield more char than their aliphatic analogues. Polystyrene can also be considered as an example in this category, and has been shown to produce varying amounts of char residue especially when it is present a part of co- and ter-polymers. Char residues can be also formed *via* different routes such as cross-linking, fusion of aromatic groups, or graphitization, as in the case of step-growth polymers, such as, PDA, PA and PPe.

In the following sections, a detailed account of the commercial importance, production processes, thermal decomposition steps, production of combustible volatiles, and flammability features of two of the chain-growth polymers selected in the present study (PSt and PMMA) are given.

1.5.1 Polystyrene

Polystyrene (PSt) is a cheap, easily available and transparent thermoplastic polymer that is used for a wide number of applications, especially as foams (Lynwood, 2014). The monomer, styrene, is also copolymerised with other monomers to produce co- and/or ter-polymers, often having improved properties. These include styrene-acrylonitrile (SAN) and acrylonitrile-butadiene-styrene (ABS) polymers, styrene-butadiene rubber (SBR), etc. Furthermore, there are two types of polystyrene foams available: expanded polystyrene (EPS) and extruded polystyrene (XPS). Expanded polystyrene is used for food packaging applications and XPS, which is a higher density foam, is used in the building sector (Sayadi, *et al.*, 2016).

Polystyrene is made up of repeating styrenic units, which can be easily obtained by polymerizing styrene in the presence of certain initiators, or at elevated temperatures. Suspension polymerization is one of the industrial techniques commonly used for producing styrene foams. In this process, styrene monomer is suspended in water as small droplets with the aid of a suspending agent, under a high-shear stirring. Polymerization is then carried out in the presence of an initiator, such as benzoyl peroxide, at higher temperatures to yield bead-like particles (O'dian, 2004).

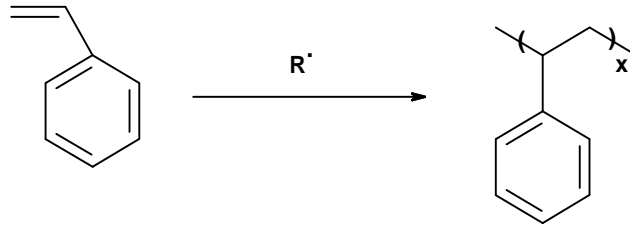


Figure 1.3 A scheme showing the polymerization of styrene to form polystyrene (where $R\cdot$ denotes the initiating species)

The polystyrene beads, thus obtained, can be expanded (expanded polystyrene: EPS) for end uses in three steps:

- Pre-expansion: grain-shaped PSt beads are expanded up to 50 times their original size by using a blowing agent such as pentane, or steam
- Conditioning: the expanded beads are then stored in appropriate containers for a maturation period before the moulding process
- Moulding: in this step, the pre-expanded PSt beads are further expanded in a mould in the presence of steam thereby moulding them into blocks or boxes or any desired shapes for the end use.

Expanded polystyrene (EPS) is widely used as a light weight insulating material for buildings owing to several desirable attributes. The characteristics of EPS that makes it popular as an insulating material in the construction sector include:

- Availability and low cost
- Can be processed easily
- Light weight, transparent and ease of recycling
- Excellent thermal insulator
- Good shock absorbent quality
- Water resistance, and can act as a vapour, air and dust barrier
- Good load bearing capacity
- Easy installation and maintenance

a. Flammability of styrenic materials

One of the disadvantages, despite its useful characteristics, is the high flammability of polystyrene. When ignited, polystyrene and its copolymers can burn quickly with a visible flame, releasing volatiles into the environment including styrene monomer, oligomers, lower hydrocarbons such as benzene, lower alkylbenzenes, etc. (Price, *et al.*, 2007). During the burning process, polystyrene can also melt, flow and drip, which can lead to an increased fuel load feeding into enhanced flame spread (Joseph & Tretsiakova-McNally, 2015). Generally, styrenic polymers produce minimal amounts of char residues, especially upon combustion.

b. Mechanisms of thermal decomposition of polystyrene

Polystyrene homopolymer, generally, starts degrading at a temperature around 270°C and continues until 425°C under normal conditions in air. Through random main-chain cleavages and associated mechanisms, PSt forms varying amounts of a number of compounds such as styrene, benzaldehyde, styrene oxide, acetophenone, and 1-phenylethanol. Styrene and benzaldehyde are found to be the prominent fractions among the decomposition products (Ebdon, *et al.*, 2000). Like the majority of main-chain carbon polymers, the thermal decomposition of polystyrene generally occurs in three steps: initiation, propagation and termination, which follows a free-radical chain mechanism (McNeill, *et al.*, 1990):

- **Initiation:** decomposition of polystyrene can take place *via* two routes, i.e., random scission or chain-end scission. In random chain scission, two radicals are formed, one primary radical (R_p) and one secondary benzyl radical (R_{sb}) with a strong benzylic resonance. In the chain-end scission mechanism, one secondary benzyl radical (R_{sb}) and the resonantly stabilized allyl benzene radical (R_a) are formed. The reaction mechanisms are shown below (Figure 1.4):

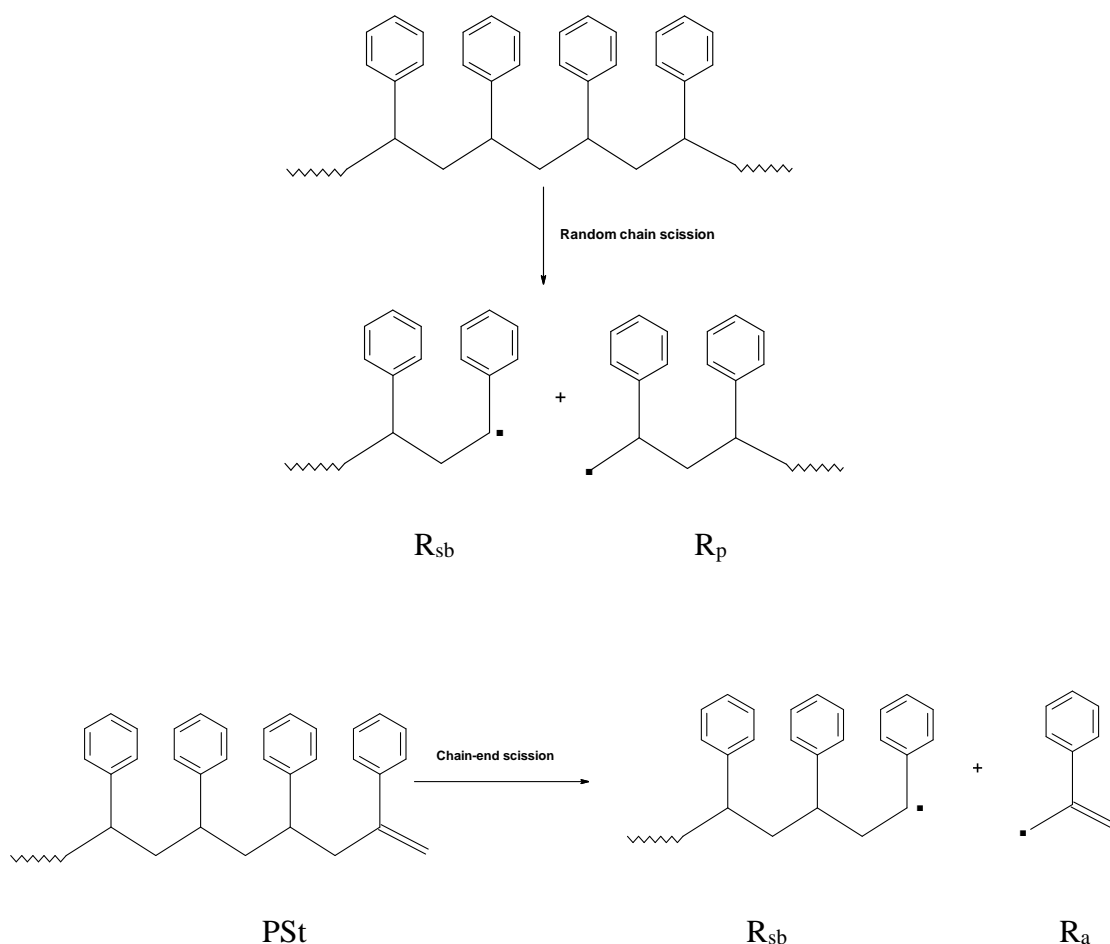


Figure 1.4 A schematic representation of mechanism of polystyrene decomposition (where the free radical species are denoted by R)

- Propagation: The generated free radicals are propagated through hydrogen abstraction and unzipping reactions. There are two types of hydrogen abstraction reactions: intermolecular and intramolecular abstractions.
- Termination: Termination can occur by either recombination, or disproportionation mechanisms of various active radical fragments.

1.5.2 Polymethyl methacrylate (PMMA)

Polymethyl methacrylate is an important member of the class of acrylic polymers and is used widely for industrial as well as household purposes. It has excellent properties such as transparency, high light transmission, good impact strength, less prone to chemical

attack and weathering, and UV resistance (Poth, *et al.*, 2011). Commercially, PMMA-based materials are used in sectors, such as construction and architecture, lighting, automotive and transportation, electronics, medical, etc. It is synthesized from its monomer, methyl methacrylate using various polymerization techniques, primarily utilizing a free radical route (Kricheldorf, 1991). Furthermore, copolymerization reactions of PMMA with other monomers yield hybrid materials that often exhibit some additional desirable properties.

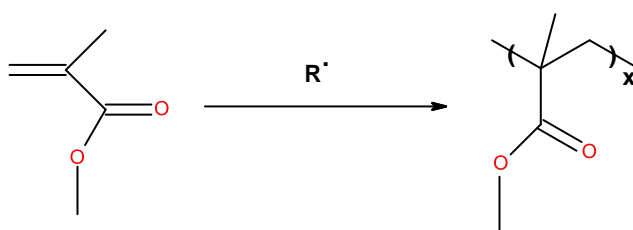


Figure 1.5 A scheme showing the polymerization of methyl methacrylate to form PMMA

Polymethyl methacrylate is mainly used as an alternative to borosilicate glass, and as a component in acrylic paints. Since its density is half that of glass (1190 kg m^{-3}), this makes it lighter than glass. The transparency and relatively non-toxic nature of PMMA make it suitable for the manufacturing of windows and the end-products are usually known as Plexiglas, Lucite, etc. Lucite is also used for making toilet and shower units. Some other uses of transparent PMMA sheets include outdoor signs, lenses, light covers, aircraft glazing, toys, etc. In building applications, PMMA is mainly used in ceilings, roofing, walls and wall frames as a replacement for glass.

Polymethyl methacrylate is also a component of acrylic paints that are produced as emulsions, along with other additives such as acetates, xylene, toluene, and colouring pigments. Acrylic paints are fast-drying coatings, and are water resistant when dry, but can be diluted with water prior to coating. Polymethyl methacrylate is also used in varnishes, stains, and resins also known as 'acrylic resin', and the filaments for 3-D printing.

In summary, the salient properties of PMMA which makes it one of the widely used plastics, include the following:

- Availability, processability, low cost, and low-toxicity
- Transparency as comparable to glass
- Light weight, and scratch resistance
- UV- and weather-resistance

a. Flammability of acrylic resins

The thermal depolymerisation of PMMA involves the unzipping of the polymer chain, resulting in the complete recovery of its monomer methyl methacrylate (Fateh, *et al.*, 2016). When ignited PMMA can burn with a sustained, bright and smoky flame, and generally produces a fruity smell. In the presence of air, PMMA starts burning at 460°C leading to complete combustion resulting in the formation of carbon dioxide and water as by-products (Price, *et al.*, 2007; Price, *et al.*, 2001). The decomposition process takes place in three stages during a programmed heating in a controlled atmosphere as follows:

- 165°C – scissions of the bonds between monomer units of the head-to-head type linkages
- 270°C – scissions at the chain-ends with vinylidene ends
- 350°C – random scissions in the polymer chain

These stages were generally found in PMMA synthesized through a free-radical mechanism. However, when synthesized *via* an anionic route, the decomposition often takes place only in one stage at 360°C by random chain scission.

The initial stage of decomposition consists of random chain scission that can proceed to chain-end scission. The unzipping of the main chain, leading to monomer regeneration, takes place in the propagation stage. Almost 90% or more of the monomer can be recovered through this process. Generally at higher temperatures, a series of complex reactions take place resulting in the formation of decomposition products such as butene, methacrylic acid anhydrides, etc. (Holland & Hay, 2001)(see below in Figure 1.6).

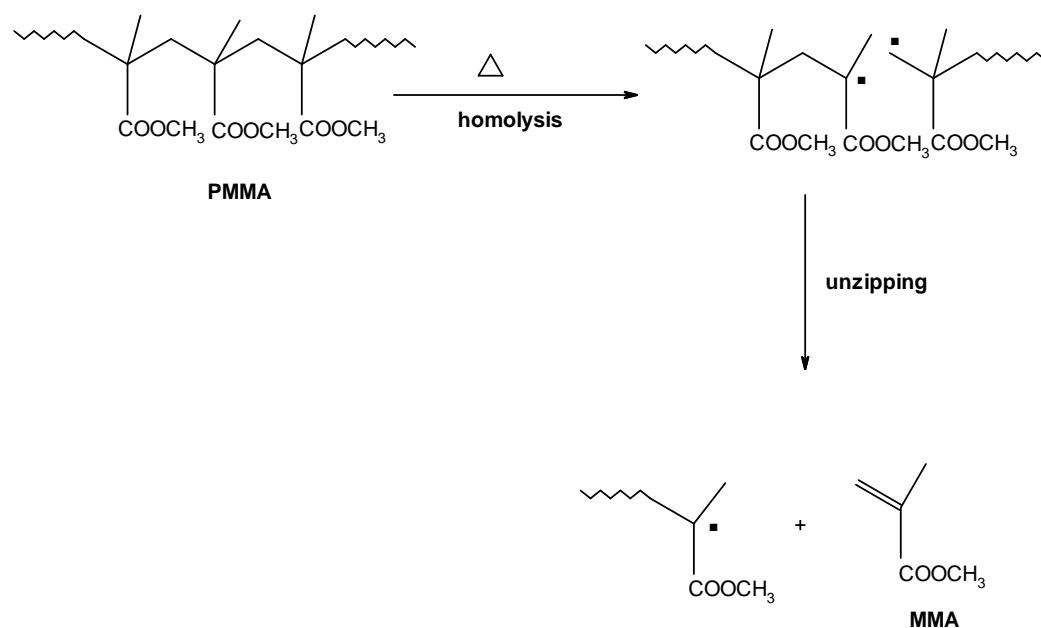


Figure 1.6 A schematic representation of unzipping reaction of PMMA on decomposition

1.6 Improving the flame retardancy of polymers – general considerations

Generally, polymeric products are widely used as a cheaper and lighter alternative for a large number applications in the construction sector, such as: facades, insulation materials, panels, frames, etc. (Cheremisinoff, 1997). Another potential application of polymeric materials is in the transport industry. Textile industries also use synthetic polymeric fibres for the preparation of clothing materials. However, for the safer and wider use of polymeric materials, it is mandatory that they satisfy some acceptable level of fire resistance. For this purpose, it is often necessary to treat the polymeric material through a suitable methodology, where an appropriate combustion inhibitory reagent (i.e. a flame retardant, FR) is incorporated into the final product. Generally, a large number of flame retardants have been used for many years to protect polymeric materials from fire hazards (Morgan, 2019). These flame retardants are mixed as additives in the polymer matrix by physical means. Another way of improving flame retardancy is to prepare inherently less flammable polymers through copolymerization with compounds that can impart fire resistance (Grand & Wilkie, 2010).

The use of FRs to impart fire retardance to common polymeric materials are well documented in the literature (Morgan, *et al.*, 2015; Schartel, *et al.*, 2016; Schartel, *et al.*,

2017; Wilkie & Morgan, 2010). Flame retardants can interact with polymers physically and/or chemically depending on their inherent nature and associated properties (Ebdon, *et al.*, 2001). Physical mechanisms include:

- Formation of a protective coating: This involves the formation of carbonaceous char on combustion, which then acts as a physical barrier between the polymer and surrounding atmosphere. This limits the supply of fuel to the system, thus hindering the combustion process. Such coatings also help in preventing the release of flammable volatiles/gases into the atmosphere.
- Cooling: During combustion, this type of FR activates certain endothermic reactions, which absorb the surrounding heat, thereby cooling the system below the temperature that is required to sustain the combustion process.
- Dilution: Flame spread can be hindered by adding certain inert additives, or fillers, to the polymer system. During flaming combustion, these additives liberate certain inert gases, which then dilute the system making it less favourable for further burning in the gaseous phase.

Flame retardants are generally active either in the condensed phase, or in the gaseous phase. In addition, upon exposure to an external heat flux, a polymer can pyrolyze with the generation of enough flammable volatiles releasing into the gaseous phase, which adds fuel to the system. These volatiles get mixed up with atmospheric oxygen forming a fuel source, leading to visible flame. The heat generated during this process is fed back to the condensed phase of the system, thus sustaining the burning process. This forms a cycle, as depicted in Figure 1.1 (Joseph, *et al.*, 2016). The introduction of a flame-retardant material, physically or chemically, into the polymer matrix can hinder some of the processes/stages either in the condensed phase, or in the gaseous phase of the system (Figure 1.7). It is relevant to note here that the physio-chemical processes occurring at the interphase are relatively hard to decipher, and hence it is the least studied among the three phases when a solid fuel undergoes decomposition /combustion (Price, *et al.*, 1999).

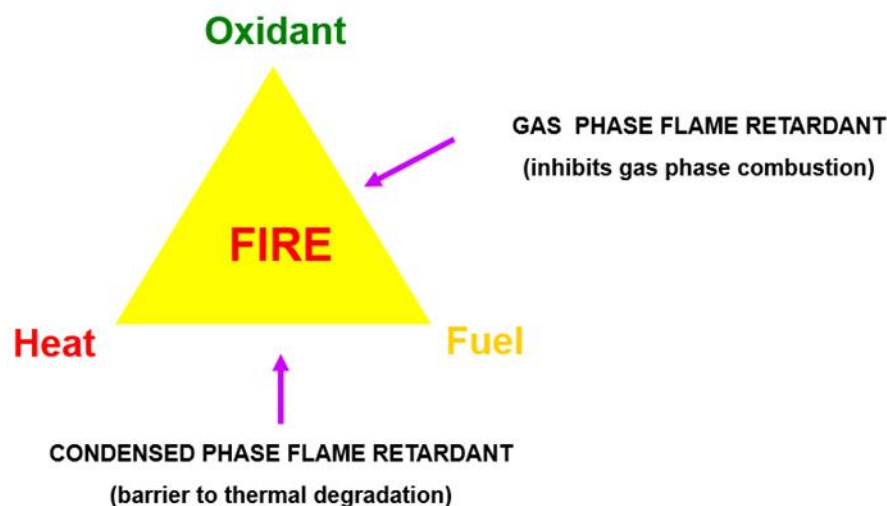


Figure 1.7 A diagrammatic representation of interruption of polymer combustion cycle

- *Condensed phase*

In a condensed phase mechanism, usually the FR compound helps in forming carbonaceous char and/or *in-situ* production of water when degraded. Char residues often form a thick layer of coating on the surface of the polymer, which prevents the release of flammable volatiles into the gaseous phase, thus obstructing the pyrolysis pathway. Intumescent coatings work by this principle (Camino, 1998; Camino & Costa, 1986). Char formation also helps in protecting the underlying polymer from further damages.

- *Gaseous phase*

Combustion of gaseous fuel is facilitated by the formation of certain free radicals. Most polymers when burned can release free radicals, which then combine with atmospheric oxygen (see also in Figure 1.2). Generally, H^{\bullet} and HO^{\bullet} are the most predominant intermediates that are responsible for the chain propagation reactions. The species, HO^{\bullet} is also responsible for the secondary oxidation of CO to CO_2 . In most cases, the free radicals formed in the vapour phase are scavenged by flame retardants, or their decomposition products, and subsequently converting these into more stable species. This in turn will interrupt the exothermic processes leading to a less efficient combustion. Most of the halogen-based flame retardants follow this mechanism (Joseph & Tretsiakova-McNally, 2011).

1.6.1 Mode of action of halogen- and phosphorus-containing flame retardants

Common commercially available flame retardants that are used for plastic products are halogen-based (bromine and chlorine), phosphorus compounds and metal hydrates. As previously mentioned, the halogenated component in a formulation often tend to volatilise, thus liberating highly active halogen atoms in the vapour phase. These atoms can then act as radical scavengers by combining with the primary propagating species, such as H^{\bullet} and HO^{\bullet} . The inhibition of flaming combustion is thus effected when the threshold amount of the propagating species falls below a critical value. On the other hand, phosphorus-based FRs predominantly act in the condensed phase, which also in fact depend on the chemical nature of the base substrate. However, elemental phosphorus and /or its oxygenated species can also exert vapour phase inhibition, as in the case of halogenated compounds. Thus the phosphorus flame retardants will often exhibit a mixed vapour phase/condensed phase effect. Other examples of less commonly used FRs include boron-, silicon- or nitrogen-containing compounds, FR synergists such as antimony trioxide and others, along with some of the newer product technologies such as nanoclays (Grand & Wilkie, 2010). The specific modes of actions of each class of flame retardants are explained below:

- *Halogen-containing compounds*

Bromine is the most effective in this category followed by chlorine (Covaci, *et al.*, 2011). Bromine and chlorine form halides with hydrogen, which are liberated over a specific range of temperature for each, acting as effective scavenging agents during combustion. Various chlorinated and brominated flame retardants are used for engineering plastics such as high impact polystyrene, epoxy resins, etc. These retardants also impart good physical properties to the parent polymer. However, owing to obvious environmental toxicity issues, the wider use of halogenated FRs have been very severely criticised in recent years, and several of these are banned completely (Ezechiáš, *et al.*, 2014).

- *Phosphorus and its compounds*

The use of phosphorus-containing compounds as flame retardants can be traced back as long ago as 1821, where Gay Lussac had described a method to modify theatre curtains for improved flame retardancy by treating them with ammonium phosphate solution (Joseph & Tretsiakova-McNally, 2011). Generally, phosphorus-based FRs and their

combustion products are less toxic than the corresponding halogen-based flame retardants. Therefore, phosphorus-based compounds are as important as halogenated retardants and to a certain extent are as effective in managing combustion phenomenon (Benin, *et al.*, 2015; Wang, *et al.*, 2017).

A large number of phosphorus-based compounds are available with a difference in their chemical environments of the phosphorus atom (Joseph & Tretsiakova-McNally, 2011). These compounds when degraded are shown to produce phosphoric acid and similar species that could inhibit the combustion process in the condensed phase. Phosphorus compounds are active in the vapour (Salmeia & Gaan, 2015) and condensed phases based on the chemical nature of the compound. Typical reactions of phosphoric acid species in the vapour phase are shown below (Grand & Wilkie, 2000).

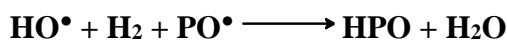
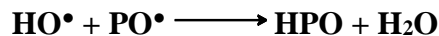


Figure 1.8 A schematic representation of the various elementary processes in the vapour phase relating to the activity of phosphoric acid

Here, PO^\bullet can be considered as the most important species, acting as a free radical scavenging agent. Some of the common phosphorus-containing compounds include: red phosphorus, phosphine oxides, inorganic phosphates, organophosphates, phosphonates, chlorophosphates, etc. Furthermore, halogenated and phosphorus-containing compounds when combined together are shown to exhibit some degree of synergism similar to halogen/antimony combination (Cullis & Hirschler, 1981). Phosphorus and nitrogen, when combined, can also exhibit synergism (Joseph & Ebdon, 2000). However, this effect can also depend on the chemical nature of the nitrogen in the modifying group (for example, amide, imide, nitrile, etc.) when present with a particular type of phosphorus-

bearing moiety (for instance, with phosphonate esters). In addition, the extent of the synergetic effect can also depend on whether both the atoms for the part of the same pendant group (Joseph, & Tretsiakova-McNally, 2012b). Furthermore, P/N- containing compounds such as phosphorylaminoesters and phosphoramides are also tested for enhanced flame retardant properties (Bakos, *et al.*, 1982).

The efficiency of phosphorus containing compounds in the additive as well as the reactive categories is well documented in the literature (Joseph & Tretsiakova-McNally, 2011; David, *et al.*, 2012). Organophosphorus compounds containing P-C bonds also have good thermal and hydrolytic stabilities. The efficiency of phosphorus-based compounds generally depends on several factors: chemical environment and oxidation state of the P atom; volatility; nature of the decomposition products formed upon thermolysis etc. Condensed-phase activity of phosphorus compounds, predominantly, involves char formation which is facilitated by the dehydration of the polymeric structure leading to cyclization, cross-linking and aromatization/graphitization (Grand & Wilkie, 2000). Cross-linking can be also induced by the decomposition by-products of the phosphorus compounds. For polymers with hydroxyl, or amino, groups in their monomeric units, such as in the case of cellulose or wool, phosphorus compounds work mainly in the condensed phase. In the case of olefin-based polymers, these compounds act mainly in the gaseous phase by scavenging free radicals like H[•], HO[•] and preventing their oxidation.

The phosphorus containing compounds that we have used for the present study include additive and reactive types. Additives are simply added to the monomer/initiator mixture during polymerization to form physical mixtures. Reactive types, on the other hand, include phosphorus-based compounds that can be polymerized by adding them into the main monomer mixture during the syntheses of copolymers (Ebdon, *et al.*, 2001; Price, *et al.*, 2001).

1.6.2 Passive fire protection of PSt and PMMA

Among the chain-growth polymers, the present study is focused on improving the flame retardant properties of polystyrene and polymethyl methacrylate (Ebdon, *et al.*, 2000; Ebdon, *et al.*, 2000; Price, *et al.*, 2005). The flame retardation of styrenic and acrylic polymers using covalently bound phosphorus-containing moieties is well documented in

the literature (Joseph & Tretsiakova-McNally, 2012a; Joseph & Tretsiakova-McNally, 2011; Price, *et al.*, 2008; Price, *et al.*, 2007; Joseph & Tretsiakova-McNally, 2012b; Tretsiakova-McNally & Joseph, 2015; Wyman, *et al.*, 2006; Dumitrascu & Howell, 2011; Dumitrascu & Howell, 2012; Röchow, *et al.*, 2018; Vahabi, *et al.*, 2012; Vahabi, *et al.*, 2012).

Recent studies have shown that incorporating inorganic fillers such as magnesium hydroxide, graphene oxide and modified nanoparticles such as clays, silica etc. into polystyrene matrix reduces the peak heat release rate and improves the overall flame retardancy of the polymer (Edenharter, *et al.*, 2016). In a related study, it was shown that the polymerization of styrene in the presence of organic phosphorus compounds and/or its modification with organic clays improves the flame retardant properties and reduces oxygen consumption (Jankowski & Kedzierski, 2011). Alternatively, blending polystyrene with other polymers that are more flame retardant such as polyvinylidene fluoride, polyamides, etc., can offer better properties (Cao, *et al.*, 2013; Kausar, *et al.*, 2017).

Similarly, some recent studies have also shown that PMMA modified with several nano-fillers, or blends, using different techniques, resulted in improved fire resistance. One of these uses a sol-gel method to prepare organic-inorganic hybrids of PMMA with a silane-containing phosphorus and nitrogen compound (Ebdam, *et al.*, 2017; Jiang, *et al.*, 2014). This method was shown to improve the charring process and also highlighted the synergism among phosphorus, nitrogen and silicon. Other studies have shown that incorporating certain additives such as layered double hydroxides and alumina nanoparticles into PMMA matrix is useful in reducing the peak heat release rate obtained from cone calorimeter measurements, thus enhancing overall flame retardancy of the systems (Mohammadi & Davoodi, 2018; Zhu, *et al.*, 2012).

Most of the studies in recent years have focused on varying the ratios of different components in blends, incorporating necessary fillers with varied chemical constitutions, and then monitoring the thermal properties (decomposition temperature, heat release rates, etc.), and improvements in the glass transition temperatures, etc. Even though these studies have demonstrated an increase in the overall flame retardant properties, as identified through some prescriptive laboratory-scale techniques/tests, they still remain predominantly in the realm of an academic pursuit. From a practical point of view, the

important facts that need due consideration while formulating any FR strategy should include: cost-effectiveness and ease of processing, and hence the commercial viability; environmental implications of the fillers/additives; the overall efficacy of the modifying compounds in the case of a fire scenario; etc. In this context, it is clear from the previous discussions that phosphorus-containing compounds are similar to many of the new as well as tried-and-tested compounds, like the metallic oxides and/or other hybrid versions.

Given the renewed interest in phosphorus-containing FRs, especially as alternatives to environmentally harmful halogenated compounds, the desirable attributes of several classes of them were explored through the current project. Thus, the additives used in the present study included: phosphine, phosphine oxide, DOPO, phosphites, phosphate and phosphonates. In the *reactive* category, polymerizable compounds, such as aliphatic and aromatic phosphonates, phosphorus-nitrogen (P/N) containing and phosphate esters were used. The above list of compounds are ones where the phosphorus atom is in different chemical environments and different oxidation states (i.e. oxidation number III or V). In the present study it was also attempted to identify the variation in the flame retardation, if any, brought about by the differences in the chemical nature and/or oxidation state of the phosphorus atom, apart from the loadings, among the chosen additives/reactives. Furthermore, the relative predominance of the condensed- and gaseous-phase activities of the modifying groups in each case were investigated.

1.7 Passive protection coatings for ferrous metals

Another interesting fact about phosphorus-containing polymers is that they can mitigate, to some degree the effects of biofouling and corrosion occurring to various ferrous metals, when used as protective ingredients in formulations (Pospiech *et al.*, 2017; Pospiech *et al.*, 2013). The significance of these properties are mainly related to marine structures, both moving and stationary, where humidity, salinity and many other such potentially harsh environmental conditions are prevalent. These marine structures are mostly manufactured from different types of steel or iron alloys, and current practices/coatings are either inefficient, or have detrimental effects on the surrounding environment (Kepler, *et al.*, 2000; Kumar, *et al.*, 2006; Nanishi & Nakayama, 1990).

When in contact with fresh water from inland sources, or saline water from oceans or seas, structures made of concrete/steel tend to absorb the aqueous media over the course of their lifetime. Since concrete is microporous in nature, the permeation of gases and water is relatively unimpeded and often reaches the inner steel reinforcements. In addition, when the concentration of chloride ions present in seawater reaches a threshold value, it can initiate corrosion of the steel parts. These chloride ions also catalyse the corrosion mechanism, which can further accelerate the deterioration of steel structures, thus eventually leading to collapse of the entire system (Torres-Acosta & Martínez-Madrid, 2003; Val & Stewart, 2003).

The presence of atmospheric oxygen generally accelerates the electrochemical corrosion process in metallic structures that are above the water level and exposed to the natural environment (Figure 1.9). However, the effect of oxygen in driving corrosion to a higher degree is limited, and slows down, as the structures go deeper into seawater. The extent and degree of corrosion of the base substrate also depends on the pH, as well as the ionic conductivity of the electrolyte solution constituting the galvanic cell that underpins the essential electrochemical processes(s) driving the kinetically-controlled phenomena of corrosion. Generally speaking, chloride ion ingress is the predominant factor governing the corrosion mechanism of metals in contact with saline water (Bird, *et al.*, 2001).

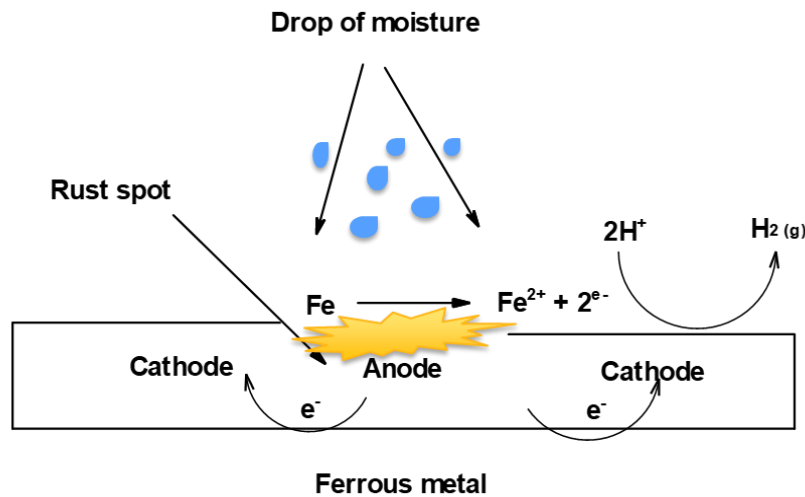


Figure 1.9 A schematic representation of the mechanism of corrosion reaction forming rust on ferrous metals

Some of the modified systems, produced in the present project, were also screened for their anti-corrosion properties. In addition, two relatively straightforward and faster

laboratory-scale techniques to phenomenologically follow the extent of corrosion in mild steel specimens under controlled conditions were successfully explored and demonstrated. Here, one of the techniques involved quantitative determination of Fe(III) in aqueous extracts, through ICP/OES, whereas the other method utilized an in-house proprietary software.

1.8 Overall aim of the project

The overarching aim of the present work was to develop passive fire protection strategies for some commercially important synthetic polymeric materials with a view to improving their overall performance, especially when used as structural components in the construction sector.

1.8.1 Individual objectives

In order to achieve the overall aim, the following individual objectives of the programme were identified, which are given below:

- Preparation of homopolymers of aniline, pyrrole and dopamine
- Syntheses and characterization of precursors, and phosphorus- and/or phosphorus- and nitrogen-containing monomers and additives (GC/MS, FT-IR and NMR)
- Syntheses of homo- and copolymers based on styrene and methyl methacrylate using standard radical reactions through solution, aqueous-slurry, suspension, emulsion and bulk polymerization techniques
- Elucidation of the structures and compositions of the recovered polymeric materials, primarily, through NMR spectroscopy
- Thermal and calorimetric characterization of the virgin and modified polymeric systems (step-growth and chain-growth polymers produced through bulk method) via standard means (TGA, DSC, PCFC and ‘bomb’ calorimetry)
- Identification of general trends, if present, amongst relevant empirical data, primarily through thermal and calorimetric techniques

- Identification of the elements of the mechanism(s) of fire retardance operating in the condensed- and vapour-phase (pyrolysis-GC/MS, solid-state NMR and ICP/OES)
- Evaluation of the corrosion resistance of the selected film-forming products and formulations

CHAPTER 2: MATERIALS AND METHODS

2.1 Materials

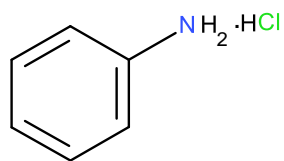
All the chemicals, reagents and solvents used in the present study were purchased from Aldrich Chemical Company, except the following: ammonium persulfate, sodium dodecylsulfate, tris-HCl buffer, calcium phosphate, aniline hydrochloride, 9,10-dihydro-9-oxa-10-phosphaphenanthrene 10-oxide (DOPO) and diethyl-1-propylphosphonate (Thermofisher Scientific); iron (III) chloride (Alfa Aesar). Generally, the solid compounds were used as received, whereas liquid reagents and solvents were, optionally, dried by keeping them over molecular sieves (4 Å). Furthermore, thermally labile initiators and monomers were stored under sub-ambient temperatures in a refrigerator, or in a freezer, as the case may be. The inhibitors (typically hindered phenolic compounds, such as hydroquinone monomethyl ether and *tert*-butyl catechol), were removed from the styrene and methacrylic monomers by passing through proprietary inhibitor removal columns, purchased from Aldrich Chemical Company, or through a column containing basic alumina, prior to use.

2.2 Methods

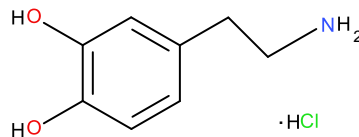
2.2.1 Synthesis of step-growth polymers

The homopolymers of pyrrole, aniline and dopamine were prepared by polymerization reactions facilitated through an oxidative route, adopted from the literature, i.e. by using an appropriate oxidizing agent, in aqueous media (Boeva & Sergeyev, 2014; Brezoi, 2010; Liebscher, *et al.*, 2013; Liu, *et al.*, 2014) (see Table 2.1). The exact procedure, including the mode of recovery of the expected product varied according to the specific monomer in question and the particular initiator that was used. Furthermore, the recovered yields were also different, especially relatively low for PDA and PPe. A typical procedure consisted of initially dissolving/dispersing the required amount of monomer in deionized water with stirring, followed by dropwise addition of the initiator. In the case of polymerizations involving aniline hydrochloride and dopamine hydrochloride, the reactions were carried out at ambient temperature, whereas for pyrrole a lower temperature was used (*ca.* 5°C). After the required reaction period, the formed solids were filtered through a quantitative filter paper, or optionally by centrifugation at 4000 rpm, and subsequently dried at *ca.* 70°C for at least 48 h before further examinations.

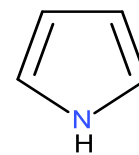
a. Monomers



Aniline hydrochloride

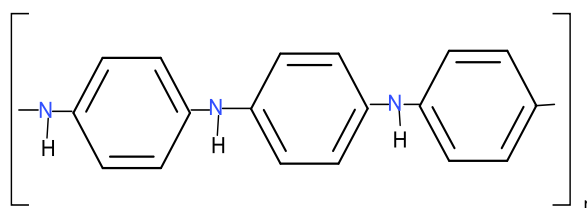


Dopamine hydrochloride

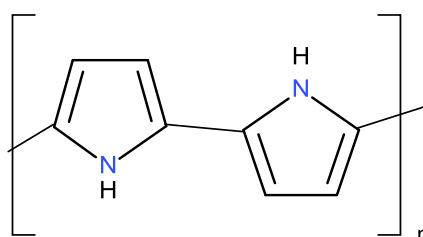


Pyrrole

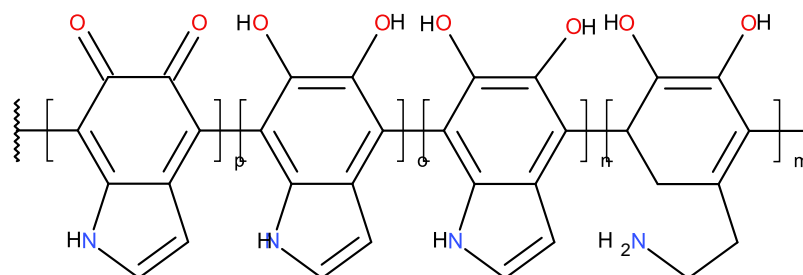
b. Polymers



Polyaniline



Polypyrrole



Polydopamine

Figure 2.1 A schematic representation of step-growth polymers (i.e. structures of the monomers and polymers)

Table 2.1 Preparative data for step-growth polymers

Sl. No.	Monomer (g or mL)	Solvent (DI water, mL)	Initiator (g or mL)	Time (h)	Yield (wt.%)
1	Aniline hydrochloride (2.59 g)	50	KMnO ₄ (1.57 g)	20	63
2	Dopamine hydrochloride (1.00 g)	90	Tris-HCl (10.0 mL, pH = 10)	20	11
3	Pyrrole (4.50 mL)	50	FeCl ₃ (1.00 g)	20	7.0

2.2.2 Procedures for coating the step-growth polymers

a. *In-situ* process

Mild steel substrates of dimensions 1 cm × 1 cm × 1 mm were cut from a larger piece. The substrates were then subjected to acid pickling by placing them in concentrated nitric acid for two days with a view to removing any unwanted oxide layers and other surface impurities. The acid-treated substrates were washed several times with acetone and deionized water, and then dried in an air oven at *ca.* 70°C for several hours prior to use. Homopolymerizations of the monomers were then performed in the presence of the mild steel specimens in an attempt to coat the formed polymer onto the surface of the specimen *in-situ*. The experiments were also repeated with PMMA segments (1 cm × 1 cm × 1 mm) instead of mild steel. It was found that the step-growth polymers did not form smooth and coherent coatings on both the substrates.

b. Hot powder process

Stainless steel substrates (1 cm × 1 cm × 1 mm) were first cleaned to remove any unwanted oxide layers, and other impurities on the surfaces *via* acid pickling, followed by washing a few times with acetone and deionized water. The purified substrates were then kept at *ca.* 70°C in a hot air oven for least 2 h before coating. As a trial run, *ca.* 1 g of polyaniline (PA) in finely powdered form was dispersed in 50 mL of methanol/water solution (1:1 by volume). This dispersion of PA in water/methanol mixture was then

poured directly onto the warm substrates uniformly, and left in the fume cupboard to facilitate the evaporation of the solvent from the specimens. The idea here was to facilitate the formation of a uniform coating of PA onto the stainless steel surfaces after the evaporation of the solvent. Again, the method failed to produce a uniform and cohesive layer of the polymers on the steel surface. This effectively demonstrated that condensation polymers did not exhibit enough adhesive forces with the surface of the substrates. In addition, it is to be assumed that the residual forces that were primarily responsible for facilitating the formation of a uniform and adherent coating onto the surface of the base material were feeble, if at all present.

2.3 Chain-growth polymers

Prior to the syntheses of polymers based on St and MMA, one of the additives that was not available commercially was synthesized. This compound was subsequently used as an additive for the PSt and PMMA polymers produced through the bulk technique.

2.3.1 Synthesis of the additive (diethylbenzylphosphonate)

The additive was synthesized using the *Michaelis-Arbuzov* reaction. The required amount of benzyl bromide (23.8 mL, 0.2 mol) was mixed with triethyl phosphite (34.3 mL, 0.2 mol), and the mixture was refluxed at 90°C for 8 h, followed by heating at 140°C for an extra 2 h. The reaction mixture was subsequently rotatory evaporated at an elevated temperature (*ca.* 90°C) until the unspent reactants were removed from the product. The product was used without further purification.

Yield = 45.5 g (0.19 mol; 95 mol% - i.e. near quantitative yield)

- ¹H NMR (600 MHz, CDCl₃): δ 7.27 (m, 5H, Ar), 3.98 (m, 4H, -P-O-CH₂-CH₃), 3.14 (d, 2H, -P-CH₂-Ar), 1.21 (t, 6H, -P-O-CH₂-CH₃)
- ³¹P NMR (243 MHz, CDCl₃): δ 26.41
- GC/MS: Retention time = 8.00 min; [M]⁺-137 = 91 (benzylic radical: corresponding to the most abundant species)

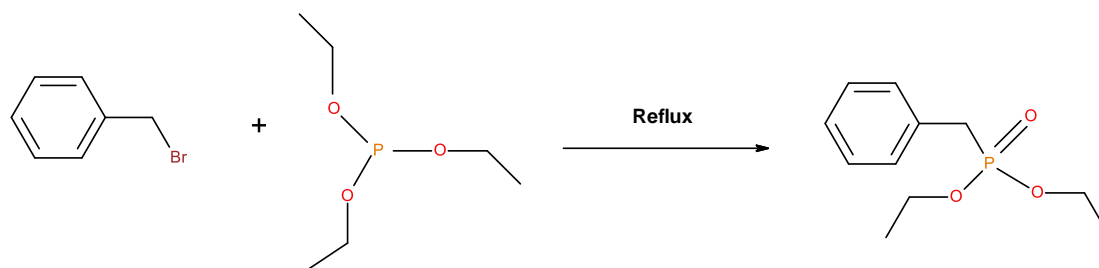


Figure 2.2 A schematic representation of the synthesis of diethylbenzylphosphonate

2.3.2 Synthesis of precursors to monomers

a. Synthesis of acryloyl chloride

Acryloyl chloride was prepared from acrylic acid and benzoyl chloride by a rapid distillation process (Stempel Jr, *et al.*, 1950). A 1:3 mixture of acrylic acid (50 mL, 0.73 mol) and benzoyl chloride (*ca.* 292 mL, 2.5 mol) were mixed and distilled rapidly in the presence of hydroquinone (*ca.* 1 g) in a 1 litre round-bottom flask fitted with a double-walled water condenser and a receiver. The fraction boiling at 60-70°C (*ca.* 20 mm Hg pressure) was collected. The final product in the liquid form was used for further syntheses without any purification.

Yield: (22g, 0.25 mol; 34 mol%)

Given the very reactive nature of the product, especially towards moisture, its authenticity was primarily inferred from the boiling point, and from careful comparison of the FT-IR spectra with a known sample that was commercially available.

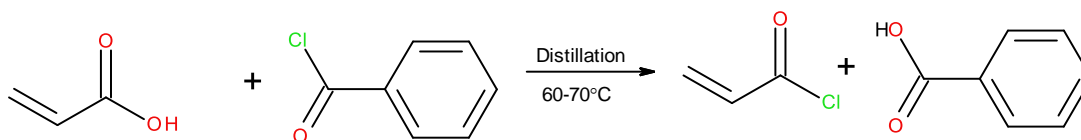


Figure 2.3 A schematic representation of the synthesis of acryloyl chloride

b. Synthesis of diethyl(1-hydroxyethyl)phosphonate (DEHEP)

In a typical procedure (Liepins, *et al.*, 1978), 30 mL (0.5 mol) of acetaldehyde, 32 mL (0.25 mol) of diethylphosphite and 40 mL of dichloromethane (DCM) were placed in a 250 mL round-bottom flask fitted with a double-walled water condenser and a bubbler. The contents of the flask were stirred, flushed with argon and cooled in an ice bath. About 1 mL of tetramethyl guanidine (TMG) was then added dropwise to the reaction mixture. An exotherm was observed, and the temperature of the reaction mixture was kept below 5°C by cooling with ice/water mixture. After the addition of TMG was complete, the reaction mixture was brought to room temperature and stirred for a further period of 2 h. The contents of the flask were washed with a single portion of saturated brine and the organic layer was separated and dried over sodium sulfate, filtered, and the volatiles were stripped by rotary evaporation to isolate DEHEP. This intermediate was used for the subsequent esterification reaction without further purification.

Yield: 35 g (0.2 mol; 80 mol%)

- ^1H NMR (600 MHz, CDCl_3): δ 4.99 (s, 1H, -OH), 4.11 (m, 4H, -P-CH₂-), 3.97 (m, 1H, -P-CH-), 1.38 (m, 3H, CH₃CH (OH)-), 1.28 (m, 6H, -CH₂-CH₃)
- ^{31}P NMR (243 MHz, CDCl_3): δ 26.30

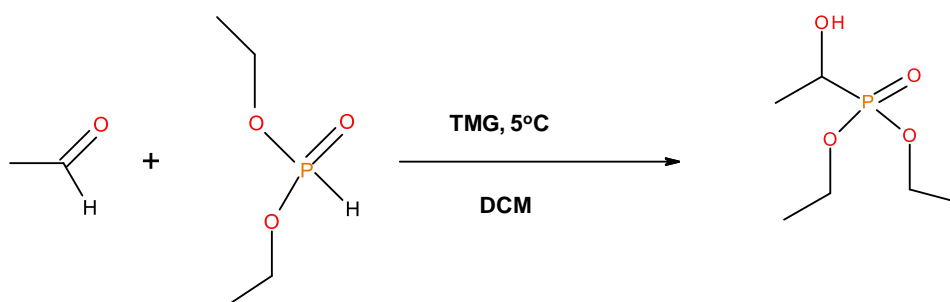


Figure 2.4 A schematic representation of the synthesis of diethyl(1-hydroxyethyl)phosphonate (DEHEP)

c. Synthesis of precursor to hydroxyphosphoramino ester

The synthetic procedure was adopted from a literature precedent (Ebdon, *et al.*, 2008), and is given below:

Triethylamine, TEA, (18 mL, 0.13 mol) and 2-(methylamino)ethanol, MAE (8 mL, 0.1 mol) were dissolved in 200 mL of dichloromethane (DCM) in a three-necked 500 mL round-bottom flask. Argon was purged through the mixture for about 30 min with stirring by placing it in an ice bath. Diethylchlorophosphate (DECP: 14.4 mL, 0.1 mol) was then added drop-wise to the reaction mixture under the argon atmosphere over a period of 1 h. A white precipitate of triethylamine hydrochloride was formed. After the addition of DECP, the reaction mixture was brought to room temperature and allowed to stir overnight. The resultant slurry was then rotary evaporated under reduced pressure to remove the solvent (DCM), which yielded a yellow oil containing a small amount of trimethylamine hydrochloride salt suspended in it. The oil was further dissolved in ethyl acetate (EtAc: 100 mL), filtered to remove any dissolved solids and finally rotary evaporated again under vacuum leaving a clear pale-yellow liquid, which was used as a precursor to make the final product without further purification.

Yield: 21 g (0.1 mol; ~100 mol%- i.e., near quantitative yield)

- ^1H NMR (600 MHz, CDCl_3): δ 3.99 (m, 4H, $-\text{CH}_2\text{OP}-$), δ 3.64 (t, 2H, $-\text{CH}_2\text{OH}$), 3.14 (m, 2H, $-\text{NCH}_2-$), 2.64 (d, 3H, $-\text{P-N-CH}_3$), 1.25 (t, 6H, $-\text{CH}_3\text{CH}_2\text{O}-$)
- ^{31}P NMR (243 MHz, CDCl_3): δ 11.70

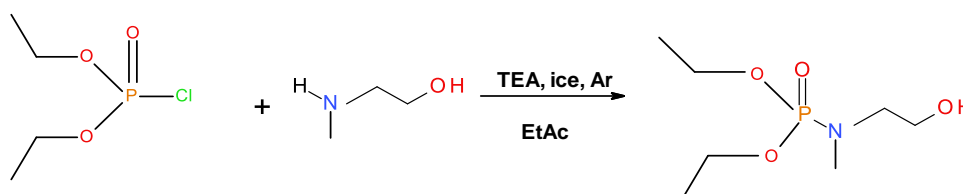


Figure 2.5 A schematic representation of the synthetic route to the precursor for hydroxyphosphoraminoester

2.3.3 Syntheses of monomers

a. Synthesis of diethyl-1-(acryloyloxyethyl) phosphonate (DE-1-AEP)

The required procedure was adopted from a literature precedent (Liepins, *et al.*, 1978). Here, a mixture of 18.2 g (0.1 mol) of DEHEP, 13.1 g (0.13 mol) of TEA and 200 mL of anhydrous DCM were stirred in a 500 mL round-bottom flask, under argon, in an ice bath for about 30 min. To this mixture, 10.02 g (0.1 mol) of acryloyl chloride was added dropwise under an argon blanket. After the complete addition of acryloyl chloride, the reaction mixture was brought to room temperature, and the reaction was allowed to proceed overnight. A white precipitate of trimethylamine hydrochloride was formed, which was then filtered. The remaining solution was washed with deionized water (4×50 mL), dried over anhydrous sodium sulfate, and concentrated in a rotary evaporator to yield a pale-yellow oil. This monomer was employed for the required polymerization reactions without further purifications.

Yield: 13 g (0.06 mol; 60 mol%)

- ^1H NMR (600 MHz, CDCl_3): δ 6.40 (d, 1H, vinyl), 6.10 (dd, 1H vinyl), 5.83 (d, 1H, vinyl), 5.28 (dq, 1H, $-\text{CHCH}_3$), 4.11 (m, 4H, $-\text{POCH}_2-$), 1.44 (dd, 3H, $-\text{CHCH}_3$), 1.26 (t, 6H, $-\text{P-O-CH}_2\text{CH}_3$)
- ^{31}P NMR (243 MHz, CDCl_3): δ 21.39
- GC/MS: Retention time = 5.7 min; $[\text{M}]^+-125 = 111$ (phosphonate species : corresponding to the most abundant species)
-

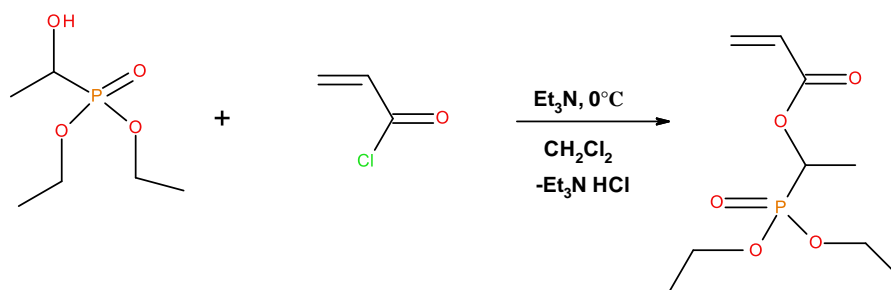


Figure 2.6 A schematic representation of the synthesis of diethyl-1-(acryloyloxyethyl) phosphonate (DE-1-AEP)

b. Synthesis of diethyl-*p*-vinylbenzyl phosphonate (DEpVBP)

Potassium *tert*-butoxide (11.22 g, 0.1 mol) was first dissolved in dry tetrahydrofuran (THF: *ca.* 50 mL). This was then added dropwise to a cold (*ca.* 5°C) mixture of diethyl phosphite (12.88 mL, 0.1 mol) and *p*-vinylbenzyl chloride (14.09 mL, 0.1 mol) in THF (*ca.* 30 mL) over a period of 1-2 h. After the addition, the reaction was then brought to room temperature and allowed to proceed for another hour. The resulting slurry was then filtered, diluted with diethyl ether (DEE, 200 mL) and washed with deionized water for 4 times (4 × 50 mL). The remaining organic layer was then dried over anhydrous sodium sulfate for around 2-3 h and concentrated *in vacuo* to yield a colourless, viscous oil. Yield: 20.4 g (mixture of the phosphonate and vinylbenzyl chloride, as shown by GC/MS).

Any unreacted vinylbenzyl chloride (as inferred from the GC/MS measurement) in the product was removed by a technique called silica ‘plug’ chromatography (Wyman, *et al.*, 2006). Typically in this method, 10 g of the crude product was mixed with 40 g of silica-60 gel in 100 mL of dichloromethane (DCM). This slurry was then rotary evaporated under vacuum to get a dry and intimate mixture of the crude product with silica gel. This mixture was loaded into a column and washed down quickly with petroleum ether (600 mL) to elute the unreacted vinylbenzyl chloride, followed by a further wash down of the mixture with 400 mL of ethyl acetate. Finally, the purified product was obtained by evaporating the ethyl acetate from the solution *in vacuo*.

Overall yield: *ca.* 7.0 g, (0.03 mol; 30 mol%)

- ^1H NMR (600 MHz, CDCl_3): δ 7.03 (dd, 2H, Ar-H), 7.92 (dd, 2H, Ar-H) 6.36 (dd, 1H, $\text{CH}=\text{C}$), 5.40 (d, 1H, $\text{C}=\text{CH}_2$), 4.90 (d, 1H, $\text{C}=\text{CH}_2$), 3.68 (dq, 4H, O- CH_2), 2.81 (d, 2H, $-\text{CH}_2\text{-P}$), 0.92 (t, 6H, $-\text{O}-\text{CH}_2\text{CH}_3$)
- ^{31}P NMR (243 MHz, CDCl_3): δ 26.56
- GC/MS: Retention time = 9.1 min; $[\text{M}]^{+}$ = 254

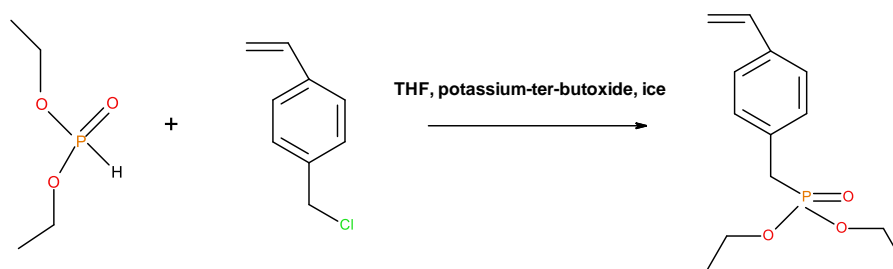


Figure 2.7 A schematic representation of the sSynthetic route to diethyl-p-vinylbenzyl phosphonate (DEpVBP)

c. Synthesis of diethyl-2-(acryloyloxy)ethyl phosphate (DEAEPa)

The synthetic procedure was adopted from the literature (Nair, *et al.*, 1988).

In a three-necked 500 mL round-bottomed flask, 2-hydroxyethyl acrylate, HEA (11.5 mL, 0.1 mol), TEA (20 mL, 0.14 mol) and 0.25 g of cuprous chloride were dissolved in anhydrous diethyl ether, DEE (100 mL) with stirring and under argon at *ca.* 0°C for 30 min. Diethyl chlorophosphate, DECP (14.5 mL, 0.1 mol) in 25 mL of DEE, was then added dropwise to the mixture over a period of one hour. The reaction mixture was brought to room temperature and the reaction was then allowed to proceed for another 48 h. A white precipitate of triethylamine hydrochloride salt was formed, which was then removed through filtration. The filtrate was washed with deionized water (4 × 50 mL) and dried over anhydrous sodium sulfate overnight. The resultant solution was then subjected to rotary evaporation to remove DEE, which resulted in a pale-yellow oil. This product was used without further purification.

Yield: 9 g (0.04 mol; 40 mol%)

- ^1H NMR (600 MHz, CDCl_3): δ 6.48 and 6.11 (m, 2H, $\text{CH}_2=\text{CH}$), 5.88 (dd, 1H, $\text{CH}_2=\text{CH}$), 4.40- 3.83 (m, 8H, $-\text{OCH}_2-$), 1.34 (t, 6H, $-\text{O}-\text{CH}_2-\text{CH}_3$)
- ^{31}P NMR (243 MHz, CDCl_3): δ 0.5
- GC/MS: Retention time = 7.8 min; $[\text{M}]^+-197 = 55$ (cleavage of carbonyl ester group)

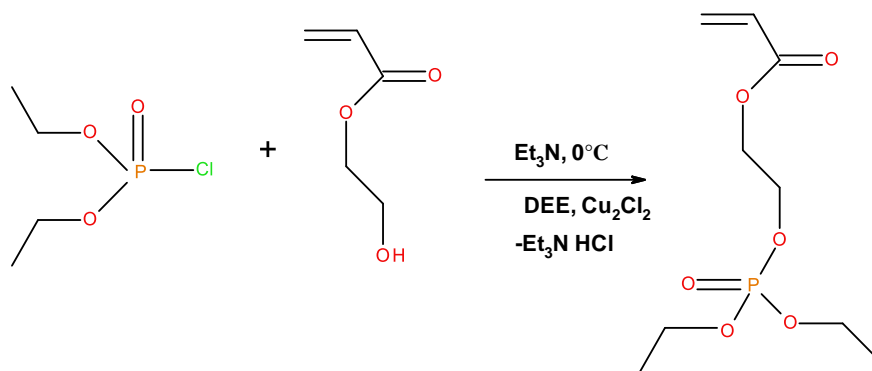


Figure 2.8 A schematic representation of the synthetic route to diethyl-2-(acryloyloxy)ethyl phosphate (DEAEPa)

d. Synthesis of acrylic acid-2-[(diethoxyphosphoryl) methyl amino] ethyl ester (ADEPMAE)

The required product was obtained through a previously published synthetic method (Ebdon, *et al.*, 2008). In a three-necked, 500 mL round-bottom flask, *ca.* 10.55 g (0.05 mol) of the hydroxyphosphonate precursor and 10.5 mL (0.07 mol) of TEA were dissolved in 125 mL ethyl acetate under an argon atmosphere. Acryloyl chloride (4.1 mL, 0.05 mol) dissolved in 50 mL of ethyl acetate was then added dropwise, slowly to the reaction mixture with stirring. A white precipitate of triethylamine hydrochloride was formed. The contents of the RB flask were then brought to room temperature and the reaction was allowed to proceed overnight under an argon blanket. The following day, the resulting mixture was concentrated by rotary evaporation to remove ethyl acetate to yield a pale-yellow oil with a white solid suspended in it. The solid was filtered using a Buchner funnel, and washed with EtAc (50 mL) to extract the oil. The EtAc was then removed in vacuum to leave a pale-yellow oil as the crude product. This product was used as obtained.

Yield: 12.2 g, (0.05 mol; ~100 mol% - i.e., near quantitative yield)

- $^1\text{H NMR}$ (600 MHz, CDCl_3): δ 6.38 [dd, 1H, $(-\text{O}_2\text{C})\text{CH}=\text{C}(\text{H})\underline{\text{H}}$], 6.06 [dd, 1H, $(-\text{O}_2\text{C})\text{CH}=\text{CH}_2$], 5.79 [dd, 1H, $(-\text{O}_2\text{C})\text{CH}=\text{C}(\underline{\text{H}})\text{H}$], 4.21 (t, 2H, $\text{CH}_2\text{CH}_2\text{O}-$), 3.95 (q, 4H, $\text{CH}_3\text{CH}_2\text{OP}-$), 3.28 [m, 2H, $\text{PN}(\text{CH}_3)\text{CH}_2\text{CH}_2\text{O}$], 2.65 (d, 3H, NCH_3), 1.24 (t, 6H, $\text{CH}_3\text{CH}_2\text{OP}-$)

- ^{31}P NMR (243 MHz, CDCl_3): δ 10.37.
- GC/MS: Retention time = 7.1 min; $[\text{M}+1]^{+} = 266$

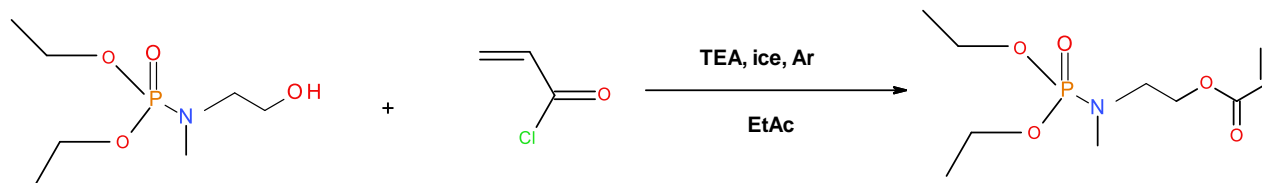


Figure 2.9 A schematic representation of the synthetic route to acrylic acid-2-(diethoxyphosphoryl) methyl amino ethyl ester (ADEPMAE)

2.3.4 Chain-growth polymerization techniques (homo- and co-polymers)

a. Syntheses of chain-growth polymers based on methyl methacrylate and styrene

A typical procedure for solution polymerization:

All solution polymerizations were carried out in toluene as the solvent. In a typical procedure, a solution of the monomer(s) in toluene was first stirred in a 250 mL three-necked, round-bottom flask fitted with a double-walled water condenser. Argon was then purged through this mixture at room temperature for 30 min to remove any dissolved air. The required amount of initiator (benzoyl peroxide: BPO) was then added slowly to the reaction mixture, and the polymerization was allowed to proceed at 60°C for *ca.* 7 h. The formed polymer was recovered by precipitating the reaction mixture to an excess of petroleum ether (boiling point $40\text{-}60^\circ\text{C}$) for MMA-based polymers, and methanol, or absolute alcohol, for styrene-based polymers, as the non-solvent. The precipitated polymeric product was collected using filtration through a G_4 sintered funnel and dried (at least for 24 h in a vacuum oven kept at *ca.* 60°C). The dried polymers were dissolved in dichloromethane and re-precipitated into the non-solvent, washed with several aliquots of the non-solvent, and dried again at 60°C for at least two days in a vacuum oven, before further examination.

Table 2.2 Preparative data for chain-growth solution polymerization reactions of PMMA-based polymers (feed ratio, 9:1)

Sl. No.	Monomer MMA (mL)	Co-monomer (g)	Solvent: toluene (mL)	Initiator, BPO (mg)	Recovered yield (wt.%)
1	15.0	---	15	70	47.5
2	12.0	DE-1-AEP, 2.95	20	80	4.30
3	12.0	ADEPMAE, 3.31	20	80	15.1
4	11.3	DEAEPa, 4.73	20	80	8.20
5	5.00	DEpVBP, 1.34	10	40	35.4

Table 2.3 Preparative data for chain-growth solution polymerization reactions of PSt-based polymers (feed ratio, 9:1)

Sl. No.	Monomer St (mL)	Co-monomer (g)	Solvent: toluene (mL)	Initiator BPO (mg)	Recovered yield (wt.%)
1	15.0	---	15	70	17.8
2	13.0	DE-1-AEP, 2.95	20	80	49.5
3	13.0	ADEPMAE, 3.31	20	80	48.2
4	13.0	DEAEPa, 3.15	20	80	8.20
5	5.40	DEpVBP, 1.34	10	40	62.0

A typical procedure for the preparation of polymers based on MMA and styrene by aqueous- slurry method:

A three-necked 250 mL round bottomed flask, containing 100 mL of deionized water, was fitted with a magnetic stirrer, a water condenser and a bubbler. This was stirred for *ca.* 30 min with argon bubbling through it. Then the required amount of monomer was added to this and further stirred under argon for about 10 min. Sodium metabisulfite (SMBS: 0.5

g) in 15 mL of deionized water was added to the reaction mixture, followed by ammonium persulfate (APS: 0.125 g in 15 mL of deionized water). The reaction mixture was brought to 40°C, and the polymerization was allowed to proceed for 16 h under a blanket of argon. The aqueous- slurry formed was filtered through a qualitative filter paper, and the polymer obtained was washed with deionized water several times, followed by methanol, to remove traces of unreacted monomer. The polymer was dried in a vacuum oven (*ca.* 60°C) for at least 72 h before further examination.

Table 2.4 Preparative data for aqueous-slurry polymerizations

Sl. No.	Monomer (mL)	Water (mL)	SMBS (g)	APS (g)	Recovered yield (wt.%)
1	MMA, 6.4	100	0.500	0.125	73
2	Styrene, 6.5	100	0.500	0.125	58

A typical procedure for suspension polymerization of styrene-based polymers:

This type of polymerization was carried out in an aqueous medium to obtain polymers in the form of fine beads. In the first step, argon gas was passed through an appropriate volume of deionized water in a round-bottom flask for about 30 min. Then, the required amount of dispersing agent, polyvinyl pyrrolidone (PVP) with calcium phosphate were added with stirring under a blanket of argon. The temperature was then raised to 80°C. After reaching the required temperature, a mixture of required amount of the initiator, benzoyl peroxide, in the monomer(s) was then added to the system. The mixture was stirred for 3 to 5 h under argon at 80°C. The final product was washed a couple of times with water followed by methanol. After purification, the formed polymer was kept in a vacuum oven for drying for 2-3 d at 40-50°C.

Table 2.5 Preparative data for suspension polymerization reactions of homo- and co-polymers of styrene in the 9:1 ratio

Sl. No.	Styrene (mL)	Co-monomer (g)	Water (mL)	PVP (g) /Ca ₃ (PO ₄) ₂ (g)	BPO (g)	Recovered yield (wt.%)
1	10.0	---	180	0.15/0.60	0.15	70.0
2	5.20	DE-1-AEP, 1.18	180	0.15/0.60	0.15	38.0
3	6.80	ADEPMAE, 1.76	180	0.15/0.60	0.15	38.0
4	10.3	DEAEPa, 2.52	180	0.15/0.60	0.15	59.0
5	11.4	DEpVBP, 2.82	180	0.15/0.60	0.15	53.0

Table 2.6 Preparative data for suspension polymerization reactions of co-polymers of styrene in the 8:2 ratio

Sl. No.	Styrene (mL)	Co-monomer (g)	Water (mL)	PVP (g) /Ca ₃ (PO ₄) ₂ (g)	BPO (g)	Recovered yield (wt.%)
1	6.10	DE-1-AEP, 3.15	180	0.15/0.60	0.15	69.0
2	4.60	ADEPMAE, 2.65	180	0.15/0.60	0.15	15.0
3	3.10	DEAEPa, 1.68	180	0.15/0.60	0.15	29.0
4	6.10	DEpVBP, 3.40	180	0.15/0.60	0.15	78.0

A typical procedure for emulsion polymerization of styrene and methyl methacrylate:

A typical procedure for the emulsion polymerization included the monomer and water in the 1:2 ratio. Initially, *ca.* 100 mL of deionized water and an appropriate amount of emulsifying agent (sodium dodecyl sulfate and potassium orthohydrogen phosphate) were taken in a round-bottom flask. Nitrogen was passed through this mixture for about 30 min, with stirring. The temperature was then increased to 70°C. After attaining the required temperature, the required amount of monomer was added dropwise to the mixture. Finally, the initiator, dissolved in about 2-3 mL of deionized water, was added to the system with vigorous stirring. The reaction was continued for 6 h at 70°C. The resulting solution was milky-white in colour with the appearance of a colloid.

Table 2.7 Preparative data for chain-growth emulsion polymerization reactions of St and MMA

Sl. No.	Monomer (mL)	Water (mL)	Emulsifying agents: SDS (g)/KH ₂ PO ₄ (mg)	APS (mg)	Solid content (mg/mL)	Remarks
1	MMA, 50	100	1.0 g/ 55 mg	125	161	white, colloidal liquid
2	St, 50	100	1.0 g/ 55 mg	125	245	white, colloidal liquid

A typical procedure for bulk polymerization:

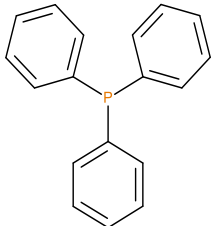
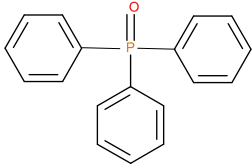
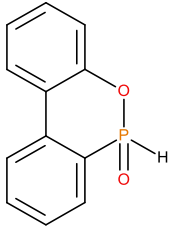
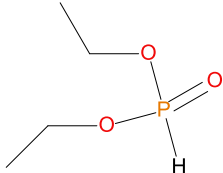
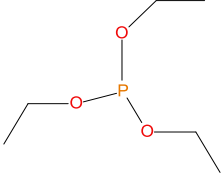
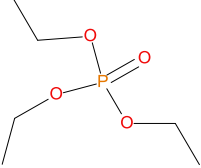
- *PMMA-based bulk polymers*

In this method, the required amount of monomer(s) and initiators were stirred thoroughly in a conical flask under a nitrogen atmosphere for *ca.* 1 h at 70-80°C, until a visible increase in the viscosity was observed. Subsequently, the required amount of the additive/reactive was added, and stirred for another 1 h, and the mixture was subsequently poured into an aluminium pan of *ca.* 50 mL volume and the pan stoppered with an aluminium lid. The pan was placed in an air oven preheated at 40°C and kept for curing for about 20 h. During the second stage of curing, the temperature of the oven was raised to 60°C for 8 h. Finally, after another 20 h of curing at 80°C, the pan was cooled to room temperature. The final solid plaque, in the shape of the aluminium pan, was extracted from the pan. In the present study, a fixed phosphorus loading of 2 wt.% was used in case of each of the additive/reactive.

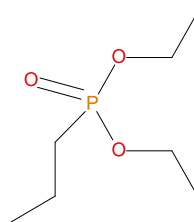
- *PSt-based bulk polymers*

The required amount of monomer(s) and initiators were stirred thoroughly in a conical flask under a nitrogen atmosphere for *ca.* 5 h at 70°C, until a visible increase in the viscosity was observed. The required amount of the additive/reactive was then added, and stirred for another 1 h, and the mixture was subsequently poured into an aluminium pan of *ca.* 50 mL volume and the pan stoppered with an aluminium lid. The pan was placed in an air oven preheated at 40°C and kept for curing for about 20 h. In the second stage of curing, the temperature of the oven was raised to 60°C for 8 h. After another 20 h of curing at 80°C, the pan was allowed to cure again for a period of 3 h at 100°C before being cooled to room temperature. The final plaque was then extracted from the aluminium pan. Again, a fixed phosphorus loading of 2 wt.% was used.

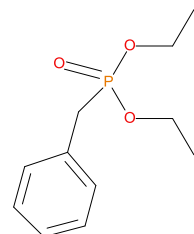
Table 2.8 Various additives and reactives used for the bulk polymerization of styrene and MMA

Sl. No.	Additive/reactive	Structure
1.	Triphenylphosphine (TPP), <i>additive</i>	
2.	Triphenylphosphineoxide (TPPO), <i>additive</i>	
3.	9,10-Dihydro-9-oxa-10-phosphaphenanthrene-10-oxide (DOPO), <i>additive</i>	
4.	Diethylphosphite (DEHPi), <i>additive</i>	
5.	Triethylphosphite (TEPi), <i>additive</i>	
6.	Triethylphosphate (TEPa), <i>additive</i>	

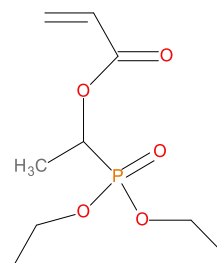
7. Diethylpropylphosphonate (DEPP), *additive*



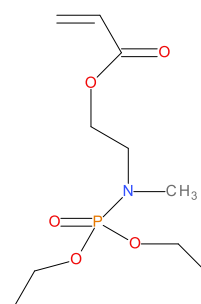
8. Benzylphosphonate (DEBP), *additive*



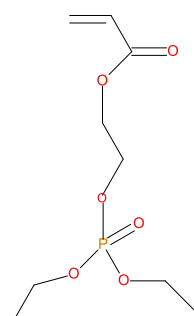
9. Acrylic phosphonate (DE-1-AEP), *reactive*



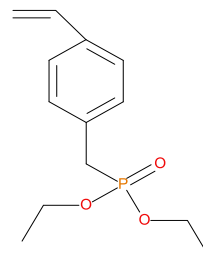
10. P/N (ADEPMAE), *reactive*



11. Acrylic phosphate (DEAEPa), *reactive*



12. Vinylbenzylphosphonate (DEpVBP),
reactive



The following steps were used to calculate the amounts of additives/reactives in each case for a P-loading of 2 wt.%, for instance, in the case of MMA. Essentially, the same steps were used in the case of styrene.

Let the weight fraction of the additive be x , and that of the main monomer (methyl methacrylate, MMA) be $(1 - x)$.

The algebraic equation for calculating the weight percentage of phosphorus in an additive/reactive is:

$$\text{Weight \% of P} = 31 \times 100 \times x' / [100 \times (1 - x') + MWa \times x']$$

where 31 is the atomic mass of phosphorus, 100 is the molecular weight of MMA, x' is the mole fraction of the additive and MWa is the molecular weight of the additive/reactive.

Here, the weight percentage of phosphorus required for the syntheses of the bulk samples, in each case, is fixed as 2%. Therefore, the equation can be re-written as:

$$2 = 31 \times 100 \times x' / [100 \times (1 - x') + MWa \times x']$$

The value of x' can be found from the above equation.

Weight fraction of the additive/reactive required is calculated by substituting the value of x' (obtained above) in the following equation:

$$x = MWa \times x' / [100 \times (1 - x') + MWa \times x']$$

Therefore, for 50 g of reagents, the amounts required can be calculated as:

$$MMA = 50 \times (1 - x) \quad \text{and}$$

$$\text{Additive/reactive} = 50 \times x$$

In the following tables (Tables 2.9 and 2.10), the respective masses of the additives/reactives for MMA and St, calculated using an Excel spreadsheet are given:

Table 2.9 Details of the preparative data for MMA-based bulk polymers

Sl. No.	MMA (mL)	Additive/reactive	Formula weight	Additive/reactive weight (g/mL)	BPO/dicumyl peroxide (mg)
1	40.00	---	---	--	40.0/20.0
2	44.20	TPP	262	8.46 g	54.0/27.0
3	43.65	TPPO	278	8.97 g	53.0/26.5
4	45.80	DOPO	216	6.97 g	53.0/26.5
5	48.46	Diethylphosphite	138	4.15 mL	52.0/26.0
6	47.50	Triethylphosphite	166	5.50 mL	53.0/26.5
7	46.95	Triethylphosphate	182	5.48 mL	53.0/26.5
8	37.61	Diethylpropylphosphonate	180	4.65 g	43.0/21.5
9	36.29	Diethylbenzylphosphonate	228	5.88 g	44.0/22.0
10	22.50	DE-1-AEP monomer	236	3.81 g	26.0/13.0
11	22.05	ADEPMAE monomer	265	4.27 g	26.0/13.0
12	22.30	DEAEPa monomer	252	4.06 g	26.0/13.0
13	22.24	DepVBP monomer	254	4.10 g	26.0/13.0

Table 2.10 Details of the preparative data for St-based bulk polymer

Sl. No.	Styrene (mL)	Additive/reactive	Formula weight	Additive/reactive weight (g/mL)	BPO/dicumyl peroxide (mg)
1	50.00	---	---	---	50.0/25.0
2	36.57	TPP	262	6.76 g	44.0/22.0
3	36.10	TPPO	278	7.17 g	43.0/21.5
4	37.90	DOPO	216	5.57 g	43.0/21.5
5	40.09	Diethylphosphite	138	3.56 mL	44.0/22.0
6	39.29	Triethylphosphite	166	4.42 mL	44.0/22.0
7	38.84	Triethylphosphate	182	4.40 mL	44.0/22.0
8	39.00	Diethylpropylphosphonate	180	4.65 g	44.0/22.0
9	37.53	Diethylbenzylphosphonate,	228	5.88 g	44.0/22.0
10	23.32	DE-1-AEP monomer	236	3.81 g	26.0/13.0
11	23.00	ADPMAE monomer	265	4.27 g	26.0/13.0
12	23.00	DEAEPa monomer	252	4.07 g	26.0/13.0
13	23.00	DEpVBP monomer	254	4.10 g	26.0/13.0

2.3.5 Preparation of test solutions for determination of P and Fe(III) contents

The char residues for P-analysis were obtained by subjecting the PMMA- and PSt-based bulk polymers to forced flaming combustion. In order to obtain enough char residues, smaller pieces of the polymeric materials, produced through the bulk polymerization route, were taken in a porcelain crucible. These pieces were made to undergo flaming combustion using a butane torch. It is relevant to note here that the application of the pilot greatly varied in each case, which in turn dependant on the combustibility of the material in question. These samples were first accurately weighed (*ca.* 10-15 mg, in triplicate), and were digested by boiling with a mixture of 3 mL of AR conc. HNO₃ and 2 mL of AR conc. HClO₄ in 50 mL beakers. Upon digestion of the contents, the resulting solutions were quantitatively transferred to a 25 mL volumetric flask and the solution were made

up to the mark with deionized water. In the case of incomplete digestion, as inferred from the presence of residues, the contents were first filtered using a qualitative filter paper before making up to the required volume. The prepared solutions were transferred to 15 mL sample tubes before being introduced into the ICP/OES instrument (Shimadzu ICPE-9000). Measurements on each of the samples were repeated three times, and the corresponding average value is reported in each case. Quantitative assessments of the phosphorus content in the samples were deduced by constructing a calibration plot, with a standard solution of KH_2PO_4 , in accordance with Beer-Lambert law (Figure 2.10).

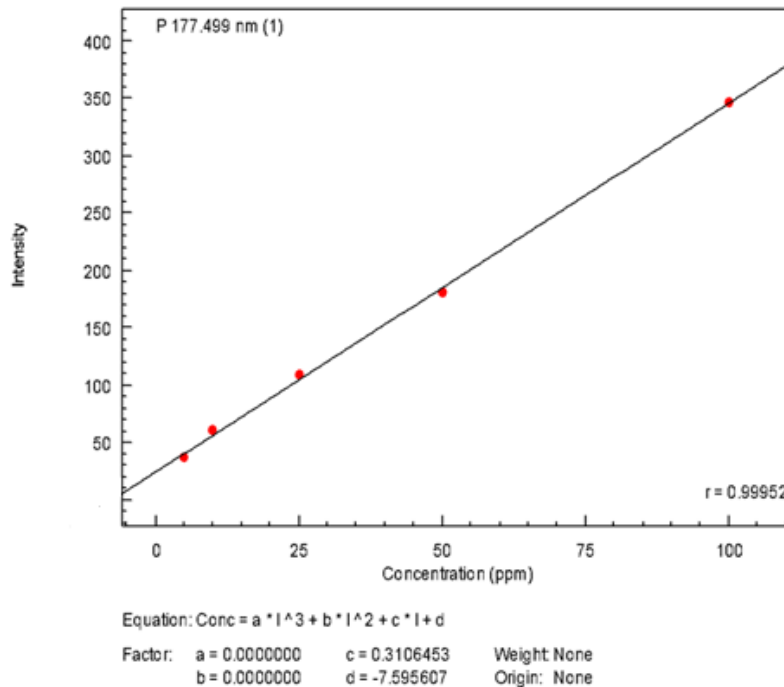


Figure 2.10 Calibration curve (Beer-Lambert plot) for phosphorus

Corrosion studies of mild iron/mild steel specimens

Fe(III) contents of aqueous solutions can be measured using ICP/OES (Malel & Shalev, 2013). In the present work, this method was explored for measuring the degree of corrosion of iron nails where the test specimens were dipped in different aqueous media (i.e. in deionized and seawater). After specified periods, samples were taken out of the test solutions, washed with DI water, and the particulate matter (indicating corrosion) was

digested by boiling it with 5 mL of AR conc. HNO₃. Once the digestion was affected, the clear solution was cooled to room temperature and was made up to a specified volume in a volumetric flask. The Fe(III) content of each of the solutions was then quantified using ICP/OES. Here, the Beer-Lambert plot was constructed for calculating the Fe(III) content in each case using a standard aqueous solution of Fe(III) (see in Figure 2.11).

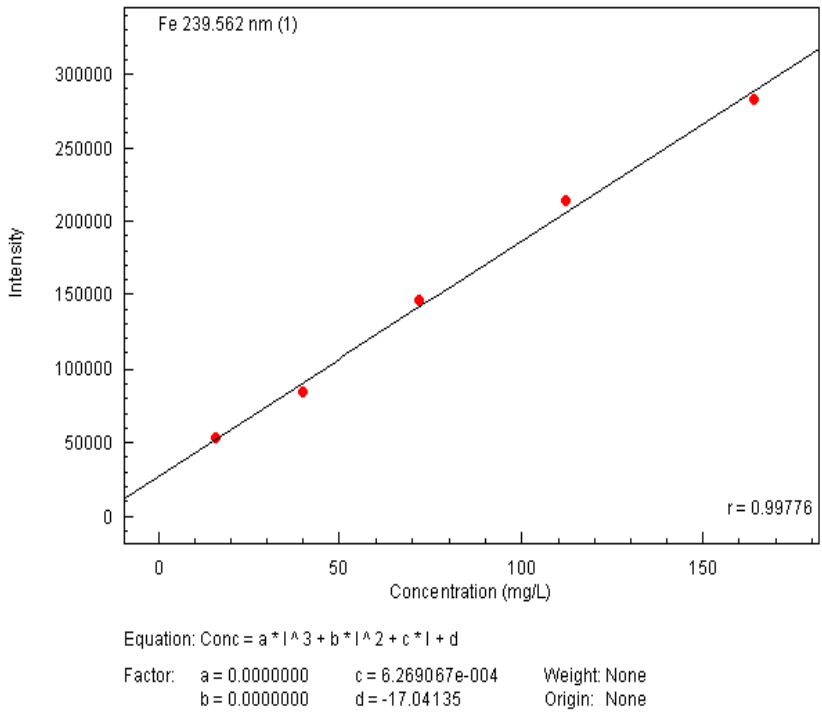


Figure 2.11 Calibration curves (Beer-Lambert plot) for Fe(III)

Plots of Fe(III) content versus time (in hours, or days) in the case of iron nails dipped in sea water were constructed and are given in Figures 2.12 and 2.13.

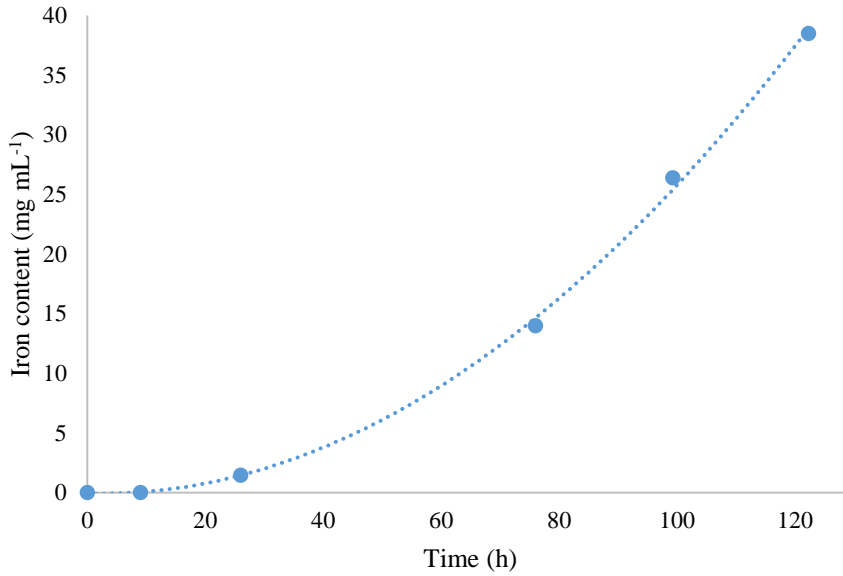


Figure 2.12 Plot showing an increase in the degree of corrosion of the first set of test samples (iron nails) kept in sea water at specified intervals of time as revealed by the corresponding increases in the concentrations of Fe(III) ions

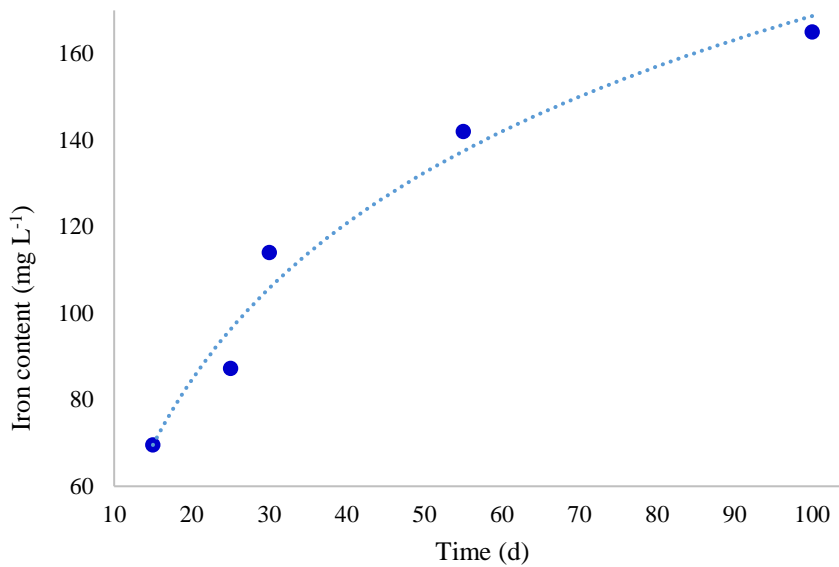


Figure 2.13 Plot showing an increase in the extent of corrosion of the second set of iron samples (nails) in sea water at specified intervals of time as revealed by the corresponding increases in the concentrations of Fe (III) ions

As can be seen from the above figures, the concentration of the Fe(III) species increased with time (after an induction period). Thus the present work demonstrated a laboratory-

scale, quick and easy methodology that can be used to measure the rate of corrosion utilizing the ICP/OES technique. The data obtained can then be plotted against time to analyse the rate of release of iron over a certain period of time, thus aiding in understanding the phenomenological evolution of the extent of corrosion of the samples in various aqueous media.

As a variation to the above procedure, we subsequently prepared various uncoated and coated mild steel substrates (thin segments: 1 cm × 1 cm × 1 mm). For the purpose of coating, two of the modified PMMA polymers with phosphorus-containing reactives were chosen (DE-1-AEP, or DEAEPA). Initially, the cleaned metallic specimens were kept immersed in solutions of the above polymers in DCM, and were subsequently allowed to dry in a fume cupboard until a coherent layer of the material onto the substrate was obtained. The coated substrates were then immersed in deionized, or sea water, for specific periods of time. After these intervals the samples were retrieved, and the resultant solutions were subjected to Fe(III), and optionally phosphorus analyses, using the ICP/OES technique (see in Tables 2.11 and 2.12 below for the preparative data).

In table shown below, the masses of various uncoated mild steel substrates, before immersing in the aqueous media (initial mass) and after immersing for specified time durations (final mass) are given.

Table 2.11 Preparative data of uncoated (US) mild steel substrates immersed in deionized (DIW) and sea water (SW) to different time intervals (days)

Sl. No.	Sample	Medium	Initial mass (g)	Time (d)	Final mass (g)
1	US 1	DIW	1.0743	8.0	1.0735
2	US 2	DIW	1.2261	15	1.2243
3	US 3	DIW	1.0875	22	1.0855
4	US 1	SW	1.1520	8.0	1.1513
5	US 2	SW	0.9916	15	0.9892
6	US 3	SW	1.0471	22	1.0440

Similarly, the table below shows the masses of coated mild steel substrates before immersion in aqueous media (initial mass) and after immersing for 22 days (final mass) are shown.

Table 2.12 Preparative data of coated mild steel substrates immersed in deionized (DIW) and sea water (SW) to different time intervals (22 days)

Sl. No.	Coating formulation	Medium	Initial mass (g)	Final mass (g)
1	PMMA	DIW	1.1879	1.1844
2	PMMA	SW	1.2716	1.2692
3	MMA+DE-1-AEP	DIW	1.2369	1.2116
4	MMA+DE-1-AEP	SW	1.0819	1.0600
5	MMA+ DEAEpa	DIW	1.2995	*---
6	MMA+ DEAEpa	SW	1.3072	*---

*here masses were not be ascertained accurately as the samples could not be effectively retrieved from the glass vials

2.4 Analytical instrumentation and techniques

2.4.1 Inductively-Coupled Plasma Optical Emission Spectroscopy (ICP/OES)

This is a multi-elemental analysis technique, generally used to identify the presence of various elements in a compound. It can be used for quantitative as well as qualitative measurements. Here, diluted sample solutions are introduced into the core of inductively coupled argon plasma which operates at a temperature of approximately 8000°C. At this temperature, all elements become thermally excited and emit light at their characteristic wavelengths upon relaxation to their ground states. This light is collected in the spectrometer and is passed through a diffraction grating that serves to resolve the light into a spectrum of its constituent wavelengths. Within the spectrometer, the diffracted light is then collected according to the wavelength and the signal amplified to yield an intensity measurement that is proportional to the elemental concentrations.

In the present work (see section 2.3.5 above), ICP/OES was employed to determine the rate of corrosion of nails/mild steel samples by plotting the iron content *versus* time (in

hours) for each sample set. The concentration for Fe(III) was then obtained from the Beer-Lambert plot constructed by employing a standard ferric salt solution (Olesik, 1991). Essentially the same procedure was used to estimate the phosphorus contents of the digested char residues (as phosphates in the aqueous phase).

2.4.2 Morphological and structural analyses of the materials

a. Fourier-Transform Infrared (FT-IR) Spectroscopy

Infrared spectroscopy is a standard technique frequently used to identify the important functional groups present in a sample. This technique can be used to obtain both quantitative as well as qualitative information regarding the chemical nature of the sample. For the present study, a Perkin-Elmer 1600 model instrument was used, in which infrared radiation in the range 4000 to 600 cm^{-1} is absorbed by the test sample in the attenuated total reflectance (ATR) mode. For both liquid and solid samples, a few milligrams were used as neat, and were mounted onto the diamond crystal stage. The spectrum of absorbance *versus* wavenumber is generated for each of the samples, after appropriate baseline correction for each run (number of scans: 32; resolution: 4 cm^{-1}), aiding in identifying various functional groups present within their structure (Nikolic, 2007). In the present project, the FT-IR spectroscopy was employed for a variety of purposes, such as: checking the authenticity/structural features of starting materials, intermediates and products, and in the latter case this included polymeric products; for identification of residual monomer(s), if present, in the polymers produced through the bulk method; analyses of partially burned polymeric samples; etc.

b. Nuclear Magnetic Resonance (NMR) Spectroscopy

With a view to obtaining the purity and structure of the additives, precursors, monomers and polymeric materials, a Bruker 600 MHz instrument was employed, and the spectra were run in deuterated solvents (CDCl_3 , or d_6 -DMSO) at ambient probe conditions. The solid-state NMR (^{31}P , and optionally ^{13}C , with CP/MAS mode) spectra of the polymer/char residues was obtained using a 500 MHz Bruker Avance III spectrometer working at ambient probe conditions. A 4 mm H/F-X double resonance probe was used

to record ^{13}C and ^{31}P NMR spectra, typically at 10 kHz rotor speed, and the signals were calibrated against phosphoric acid as the external calibrant. In both cases, the raw data were processed by using a proprietary software from the manufacturer (TopSpin 4.0.8).

c. Gas Chromatography/Mass Spectrometry (GC/MS)

For the GC/MS runs, a GCMS-QP2010 instrument equipped with a capillary column with specifications as follows was used: ZB-5MS; length: 30 m; thickness: 0.5 μm ; diameter: 0.25 mm. The column oven temperature was set at 45°C and the injection temperature was set at 250°C. The carrier gas pressure was maintained at 86.6 kPa, with a column flow rate of 1.5 mL min^{-1} where the total flow was set at 154.4 mL min^{-1} . The GC was coupled to the mass spectrometer which utilized electron impact ionization. The associated operating parameters of the MS were as follows: ion source temperature: 250°C, interface temperature: 300°C; solvent cut time: 3 min; GC program time: 12.2 min).

d. Pyrolysis-GC/MS

Pyrolysis-GC/MS was performed with the pyrolysator Pyroprobe 5000 (CDS Analytical, Inc., Oxford, PA, USA) with a platinum filament coupled with a gas chromatograph GC7890A (Agilent Technologies, Santa Clara, CA, USA) with GC column HP-5MS (non-polar, length: 30 m; inner diameter: 250 μm ; layer thickness: 0.25 μm , Agilent Technologies, Santa Clara, CA, USA). The carrier gas was helium with a gas flow rate of 1 mL min^{-1} . The GC was equipped with a mass-selective detector (MSD 5975C inert XL EI/CI, Agilent Technologies, Santa Clara, CA, USA) with a mass scan range between 15-550 m/z and EI at 70 eV. The samples were pyrolyzed at the temperatures of maximum mass losses found in TGA. The inlet temperature of the GC was variable, the oven temperature program was fixed (2 min at 50°C; heating with 12°C min^{-1} to 280°C).

2.4.3 Thermal and calorimetric analysis

a. Thermogravimetry (TGA)

This technique is used to study the thermal behaviour of materials, especially the decomposition behaviour that is generally monitored in terms of mass loss (wt.%) over a set range of temperature. It can also provide information of the ‘non-combustible’ char residues obtained upon decomposition. In this technique, a sample is subjected to a pre-set heating regime under a controlled atmosphere (such as air, or nitrogen, or oxygen). The TGA runs on the polymeric products were run, in a nitrogen atmosphere, at $10^{\circ}\text{C min}^{-1}$ and $60^{\circ}\text{C min}^{-1}$, from 30 to 900°C , using a Mettler-Toledo instrument with a gas flow rate of 50 mL min^{-1} . The runs were done in triplicate, and it was found to be highly reproducible in that the associated thermograms were found to be perfectly overlapped on each other. The set heating rate of $60^{\circ}\text{C min}^{-1}$ was chosen with a view to comparing and correlating the results from the TGA experiments to those of other calorimetric techniques, such as the pyrolysis combustion flow calorimetry (PCFC) technique (Prime, *et al.*, 2009) .

b. Differential Scanning Calorimetry (DSC)

In this thermal analysis technique, the heat capacity of a sample is measured over a temperature range as the heat flow to the system changes according to the controlled temperature program. Important transitions such as melting, glass transition, crystalline phase transition, curing, etc. can be identified with much ease and speed (Menczel, *et al.*, 2009). In the present study, DSC runs were primarily used to estimate the heats of pyrolysis of the various polymeric materials. For this purpose, the thermograms were recorded in a nitrogen atmosphere, at a heating rate of $10^{\circ}\text{C min}^{-1}$, from 30 to 550°C , using a Mettler-Toledo instrument. The reproducibility of the DSC tests were optionally checked, and found to be quite acceptable.

c. Pyrolysis Combustion Flow Calorimetry (PCFC)

This technique, also known as ‘microscale combustion calorimetry’ (MCC), is a small-scale calorimetric testing method used to analyse the fire behaviour of various solid materials when subjected to a forced non-flaming combustion, under anaerobic, or aerobic, conditions (ASTM D7309). The seminal work behind this technique was carried

out at the Federal Aviation Administration in USA in the late 1990's. This method is assumed to reproduce and decipher the condensed and gaseous parts of flaming combustion, in a non-flaming test regime, through a rapid and controlled pyrolysis of the sample in an inert atmosphere (i.e. in nitrogen) followed by high-temperature oxidation (i.e. combustion) of the pyrolyzate components in the presence of oxygen. The main advantage of using PCFC is that only a very small quantity (mg) of a sample is required, and the test method often provides information regarding useful combustion parameters of the test sample, such as, peak heat release rate (pHRR), temperature to pHRR, total heat released (THR), heat release capacity (HRC), effective heat of combustion (EHC/ h_c) and percentage of char yield. Although PCFC is able to provide some of the useful data regarding heat-related parameters in the smaller scale, correlation of the available data with real fire scenarios is still limited. In the present work, PCFC runs were carried out in some chosen substrates (mainly step-growth polymers) at 1°C min^{-1} , using an FTT microscale calorimeter using method A- i.e., in an atmosphere of nitrogen. (Lyon & Walters, 2004; Cogen, *et al.*, 2009; Sonnier, *et al.*, 2012).

d. 'Bomb' Calorimetry

'Bomb' calorimetry measurements were performed on an IKA C200 instrument (IKA, Oxford, UK). Pelleted samples, weighing *ca.* 0.5 g, were placed inside a 'bomb' cell. The 'bomb' was filled with pure oxygen up to 30 bar, and the sample was subsequently ignited. The instrument was periodically calibrated using recrystallized benzoic acid. The final calorific values were displayed by the instrument using built-in software. For each sample, triplicate runs were performed.

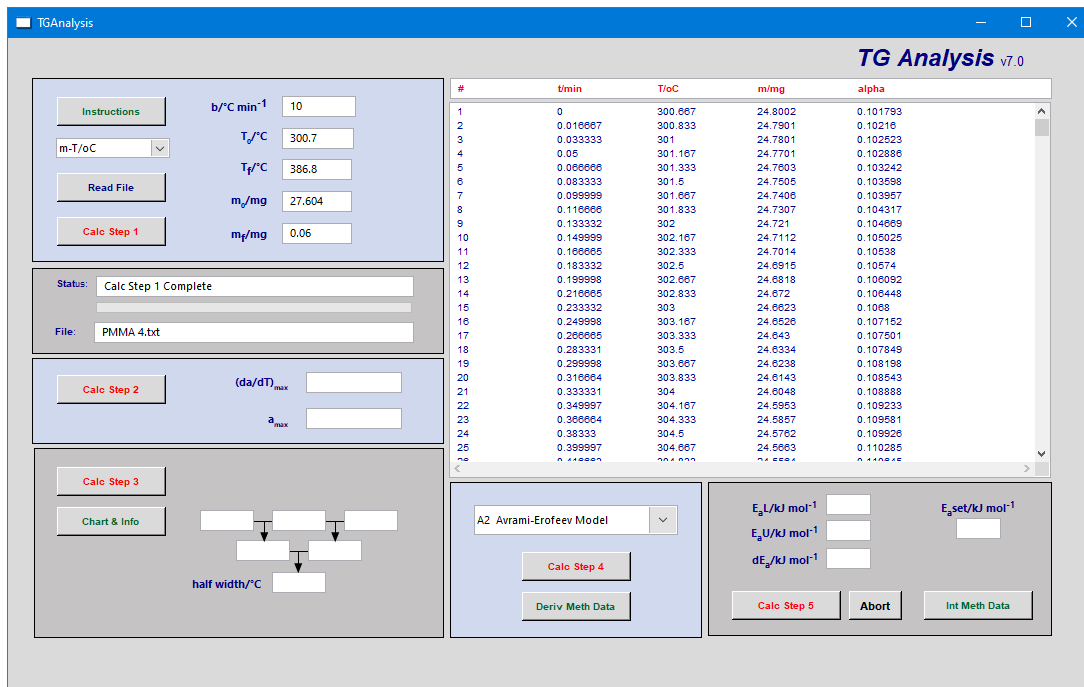
2.4.4 Software used for data analyses and imaging

2.4.4.1 Software for Thermogravimetric Analyses (TGA)

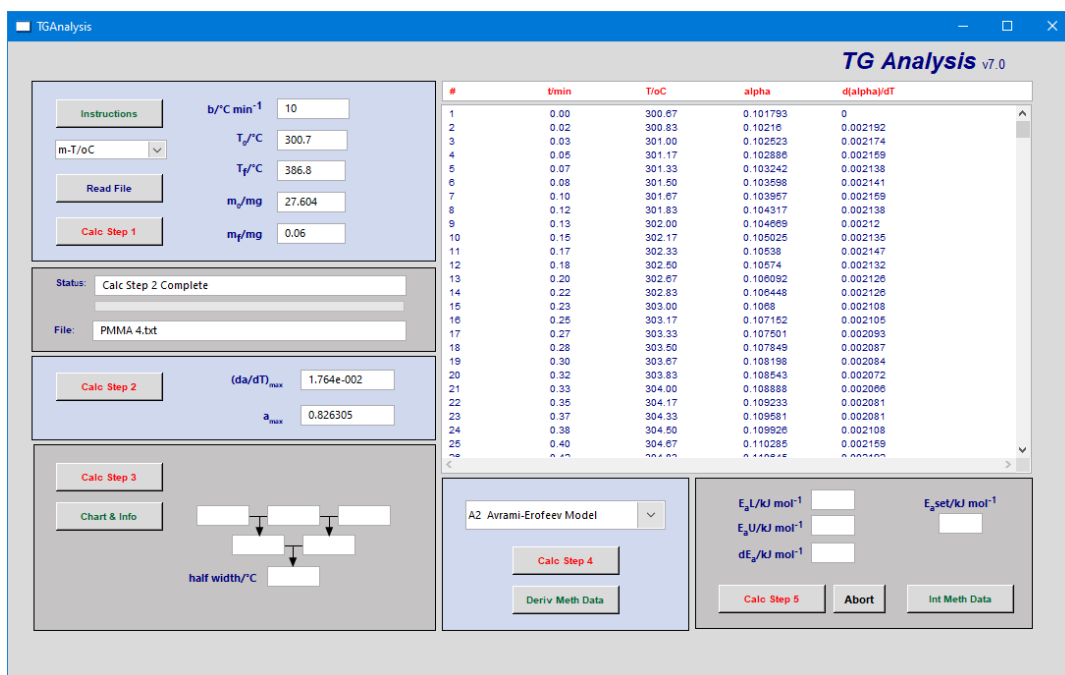
This method was based on an algorithm and its accompanying software reported in the literature (Bigger, *et al.*, 2015; Bigger, *et al.*, 2015). In this approach, one of the non-isothermal thermograms is chosen. In the present study, in all cases, the thermograms obtained at a relatively low heating rate of $10^\circ\text{C min}^{-1}$ were chosen as this is expected to capture most of the underlying steps in the thermal degradative pathway of the substrate

in question. As the first step, the data comprising the thermogram were transferred into an Excel file for subsequent processing, which primarily involved identifying the main step of decomposition. The following procedure was adopted and is illustrated here for the sample PMMA obtained through bulk polymerization, as an example.

1. The initial mass of the sample is taken as m_i and final mass as m_f , and they are first identified from the TGA plot. The average values of the regions where the mass does not change significantly are chosen.
2. Next, the corresponding degree of conversion, α , is calculated using $\alpha = (m_i - m_t)/(m_i - m_f)$, m_t is the mass at a particular time, t . The range of α values chosen should be as large as possible but should also avoid those values of α that are close to 0 and 1 where the uncertainties are too high.
3. The values of T and the masses in the range of α values selected are copied into a new excel workbook and the file is saved in tab delimited text (.txt) format.
4. This file is then opened in the software using the *Read File* button and the desired input file (e.g. m-T/°C) and the required heating rate is set as required (10°C). When the data are successfully loaded a message appears in its status field with the name of the input file in the 'File' field.
5. The values of m_i and m_f calculated in 1 is to be entered in the appropriate fields
6. Click the Calc Step 1 button to perform the initial calculations.

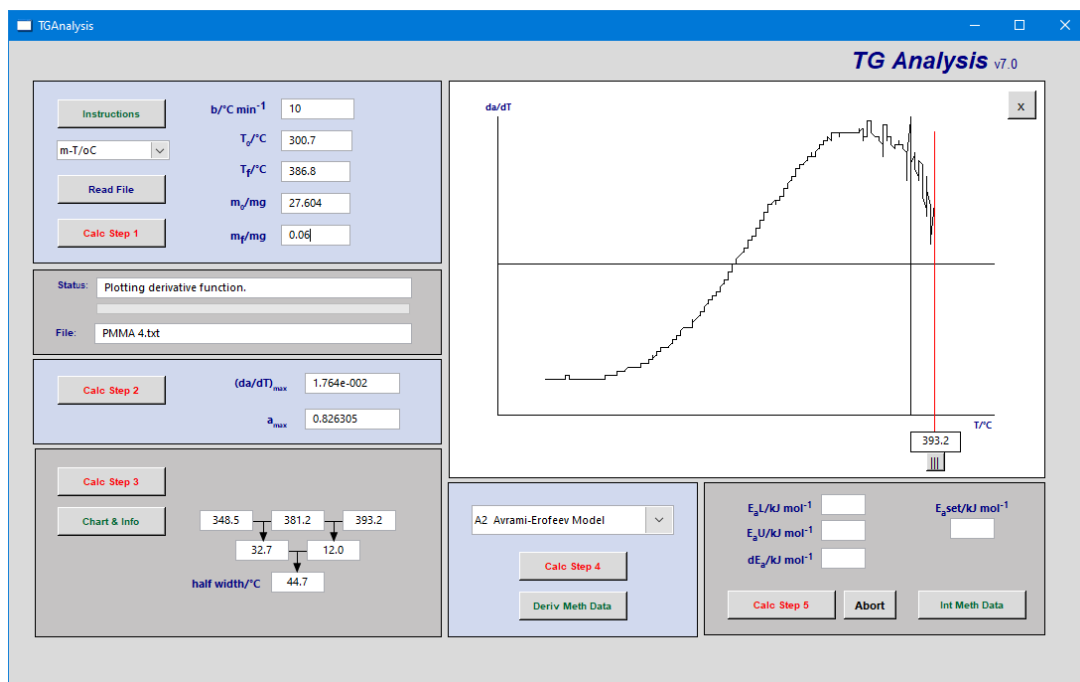


7. Next, click the Calc Sep 2 button which will calculate the $(da/dT)_{\max}$ and α_{\max} values.

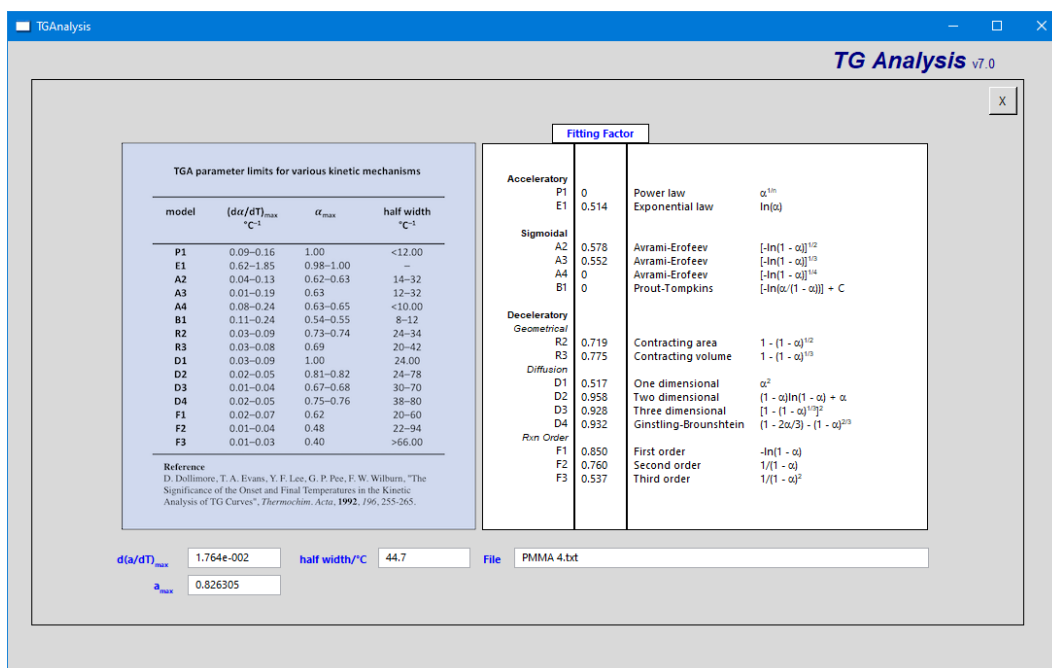


8. Click Calc Step 3 button, which will produce the da/dT versus $T/^\circ\text{C}$ along with a horizontal line (half-height line) whose vertical axis intercept is half of the maximum da/dT values. The cursor which appears can be moved along the

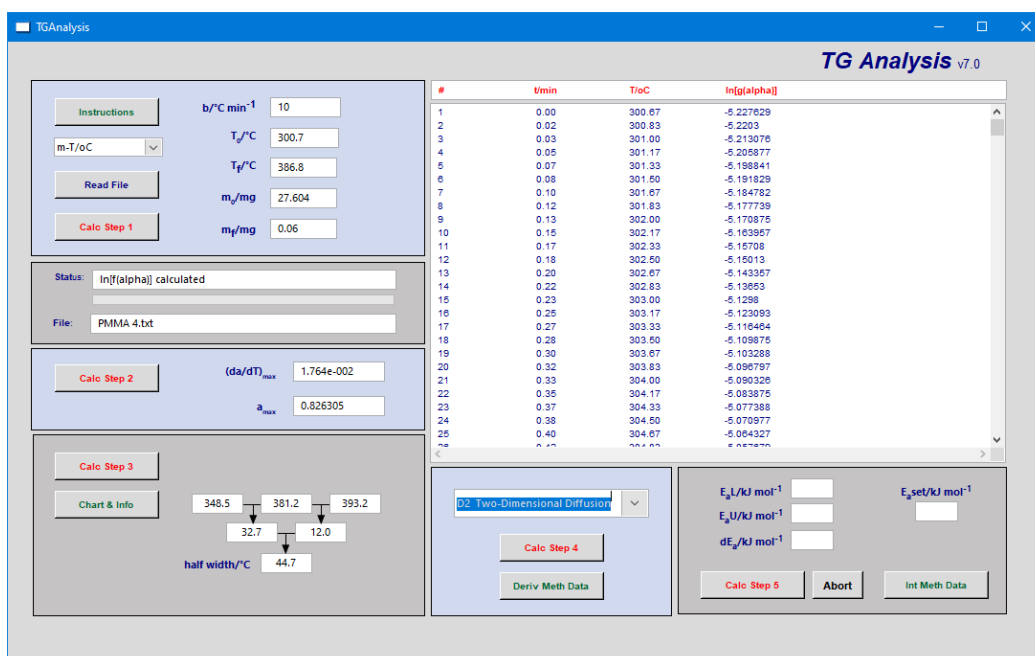
temperature axis and the cursor handle is used to determine the lower and upper temperatures where the plot intersects the half-height line.



- The Chart and Info button displays a listing of the kinetic models that can be used to fit the data along with a fitting parameter, ρ , for each model. This chart can be used to identify the most appropriate model for fitting the data. In the present work, D2-two dimensional diffusion model was used for PMMA-based samples, whereas, for PSt-based, materials F1-first order model was employed.

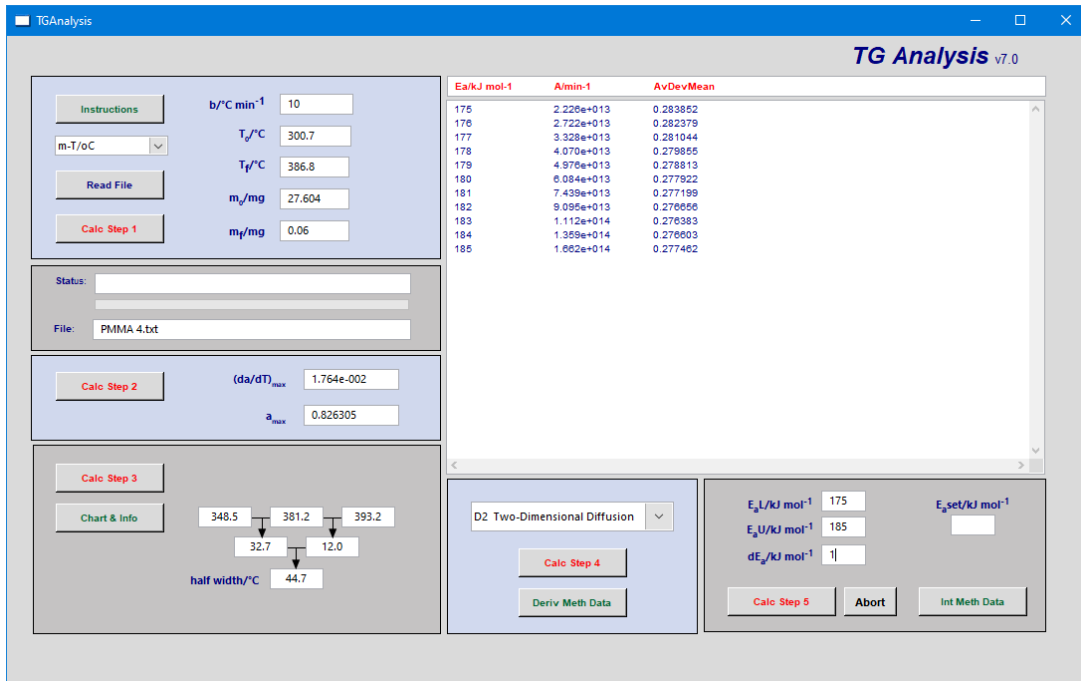


10. Select the required model that has a fitting factor close to 1 from the pull-down menu and click Calc Step 4 which will produce a $\ln[g(\alpha)]$ that are needed to extract the activation energy and Arrhenius factor in the next step (here, $g(\alpha)$ is an integral function as defined through equation (4) in section 3.5.2.



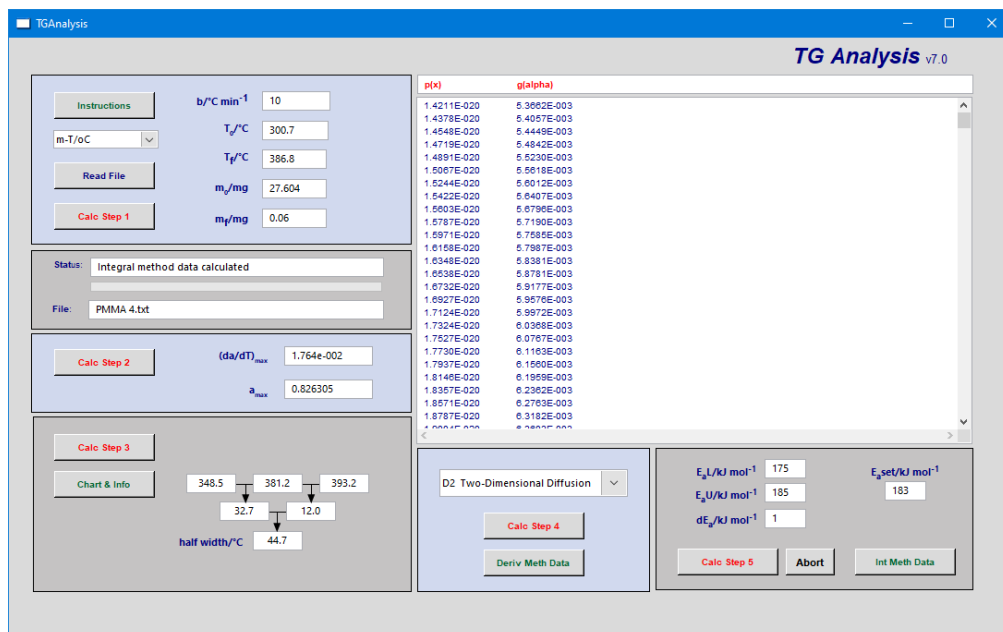
11. Start by scanning a wide range of E_a values with large incremental steps until a satisfactory convergence is reached. To determine the activation energy E_a , an iterative numerical calculation is performed on the data, the convergence to the

best fit is indicated by a minimum value of the averaged sum of the squares of the residuals.



12. Once the E_a value is optimized, the corresponding Arrhenius A -factor can be obtained from the output window in this stage. In this case, the E_a value for PMMA was found to be 183 kJ mol^{-1} .

13. Enter the optimized E_a into the E_a 'field' and click the Int Meth Data to obtain values of $g(\alpha)$ versus $p(x)$. Here, $p(x)$ is an integral function as defined through equation (6) in section 3.5.2.



14. These data will be automatically transferred to the clipboard and can be pasted directly into Excel to produce a plot of $g(\alpha)$ versus $p(x)$. This plot should be linear and pass through the origin. This step is critical to confirm the appropriate fit of the kinetic model and the reliability of the E_a and Arrhenius factor values obtained. The actual choice of an appropriate model, in the case of PMMA- and PSt-based substrates are given in detail in section 3.5.2 (Chapter 3).

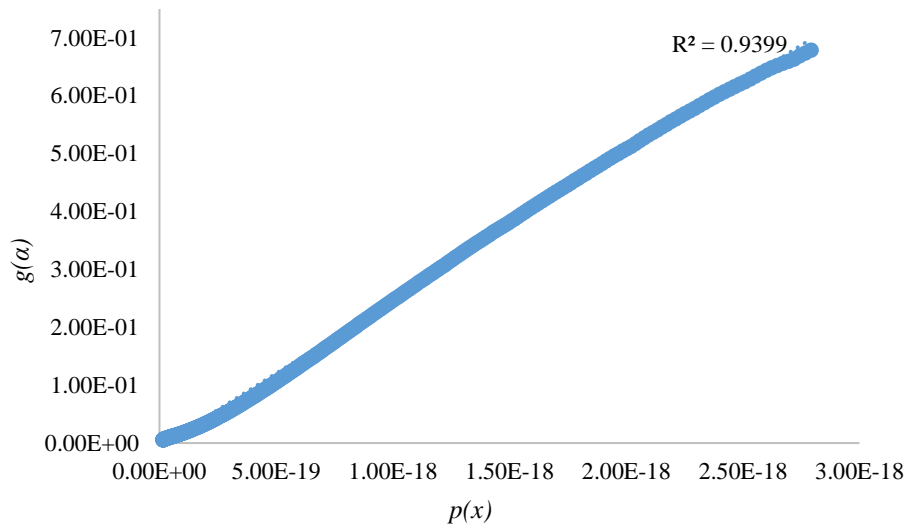


Figure 2. 14 A plot of $g(\alpha)$ vs. $p(x)$ obtained from the TGA software run of the PMMA bulk sample.

2.4.4.2 Imaging software for corrosion studies

This software was used to gauge the surface morphology of a mild steel specimen undergoing corrosion from its photographic images based on an imaging technique and accompanying software described in the literature (Bigger, *et al.*, 2017; Tawakkal, *et al.*, 2017). Here a mild steel specimen, having dimensions of *ca.* 10 cm \times 10 cm \times 1 mm, was chosen for the study. The surface of the specimen was initially smoothed using a fine-grade sandpaper and was then thoroughly cleaned by immersing it in conc. HNO_3 for *ca.* 48 h. The specimen recovered from the acid bath was subsequently washed with deionized water and dried in an air oven at *ca.* 70°C for a few hours prior to the start of the experiment. The specimen was mounted onto the wall and the free surface was exposed to the ambient conditions of the laboratory. The exposed surface was sprayed with deionized water, intermittently for the first two weeks followed by an aqueous

solution containing NaCl (10 wt.%) for another two weeks, with a view to accelerating the rate of corrosion. Digital photographs of the exposed surface were taken periodically, using a hand-held camera, in each instance where the intensity of the lightening was held constant.

The photographs thus obtained were processed by the in-house software. For this, the images were first 'cropped' to a pre-determined size (*ca.* 300 × 300 pixels). The 'cropped' photographs were then uploaded to the software, where the coloured pictures were converted to black-and-white images. In order to yield the final results, in percentage of black pixels, at a specific point which appeared to be representative of the morphological feature of a region that underwent corrosion, was selected through visual observation. Here, it is also relevant to note that an *optimum* value for the 'range' pertaining to the colour was manually chosen. It is also relevant to note that in each case, the 'range' was also varied as the intensities of the colour of the corroded regions were found to be different with time. Subsequently, the software automatically assigned black pixels to all points that underwent corrosion, whereas the rest of the matrix was depicted through white pixels. The output from the software and a plot of percentage of black pixels *versus* time are given in Chapter 3; Section 3.6.1; Figures 3.104 and 3.105, pages 161 -166.

CHAPTER 3: RESULTS AND DISCUSSION

3.1 Synthesis of step-growth polymers

Several studies have shown that condensation polymers, such as polydopamine, polyaniline and polypyrrole, possess good thermal stabilities/fire resistance and anti-corrosion/anti-microbial properties (Cho, *et al.*, 2015; Liu & Oliveira, 2007; Valença, *et al.*, 2015; Fang, *et al.*, 2007; Peikertová, *et al.*, 2011; Varesano, *et al.*, 2013; Boomi, *et al.*, 2014). This was the primary reason for choosing these polymers during the initial stages of the study. The oxidative polymerization (Coleman, 2019) of the corresponding monomers were found to be successful, resulting in the desired products with varying yields. All the polymers were obtained as fine, black powders. Here, it is also relevant to note that owing to the very limited solubility of these condensation polymers in common deuterated solvents, the solution-state NMR spectra could not be recorded. Therefore, the formation of desired polymers was, primarily, confirmed from their FT-IR spectra (see in Figures 3.1, 3.2 and 3.3).

3.2 Characterization of step-growth polymers

a. Structural characterization (FT-IR spectroscopy)

1. Polyaniline

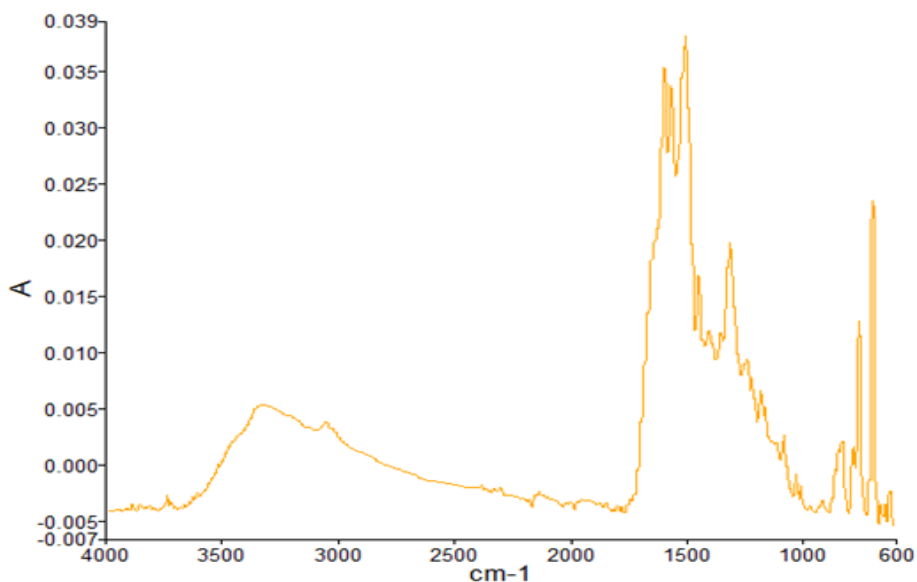


Figure 3.1 FT-IR spectrum of polyaniline: ordinate represents absorbance in arbitrary units and abscissa the wavelength in cm^{-1}

As expected, the spectrum showed signals from –N-H stretching, and absorptions owing to the aromatic structures with a signal at 3347 cm^{-1} , and signals at 694 cm^{-1} and 750 cm^{-1} , respectively (Singu, *et al.*, 2011). In addition, the spectrum also exhibited certain characteristic skeletal vibrations centered around 1300 cm^{-1} and 1500 cm^{-1} (see also in Figure 3.1).

2. Polypyrrole

The following signals were observed in the spectrum (Figure 3.2) which can be assigned as follows: 1554 and 1474 cm^{-1} - fundamental vibrations of the polypyrrole ring; 1294 and 1049 cm^{-1} -due to the =C–H in-plane vibrations; 1196 cm^{-1} can be assigned to the –C–N stretching vibrations (Fu, *et al.*, 2012). The signal around 2100 cm^{-1} can be assigned to a weaker –C–H stretching, and the broader band situated around 1800 cm^{-1} maybe owing to characteristic skeletal vibrations.

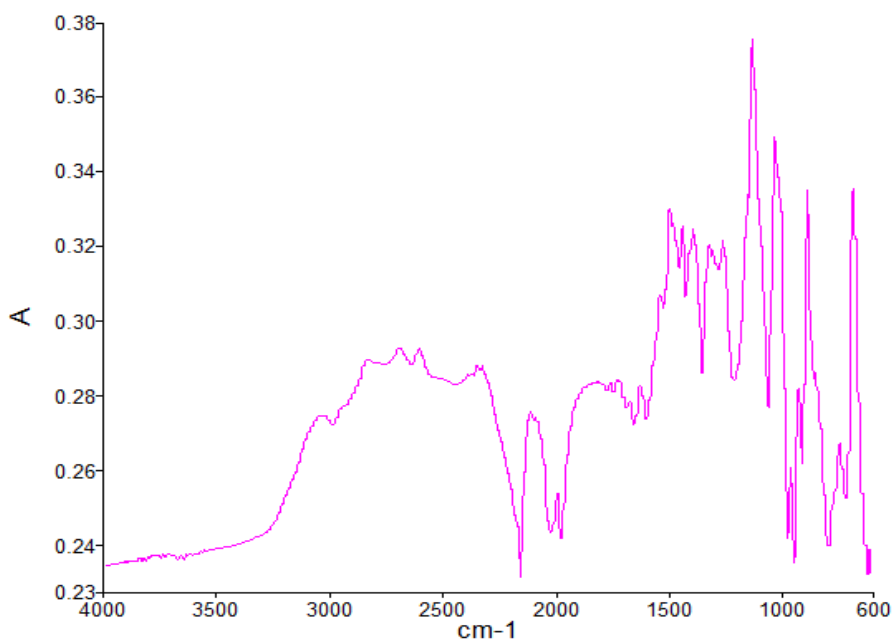


Figure 3.2 FT-IR spectrum of polypyrrole: ordinate represents absorbance in arbitrary units and abscissa the wavenumber in cm^{-1}

3. Polydopamine

As can be seen from the spectrum, shown in Figure 3.3 below, the broader peak around 3231 cm^{-1} denotes the phenolic –O–H and the –N–H stretching vibrations, from the primary and ring imino groups. The other absorptions can be assigned to: 1607 cm^{-1} ,

-C=O stretching; 1515 cm^{-1} , both -C=C and -C=N stretching vibrations; 1289 cm^{-1} ,
-C-O stretching (Luo, *et al.*, 2015).

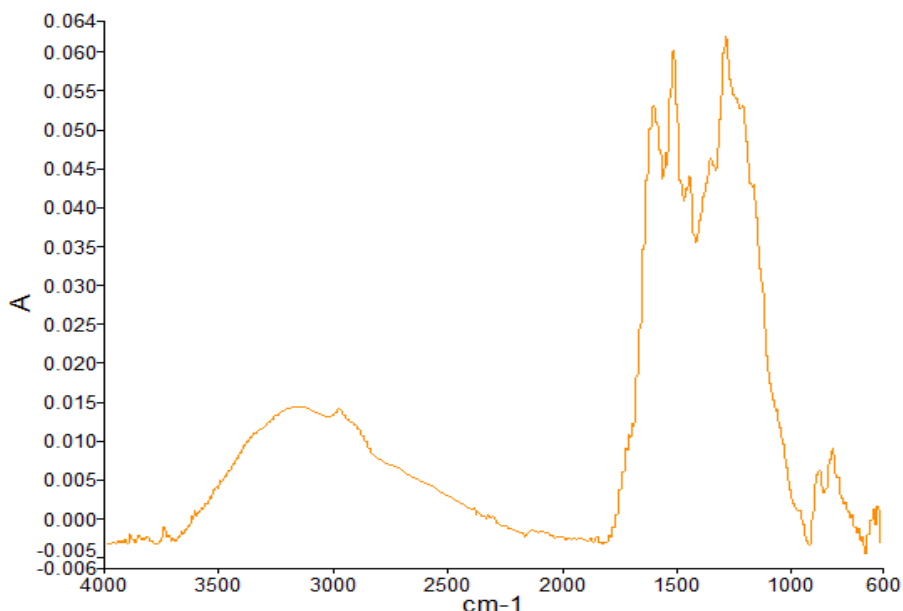


Figure 3.3 FT-IR spectrum of polydopamine: ordinate represents absorbance in arbitrary units and abscissa the wavenumber in cm^{-1}

b. Thermal characterization (TGA)

The step-growth polymers were subjected to thermogravimetric analyses, where the samples were degraded in an atmosphere of nitrogen at two heating rates of $10^\circ\text{C min}^{-1}$ and at $60^\circ\text{C min}^{-1}$, the latter rate was used for the purpose of direct comparison with the corresponding PCFC tests (i.e. equivalent to: 1°C s^{-1}). The results thus obtained are presented in Table 3.1. Here, the temperature at which the samples lose their mass in the first instance is taken as the induction temperature.

All three materials produced significant amounts of char residues when subjected to decomposition at both the heating rates. This indicates a relatively high thermal stability of the materials, primarily owing to the resonance stability of their aromatic structures constituting the backbone of the polymeric chains. Furthermore, the overall thermal stability of the polymers was found to be relatively significant (i.e. the ability to withstand up to $700\text{-}900^\circ\text{C}$ with only 50 wt.% mass loss), even though some degree of decomposition was observed during the initial phase of the TGA runs. This initial mass

loss can be attributed to the elimination of some low molecular-weight volatiles from the parent polymeric chains (i.e. through random chain scissions and/or through functional group condensation reactions, inter-, or intra-molecular, in nature) (Jakab, *et al.*, 2007; Kulkarni, *et al.*, 1989).

Table 3.1 TGA data of the step-growth samples at heating rates $10^{\circ}\text{C min}^{-1}$ and $60^{\circ}\text{C min}^{-1}$

Sl. No.	Sample	Heating rate ($^{\circ}\text{C min}^{-1}$)	Induction temp ($^{\circ}\text{C}$)	Temp at 50 wt.% ($^{\circ}\text{C}$)	Residue at 500°C (wt.%)	Final residue at 800°C (wt.%)
1	Polyaniline	10	47	864	66	54
2	Polyaniline	60	85	900	67	59
3	Polypyrrole	10	39	765	67	47
4	Polypyrrole	60	63	900	74	61
5	Polydopamine	10	40	672	63	44
6	Polydopamine	60	68	728	65	47

Another interesting pattern observed in the case of all three polymers at the faster heating rate ($60^{\circ}\text{C min}^{-1}$) is that their initial thermal stabilities (as indicated by the values of the induction temperatures), as well as the char yields, increased significantly as compared to those observed at the lower heating rate ($10^{\circ}\text{C min}^{-1}$). This trend was also observed in the values for the temperature corresponding to 50 wt.% mass loss. Both these attributes of the materials point towards their inherent flame-resistant properties, especially, given that faster heating rates are usually encountered in real fire scenarios. The thermograms obtained at both heating rates are given below in Figures 3.4 to 3.9.

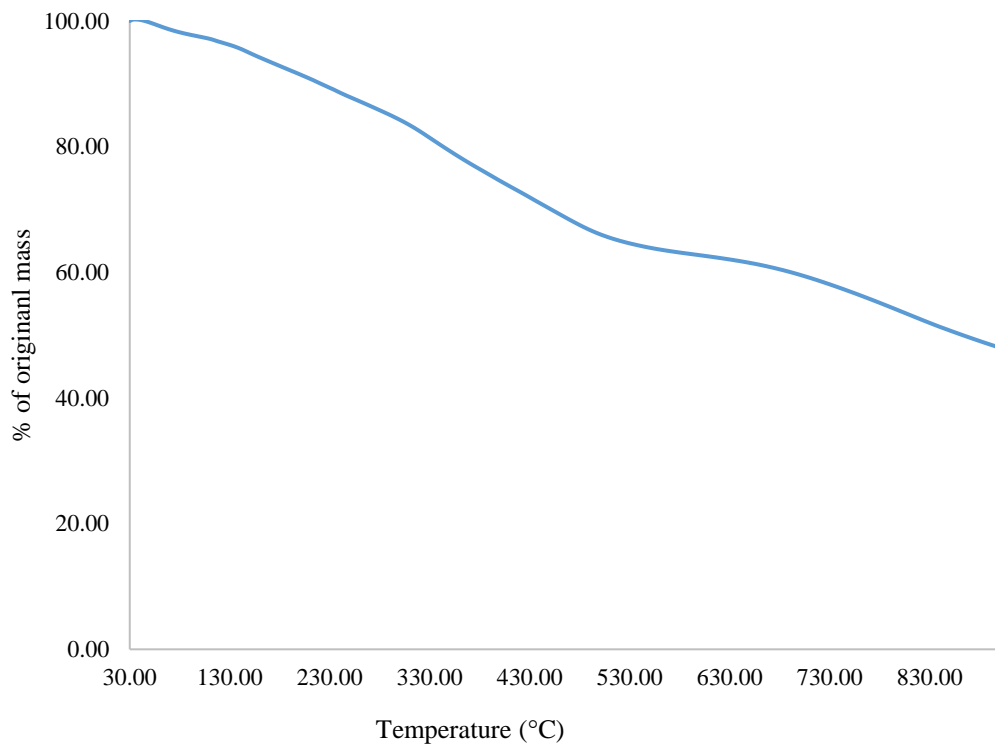


Figure 3.4 Thermogram of polyaniline at a heating rate of 10°C min⁻¹

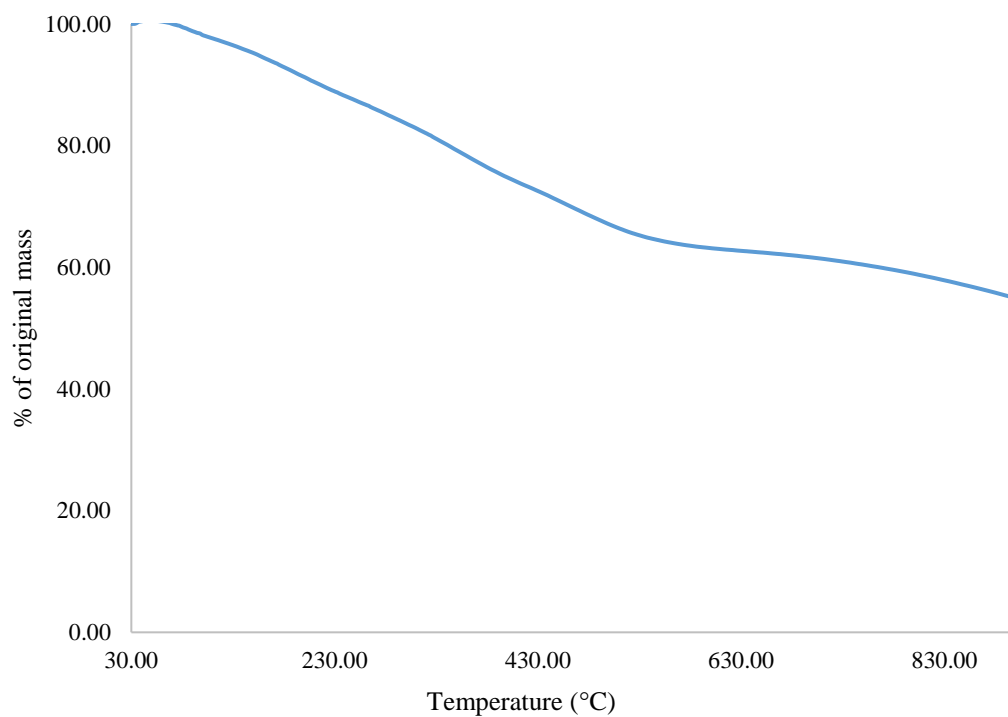


Figure 3.5 Thermogram of polyaniline at a heating rate of 60°C min⁻¹

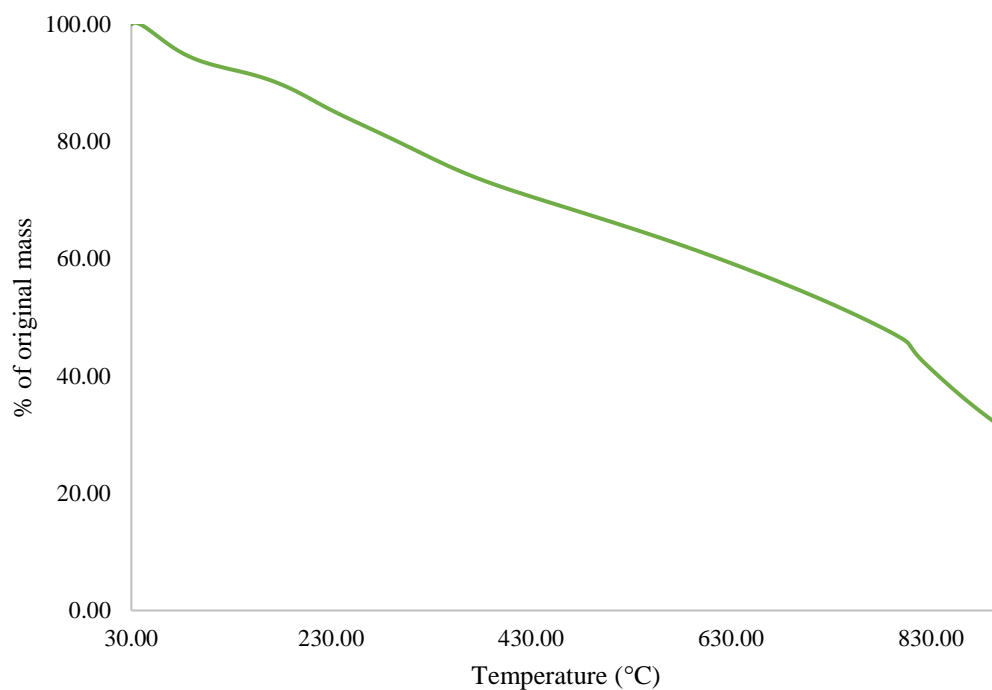


Figure 3.6 Thermogram of polypyrrole at a heating rate of 10°C min⁻¹

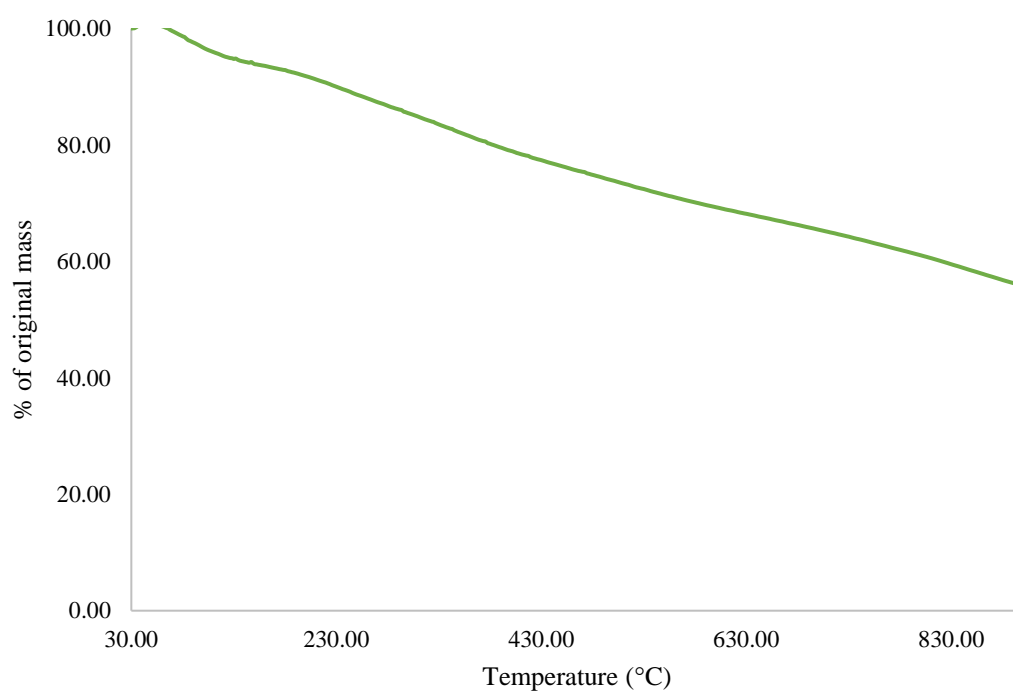


Figure 3.7 Thermogram of polypyrrole at a heating rate of 60°C min⁻¹

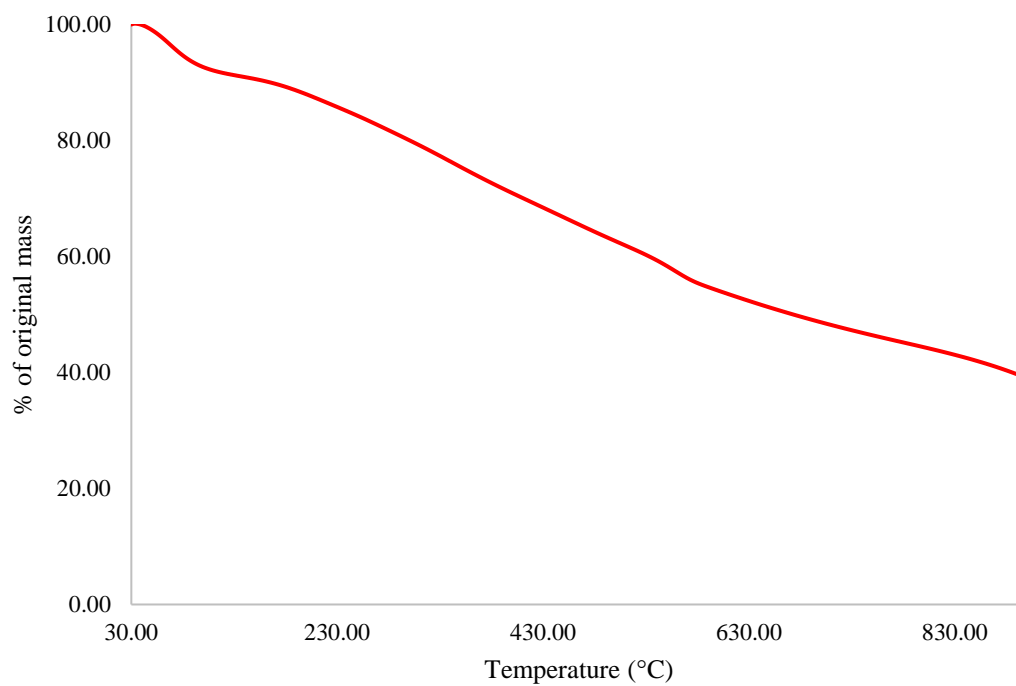


Figure 3.8 Thermogram of polydopamine at a heating rate of $10^{\circ}\text{C min}^{-1}$

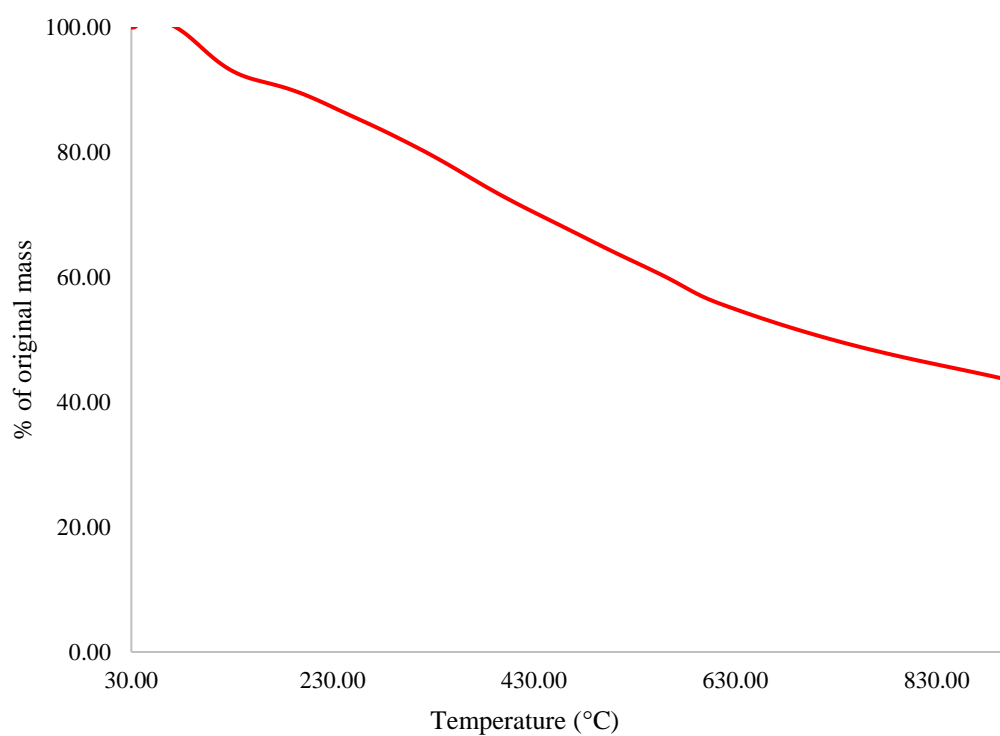


Figure 3.9 Thermogram of polydopamine at a heating rate of $60^{\circ}\text{C min}^{-1}$

As can be seen from the above figures, the general profiles of the thermograms for the three materials obtained under the two heating rates, showed a slow and steady mass loss resulting in relatively significant amounts of char residues. This attribute suggests that the step-growth polymers have a potential to be used as fire-proofing barrier materials for suitable substrates.

c. Calorimetric evaluation (DSC)

The differential scanning calorimetric analyses of the step-growth polymers were performed, in nitrogen, and from 30-550°C, at a heating rate of 10°C min⁻¹. A heat flow *versus* temperature (or time) curve was obtained for each sample. Here, the peaks pointing upwards with respect to the base line are indicative of endothermic processes occurring within the polymer matrices, whereas the peaks pointing downwards result from exothermic reactions, if present.

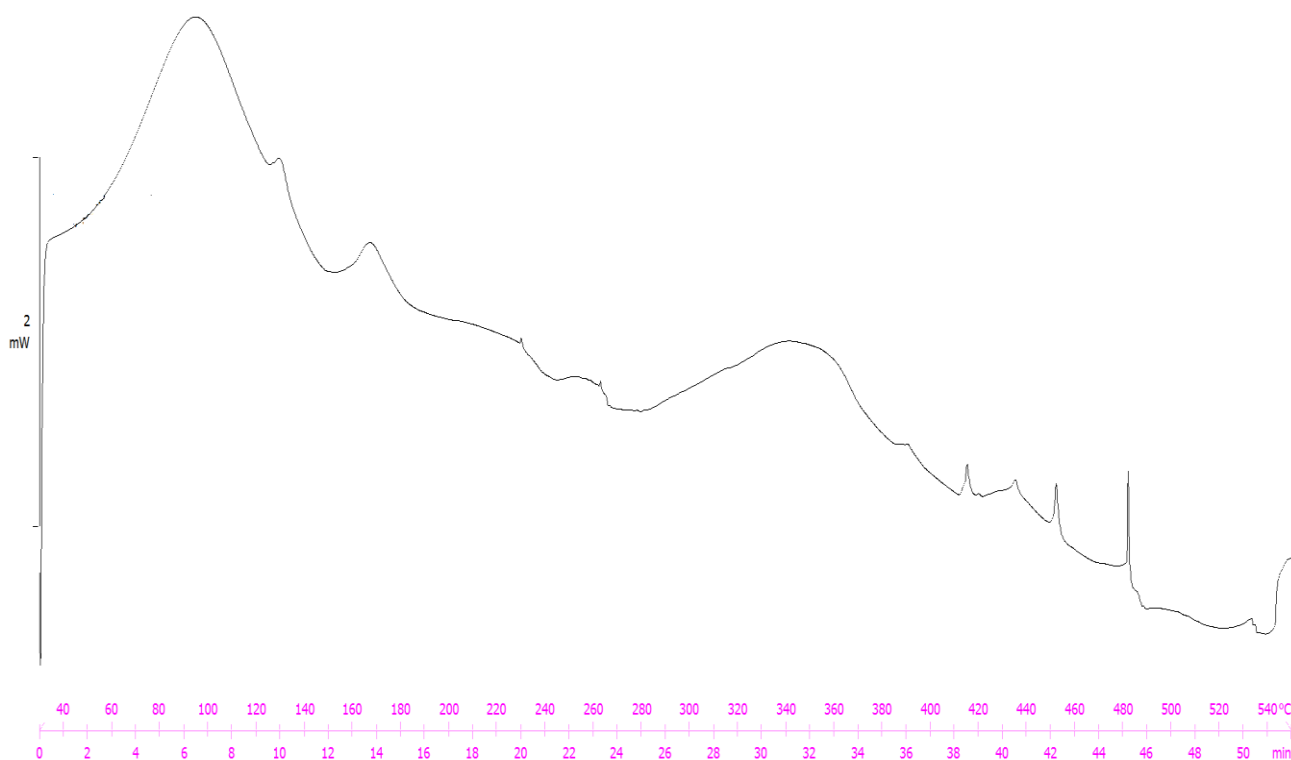


Figure 3.10 DSC curve of polyaniline at a heating rate of 10°C min⁻¹

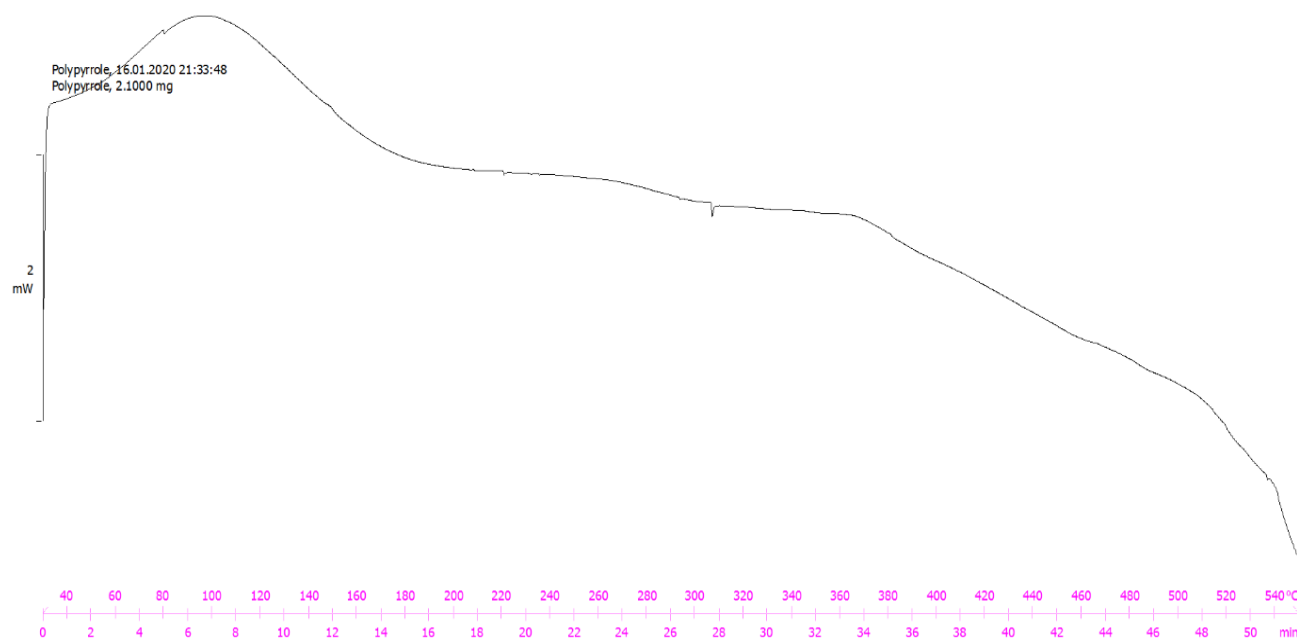


Figure 3.11 DSC curve of polypyrrole at $10^{\circ}\text{C min}^{-1}$

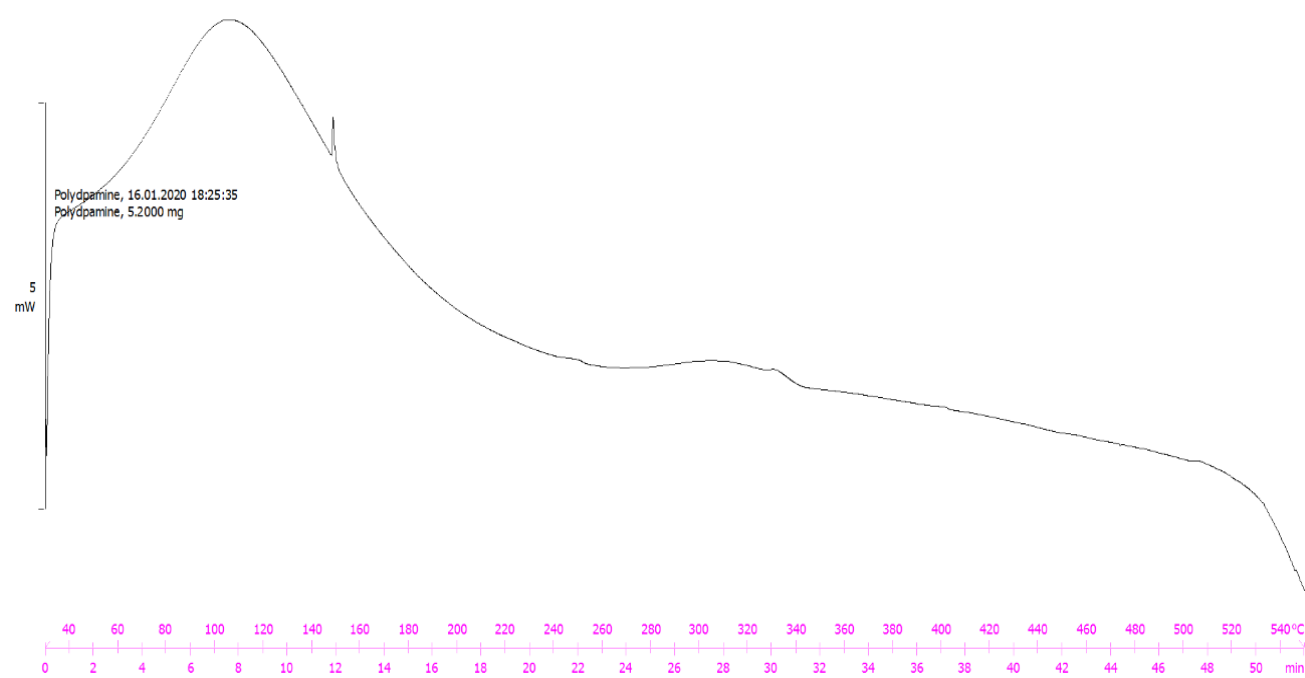


Figure 3.12 DSC curve of polydopamine at $10^{\circ}\text{C min}^{-1}$

The endothermic peak around 100°C in all three cases can be assigned to the loss of water molecules and/or other smaller volatile fragments (Matoetoe, *et al.*, 2014). It is also

interesting to note the presence of a smaller endothermic peak around 352°C for polyaniline, presumably arising from the elimination of nitrogen-containing species (Mostafaei & Zolriasatein, 2012). However, in the case of polypyrrole and polydopamine, the corresponding peak is not as prominent as in the former case.

d. Combustion attributes (PCFC)

The relevant combustion parameters of the step-growth polymers were collated by performing pyrolysis combustion flow calorimetric (PCFC) tests, in triplicate, for each material. Here the samples (*ca.* 5-15 mg) were initially degraded in an atmosphere of nitrogen (i.e. under anaerobic conditions, at a heating rate of 1°C s⁻¹), and then subjected to forced combustion in the presence of air. The average of the values of the relevant parameters that were obtained from the PCFC runs are tabulated in Table 3.2 below.

Table 3.2 PCFC data of the step-growth polymers performed at a heating rate of 1°C sec⁻¹

Sl. No.	Samples	Temp to pHRR (°C)	pHRR (W g ⁻¹)	THR (kJ g ⁻¹)	HRC (J g ⁻¹ K ⁻¹)	Char yield (%)	EHC (kJ g ⁻¹)
1	Polyaniline	455	22.1	5.8	25.3	63	15.5
2	Polypyrrole	119	4.60	2.3	8.00	73	8.60
3	Polydopamine	170	10.6	1.9	5.00	54	4.10

From the PCFC data of the step-growth polymers given above, it can be clearly seen that all three polymers have good flame-retardant properties, as revealed by the relative low values for peak heat release rate (pHRR), total heat released (THR), heat release capacity (HRC) and effective heat of combustion (EHC), especially, compared to some common commodity plastics. For example, the corresponding values for unmodified PMMA and PSt are much higher compared to the step-growth polymers (PA, PPe and PDA) (Tretsiakova-McNally & Joseph, 2015). Amongst the three materials, polyaniline appeared to be more thermally stable, in terms of the value of its Temp to pHRR; however, it has relatively higher values for pHRR, THR, HRC and EHC. The relatively lower values for Temp to pHRR for PPe and PDA can be attributed to their initial

decomposition resulting in combustible volatiles. On the other hand, polydopamine showed the least values for total heat release (THR), heat release capacity (HRC) and effective heat of combustion (EHC) values, thus indicating its superior combustion inhibitory effects. It can also be noted that polypyrrole has the lowest values for pHRR, and maximum char yield. The deviances among the PCFC parameters of the three polymers can be thought of arising from their inherent differences in their chain structures (i.e. tertiary amino functions in polyaniline *versus* heterocyclic aromatic structures in polypyrrole and polydopamine).

In summary, the results from the thermal and calorimetric measurements of the step-growth polymers suggested that they are endowed with good thermal stability and combustion resistance, thus making them ideal candidates for the use as fire-resistant coatings on substrates of interest. Therefore as the next step, the polymers were tried as surface coatings on some mild steel/PMMA substrates. Here, two simple, laboratory-based methods were adopted with a view to obtaining the required polymeric layer onto the material (an *in-situ* process and a hot-powder method).

In the first instance, the syntheses of the polymers were carried out in the presence of the mild steel/PMMA substrate, with a view to allowing the polymers thus formed to create a uniform coating onto the substrates, *in-situ*. However, it was found that the products obtained were not able to form any smooth and uniform coatings. In the second method, dispersions of polymers in water/methanol mixtures were applied onto pre-heated mild steel substrates, with a view to obtaining a uniform layer upon the evaporation of the solvent. Here, the heated surfaces (*ca.* 70°C) were expected to provide a more favourable base substrate for binding the polymer to the surfaces. However, this method also failed to produce any coherent coating. Here, elevated temperatures (i.e., 120°C or above) were not tried as this is bound to result in substantial decomposition of the polymers.

Therefore, it is to be concluded that a uniform coating of these step-growth polymers can only be achieved by using specialized techniques, such as electroplating/electrospinning. As these techniques are relatively expensive and harder to be implemented in the case of larger structural components, the focus of the investigation was shifted to the chain-growth polymers as they are more easily processable. Hence, two of the commercially important polymers, polystyrene (PSt) and polymethyl methacrylate (PMMA), were chosen for obvious reasons (see in chapter 1, section 1.2, pages 2 and 3).

3.3 Synthesis of the additive, precursors and co-monomers

All additives used in the present work were available commercially except diethylbenzylphosphonate, which was synthesized using the *Michaelis-Arbuzov* reaction (Bhattacharya & Thyagarajan, 1981). Furthermore, several precursor compounds and/or monomeric components were synthesized following established literature methods (Stempel Jr, *et al.*, 1950; Liepins, *et al.*, 1978; Ebdon, *et al.*, 2008; Wyman, *et al.*, 2006; Nair, *et al.*, 1988). These included: acryloyl chloride, diethyl-(1-hydroxyethyl)phosphonate (DEHEP), hydroxyphosphorlaminoester, diethyl-1-(acryloyloxyethyl)phosphonate (DE-1-AEP), diethyl-*p*-vinylbenzylphosphonate (DEpVBP), diethyl-2-(acryloyloxy)-ethylphosphate (DEAEPa) and acrylic acid-2-[(diethoxyphosphoryl) methyl amino] ethyl ester (ADEPMAE). It is also relevant to note that the specific procedure for the synthesis of DEpVBP was through a *Michaelis-Becker* route, which was found to be quite facile under relatively mild conditions (Wyman, *et al.*, 2004). Here, the reaction proceeded rapidly at sub-ambient temperatures to yield the desired product. This concomitantly eliminated the requirement to heat the reaction mixture, often at its reflux point as encountered in a classic *Michaelis-Arbuzov* procedure. Furthermore, carrying out the reaction at elevated temperatures can also result in premature thermal polymerization of the starting vinyl reactant and/or product. Overall, the synthetic procedures were found to be quite facile, furnishing the desired products in appreciable yields and with an acceptable level of purity. The chemical structures of these compounds were inferred from ^1H and ^{31}P NMR spectra, and through GC/MS analyses.

3.4 Synthesis of chain-growth polymers

1. Homopolymers of MMA and St

As a preliminary step, various and established laboratory-scale chain-growth polymerization methods were tried, i.e., solution, bulk, aqueous-slurry, suspension and emulsion. It is also relevant to note that the nature of the free radicals and/or the media were different in each case. The homopolymers of MMA and St were synthesized based on the above mentioned methods also with a view to analyzing the resultant conformational features (i.e. tacticity) of the polymeric chains formed, utilizing high-field NMR spectroscopy. It is to be noted here that the aqueous-slurry route is the common industrial practice for the production of polyacrylonitrile (PAN) (Ebdon, Huckerby, & Hunter, 1994; Ebdon, T. Huckerby, & Hunter, 1994), whereas PSt is commonly made

through suspension and PMMA through bulk and emulsion routes. The yields in each case are given in Tables 3.3 and 3.4.

Table 3.3 Preparation of PMMA *via* different polymerization routes

Sl. No.	Method	Recovered yield (wt.%/solid content)
1	Solution	48 %
2	Aqueous-slurry	73%
3	Suspension	*---
4	Emulsion	161 mg/mL
5	Bulk	> 97%

*failed to produce any polymeric product

Table 3.4 Preparation of PSt *via* different polymerization routes

Sl. No.	Method	Recovered yield
1	Solution	18 %
2	Aqueous-slurry	58%
3	Suspension	70%
4	Emulsion	245 mg/mL
5	Bulk	> 97%

The detailed structures of the initiating species are given in Figures 3.13 and 3.14. The conformational features of the main chains of the homopolymers, produced through the different chain-growth techniques, were deduced from the relevant regions of the high-field (600 MHz) solution-state NMR spectra (PMMA: ^1H and PSt: ^{13}C), and are given in Figures 3.15 to 3.18 (as examples). From the proton spectra of PMMA, the stereochemical placements of the *meso* (**m**) and *racemic* (**r**) tetrads and pentads can be identified (Koenig, 1999; White & Filisko, 1982). Whilst such obvious assignments are not generally possible by looking at the relevant regions of the ^{13}C spectra of PSt (i.e. the *ipso*, methylene and

methine carbons), the fine structural features of the signals confirm that predominantly an atactic polymer is formed (Cheng & Lee, 1996).

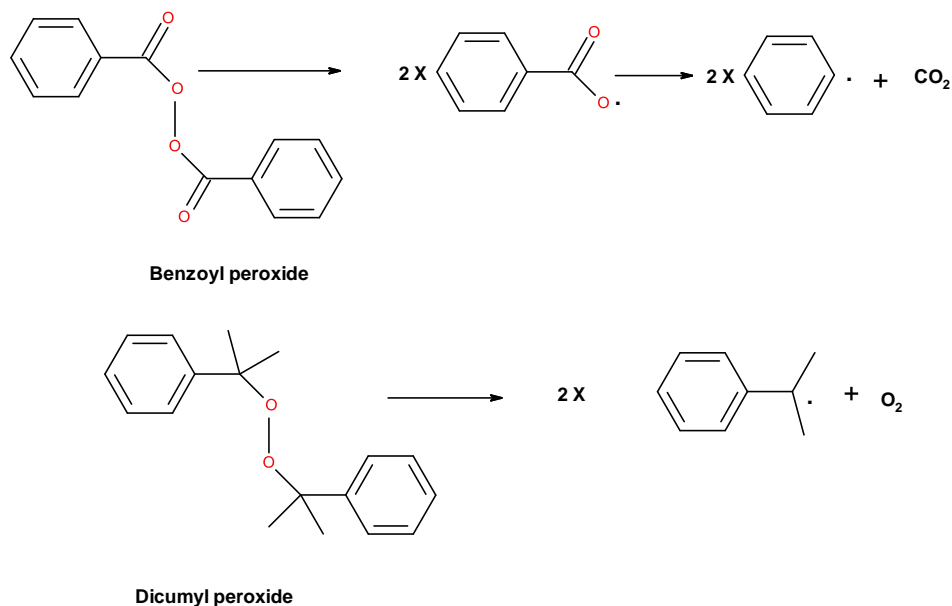


Figure 3.13 A schematic representation of the initiating species from benzoyl peroxide and dicumyl peroxide (Moad & Solomon, 2006)

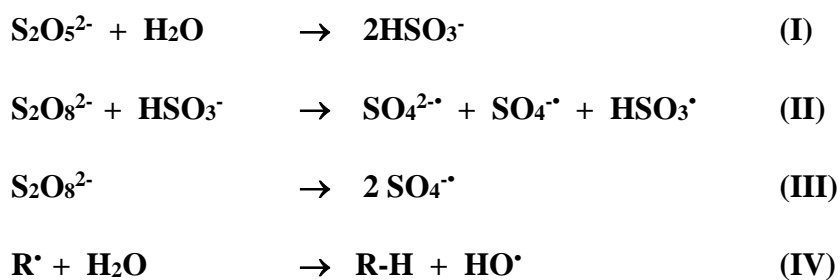


Figure 3.14 A schematic representation of the initiating species from ammoniumpersulfate/sodium metabisulfite redox pair (Ebdon, *et al.*, 1994; Ebdon, *et al.*, 1994a)

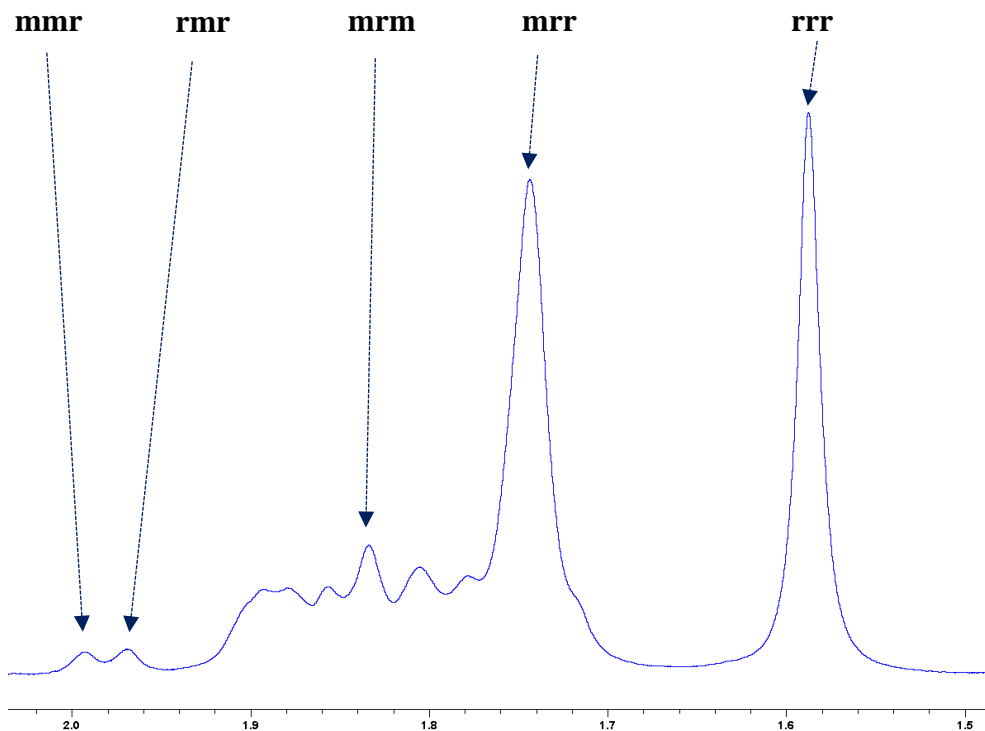


Figure 3.15 ¹H NMR spectrum of PMMA obtained through the aqueous-slurry route: region predominantly showing the syndiotactic placements of the β -CH₂ protons

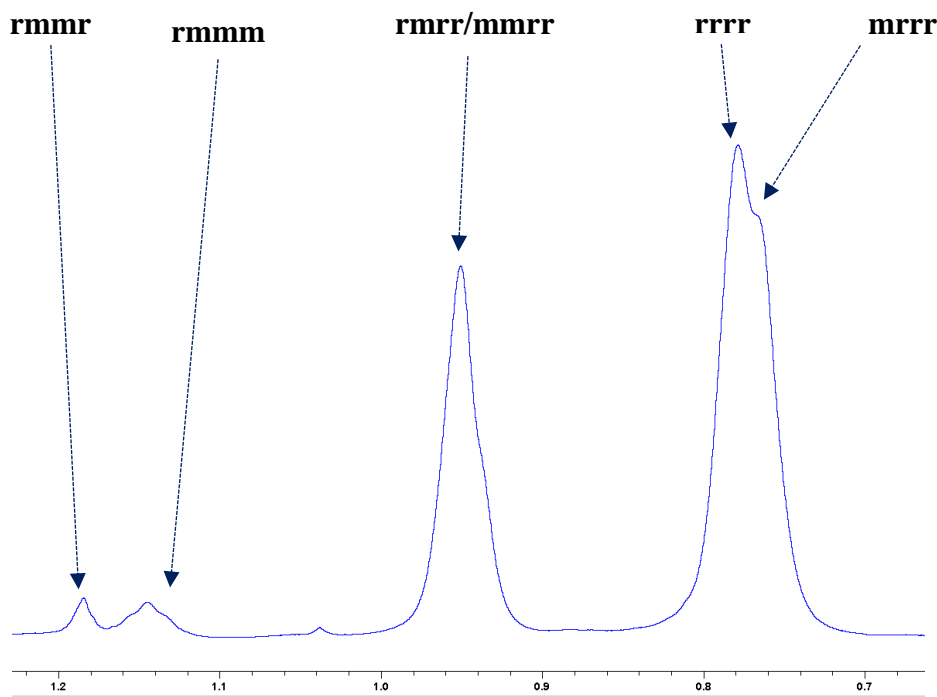


Figure 3.16 ¹H NMR spectrum of PMMA obtained through the aqueous-slurry route: region predominantly showing syndiotactic placements of the α -CH₃ protons

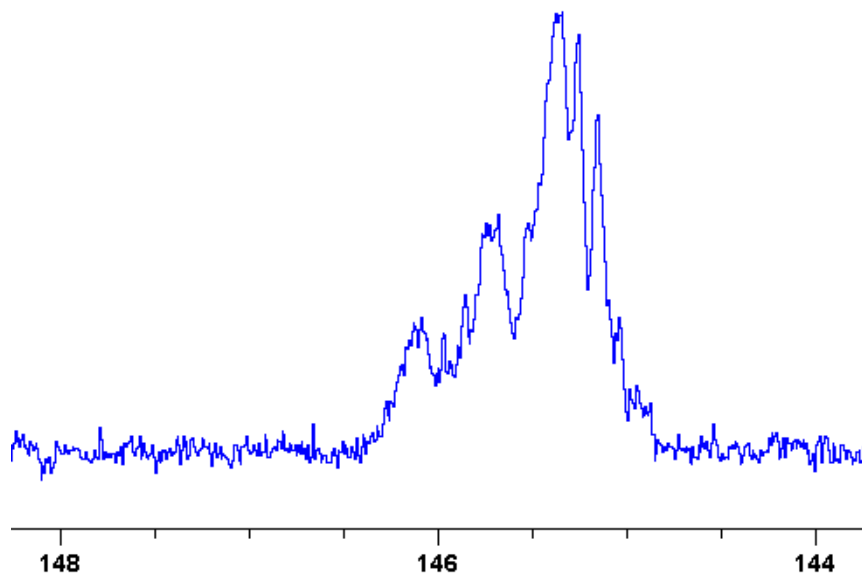


Figure 3.17 ¹³C NMR spectrum of PSt obtained through the emulsion route: region of the ipso-carbons predominantly showing atactic placements (Cheng & Lee, 1996)

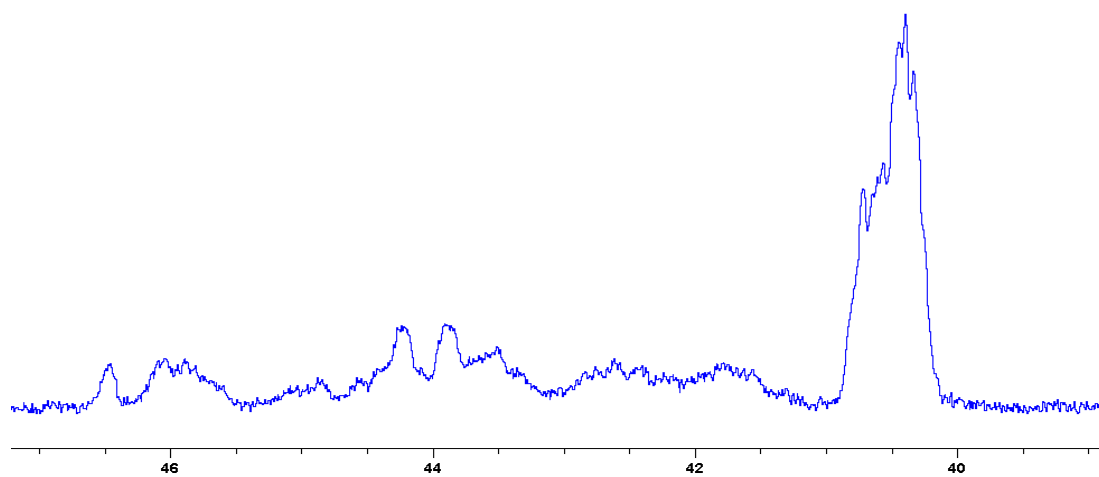


Figure 3.18 ¹³C NMR spectrum of PSt obtained through the emulsion route: region of the methine and methylene carbons predominantly showing atactic placements (Cheng & Lee, 1996)

It is interesting to note that, regardless of the nature of the initiating radicals and/or the media, predominantly syndiotactic PMMA and atactic PSt were obtained. These effects cannot be easily explained as the stereo-regular placements in the case of PMMA, or the lack of it as in PSt, can be influenced by a variety of factors, such as the resonance stability of the growing chain-ends, the preferred stereo-chemical disposition of the incoming monomeric units and the associated electronic effects, etc. (Coleman, 2019). The tacticity of PMMA and PSt are relatively less important, as they are typical amorphous polymers, when compared to some predominantly fibre-forming polymers, such as polypropylene, polyacrylonitrile, polyamides, etc. However, the conformational features of polymers can exert varying degrees of influence in some of the characteristic physical properties, such as their glass transition temperatures. Hence, the tacticity features can have an indirect bearing on the melt-processing and blending of the parent polymer matrices with other compounds for making hybrid materials. The preferred propagation steps can also indirectly affect molecular weight and/or its distribution during the production process. Therefore, it is important to study the conformational features in the present context, as the end use of these systems (i.e. as plaques, or as insulating materials, or as protective films, etc.) will depend, in turn, on the processability parameters of the pre-formed polymers.

The solution polymerizations were mainly conducted in order to gauge the polymerizability of the synthesized co-monomers with MMA and St (Ebdon, *et al.*, 2000), whereas aqueous-slurry, bulk, suspension, and emulsion routes were used to explore the feasibility of functionalization of the base polymers through the latter routes at a laboratory scale. Furthermore, PMMA- and PSt-based polymers are produced industrially for various purposes, through similar routes, with specific end-uses, such as: transparent and weather-resistant plaques through casting from neat monomers (Ebdon, Hunt, *et al.*, 2000; Price, *et al.*, 2001); beads for expandable foams; film-forming coatings based on aqueous acrylic formulations; etc.

2. Copolymers of MMA and St with the functional co-monomers

The composition of the copolymers, produced through solution and suspension routes, were primarily inferred from their ¹H NMR spectra (Table 3.6). Typically, this involved comparing the integral areas of appropriately assigned signals arising from particular monomeric units in question, or the area from a particular monomeric unit to the total

area of the copolymer, as the case may be. For example, for the copolymer formed from MMA and DEpVBP (Figure 3.19), the following steps were performed:

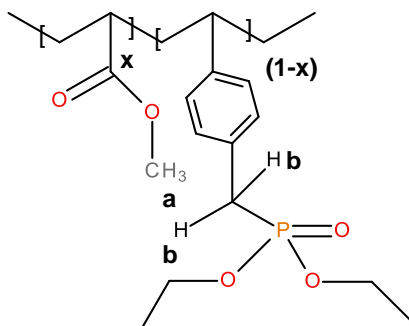


Figure 3.19 Structure of the copolymer of MMA and DEpVBP

Let x be the mol fraction of MMA, and therefore $(1-x)$ will be the mol fraction of DEpVBP units.

$$\text{Area of } \mathbf{a} \text{ protons} = 2.7205 \propto 3x$$

$$\text{Area of } \mathbf{b} \text{ protons} = 0.2574 \propto 2(1-x)$$

Dividing the above relations, and then solving for x , we get, $x = 0.88$ (mol fraction of MMA units); therefore, mol fraction of DEpVBP units is $= (1 - 0.88) = 0.12$

Hence, the wt.% of phosphorus in the copolymer can be calculated as follows (here the formula mass of MMA is 100 and that of DEpVBP is 254)

$$P(\text{wt. \%}) = \frac{(0.12 \times 31 \times 100)}{(0.88 \times 100) + (0.12 \times 254)} = 3.1$$

Essentially, the same procedure was adopted for determining the composition and wt.% of P in each case (see in Table 3.5)

Table 3.5 Styrene and PMMA-based polymers via the solution route in the 9:1 (monomer:co-monomer) ratio; reaction time: *ca.* 6 h.

Sl. No.	Monomers in the feed	Recovered yield (wt.%)	Composition of the polymer (mol fraction)*	P content (wt.%)	N content (wt.%)
1	MMA	47.5	1.00/0.00	---	---
2	MMA/DE-1-AEP	4.30	0.87/0.13	3.4	---
3	MMA/ADEPMAE	15.1	0.92/0.08	2.2	1.0
4	MMA/DEAEPa	8.20	0.64/0.36	7.2	---
5	MMA/DEpVBP	35.4	0.88/0.12	3.1	---
6	Styrene	17.8	1.00/0.00	---	---
7	St/DE-1-AEP	49.5	0.89/0.11	2.9	---
8	St/ADEPMAE	48.2	0.78/0.22	4.9	2.2
9	St/DEAEPa	8.20	0.94/0.06	1.6	---
10	St/DEpVBP	62.0	0.95/0.05	1.4	---

*from ¹H NMR

As can be seen from the above table, all copolymerizations involving the phosphorus-containing monomers *via* the solution technique were successful, resulting in copolymers that varied significantly in their compositions. Furthermore, the resultant yields were also noticeably different, and in some cases, these were relatively very low (MMA/DE-1-AEP, MMA/DEAEPa and St/DEAEPa). This effect can be attributed to the fact that the polymerization reactions were carried out in fairly dilute solutions, and that the extent of chain transfer to functional monomers can also vary. This variation in composition was expected, given that the recovered yields were also noticeably different in each case (i.e. different extents of conversion) albeit the same feed ratios and time of polymerization were used. Such deviances could also result from the different degree of polymerizability of the co-monomers (Ebdon, *et al.*, 2000). Furthermore, compositional variations are also influenced by the differences in the reactivity ratios of the co-monomer in question. In the case of the P- and N-containing copolymers, i.e. St/ADEPMAE and MMA/ADEPMAE, it was found that a phosphorus loading of 4.9 wt.% endowed the material with a nitrogen content of 2.2 wt.%, in the former case, and corresponding values in the latter case were 2.2 and 1.0 wt.%, respectively. In both cases, the presence of the P/N-monomer was found to have an apparent plasticizing effect on the parent polymeric material, i.e. making the copolymers flexible and rubbery.

Table 3.6 Styrene-based polymers via suspension route in the 8:2 (monomer:co-monomer) ratio; reaction time: *ca.* 5 h

Sl. No.	Monomers in the feed	Recovered yield (wt.%)	Composition of the polymer (mol fraction)*	P content (wt.%)	N content (wt.%)
1	Styrene	70	1.00/0.00	---	---
2	St/DE-1-AEP	69	0.64/0.36	7.4	---
3	St/ADEPMAE	15	0.87/0.13	3.2	1.5
4	St/DEAEPa	29	0.89/0.11	2.8	---
5	St/DEpVBP	78	0.93/0.07	1.9	---

*from ^1H NMR

Suspension polymerization is generally the most commonly used technique for producing polystyrene-based beads that are subsequently used as the precursors to insulating foams. The polymerization of styrene with all of the four phosphorus-containing co-monomers was studied using two different feed ratios of 9:1 and 8:2 and *via* suspension route. The second set of samples (where the feed ratio was 8:2) were characterized using NMR spectroscopy to obtain the compositions in each case. In this case also, the composition of the resultant copolymers was also found to vary widely (see Table 3.6). As mentioned earlier, the wide distribution in the composition of the polymers in terms of phosphorus loading can be considered to arise from the differences in the reactivity ratios coupled to the varying yields in each case. Thus the suspension polymerization route was found to be quite facile for chemically modifying the polystyrene matrix with phosphorus-containing groups, even though the composition of the resulting polymers cannot be fine-tuned. Albeit, this technique can be potentially adopted by industry, with minimum modifications, to produce materials that can be used as flame-retardant, insulating foams.

3.5 Bulk polymers

The most important use of MMA-based polymers is evidently as transparent plaques for various applications, where good optical clarity and enhanced weather resistance are the main pre-requisites. However for such applications, the relatively high flammability of virgin PMMA often becomes a limiting factor. In this context, the rigid solid materials

cast from PSt-based materials are not sufficiently explored to date. Hence in the present study, plaques of both PMMA and PSt were prepared (*ca.* 50 g scale) by incorporation various additives/reactives through adopting some literature precedents (Ebdon, *et al.*, 2000; Price, *et al.*, 2001). It is also relevant to note that the loading of phosphorus, in all cases, was normalized to 2 wt.%, while altering the chemical environments and oxidation states of the phosphorus atom in the admixtures. Furthermore, both the *additive* and *reactive* routes were utilized, with a view to identifying the influences, if present, between the two strategies on the combustion features of the polymeric products. In addition, given the relatively nominal loading of phosphorus (2 wt.%), any marginal improvements in the fire retardance of the modified systems as compared to the virgin polymers would be most advantageous.

The products obtained through the bulk polymerization route were also chosen for further and detailed investigations in terms of their thermal (TGA) and calorimetric (DSC) properties, as well as their combustion (PCFC and ‘bomb’ calorimetry) characteristics. It is worth noting here that the final compositions of these products through the *reactive* strategy were effectively controlled with a high degree of certainty, since the polymerization reactions were driven to near completion. Basically, this was achieved by using a mixture of low- and high-temperature initiators (benzoyl peroxide and dicumyl peroxide, respectively), and checking the structure of the final products through spectroscopic means (FT-IR and ¹H NMR). The spectra so obtained were found to be devoid of any discernable signals from the residual monomeric species indicating that the polymerizations proceeded to *ca.* 99% conversion. As expected, the products exhibited relatively high purity, when compared to polymers made through the other common chain-growth techniques, since the bulk polymerization method does not require any solvent(s)/reagent(s).

Thus the bulk synthetic route used in the present study for making PMMA- and PSt-based materials was found to be successful. In almost all cases, dense and tough polymeric plaques were formed. However, some exceptions can be noted. The DOPO-modified versions of PMMA and PSt were found to be substantially brittle, and were amenable to shattering quite easily under a mechanical strain. On the other hand, the reactively modified versions with the P- and N-containing co-monomer, ADEPMAE, were found to have a plasticizing effect on the final products, as also was observed in the case of the corresponding copolymers obtained through the solution technique. The results obtained

through the thermal and calorimetric evaluation of the products prepared through the bulk polymerization method are given, in detail, in the following sections.

3.5.1 Thermal and calorimetric characterization

a. Thermogravimetric analysis (TGA)

In this section, the relevant TGA parameters obtained for each PMMA- and PSt-based sample at a heating rate of $10^{\circ}\text{C min}^{-1}$ are presented in Tables 3.7 and 3.8, and plotted in Figures 3.20 to 3.25 and Figures 3.26 to 3.31, respectively. All the runs were carried out in a nitrogen atmosphere. The corresponding data obtained at $60^{\circ}\text{C min}^{-1}$ were primarily used for comparison with the relevant parameters obtained through the PCFC runs. The thermograms obtained for PMMA and PSt samples generally exhibited only one main decomposition step. However, during the initial phases of decomposition, some small mass losses can be also observed in almost all the cases.

Table 3.7 Some relevant parameters from the TGA analyses of PMMA-based systems

Sl. No.	Sample	Induction temp ($^{\circ}\text{C}$)	Temp at 50 wt.% ($^{\circ}\text{C}$)	Residue at 500°C (wt.%)	Final residue at 800°C (wt.%)
1	PMMA	157	362	0.4	0.3
2	PMMA+TPP	93.0	385	1.4	1.0
3	PMMA+TPPO	147	352	1.3	1.2
4	PMMA+DOPO	88.0	380	1.2	0.9
5	PMMA+DEHPi	52.0	387	6.9	7.2
6	PMMA+TEPi	74.0	375	0.7	0.7
7	PMMA+TEPa	83.0	356	0.4	0.5
8	PMMA+DEPP	98.0	358	1.1	1.1
9	PMMA+DEBP	89.0	359	2.3	2.3
10	PMMA+DE-1-AEP	97.0	395	4.5	4.1
11	PMMA+ADEPMAE	98.0	396	3.1	2.7
12	PMMA+DEAEPa	103	393	4.3	4.0
13	PMMA+DEpVBP	107	392	9.2	8.1

It can be noticed from the above table that the homopolymer (PMMA) has the highest temperature to initial mass loss (i.e. the induction point), followed by PMMA+TPPO. The corresponding value is least for PMMA+DEHPi (starting at 52°C), which can be attributed to the release of some small molecules. However, this polymeric system produced the highest amount of char among the additives. On the other hand, PMMA+DEpVBP produced maximum quantity of char amongst the reactive selected for the study. In addition, the reactively-modified systems generally exhibited relatively high thermal stabilities, in terms of the temperature at 50 wt.% decomposition (almost 30 degrees higher compared to pure PMMA), than those systems containing the additives. This can be attributed to the interference of the acrylic co-monomeric unit with the unzipping reactions of sequential parts of the methacrylate units, thereby partially blocking the usual pathway of complete decomposition of the PMMA chains to yield the monomer (Crook, *et al.*, 2010; Price, *et al.*, 2001). Furthermore, thermal cracking of the pendent phosphorus-containing moieties has been shown to be responsible for the condensed-phase mechanism which results in char formation. Previous studies have already identified that reactive compounds are generally more effective than additives (Ebdon, *et al.*, 2000; Price, *et al.*, 2001). Generally, a higher char yield in a TGA run can be indicative of an enhanced degree of activity of the modifying group in question in the condensed phase.

In the following figures, the overlays of TGA thermograms are given, which are grouped based on the physical nature of the additive, as well as on whether the modifying groups are used as an additive, or as a reactive.

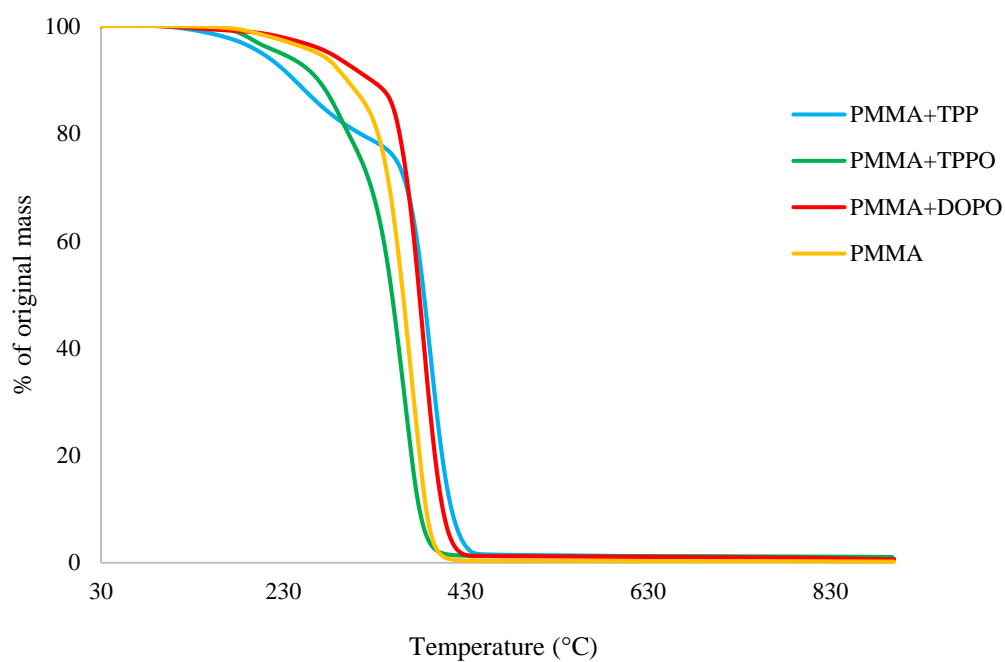


Figure 3.20 An overlay of the TGA curves of the PMMA-based materials with solid additives, at $10^{\circ}\text{C min}^{-1}$

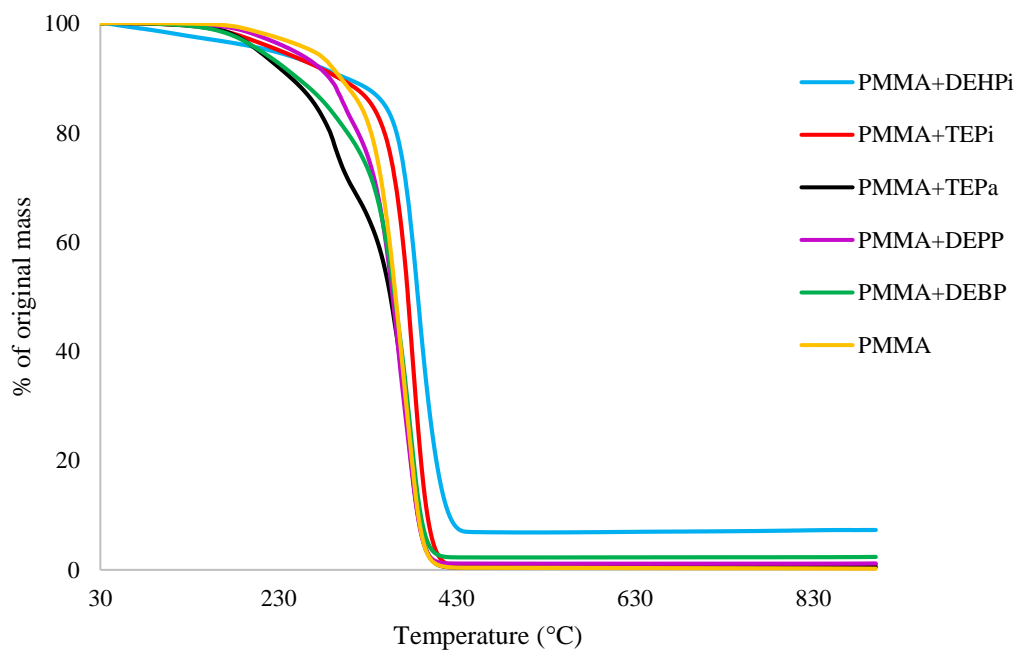


Figure 3.21 An overlay of the TGA curves of the PMMA-based materials with liquid additives, at $10^{\circ}\text{C min}^{-1}$

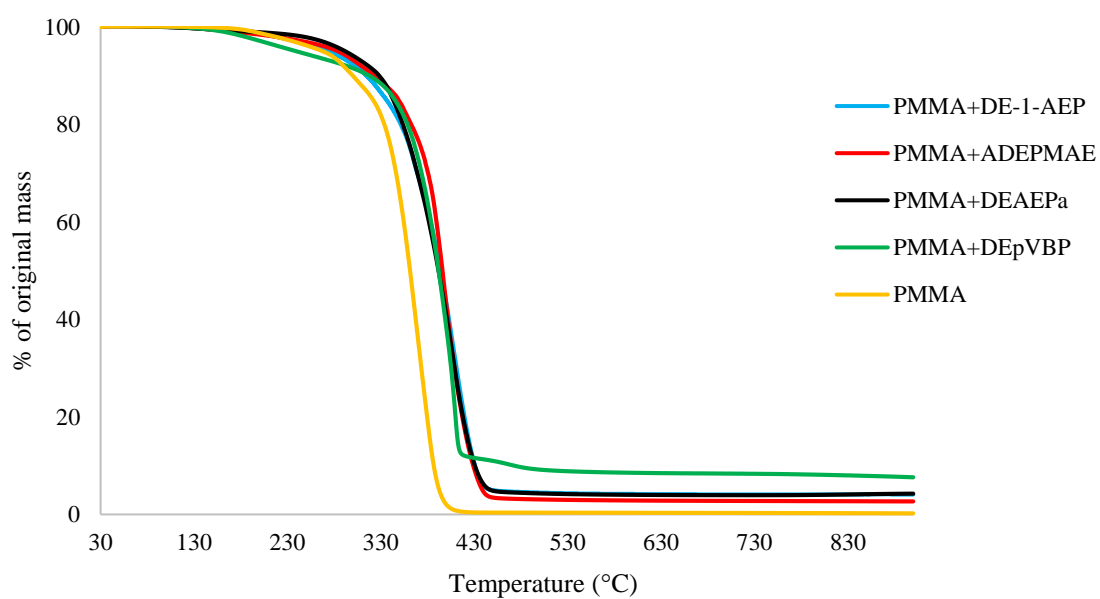


Figure 3.22 An overlay of the TGA curves of PMMA-based materials with reactives, at 10°C min⁻¹

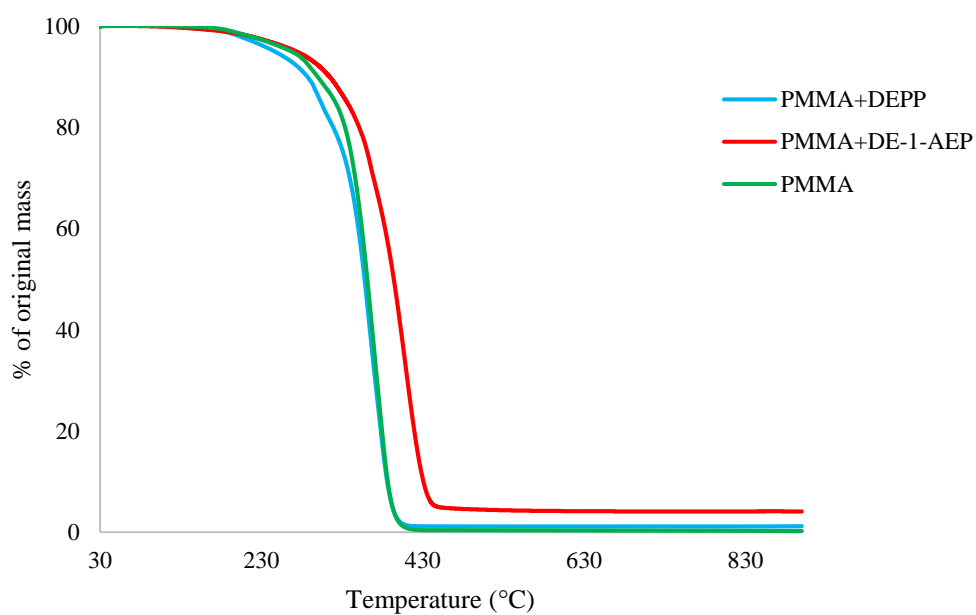


Figure 3.23 An overlay of the TGA curves of PMMA and PMMA+aliphatic phosphonate materials

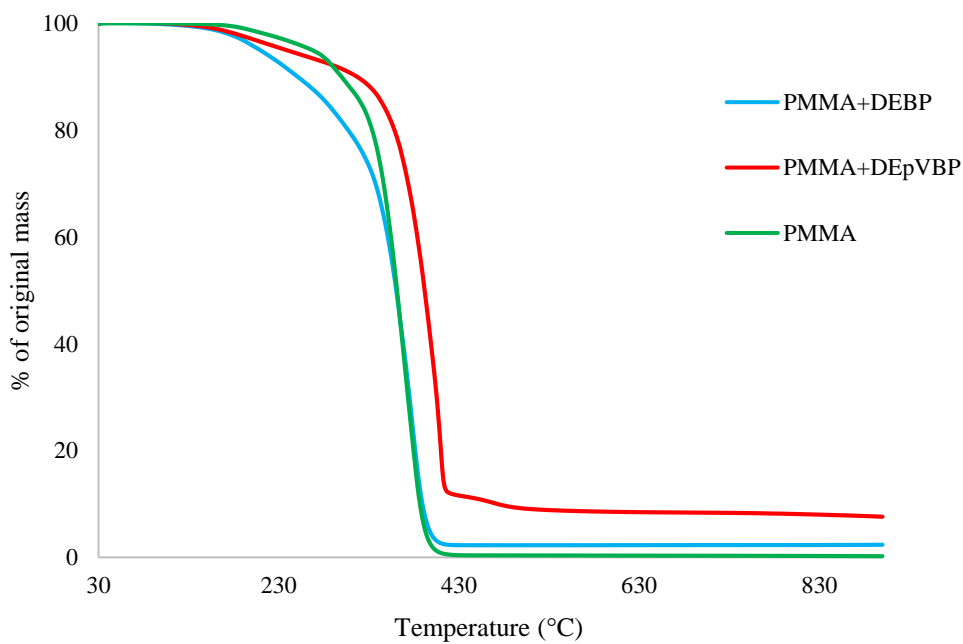


Figure 3.24 An overlay of the TGA curves of PMMA and PMMA+aromatic phosphonate materials

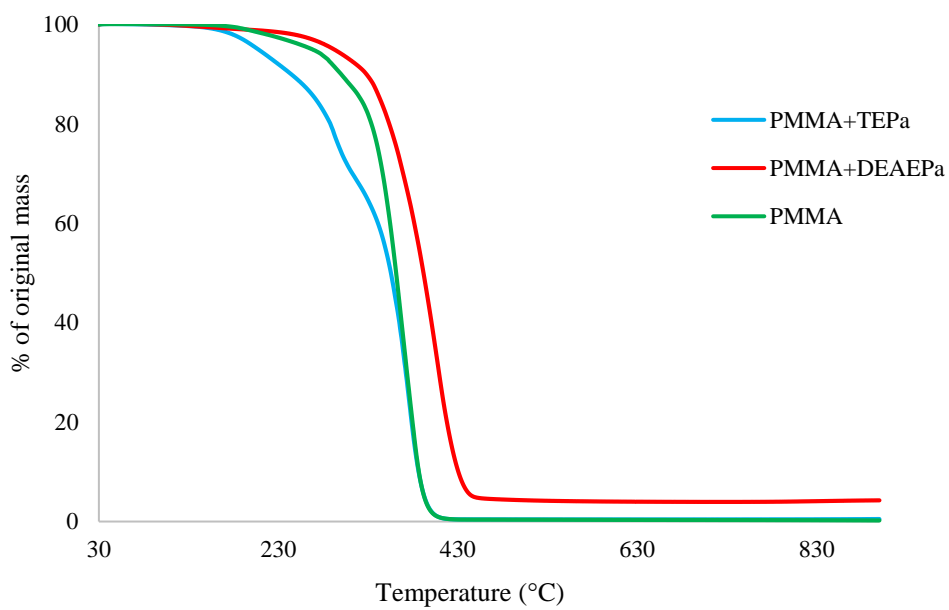


Figure 3.25 An overlay of the TGA curves of PMMA and PMMA+phosphate materials

In summary, some pertinent features regarding the thermograms of the PMMA-based systems can be noted, as follows:

1. In all cases, the products obtained through the *reactive* strategy exhibited improved thermal stabilities relative to unmodified PMMA, albeit to varying degrees. Phosphorus- containing co-monomeric units seem to effectively hinder the unzipping reaction during the decomposition of the parent polymeric chains.
2. The PMMA+DEpVBP system (where a P-containing aromatic functionality is present in the pendent group), produced the maximum amount char (i.e. 8.14 %). This is in agreement with previous published results (Ebdon, *et al.*, 2000).
3. Incorporation of ADEPMAE (i.e. the monomeric unit containing both P and N atoms) in the main chain resulted in the maximum enhancement in the stability of PMMA (i.e. 396°C at 50 wt.% mass loss). This can be attributed to P-N synergism, as reported previously in the case of polyacrylonitrile (Joseph & Tretsiakova-McNally, 2012b).
4. Some of the additives (DEHPi, TEPI, TPP and DOPO), and all of the reactive components, have aided in improving the thermal stability of the polymers possibly by delaying the decomposition process(s), which could be the result of their condensed-phase activity.
5. On the other hand, the addition of some other additives (TPPO, TEPa, DEPP and DEBP) resulted in early decomposition of the polymeric systems; but resulted in improved char yields as compared to pure PMMA. This latter effect was pronounced in the case of the additive, DEHPi, and least in the case of TEPa.

A detailed account of the analyses of thermograms of the PSt-based materials are discussed in the following section (see Table 3.8, and Figures 3.26 to 3.31). Here again, the relevant materials were grouped as in the case of PMMA-based systems (i.e. solid additives; liquid additives; reactives; additives/reactives belonging to the same chemical group: phosphonates, or phosphates)

Table 3.8 Some relevant parameters from the TGA analyses of PSt-based systems

Sl. No.	Sample	Induction Temp (°C)	Temp at 50 wt. % (°C)	Residue at 500°C (wt.%)	Final residue at 800°C (wt.%)
1	Polystyrene	129	408	0.5	0.4
2	PSt+TPP	105	408	0.2	0.0
3	PSt+TPPO	123	407	1.4	1.3
4	PSt+DOPO	118	420	1.0	0.8
5	PSt+DEHPi	73.0	441	8.1	6.9
6	PSt+TEPi	75.0	433	4.1	3.6
7	PSt+TEPa	119	424	1.8	2.1
8	PSt+DEPP	96.0	407	0.9	0.9
9	PSt+DEBP	100	415	0.9	0.8
10	PSt+DE-1-AEP	109	390	4.9	3.6
11	PSt+ADEPMAE	72.0	398	7.9	6.7
12	PSt+DEAEPa	74.0	393	6.8	5.5
13	PSt+DEpVBP	121	437	4.9	4.0

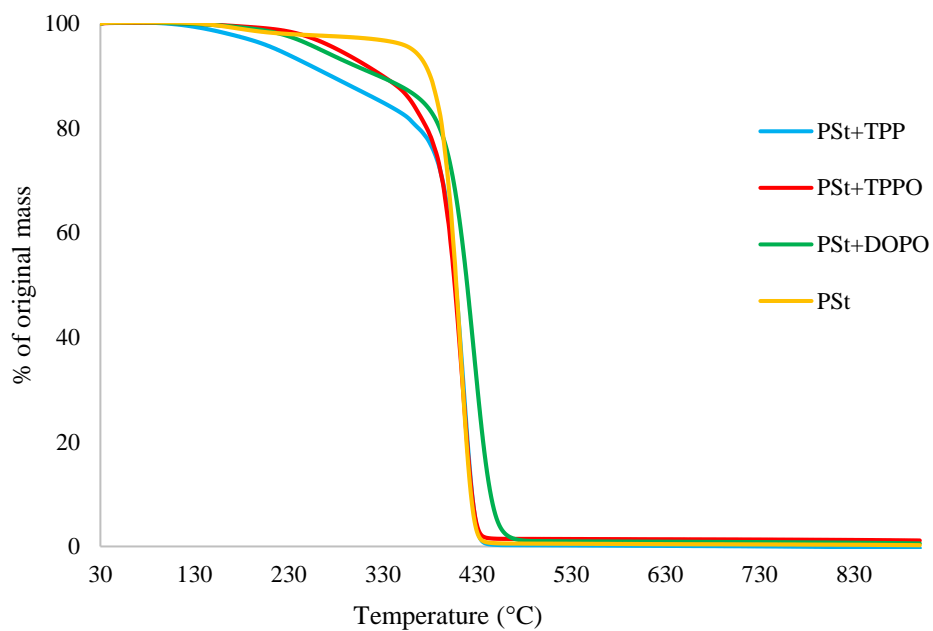


Figure 3.26 An overlay of the TGA curves of the PSSt-based materials with solid additives, at $10^{\circ}\text{C min}^{-1}$

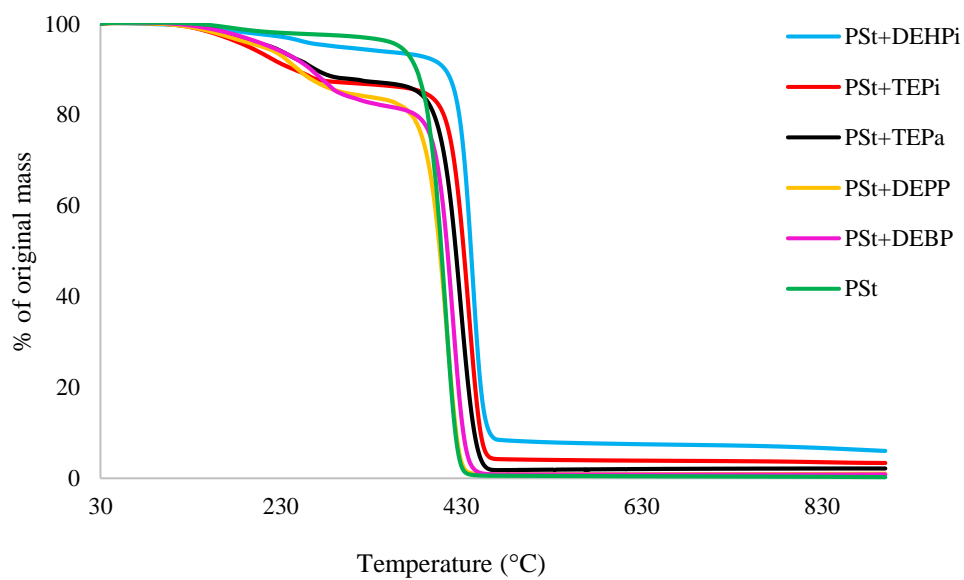


Figure 3.27 An overlay of the TGA curves of the PSSt-based materials with liquid additives, at $10^{\circ}\text{C min}^{-1}$

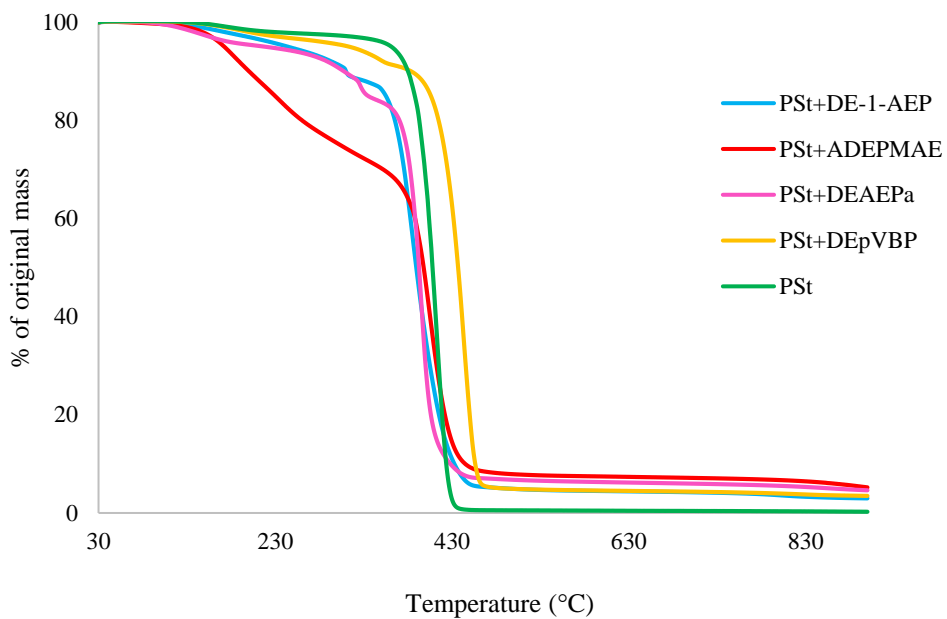


Figure 3.28 An overlay of TGA curves of the PSSt-based materials with reactives, at $10^{\circ}\text{C min}^{-1}$

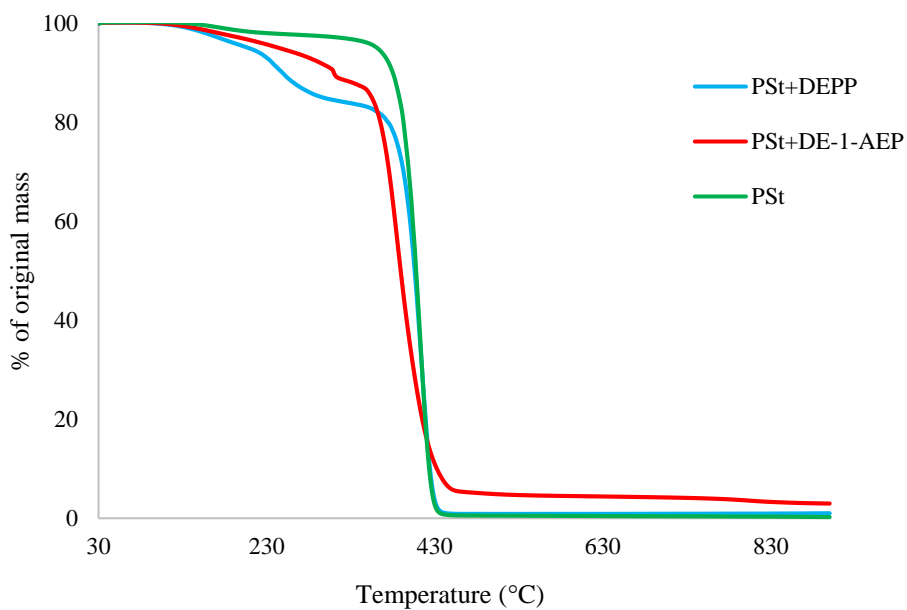


Figure 3.29 An overlay of the TGA curves of PSSt and PSSt+aliphatic phosphonate materials, at $10^{\circ}\text{C min}^{-1}$

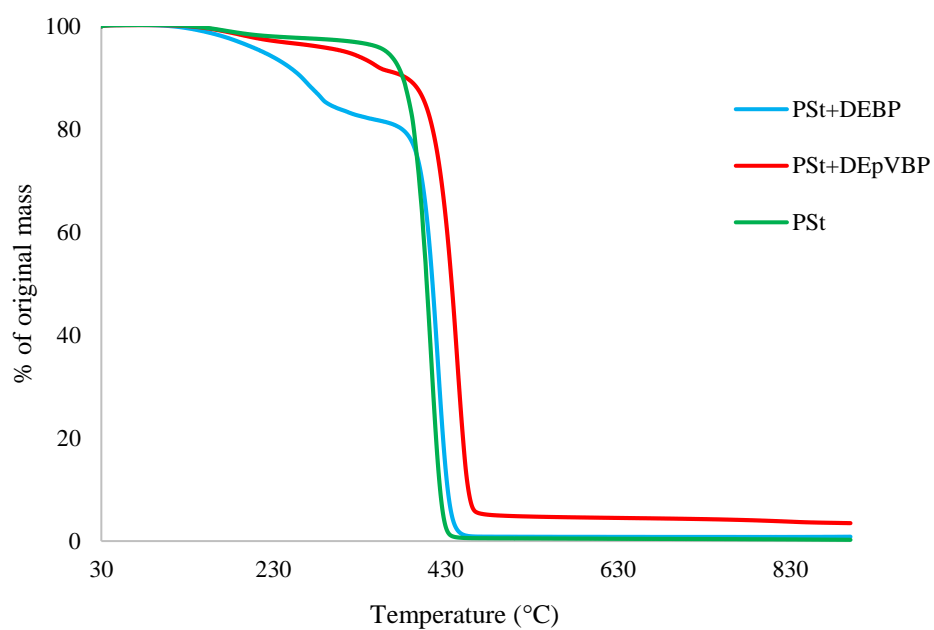


Figure 3.30 An overlay of the TGA curves of PSt and PSt+aromatic phosphonate materials, at $10^{\circ}\text{C min}^{-1}$

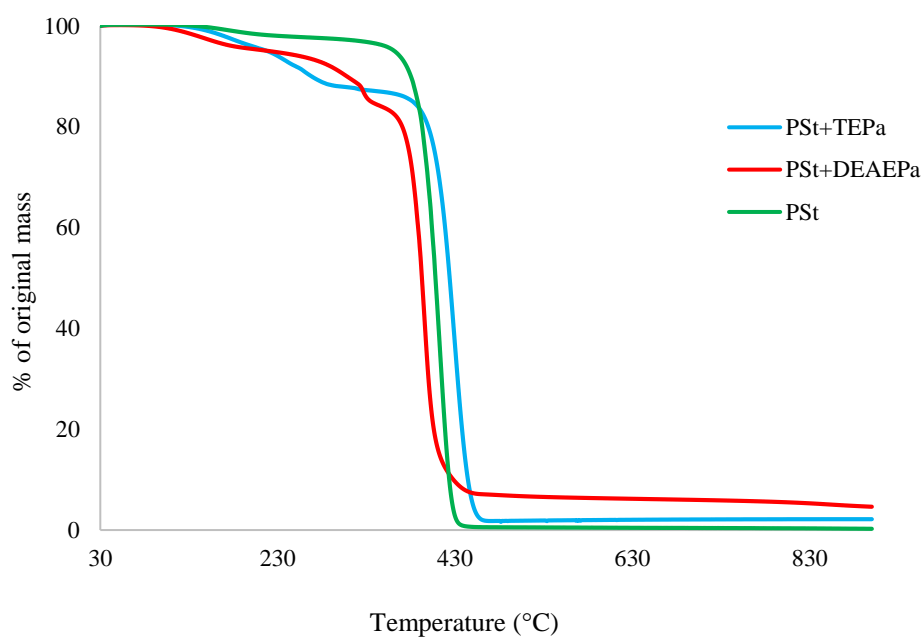


Figure 3.31 An overlay of the TGA curves of PSt and PSt+phosphate materials, at $10^{\circ}\text{C min}^{-1}$

As in the case of the PMMA-based polymers, several common similarities in the thermal behaviours can also be observed here (see Table 3.8). This leads to the following conclusions:

1. The induction temperatures seem to be lowered, to varying degrees, in the modified systems as compared to the parent polymer. As in the case of PMMA-based systems, this could be either due to the release of the additives, or owing to early thermal cracking of the pendent P-containing groups, prior to the onset of the main chain decomposition of the polymer.
2. The temperature at 50 wt.% mass loss were higher in several systems (DOPO, DEHPi, TEPI, TEPa, DEBP and DEpVBP), indicating an enhanced resistance to mass loss as compared to unmodified PSt. However, in all other systems a reverse trend was observed, except in the case of the system incorporating TPP, where the corresponding temperature remained unaltered.
3. The systems with the additive, DEHPi, and reactive, P/N monomer (ADEPMAE), produced the maximum amounts of char (6.88 and 6.71 wt.%, respectively). Other components have also assisted in producing more char (except TPP) although to different extents.

3.5.2 Kinetic analysis of the TGA thermograms

The equation for the non-isothermal kinetic analysis of TGA data is generally derived from the standard kinetic expression for an isothermal experiment, and can be given as follows (Bigger, 2015).

$$d\alpha/dt = k(T)f(\alpha) \quad (1)$$

where $f(\alpha)$ is a time-dependent function of α , the extent of reaction, $k(T)$ is a temperature-dependent rate constant, T is the absolute temperature and t is time. The function $f(\alpha)$ can take on many different forms depending on the reaction kinetics of the system under investigation.

In the case of non-isothermal kinetics, eqn. (1) can be conveniently changed from the time domain to the temperature domain, as follows (Vyazovkin, *et al.*, 2011).

$$d\alpha/dt = (dT/dt) \times (d\alpha/dT) = \beta \times (d\alpha/dT) \quad (2)$$

where β is the heating rate, which is usually maintained as a constant.

Substituting eqn. (2) in eqn. (1) and integrating between the corresponding limits of (0, T_0) and (α , T) where T_0 is the temperature at time $t = 0$ and T is the temperature at $t = t$ yields:

$$\int_0^\alpha d\alpha/f(\alpha) = (1/\beta) \int_{T_0}^T k(T)dT \quad (3)$$

Substituting the Arrhenius expression for $k(T)$ in eqn. (3) and defining $1/g(\alpha) = df(\alpha)/d\alpha$ yields:

$$g(\alpha) = (A/\beta) \int_{T_0}^T \exp(-E_a/RT)dT \quad (4)$$

where A is the Arrhenius A -factor, E_a is the apparent activation energy which is assumed to remain constant over the temperature range, and R is the ideal gas constant. The integral term in eqn. (4) is often referred to as the Arrhenius integral. Here, the valid assumption that $(A/\beta) \int_{T_0}^T \exp(-E_a/RT)dT \approx 0$ is usually made to simplify the Arrhenius integral so as to provide an analytical solution to eqn. (4) (Bigger, 2015). The resulting equation takes the following form:

$$g(\alpha) = (AE_a/R\beta) \int_x^\infty [\exp(-x)/x^2]dx \quad (5)$$

where $x = E_a/RT$ and can be written more simply as:

$$g(\alpha) = (AE_a/R\beta) \times p(x) \quad (6)$$

where the function $p(x)$ represents the integral $p(x) = \int_x^\infty [\exp(-x)/x^2]dx$.

Methods of data treatment

Vyazovkin, *et al.* (Vyazovkin, *et al.*, 2011; Vyazovkin & Wight, 1998) suggested that equations of the form depicted by eqn. (4) and those equations derived from it such as eqns. (5) and (6) represent the foundation for the so-called *integral methods* of analysis. Clearly, the analyses of TGA results utilizing such equations that require a solution to the Arrhenius integral are therefore deemed to be *integral methods* of analysis.

Conversely, the so-called *differential methods* of analysis avoid the historic difficulties that arise, for example, in solving Arrhenius integrals. This is achieved by combining eqns. (1) and (2) along with the expression for the Arrhenius equation without integrating the resulting equation:

$$d\alpha/dT = (A/\beta) \exp(-E_a/RT) \times f(\alpha) \quad (7)$$

Eqn. (8) is derived by taking the natural logarithms of both sides of eqn. (7):

$$\ln [(d\alpha/dT)/f(\alpha)] = \ln(A/\beta) - E_a/RT \quad (8)$$

An approach that utilizes the derivative $d\alpha/dT$ to process experimental data would thus be considered to be an example of a *differential* method of analysis.

In practice, the fact that all experimental data contain inherent noise can mean that one of the above methods of data analysis will produce more reliable values of the kinetic parameters than the other. It is claimed, for example, that integral methods are best suited

for integral data such as TGA data because differentiating integral data tends to magnify the noise (Vyazovkin & Wight, 1998).

Another approach to the processing of TGA data in order to obtain kinetic parameters involves the so-called *iso-conversional* methods that have an advantage of not needing to have prior knowledge of the mathematical form of $f(\alpha)$. Such methods are based on the principle that at a constant degree of conversion the rate of a reaction is only a function of temperature (Friedman, 1964; Ozawa, 1965).

Algorithms for non-isothermal TGA data analysis.

Algorithms and associated software suite were devised, in house, to facilitate a convenient method of analyses for a wide range of non-isothermal TGA data (Bigger, *et al.*, 2015; Bigger, *et al.*, 2015). These computer-based algorithms are: (i) an algorithm for identifying suitable kinetic models for fitting the experimental data based on theoretical reference characteristics calculated by Dollimore, *et al.* (Dollimore, *et al.*, 1997) for a given set of (T, α) input data and (ii) an iterative arithmetic algorithm that solves eqn. (8) without invoking assumptions, or approximations, in order to extract the two Arrhenius parameters. The overall approach delivers the so-called kinetic triplet (i.e. A , E_a and n) information and also enables one to assess whether the analysis has been appropriate in so far as the decomposition occurred by a single mechanism over the temperature range.

Algorithm to identify kinetic model

This algorithm systematically calculates from the experimental (T, α) data the values of three characteristic parameters $(d\alpha/dT)_{max}$, α_{max} and ΔT , where $(d\alpha/dT)_{max}$ is the maximum value of the derivative of α with respect to temperature, α_{max} is the value of α at which the maximum derivative value occurs, and ΔT is the half-height width of the $d\alpha/dT$ vs. T plot. The parameters are then compared with the corresponding ranges for these given in the reference data (Dollimore, *et al.*, 1997) for a number of different kinetic models, and a fit parameter, ρ , is calculated for each model. The fit parameter is such that $0 \leq \rho \leq 1$ and $\rho = 1$ is deemed to be a *perfect* fit.

Iterative numerical TGA analysis algorithm

Taking the natural logarithm of both sides of eqn. (8) and allowing for separate experimental measurements at different values of α_i as well as allowing for different values of the activation energy yields:

$$\delta_i(\alpha_i, E_{a,j}) = \ln[g(\alpha_i)] - \ln[p(\chi_i)] = AE_{a,j}/R\beta \quad (9)$$

Where $\delta_i(\alpha_i, E_{a,j})$ represents a single value of a difference function that exists for a given value of α_i and its corresponding χ_i value. The value of χ_i at a given value of $E_{a,j}$ is calculated from $\chi_i = E_{a,j}/RT_i$ where T_i is the temperature corresponding to the particular χ_i value.

Taken together, the two algorithms described herein provide a seemingly useful approach to obtaining plausible kinetic triplets for a given system under investigation provided complexities such as mechanistic changes are not encountered during the non-isothermal experiment (Bigger, *et al.*, 2015). It should be noted that for the analysis, we chose a moderate heating rate of $10^\circ\text{C min}^{-1}$ as it is assumed that at this heating rate, most of the representative decomposition pathways of the substrates are essentially captured.

As the first step, data of the unmodified PMMA bulk sample were initially used as the input for the software with a view to establishing the best-suited kinetic model. From the run, it was found out that PMMA followed the two-dimensional diffusion (D2) model (a typical value for PMMA is shown to be 180 kJ mol^{-1}). Therefore, for the ensuing analyses, this model was applied. Values of the apparent activation energy (E_a), thus obtained, for the various PMMA-based bulk samples are given in the table below (Table 3.9).

Table 3.9 Values of the apparent energy of activation (E_a) and other relevant parameters of PMMA-based samples obtained using the software (model: D2 Two-dimensional diffusion)

Sl. No.	Sample	Apparent activation energy (E_a , kJ mol ⁻¹)	A (min ⁻¹)	R ² values	α -value range
1	PMMA	183	1.11 x 10 ¹⁴	0.9399	0.1 to 0.9
2	PMMA+TPP	139	3.34 x 10 ¹⁰	0.9991	0.3 to 0.9
3	PMMA+TPPO	114	2.19 x 10 ⁸	0.9277	0.1 to 0.9
4	PMMA+DOPO	235	6.61 x 10 ¹⁷	0.9871	0.1 to 0.9
5	PMMA+DEHPi	125	4.00 x 10 ⁸	0.9038	0.1 to 0.9
6	PMMA+TEPi	173	3.46 x 10 ¹³	0.9963	0.2 to 0.9
7	PMMA+TEPa	101	6.15 x 10 ⁷	0.9714	0.4 to 0.9
8	PMMA+DEPP	137	1.61 x 10 ¹⁰	0.9344	0.1 to 0.9
9	PMMA+DEBP	109	2.67 x 10 ⁸	0.9796	0.3 to 0.9
10	PMMA+DE-1-AEP	140	6.76 x 10 ⁹	0.9526	0.1 to 0.9
11	PMMA+ADEPMAE	169	1.30 x 10 ¹²	0.9475	0.1 to 0.9
12	PMMA+DEAEPa	160	2.96 x 10 ¹¹	0.9514	0.1 to 0.9
13	PMMA+DEpVBP	121	9.13 x 10 ⁸	0.9878	0.2 to 0.8

It should be noted that the apparent activation energy obtained in each case was an average value, over the entire region pertaining to the main step of the decomposition, as observed in the respective thermograms; hence, the spread of α values were also correspondingly chosen (see the entries in the last column of the Table 3.9). In most cases, a reduction in the activation energies in the case of the modified samples can be observed. It is also relevant to note that the average values of E_a can also be influenced by their relatively lower α values (where α is around 0.1 to 0.2). Here it is to be assumed that noticeable degrees of volatilization of low-molecular weight additive (typically, in the case of some liquid compounds) can occur, where the energetic requirements are much lower than those required to break typical covalent bonds. Such an effect seems to also reflect in the correspondingly lower values for the induction temperatures in the thermograms. A graphical illustration of the variation of the E_a values for each sample is given in Figure 3.30, below. It is relevant to note that in following figures (3.32, 3.33, 3.35, 3.36, 3.50, 3.51, 3.52- 3.55) each point along the abscissa denotes a particular

polymeric system, and in all cases the same hierarchy in plotting the individual systems along the axis is retained (i.e. unmodified polymer, followed by modified versions with the solid additives, liquid additives, and finally the reactives).

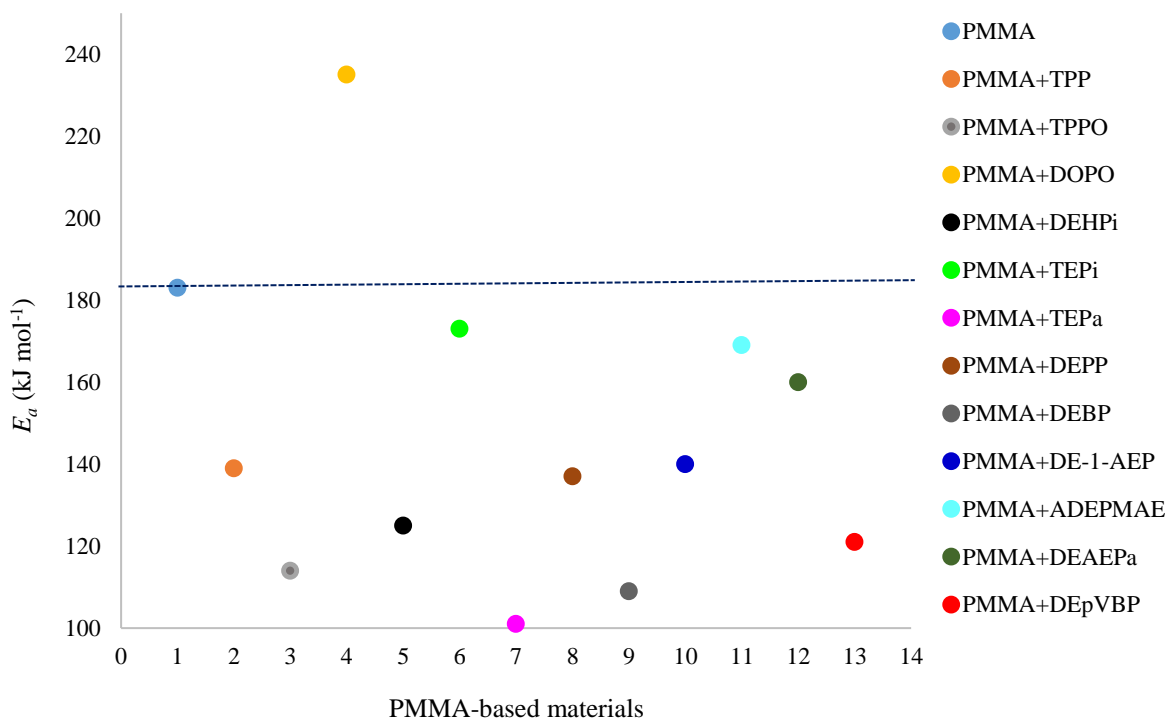


Figure 3.32 A plot of the apparent energy of activation (E_a) for the various PMMA-based materials

Here, PMMA is taken as a reference point in order to identify the extent of spread of the E_a values. The DOPO modified PMMA (yellow dot in the figure) is found to have the highest average value of the E_a (235 kJ mol⁻¹). All the other samples exhibited a lower apparent activation energy than unmodified PMMA. This seems to suggest that the presence of DOPO enhanced the thermal stability of PMMA, whereas in all other cases the modifications was found to decrease this.

The E_a values for PSt-based samples were also obtained from software runs, following the same steps as those used for the PMMA samples. It is relevant to note here that values quoted are averaged over the main decomposition step, and the range of α values were also chosen appropriately. The results are collated in the Table 3.10, below.

Table 3.10 Energy of activation (E_a) and other relevant parameters of PSt-based samples obtained using the software (model: F1 First Order)

Sl. No.	Sample	Apparent activation energy (E_a , kJ mol ⁻¹)	A (min ⁻¹)	R^2 values	α -value range
1	PSt	270	2.68×10^{20}	0.9980	0.1 to 0.9
2	PSt+TPP	118	2.69×10^8	0.9125	0.2 to 0.8
3	PSt+TPPO	162	9.52×10^{11}	0.9706	0.2 to 0.8
4	PSt+DOPO	165	8.94×10^{11}	0.9939	0.2 to 0.8
5	PSt+DEHPi	305	1.23×10^{22}	0.9943	0.1 to 0.9
6	PSt+TEPi	229	3.88×10^{16}	0.9908	0.2 to 0.8
7	PSt+TEPa	210	2.24×10^{15}	0.9935	0.2 to 0.8
8	PSt+DEPP	157	3.82×10^{11}	0.9652	0.2 to 0.8
9	PSt+DEBP	137	6.79×10^9	0.9218	0.2 to 0.8
10	PSt+DE-1-AEP	97.0	1.00×10^7	0.9815	0.1 to 0.9
11	PSt+ADEPMAE	130	3.82×10^9	0.9978	0.4 to 0.9
12	PSt+DEAEPa	216	4.26×10^{16}	0.9871	0.2 to 0.8
13	PSt+DEpVBP	223	1.08×10^{16}	0.9923	0.2 to 0.8

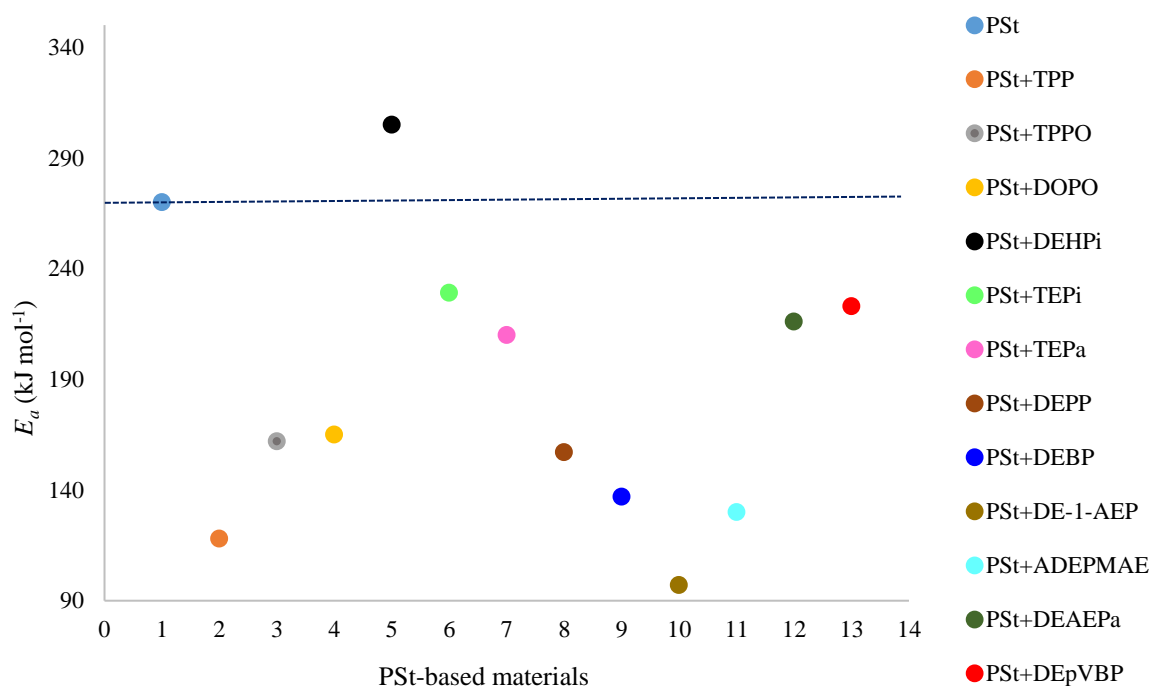


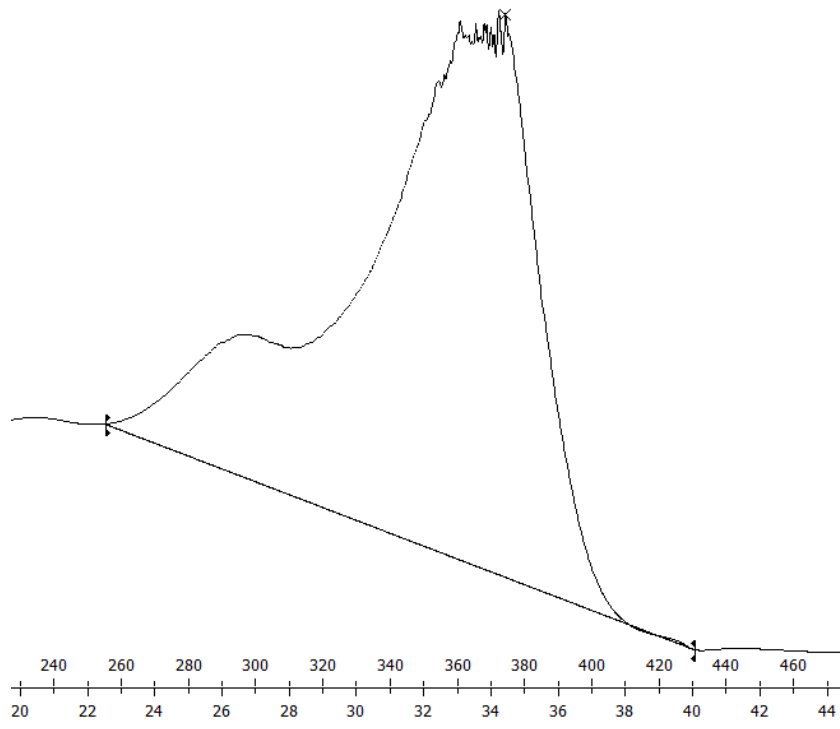
Figure 3.33 A plot of the apparent activation energy (E_a) for various PSt-based materials

The virgin polymer was found to follow the kinetic model that was in conformance with first order (F1) kinetics (E_a value typically in the region of 180 to 220 kJ mol⁻¹). Therefore, this particular model was subsequently applied in analysing all the modified versions of the styrene polymers. As in the case of PMMA samples, a reduction in the average activation energy values can be observed, except for the system containing the phosphite additive (DEHPi); here a relatively higher value (305 kJ mol⁻¹) was obtained (see in figure above). Therefore, it is to be inferred here that except in the case of DEHPi, in all other cases, the modification resulted in decreased thermal stability of the parent polymer.

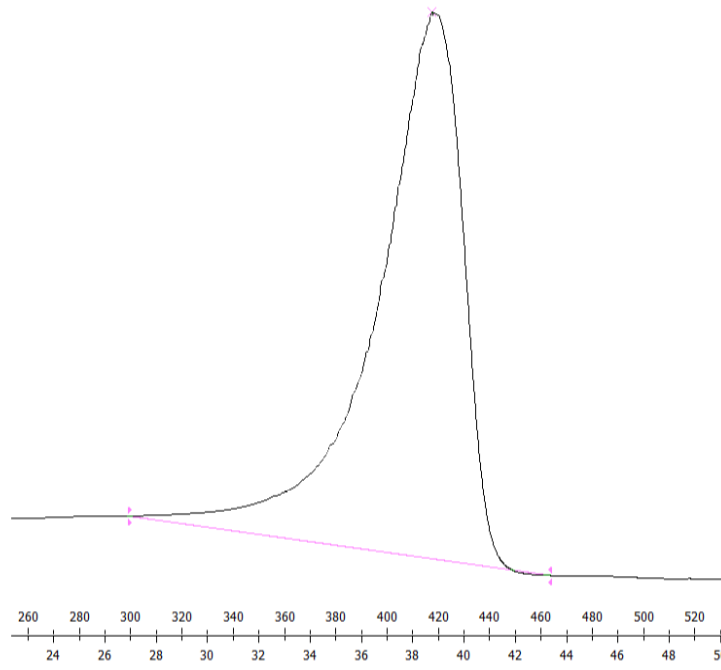
3.5.3 Differential Scanning Calorimetry

Heats of pyrolysis (ΔH_{pyro}) data for various PMMA- and PSt-based bulk samples were obtained from the DSC runs of the samples at a heating rate of 10°C min⁻¹ in the temperature range 30-550°C. The samples were accurately weighed into stoppered aluminum pans, and subsequently a pinhole was made with a view to releasing any excess pressure due to the emanating gaseous species, if present. Here, the Y-axis denotes the heat flow in mV. The ΔH_{pyro} values in each case were calculated using the following equation:

$$\Delta H_{pyro} = \frac{\text{area of the peak (mJ)}}{\text{sample weight (mg)}} \quad (10)$$



(A)



(B)

Figure 3.34 An illustration showing the deduction of the values of ΔH_{pyro} from the DSC curves in the case of unmodified polymers: (A) PMMA and (B) PSt

Given below are the results obtained for the PMMA-based bulk samples from the DSC runs as well as their corresponding ΔH_{pyro} values, calculated as per the equation shown above (eqn. 10).

Table 3.11 Heats of pyrolysis data of PMMA-based materials obtained from DSC tests

Sl. No.	Samples	Heats of pyrolysis, ΔH_{pyro} (mJ mg ⁻¹)
1	PMMA	420
2	PMMA+TPP	660
3	PMMA+TPPO	330
4	PMMA+DOPO	640
5	PMMA+DEHPi	1030
6	PMMA+TEPi	790
7	PMMA+TEPa	320
8	PMMA+DEPP	300
9	PMMA+DEBP	310
10	PMMA+DE-1-AEP	450
11	PMMA+ADEPMAE	680
12	PMMA+DEAEPa	274
13	PMMA+DEpVBP	340

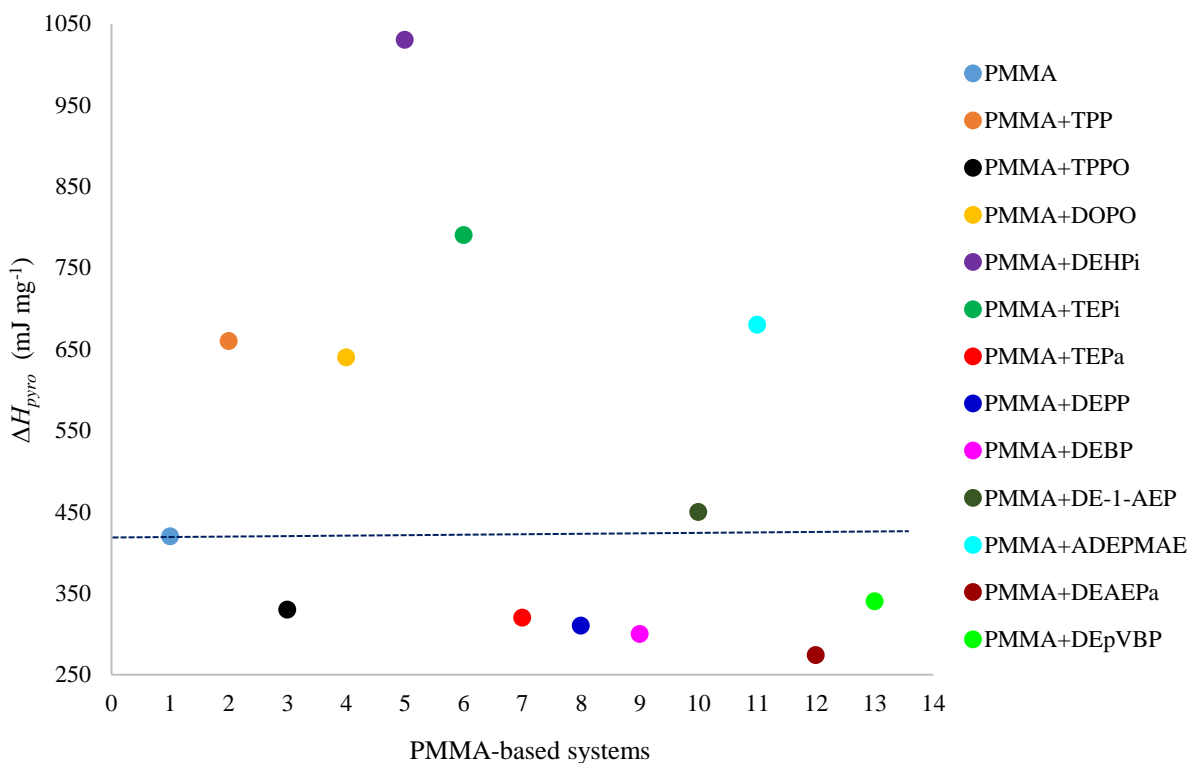


Figure 3.35 A plot of heats of pyrolysis of various PMMA-based materials

It can be observed from the Table 3.11 and Figure 3.35 that PMMA modified with TPPO, TEPa, DEPP, DEBP (additives), and DEAEPa and DEpVBP (reactives), exhibit lower values of ΔH_{pyro} than the unmodified material. The lowest value observed was that for PMMA+DEAEPa (274 mJ mg^{-1}). On the other hand, the incorporation of the additives TPP, DOPO, DEHPi, TEPi and the copolymerization with the monomers DE-1-AEP and ADEPMAE has resulted in higher values of ΔH_{pyro} , with PMMA+DEHPi being the highest (1030 mJ mg^{-1}). The relatively widespread values for heats of pyrolysis (essentially endothermic in nature) among the various systems can be thought to arise from: (i) the difference in the energy requirements accompanying the phase changes of the additives (i.e., enthalpy of vapourization); (ii) the energetic needs for bond cleavage(s) of the polymeric chains; and (iii) thermal energy requirements for the cracking of the pendent modifying group and/or altered paths of the main chain decomposition process(s), as in the case of reactively modified systems.

The heats of pyrolysis values calculated from the DSC curves for the PSt-based samples are given below (see Table: 3.12 and Figure: 3.36).

Table 3.12 Heats of pyrolysis data of PSt-based materials obtained from DSC tests

Sl. No.	Samples	Heats of pyrolysis, ΔH_{pyro} (mJ mg ⁻¹)
1	PSt	810
2	PSt+TPP	650
3	PSt+TPPO	720
4	PSt+DOPO	730
5	PSt+DEHPi	540
6	PSt+TEPi	560
7	PSt+TEPa	680
8	PSt+DEPP	690
9	PSt+DEBP	660
10	PSt+DE-1-AEP	560
11	PSt+ADEPMAE	470
12	PSt+DEAEPa	324
13	PSt+DEpVBP	520

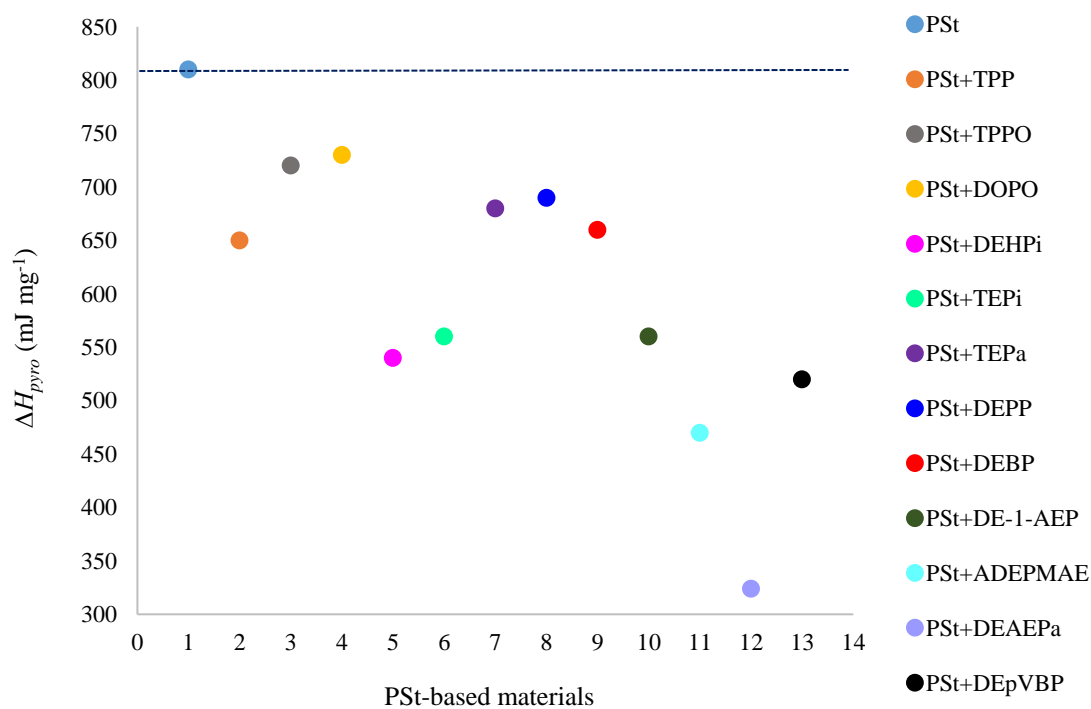


Figure 3.36 A plot of heats of pyrolysis of PSt-based materials

Here, a decrease in the values of ΔH_{pyro} in the case of the modified materials can be observed, with the PSt+DEAEPa system exhibiting the lowest value of 324 mJ mg⁻¹. On the other hand, it is interesting to note that such a trend was completely absent in the PMMA-based materials. Therefore, it is highly likely that in the case of PSt-based systems, some degree of co-operative interaction between the polymeric matrix and the modifying groups are present during the phase changes that occur during a DSC run. It is also relevant to note that the modification with phosphate co-monomer, DEAEPa, showed the least values in both the systems.

3.5.4 Pyrolysis Combustion Flow Calorimetry (PCFC)

This technique assesses the flammability of materials using only milligrams of the sample and thus can be used as a tool for screening new materials. The parameters obtained through PCFC test have been found to correlate fairly well with the conventional flame tests such as cone calorimetry, limiting oxygen index (LOI) and UL 94 (Cogen, *et al.*, 2009; Lin, *et al.*, 2007). This technique was also extensively used in the case of several commercially important thermoplastic materials (ASTM D7309) (Joseph & Tretsiakova-McNally, 2012b; Morgan, *et al.*, 2012; Scharrel, *et al.*, 2007; Sonnier, *et al.*, 2013; Tretsiakova-McNally & Joseph, 2015).

Essentially, the technique works on the principle of accurately measuring the consumption of oxygen accompanying the combustion of the volatiles produced from the test sample. Hence the method comes under the class of calorimetry called *oxygen consumption* calorimetry. This type of a calorimetry is originally based on the experimental observation that the net heat of combustion of typical organic molecules per mole of oxygen consumed is relatively a constant (i.e. 419 ± 19 kJ mol⁻¹, or 13.1 ± 0.6 kJ g⁻¹). This value was found to be largely unaffected by the chemical constitution of the material undergoing combustion. Huggett later confirmed that this result is valid for a range of combustible forest products, chemical compounds, and organic polymers, and eventually came to be known as the Huggett's principle (Huggett, 1980). Subsequently, this principle became the basis and preferred method for determining the heat released by various solid fuels undergoing flaming combustion, a classical example being the cone calorimeter (ISO: 5660; AS/NZS: 3837).

In a PCFC instrument, a linear heating program is employed (typically 1°C s^{-1}) where milligrams of a test sample (*ca.* 10 mg) is degraded in nitrogen. Here, the production of volatiles and char residues (as the case may be) are assumed to mimic what is happening to a material prior to the onset of flaming combustion in a real fire scenario. Subsequently, the volatiles are swept from the pyrolysis zone, by an inert stream of (nitrogen) to a second chamber (a tubular furnace) kept at flame temperatures (*ca.* 900°C), and a forced non-flaming combustion is affected under an atmosphere of a nitrogen/oxygen mixture (80/20 vol./vol. in the present case). The products of combustion (typically CO_2 , H_2O , and other oxides depending on the chemical composition of the solid fuel) are removed from the carrier gas stream, by using suitable scrubbers, and the transient heat release rate is calculated from the measured flow rate and the oxygen concentration, after applying a correction factor for the dispersion of the flow. The instrument produces a plot of the heat release rate (HRR in W g^{-1}).

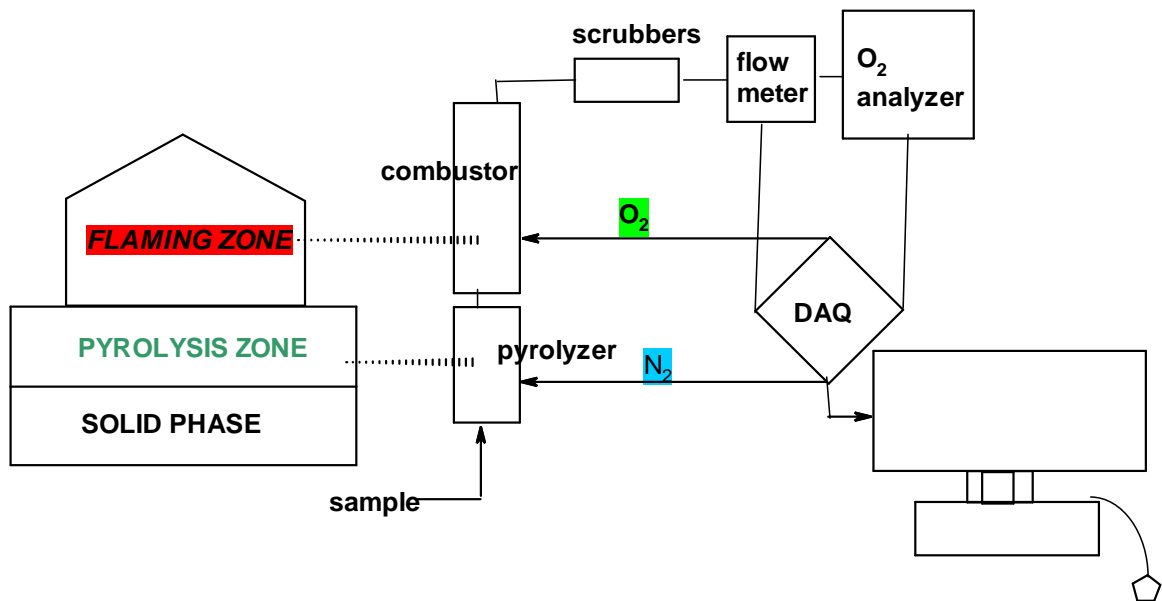


Figure 3.37 A schematic diagram of the PCFC instrument

The maximum value of the HRR (i.e. peak heat release rate: pHRR) normalized for the initial sample mass and heating rate will yield the heat release capacity ($\text{J g}^{-1} \text{K}^{-1}$). This parameter can be considered as an intrinsic property of the material, which will only

depend on the chemical constitution of the materials, and its value can be considered as the flammability parameter for the material (Solorzano, *et al.*,2019). The integration of the PCFC heat release rate curve over the time will yield the total heat released (THR), and the latter upon normalisation of the mass of the material that underwent combustion will lead to the effective heat of combustion of the material (see Table 3. 13).

$$EHC (h_c) = \frac{THR}{1-Y_p} \quad (11)$$

Where Y_p is the ratio of initial mass on the sample to mass of the char residue formed.

For example, in the case of PMMA+TPP:

$$EHC (h_c) = \frac{THR}{1-Y_p} = \frac{23.2}{1-0.43} = 24.20 \text{ kJ g}^{-1}$$

a. PMMA-based polymers

The PCFC runs for each bulk sample was performed in triplicate in order to ensure its reproducibility, and the average values are presented below in Table 3.13.

Table 3.13 PCFC data of PMMA-based materials

Sl. No.	Samples	Temp to pHRR (°C)	pHRR (W g ⁻¹)	THR (kJ g ⁻¹)	HRC (J g ⁻¹ K ⁻¹)	Char yield (wt.%)	EHC (kJ g ⁻¹)
1	PMMA	386	358	22.8	358	0.0	22.8
2	PMMA+TPP	405	339	23.2	343	4.3	24.2
3	PMMA+TPPO	373	277	23.8	283	2.9	24.5
4	PMMA+DOPO	398	413	24.8	414	0.4	24.9
5	PMMA+DEHPi	393	493	22.2	493	3.2	22.9
6	PMMA+TEPi	397	439	21.4	439	1.4	21.7
7	PMMA+TEPa	388	276	20.6	277	0.4	20.7
8	PMMA+DEPP	387	253	22.0	254	0.8	22.2
9	PMMA+DEBP	386	294	20.4	303	1.4	20.7
10	PMMA+DE-1-AEP	399	367	22.4	368	2.7	23.0
11	PMMA+ADEPMAE	420	373	22.1	372	11	24.9
12	PMMA+DEAEPa	426	336	22.3	343	0.0	22.3
13	PMMA+DEpVBP	432	271	22.5	308	5.4	23.8

It can be noticed from the table that the values of pHRR, HRC, THR and EHC of the modified samples vary to different extents, with some modified versions having higher values than the unmodified PMMA, whereas others having lower values. For example, in the case of solid additives, a noticeable reduction in the value of pHRR was observed for the TPPO modified version (277 W g^{-1}), whereas the material incorporating DOPO showed a higher value (413 W g^{-1}). The systems with the liquid additives, i.e. PMMA with DEHPi and TEPI, also showed relatively high pHRR values (493 and 439 W g^{-1} , respectively). This can be attributed to the higher volatility of the liquid samples compared to the solid versions, and that they can contribute to the fuel load, rather than showing combustion inhibitory effects. The other liquid additives used in the present study, including TEPA, DEPP and DEBP, seem to assist in reducing the pHRR values of the polymer matrix (276 , 253 and 294 W g^{-1} , respectively). The difference in the combustion inhibitory effects amongst the liquid additives can be attributed to their: volatility; chemical natures; decomposition pathways, and hence the nature and composition of the volatiles; etc. Amongst the reactively modified versions, a slight decrease in the pHRR value is only observed in the case of the sample with DEAEPa (the phosphate monomer) which tends to form phosphoric acid species more easily (Ebdon, *et al.*, 2000; Joseph & Tretsiakova-McNally, 2012a) and a noticeable drop in the case of DEpVBP- a styrenic-type monomer that can enhance the formation condensed aromatic species (Ebdon, *et al.*, 2000). The graphical representations of data pertaining to the variation of the HRRs with temperature are shown in Figures 3.38 to 3.43.

The evolution of volatile species, during the early stages of the TGA thermograms, is also reflected in the HRR curves as shoulder peaks, indicating that these fragments in effect act as fuel loads for combustion reactions in the latter stage of the PCFC tests (i.e. the second stage that involves aerobic and forced combustion at *ca.* 750°C). This attribute can also be clearly seen in the first derivative of the TGA thermograms, which favorably compare to the HRR curves, in their general and overall profiles (see Figures 3.39, 3.41 and 3.43). In short, under a programmed heating regime (i.e. 1°C s^{-1} in nitrogen, which is similar to a heating rate of $60^\circ\text{C min}^{-1}$ in TGA) as encountered in the first phase of the PCFC test, the modifying groups (both the additive compounds, or the reactive versions, as the case may be) do not seem to interact co-operatively with the decomposition of the underlying parent polymer matrix, in that they seem to fail to induce any combustion inhibitory effects.

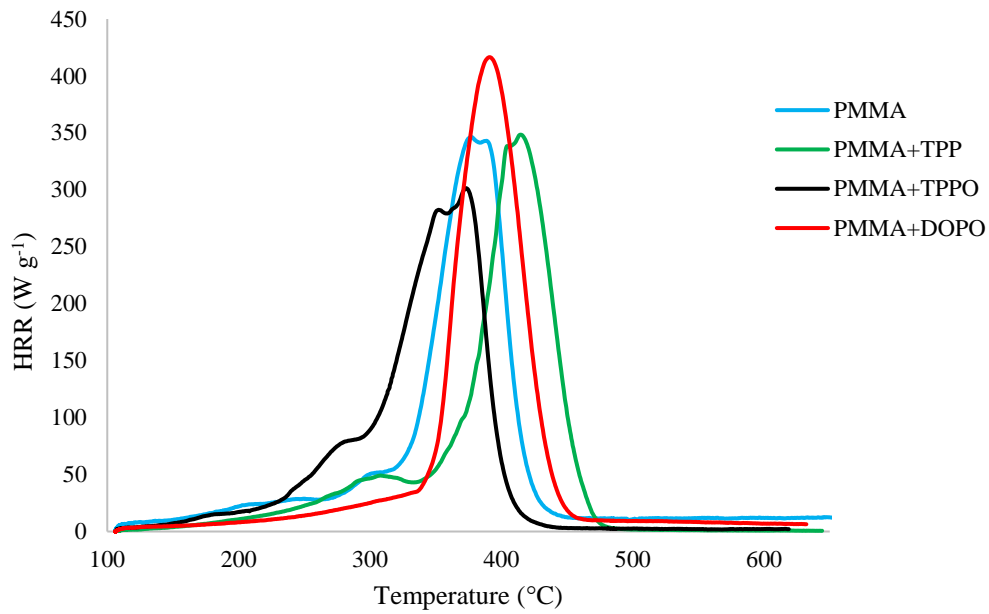


Figure 3.38 An overlay of the HRR curves obtained from the PCFC runs of all the PMMA-based systems with solid additives

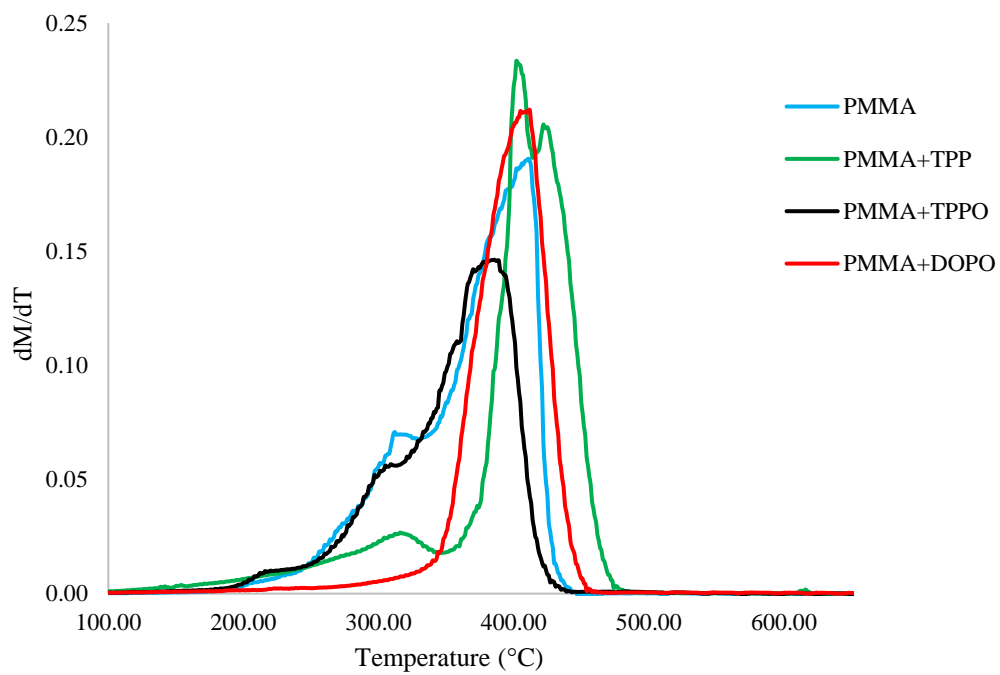


Figure 3.39 An overlay of the first derivative of the TGA curves of all the PMMA-based systems with solid additives, at $60^{\circ}\text{C min}^{-1}$

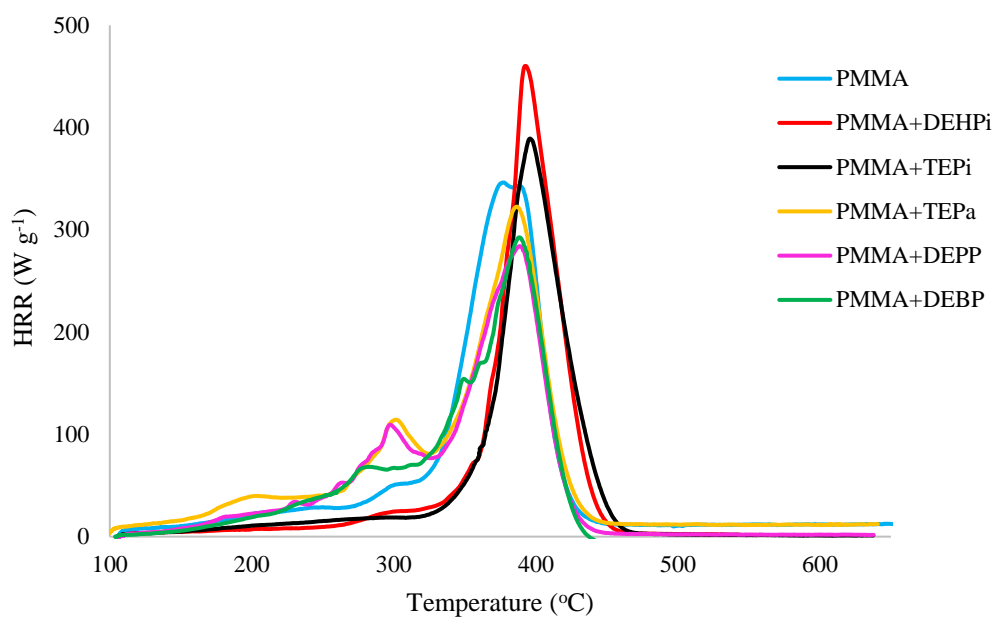


Figure 3.40 An overlay of the HRR curves obtained from PCFC runs of all the PMMA- based systems with liquid additives

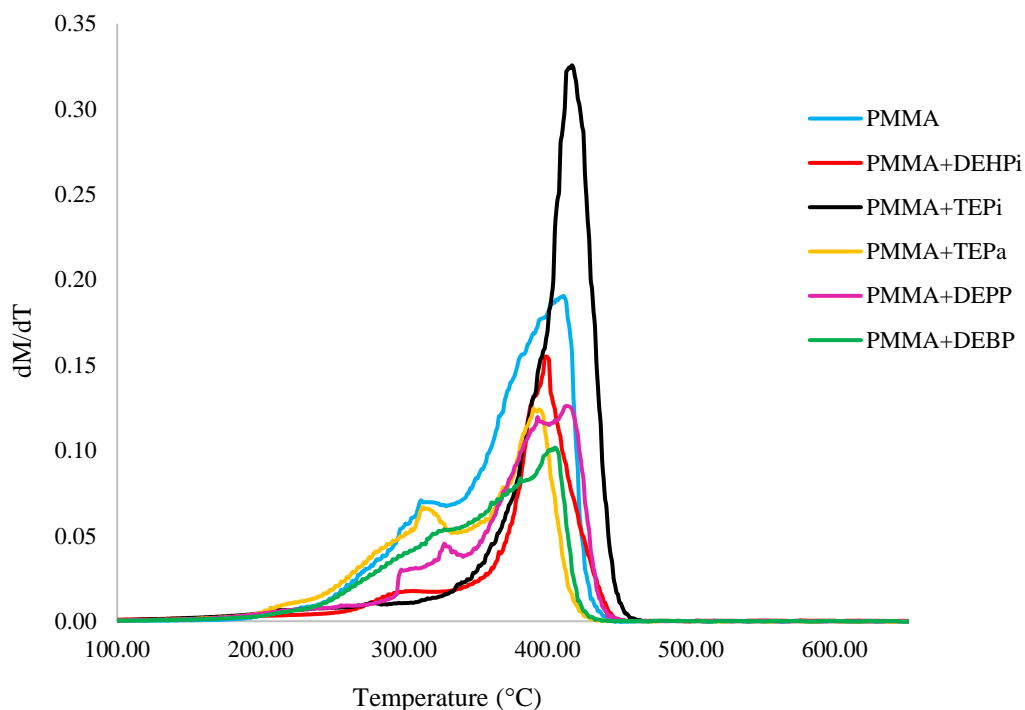


Figure 3.41 An overly of the first derivative TGA curves of all the PMMA-based systems with liquid additives, at $60^{\circ}\text{C min}^{-1}$

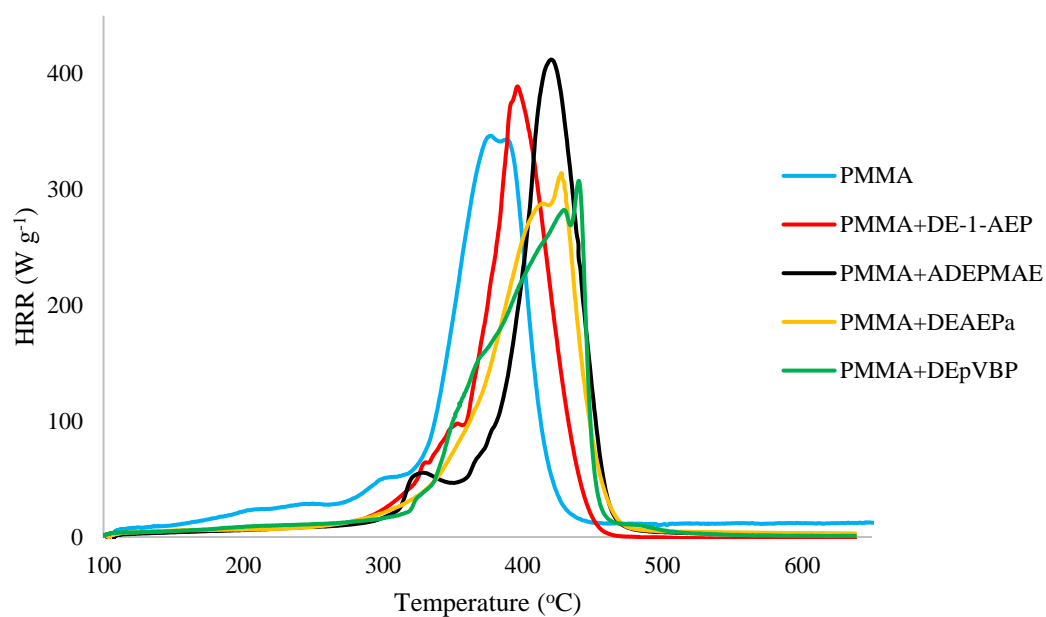


Figure 3.42 An overlay of the HRR curves obtained from the PCFC runs of all the PMMA-based systems with reactives

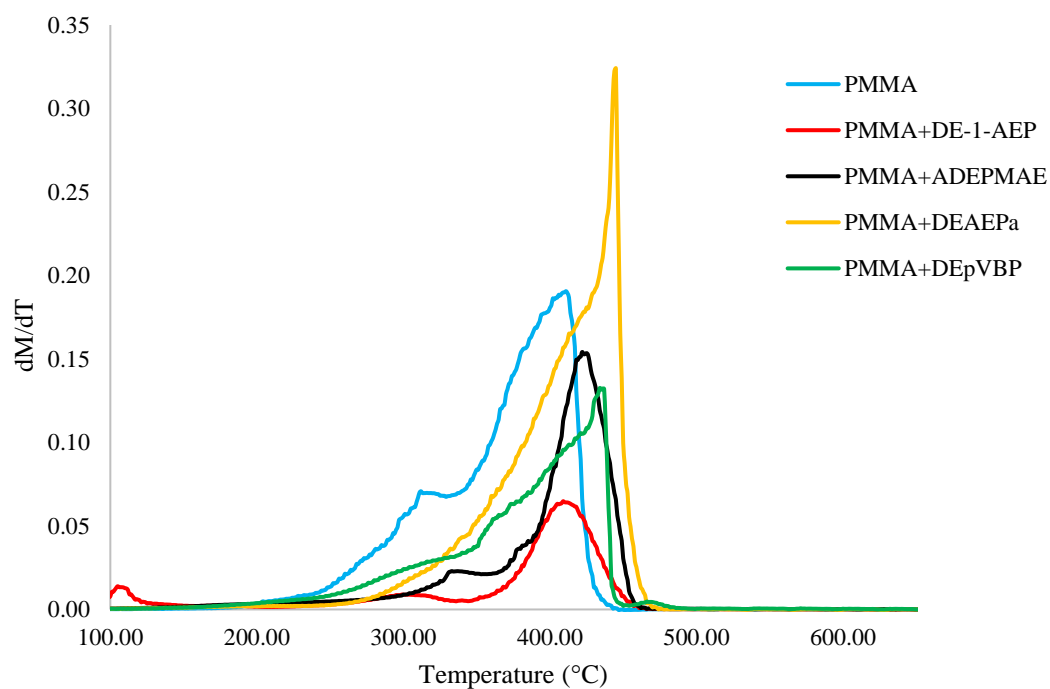


Figure 3.43 An overlay of the first derivative of TGA derivative curves of all the PMMA-based systems with reactives, at $60^{\circ}\text{C min}^{-1}$

b. Polystyrene-based polymers

The PCFC data of the PSt-based samples are shown below in Table 3.14.

Table 3.14 PCFC data of PSt-based materials

Sl. No.	Samples	Temp to pHRR (°C)	pHRR (W g ⁻¹)	THR (kJ g ⁻¹)	HRC (J g ⁻¹ K ⁻¹)	Char yield (wt.%)	EHC (kJ g ⁻¹)
1	PSt	434	840	37.1	852	4.4	38.8
2	PSt+TPP	434	682	35.9	686	6.5	38.4
3	PSt+TPPO	434	717	36.7	729	0.0	36.7
4	PSt+DOPO	446	618	36.3	621	0.0	36.3
5	PSt+DEHPi	462	778	32.9	778	5.9	35.0
6	PSt+TEPi	463	771	31.9	776	5.6	33.8
7	PSt+TEPa	444	743	34.2	772	0.0	34.2
8	PSt+DEPP	438	815	34.2	813	0.0	34.2
9	PSt+DEBP	440	792	34.5	794	0.0	34.5
10	PSt+DE-1-AEP	409	501	33.0	499	7.4	35.6
11	PSt+ADEPMAE	431	425	23.8	424	5.7	25.2
12	PSt+DEAEPa	416	757	31.9	755	6.4	34.1
13	PSt+DEpVBP	468	655	34.6	653	2.9	35.6

From the above table it can be seen that all the modified versions have lower values of the relevant parameters such as, pHRR, THR, HRC and EHC, when compared to the unmodified polystyrene sample. The material modified with the P/N-monomer, ADEPMAE, shows the lowest values for pHRR (425 W g⁻¹), THR (23.8 kJ g⁻¹), HRC (424 J g⁻¹ K⁻¹) and EHC (25.2 kJ g⁻¹), indicating that the modifying group has the most favorable effect amongst the systems under consideration. It is also relevant to note that the char yields obtained for the different samples showed a wide variability, where no underlying trend can be found.

As in the case of the PMMA systems, the first derivative of the TGA thermograms and HRR curves showed significant correspondence, and this feature was even more pronounced than the former case. In contrast to the PMMA-based polymers, the PSt-based polymers also showed a decreasing trend in the values of all the relevant parameters from the PCFC runs. This points towards the fact that, when the modified versions of the

PSt-based systems degrade, there appears to be a noticeable degree of co-operative interaction between the modifying groups and parent polymeric chains.

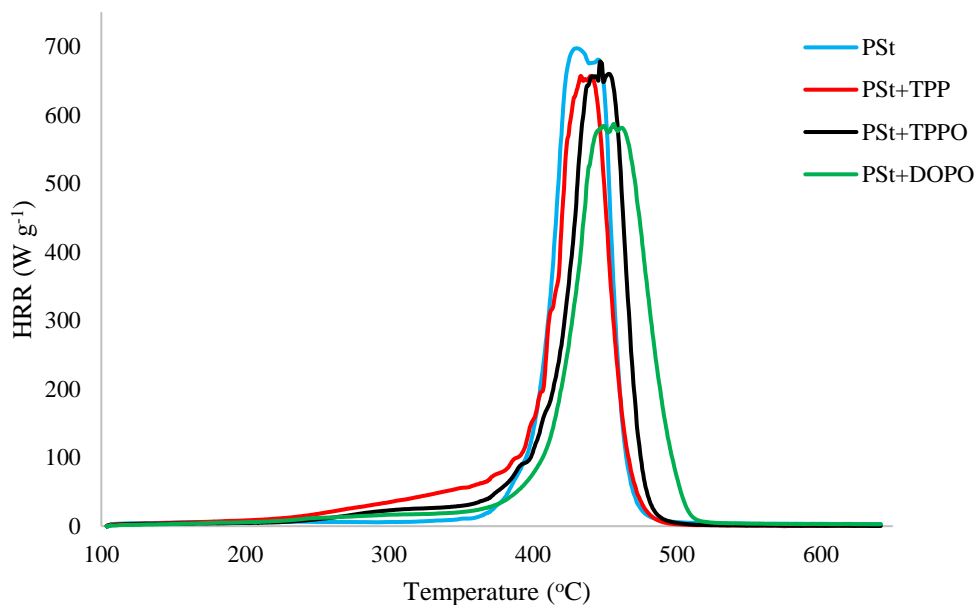


Figure 3.44 An overlay of the HRR curves obtained from the PCFC runs of all the PSt-based systems with solid additives

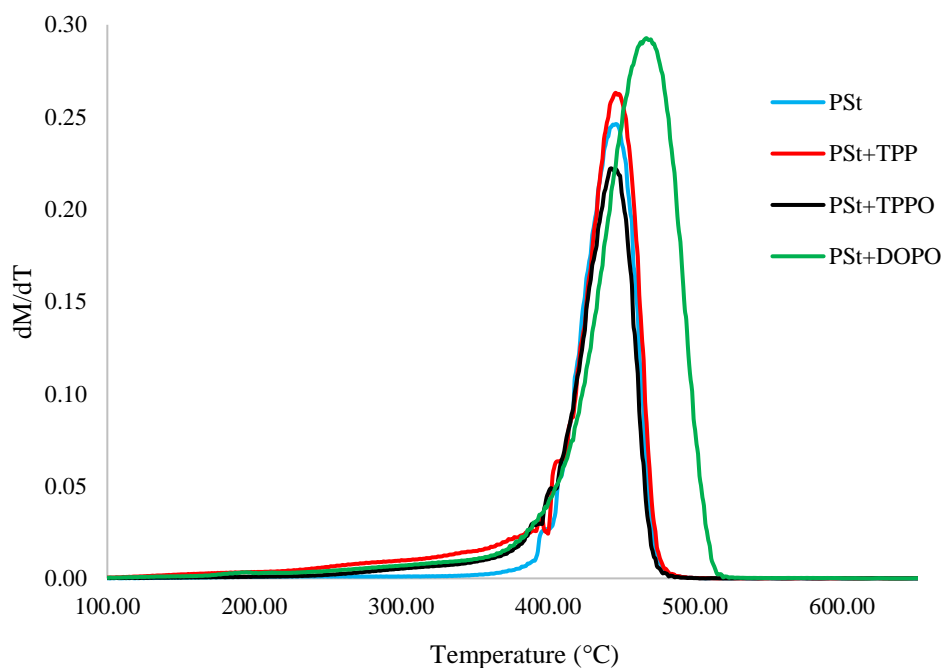


Figure 3.45 An overlay of the first derivative of TGA curves of all the PSt-based systems with solid additives, at $60^{\circ}\text{C min}^{-1}$

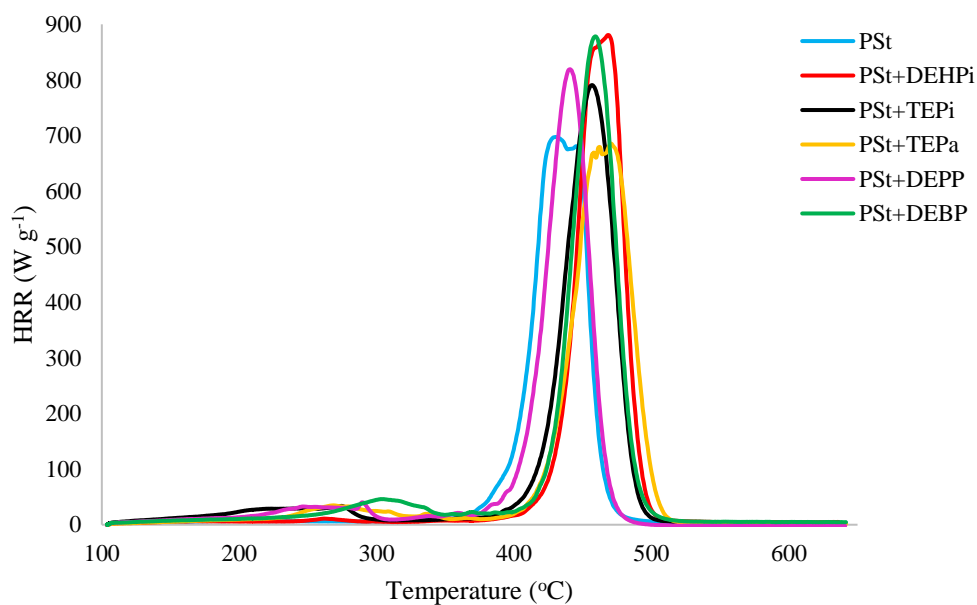


Figure 3.46 An overlay of the HRR curves obtained from the PCFC runs of all the PSt- based systems with liquid additives

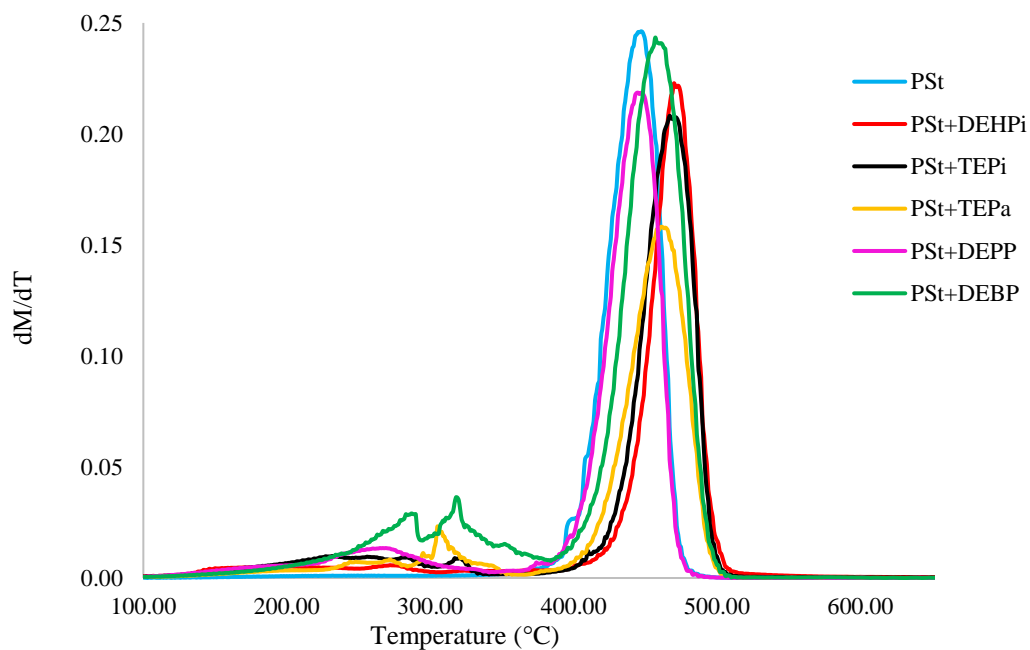


Figure 3.47 An overlay of the first derivative of TGA curves of all the PSt-based systems with liquid additives, at $60^{\circ}\text{C min}^{-1}$

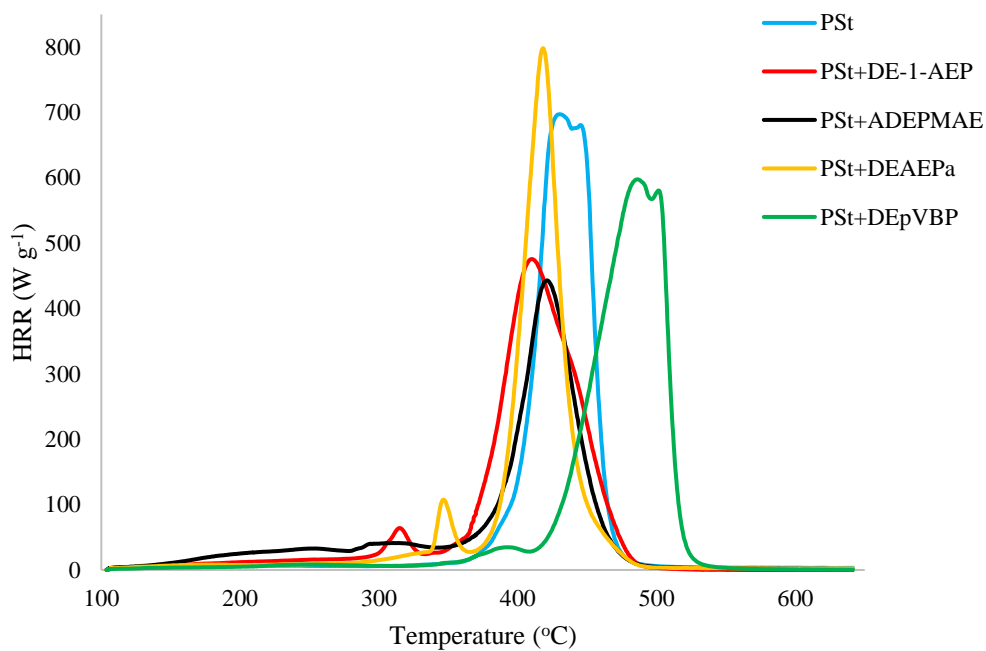


Figure 3.48 An overlay of the HRR values obtained from the PCFC runs of all the PSSt-based systems with reactives

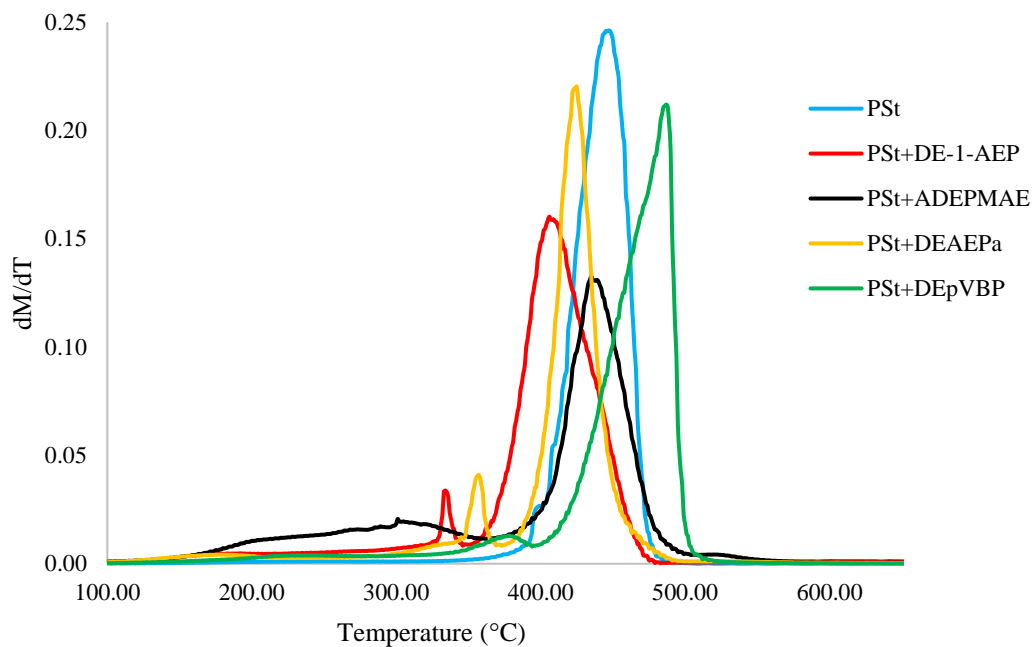


Figure 3.49 An overlay of the first derivative of TGA curves of all the PSSt-based systems with reactives, at $60^{\circ}\text{C min}^{-1}$

3.5.5 ‘Bomb’ calorimetry

The values of the heat of combustion, ΔH_{comb} , obtained through the ‘bomb’ calorimetric runs are collected in Tables 3.15 (PMMA-based samples) and 3.16 (PSt-based samples).

Table 3.15 Heats of combustion data for PMMA-based samples from ‘bomb’ calorimetric measurements

Sl. No.	*Sample	ΔH_{comb} (kJ g ⁻¹)
1	PMMA	26.24
2	PMMA+TPP	26.12
3	PMMA+TPPO	27.12
4	PMMA+DOPO	26.41
5	PMMA+DEHPi	24.87
6	PMMA+TEPi	25.42
7	PMMA+TEPa	25.74
8	PMMA+DEPP	26.55
9	PMMA+DEBP	26.56
10	PMMA+DE-1-AEP	25.27
11	PMMA+ADEPMAE	25.80
12	PMMA+DEpVBP	26.49

*the ΔH_{comb} of PMMA+ DEAEPA could not be performed

With a view to obtaining a better understanding regarding the spread of the values of the heats of combustion data recorded for each sample, a graph was plotted with ΔH_{comb} values as the ordinate and corresponding unmodified/modified materials along the X-axis (Figures 3.50 and 3.51)

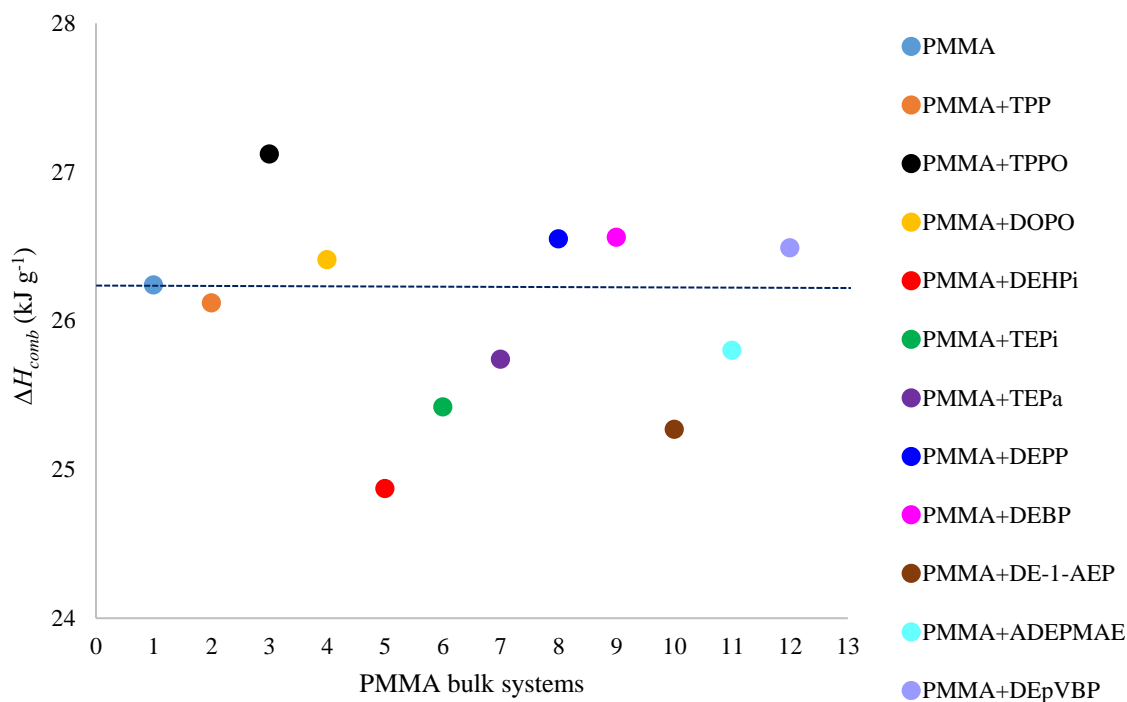


Figure 3.50 A plot of ΔH_{comb} of various PMMA-based materials

The values of the heats of combustion of the modified systems, as compared to the parent polymer, are expected to be lower when combustion inhibitory effects are in operation. However, such an effect was only noticeable in the case of PMMA with the additives, TPP, DEHPi, TEPi, TEPa, and with the reactives DE-1-AEP and ADEPMAE. Among these the PMMA+DEHPi sample showed the lowest value (24.87 kJ g⁻¹). Hence, it is to be assumed that some additives/reactive groups, upon decomposition produce volatiles which, in turn, can exert some degree of combustion inhibition. However, in the case of other modified samples (with TPPO, DOPO, DEPP and DEBP, and with the reactive monomer DEpVBP), slightly higher values of the heats of combustion were observed. Therefore, it can be inferred here that these additives/reactive group during decomposition result in volatile species that are combustible in nature, thus increasing the values of the total heat of combustion in such systems, relative to the parent polymer.

The corresponding data from the ‘bomb’ calorimetric tests of PSt-based samples are tabulated in Table 3.16 and plotted in Figure 3.51.

Table 3.16 Heats of combustion data for PSt-based samples from bomb calorimetric measurements

Sl. No.	Sample	ΔH_{comb} (kJ g ⁻¹)
1	PSt	41.50
2	PSt+TPP	41.02
3	PSt+TPPO	40.30
4	PSt+DOPO	39.50
5	PSt+DEHPi	38.70
6	PSt+TEPi	38.89
7	PSt+TEPa	38.99
8	PSt+DEPP	39.55
9	PSt+DEBP	39.13
10	PSt+DE-1-AEP	38.23
11	PSt+ADEPMAE	33.03
12	PSt+DEpVBP	39.47

*the ΔH_{comb} of PSt+ DEAEPA could not be performed

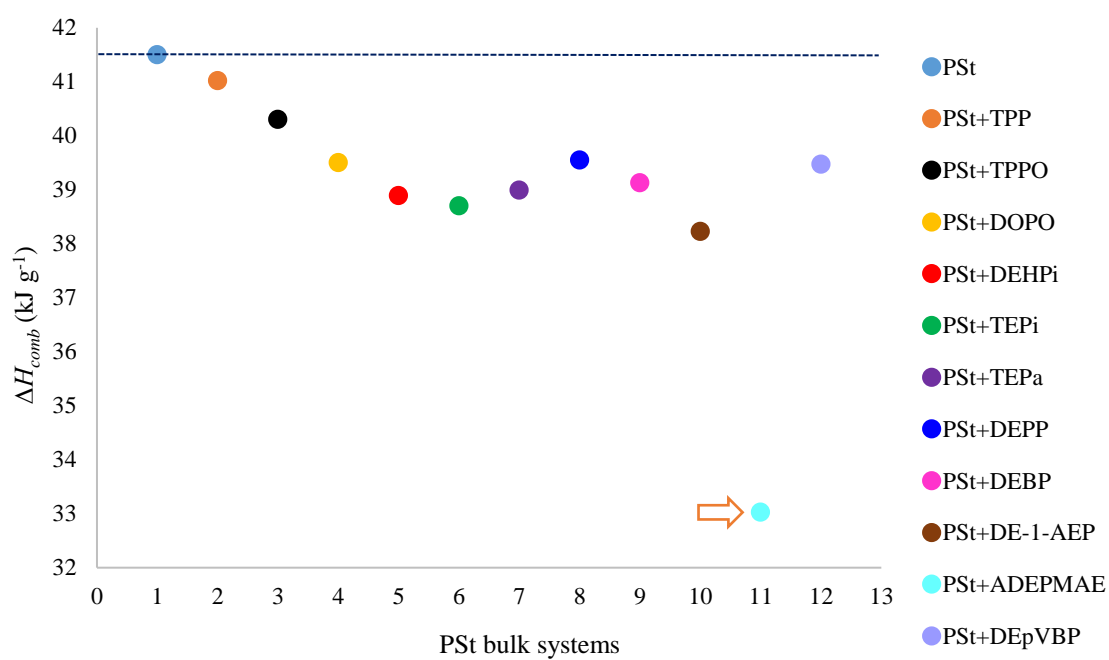


Figure 3.51 A plot of ΔH_{comb} of various PSt-based materials

In contrast to the ‘bomb’ calorimetric results obtained in the case of the PMMA-based samples, all the modified PSt-based samples showed a definite decrease in the ΔH_{comb} values as compared to the unmodified version, which clearly demonstrated the vapour-phase inhibitory effect(s) of the modifying groups. Such an effect was found to be particularly pronounced in the case of PSt modified with ADEPMAE, the P/N-containing monomer, where it may be also assumed that there is some degree of P-N synergism (Banks, *et al.*, 1994), thus exhibiting the lowest value of ΔH_{comb} , 33.03 kJ g⁻¹. It is also highly relevant to note that, generally, there may be some sort of interaction (physical or chemical) of the parent polymer matrix with the modifying groups was also evident during pyrolysis and combustion (from DSC and PCFC tests, respectively) for the PSt-based systems. However, such a generalization could not be drawn in the case of the PMMA-based systems.

3.5.6 Some generalizations among the test parameters

In the following sections, some generalizations that were found to exist amongst some of the relevant test parameters from TGA, PCFC and ‘bomb’ calorimetry techniques are presented.

The plot of the char yields, obtained through TGA (60°C min⁻¹) and PCFC runs, for the PMMA- and PSt-based samples are shown in Figures 3.52 and 3.53. Here the same hierarchy of the modifying compounds/groups are retained along the X-axis, as before. It can be noted that the TGA runs yielded less than 1 wt.% in all cases (see the points in the boxed area in figure), whereas the corresponding values in the case of PCFC tests varied widely (from 0 to 6 wt.%, except in the case of the P/N monomer: 11 wt.%). In the case of the PSt-based materials, again, no particular correspondences were observed among the values of the char yields from the two techniques (Figure 3.53). However, several systems (such as, unmodified PSt, and modified versions with, TPP, DEHPi, TEPI, DE-1-AEP, ADEPMAE, DEAEPA and DEpVBP) showed substantial char residues (ranging from, 3 to 8 wt.%) in the PCFC runs (see the points inside the red boxed area in the figure), whereas for the others the corresponding values closely resembled the char yield from the TGA runs (≤ 1 wt.%) - see the corresponding points in the blue boxed area. Furthermore, in the case of PSt-based material, several of the modifying additives/groups seem to exhibit some degree of condensed phase activity during the PCFC runs. This was

also evident in terms of enhanced char yields produced by the modified systems as compared to virgin PSt.

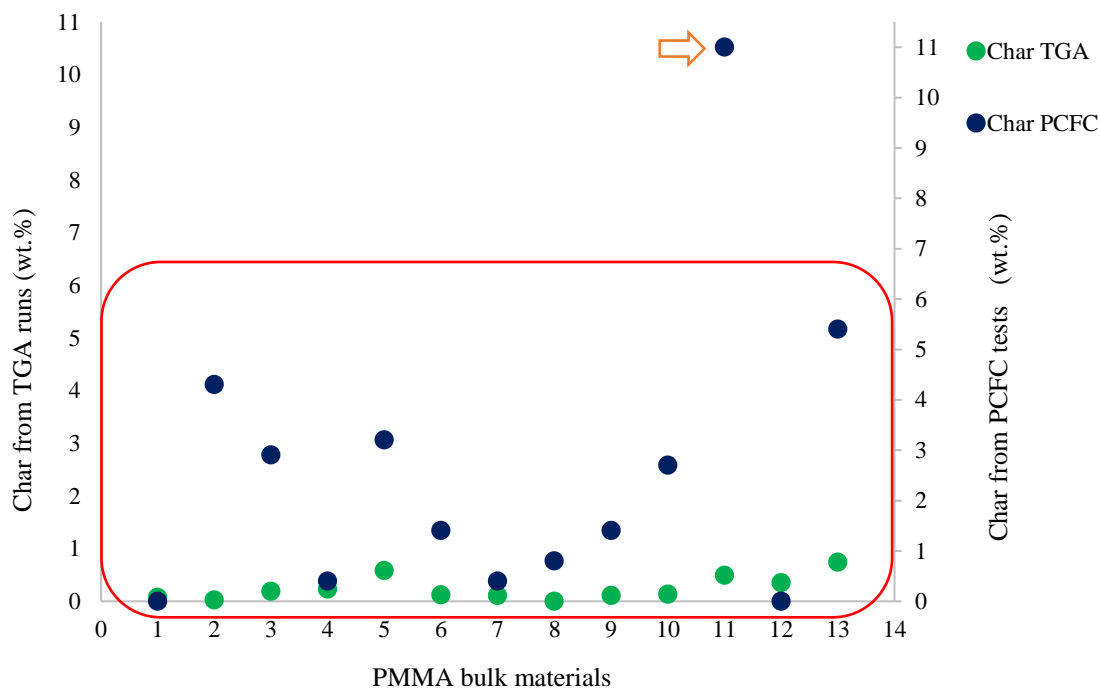


Figure 3.52 A plot of wt.% of char residues from TGA runs and PCFC tests for the PMMA-based materials

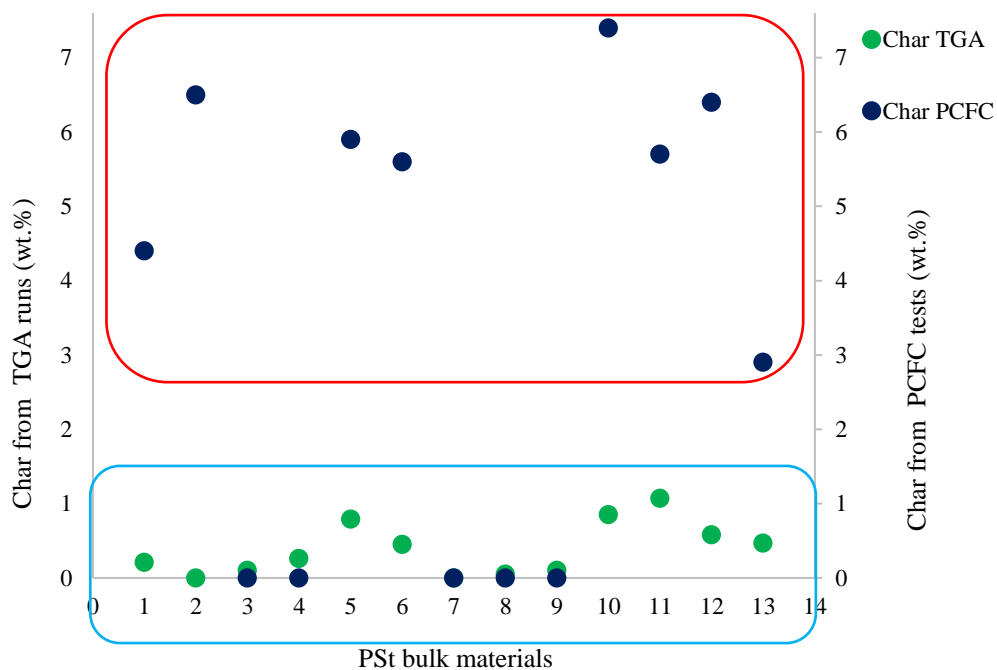


Figure 3.53 A plot of wt.% of char residues from TGA runs and PCFC tests of PSt-based materials

As the next step, the plots of the values of the combustion parameters, i.e. ΔH_{comb} and EHC), were constructed and are shown in Figures 3.54 and 3.55 (here the hierarchy of the modifying compounds/groups are maintained along the X-axis, as before).

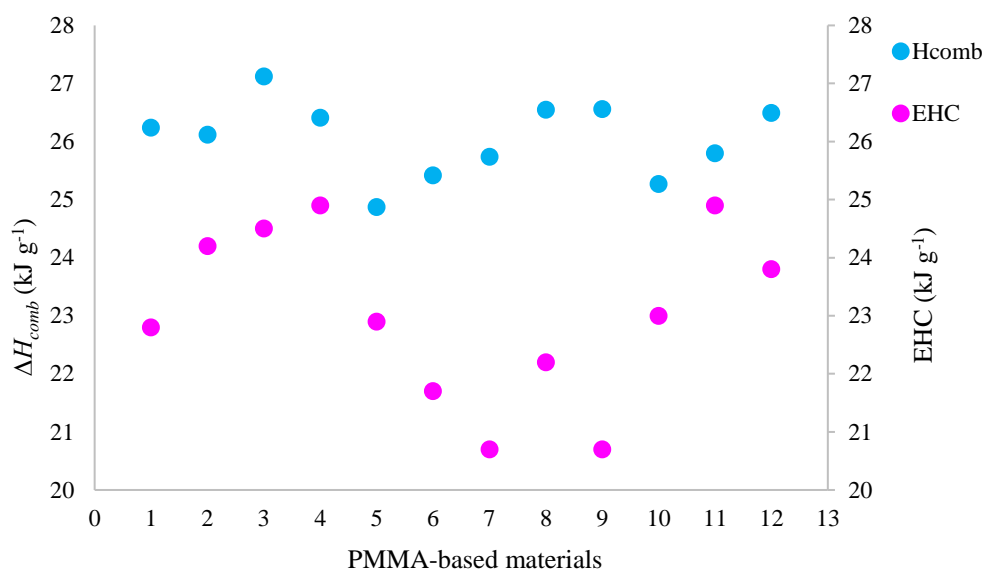


Figure 3.54 A plot of the values of ΔH_{comb} from ‘bomb’ calorimetry and EHC from PCFC runs for the PMMA-based materials

As can be seen clearly seen from the above figure, the EHC values calculated from PCFC data, where only incomplete and forced non-flaming combustion is effected, are lower than the corresponding ΔH_{comb} values obtained through ‘bomb’ calorimetric runs, where the ‘complete’ combustion of the sample is assumed to occur. Furthermore, the degree deviances between the values for each of the samples also varied widely. This can be attributed to the fact that the chemical nature of the modifying compounds/groups and the possible modes of interaction of the modifying agents with the base substrate are also different in each case.

In the case of PSt-based systems, the relative magnitude of the values of ΔH_{comb} and EHC showed more or less the same trend as in the case of PMMA-based systems. However, the extent of spread of the values was less pronounced in the case of PSt-based systems. In addition, PSt containing the P/N-monomer (ADEPMAE) exhibited significantly lower values (Joseph & Tretsiakova-McNally, 2012b); in fact its ΔH_{comb} value is even lower than the EHC values of all other systems. This, again, confirms the outstanding

combustion inhibitory effect of the monomer as is also evident in the relevant parameters obtained through TGA, PCFC and ‘bomb’ calorimetric techniques.

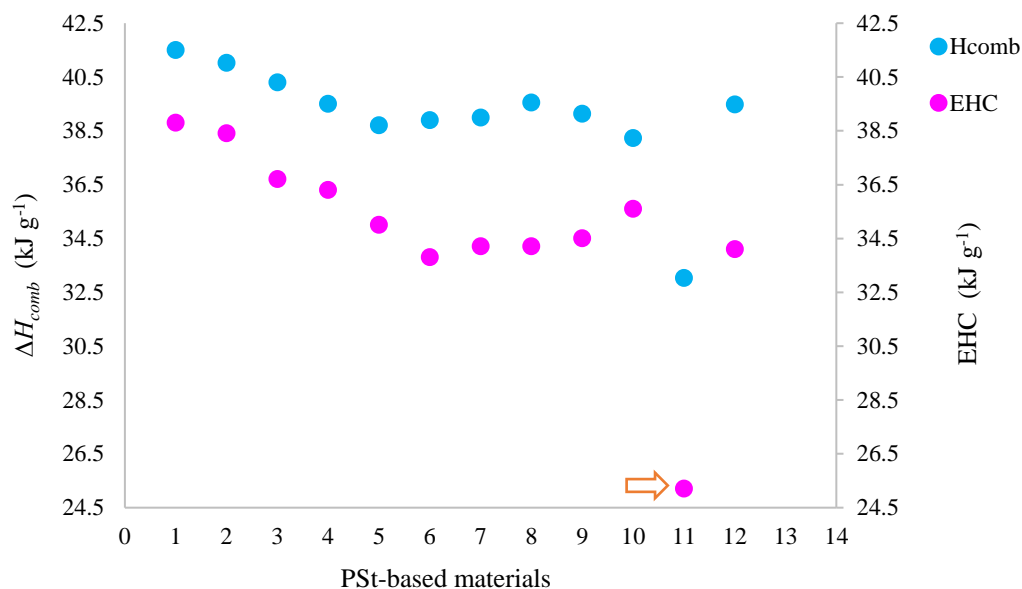


Figure 3.55 A plot of the values of ΔH_{comb} from ‘bomb’ calorimetry and EHC from PCFC runs for the PSt-based materials

3.5.7 Mechanisms of flame retardance- condensed phase

In the following sections, some possible components of mechanism(s) operating in the condensed and gaseous phases of the PMMA- and PSt-based systems are given. These were primarily inferred from the results obtained through a combination of analytical techniques (ICP/OES and solid-state NMR) and, optionally, from some hyphenated methods (GC/MS and pyrolysis-GC/MS), the latter being mainly used for gaseous phase analyses. The mechanistic aspects for PMMA- and PSt-based materials are given separately.

3.5.7.1 PMMA-based materials

a. Phosphorus contents of the char residues (ICP/OES)

The phosphorus contents of the char residues were determined through ICP/OES measurements. The reported values in Table 3.17 are averages over triplicate runs for each sample. In order to get enough char residues for the analyses (ICP/OES and solid-state NMR), smaller pieces of the samples, sourced from the plaques, were taken in 50 mL porcelain crucibles, and then made to undergo forced flaming combustion inside a fume cupboard, using a butane torch that had a flame length of *ca.* 4 cm. It should be noted that since the combustibility of the samples differed widely, the duration of the application of the pilot needed to be varied accordingly. Hence, no meaningful assessments of the char yields were made, as this essentially requires the duration of the impingement of the flame in each case to be exactly the same. Table 3.17 also includes the ratios of the P-loading in the unburnt samples (2 wt.%) to P-contents in char residues (in wt.%).

Table 3.17 Phosphorus contents of the unburned samples and char residues of PMMA-based materials

Sl. No.	Samples	wt.% of P in the unburnt sample	wt.% P in char ($\pm 1\%$)	Ratio of P in char to P in sample
1	PMMA	02	0.00	0.00
2	PMMA+TPP	2	1.97	0.99
3	PMMA+TPPO	2	2.38	1.19
4	PMMA+DOPO	2	5.55	2.78
5	PMMA+DEHPi	2	12.12	6.06
6	PMMA+TEPi	2	3.75	1.88
7	PMMA+TEPa	2	12.21	6.11
8	PMMA+DEPP	2	0.71	0.36
9	PMMA+DEBP	2	7.68	3.84
10	PMMA+DE-1-AEP	2	15.26	7.63
11	PMMA+ADEPMAE	2	35.22	17.6
12	PMMA+DEAEPa	2	9.31	4.66
13	PMMA+DEpVBP		10.02	5.01

It can be clearly noticed from the above table that several systems retained relatively higher amounts of P in the char residues (e.g. PMMA+DEHPi, PMMA+TEPa, PMMA+DE-1-AEP, PMMA+DEAEPa, PMMA+ADEPMAE and PMMA+DEpVBP), whereas the corresponding values were much lower for other materials. It is also interesting to note that the system with the P/N-monomer yielded the maximum amount of char (ratio = 17.6). The retention of P in the char residues is indicative of the condensed phase activity of the modifying compounds/groups; however, an unambiguous ranking based on the ratios of the P wt.% in the char residue to that of the unburnt material alone is not possible, especially, given that the actual char yield in each case is bound to differ substantially. Nevertheless, quantitative estimations of P in the char residues can be considered as a useful exercise, as it provides some corroborative evidence to the inferences deduced from their corresponding ^{31}P solid-state NMR spectra.

b. Solid-state NMR

Even though the char residues predominantly consist of carbon atoms, residual protons can also be present to varying amounts depending on the degree of carbonization. Therefore, scalar coupling patterns owing to the residual protons were found to be present in the ^{31}P spectra (as protons were not decoupled during the acquisition of the spectra in the present case), especially in cases where relatively larger amounts of unburnt additives/reactive moieties are present in the test samples (e.g., PMMA+TPPO). Furthermore, the signals in the solid-state NMR spectra generally are less discernable than the corresponding solution-state spectra, primarily owing to dipolar broadening. Therefore for the sake of simplicity, we compared the ^{31}P signals from the char residues with those of the additives/reactives recorded in the solution-state where a broad-band decoupling of protons was used. Here, it is to be assumed that the chemical shift values of specific ^{31}P signals do not differ largely when recorded in both states (see Table 3.18). Such an assumption was validated in the case of the solid additives (i.e. TPP, TPPO and DOPO) by recording the spectra through both techniques and comparing the chemical shift values. In the following section, ^{31}P spectra and optionally ^{13}C spectrum of chars obtained from the PMMA-based materials are given.

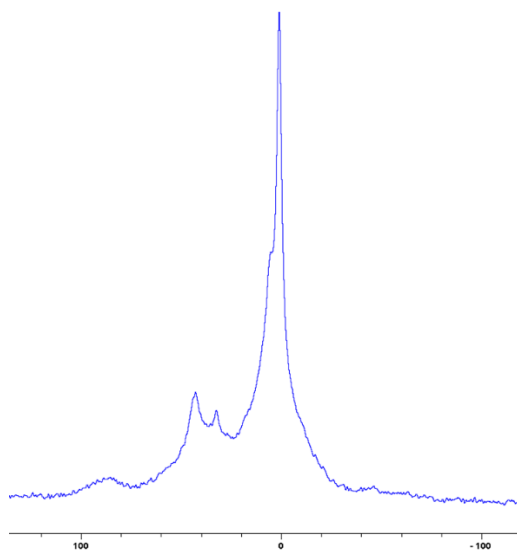


Figure 3.56 Solid-state ^{31}P -NMR spectrum of char obtained from PMMA+DOPO (the abscissa denotes the chemical shift values, δ , in ppm and the ordinate corresponds to the signal intensity in arbitrary units)

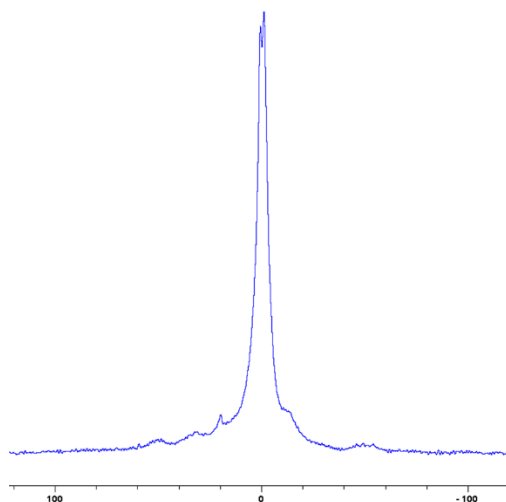


Figure 3.57 Solid-state ^{31}P -NMR spectrum of char obtained from PMMA+TPP (the abscissa denotes the chemical shift values, δ , in ppm and the ordinate corresponds to the signal intensity in arbitrary units)

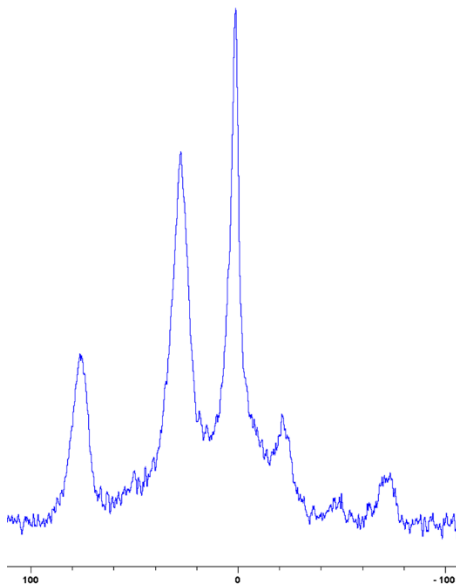


Figure 3.58 Solid-state ^{31}P -NMR spectrum of char obtained from PMMA+TPPO (the abscissa denotes the chemical shift values, δ , in ppm and the ordinate corresponds to the signal intensity in arbitrary units)

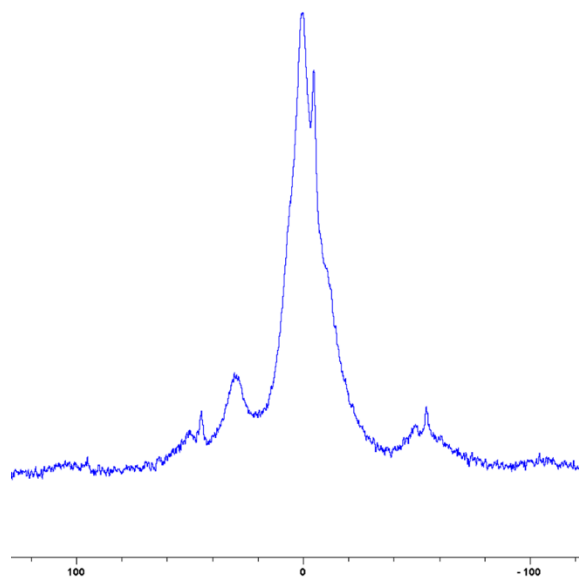


Figure 3.59 Solid-state ^{31}P -NMR spectrum of char obtained from PMMA+TEPi (the abscissa denotes the chemical shift values, δ , in ppm and the ordinate corresponds to the signal intensity in arbitrary units)

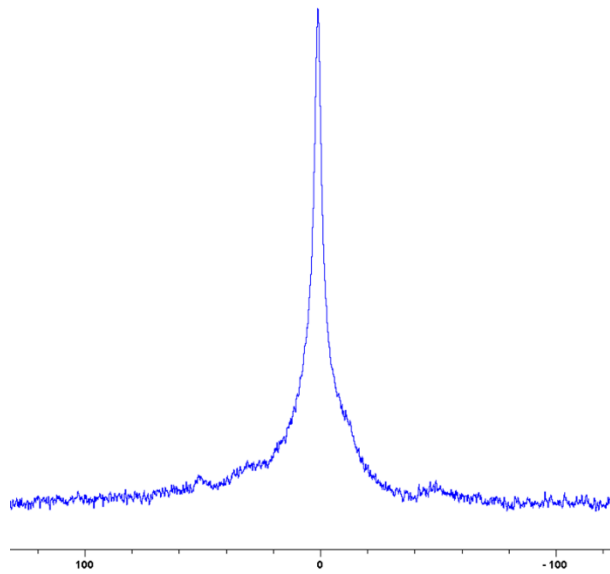


Figure 3.60 Solid-state ^{31}P -NMR spectrum of char obtained from PMMA+TEPa (the abscissa denotes the chemical shift values, δ , in ppm and the ordinate corresponds to the signal intensity in arbitrary units)

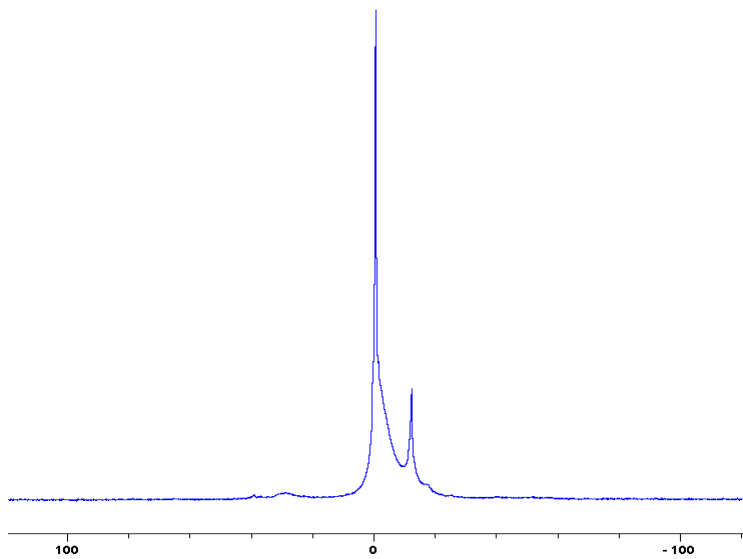


Figure 3.61 Solid-state ^{31}P -NMR spectrum of char obtained from PMMA+ADEPMAE (the abscissa denotes the chemical shift values, δ , in ppm and the ordinate corresponds to the signal intensity in arbitrary units)

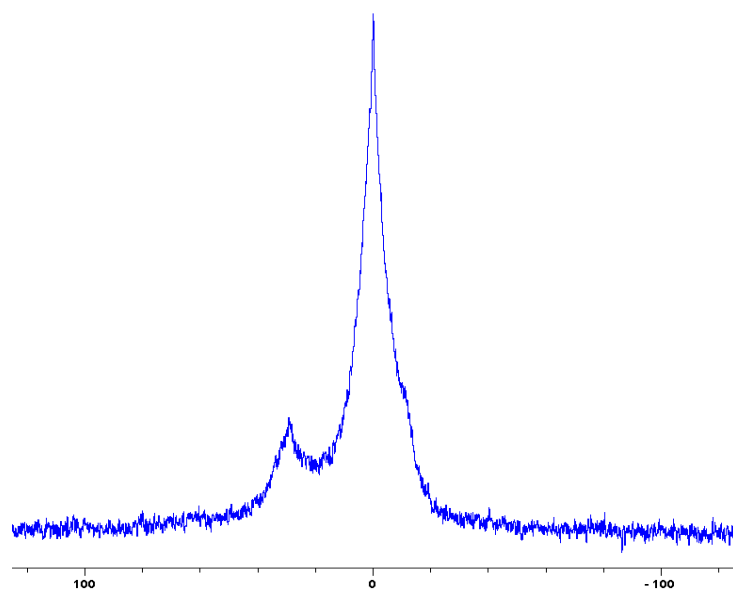


Figure 3.62 Solid-state ^{31}P -NMR spectrum of char obtained from PMMA+DE-1-AEP (the abscissa denotes the chemical shift values, δ , in ppm and the ordinate corresponds to the signal intensity in arbitrary units)

-C=O groups from anhydride linkages

aromatic char precursors

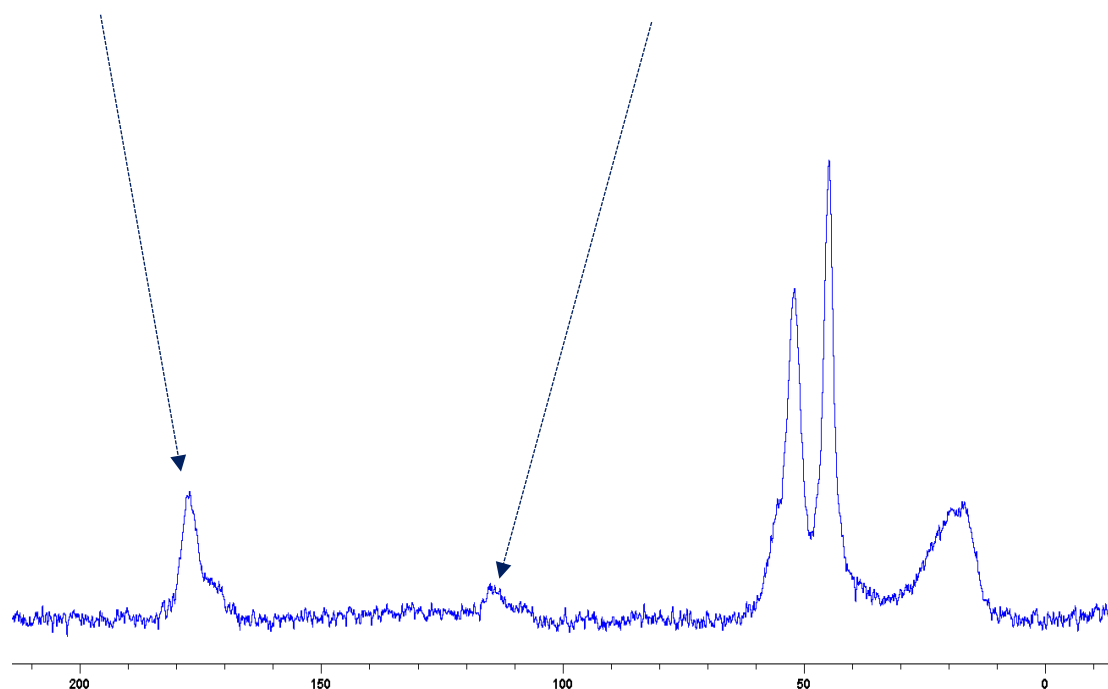


Figure 3.63 Solid-state ^{13}C -NMR spectrum of char obtained from PMMA+DE-1-AEP (the abscissa denotes the chemical shift values, δ , in ppm and the ordinate corresponds to the signal intensity in arbitrary units)

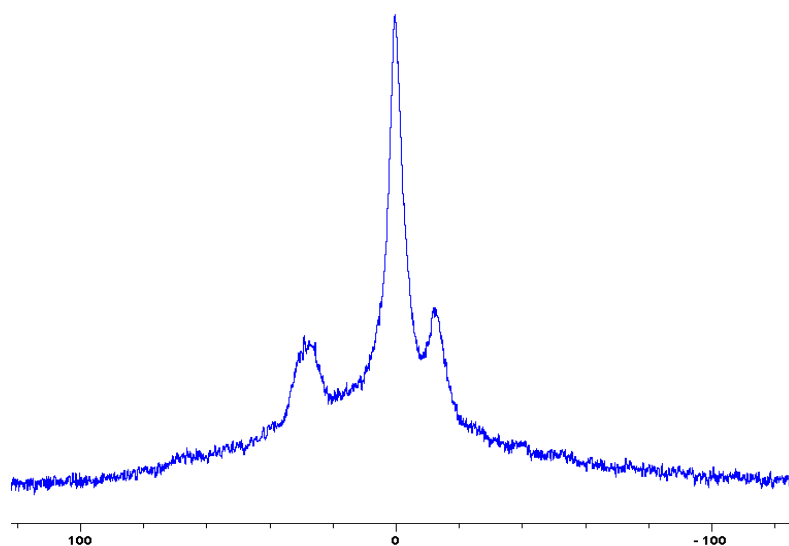


Figure 3.64 Solid-state ^{31}P -NMR spectrum of char obtained from PMMA+DEpVBP (the abscissa denotes the chemical shift values, δ , in ppm and the ordinate corresponds to the signal intensity in arbitrary units)

Table 3.18 The ^{31}P chemical shift values (δ , in ppm) of the additives/reactives and char residues of PMMA-based materials

Sl. No.	Additive	δ value for ^{31}P of the additives # (solution-state)	δ value for ^{31}P of the char residue-prominent signal (solid-state)
1	TPP	-7.10	-0.3
2	TPPO	27.6	1.6
3	DOPO	16.7	1.3
4	DEHPi	7.30	*---
5	TEPi	7.30	0.0
6	TEPa	-1.00	1.3
7	DEPP	32.2	*---
8	DEBP	26.4	*---
9	DE-1-AEP	21.4	-0.3
10	ADEPMAE	10.4	-1.3
11	DEAEPa	0.50	*---
12	DEpVBP	26.6	0.3

#recorded with broad-band proton decoupling

*not recorded

Generally, the presence of ^{31}P signals around $\delta = 0$ ppm can be considered to arise from ‘phosphorus’ acid species from the thermal cracking of the P-bearing additives/groups (Ebdon, *et al.*, 2000). The formation of such acidic species is especially feasible in the case of phosphites, phosphates, phosphonate/phosphorlamino esters (see Figure 3.68). The ‘phosphorus’ acid species thus formed can condense to form polyphosphoric acid species, where the ^{31}P signal shifts slightly to the negative region. Such condensation reactions can also result in cross-linking of chains, as shown to occur in the case of PSt-based polymers (see also Figure 3.78). Generally, the sharper signals nearer to 0 ppm can be clearly assigned to ‘free’ (i.e., unbound) phosphoric acid. In both cases, this can lead to a broadening of the signal when compared to the signals arising from more readily mobile ‘phosphorus’ acid species which remain in the char structure as unattached entities (see, for example, in the case of PMMA+ADEPMAE).

It is also reported in the literature that, in the case of PMMA-based systems, the ‘phosphorus’ acid species further trans-esterify the ester groups in the PMMA chain leading to pendent carboxylic acid functions which, under the influence of heat, subsequently forms anhydride links (Ebdon, *et al.*, 2000). The anhydride links once formed can undergo decarboxylation reactions (see in Figure 3.63), Diels-Alder type additions, etc., and thus eventually resulting in precursors for carbonaceous char (see also in the FT-IR spectrum given in Figure 3.67). In the case of the aromatic phosphine/phosphine oxide, it is more likely that the ^{31}P signal originates from the unburnt additives and, in some instances, the signal pattern also seems to incorporate the ^1H - ^{31}P couplings. With the limited amount of information in hand from the solid-state NMR spectra, and through complementary inferences made from the results of the hyphenated technique (pyrolysis-GC/MS), the shift of the signals towards the range, $\delta \sim 0$ - 2 ppm in the cases of TPP, TPPO and DOPO cannot be easily explained.

c. FT-IR spectroscopy

The FT-IR spectra of ‘partially’ burnt materials from PMMA (by igniting the tip of a solid piece) and some optional modified systems recorded in the ATR mode are shown in Figures 3.65 to 3.67. The formation of carboxylic acid groups and anhydride linkages can be clearly seen in the spectra of the ‘partially’ burnt residues from the modified systems, whereas such features are absent in the spectrum obtained from the virgin

material. Complementary information regarding the formation of anhydride linkages and the formation of aromatic species is also found in ^{13}C NMR spectra of the char residues (Figure 3.63).

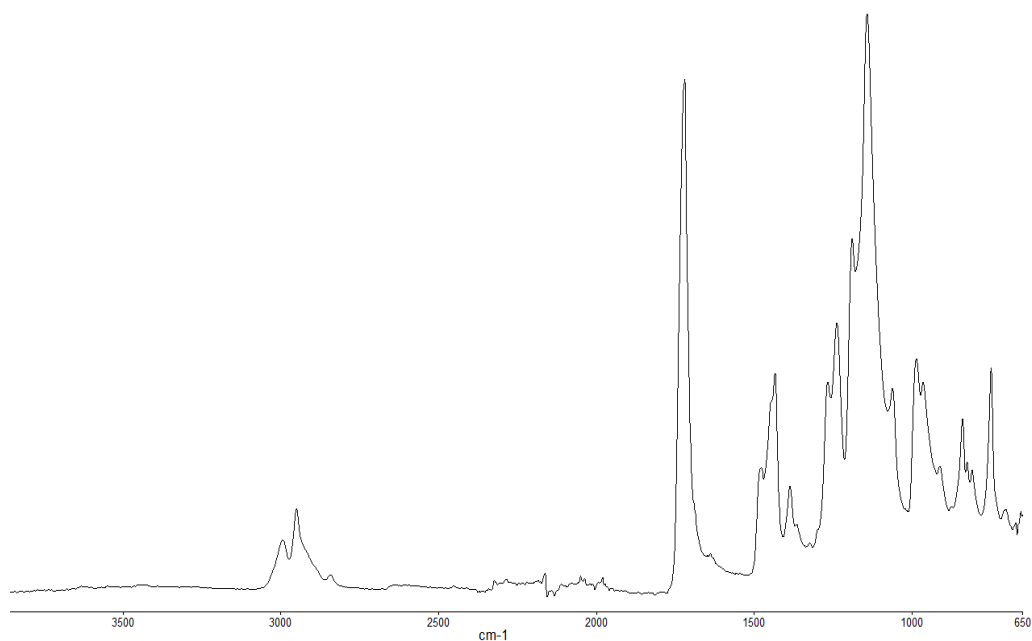


Figure 3.65 FT-IR spectrum of PMMA (unburnt sample)

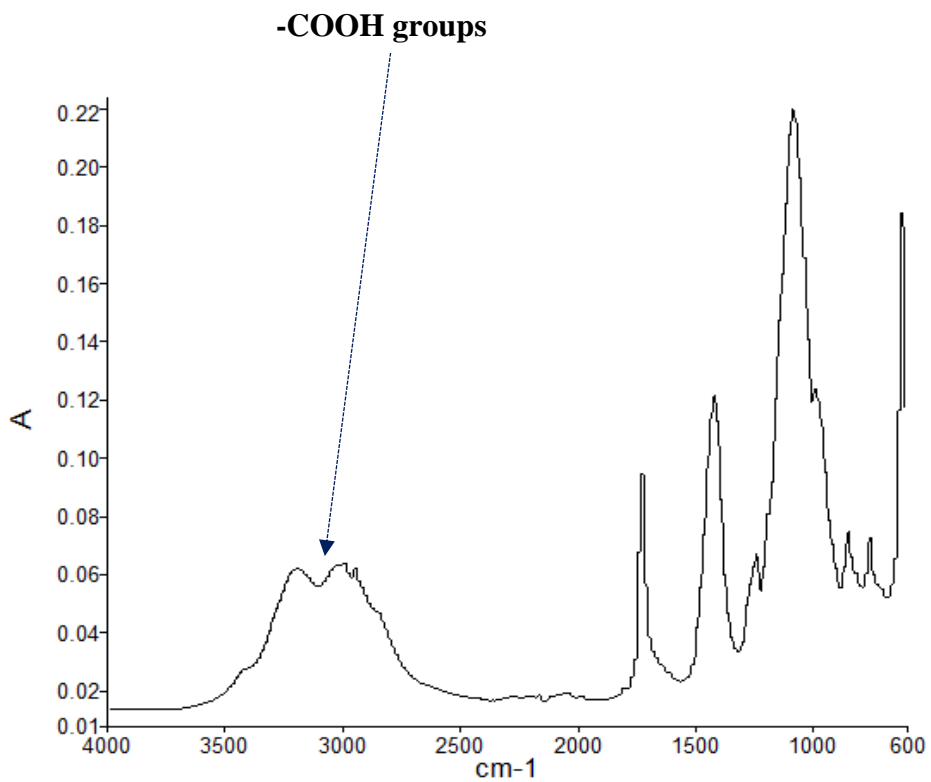


Figure 3.66 FT-IR spectrum of PMMA+DEpVBP (partially burnt sample)

anhydride linkages

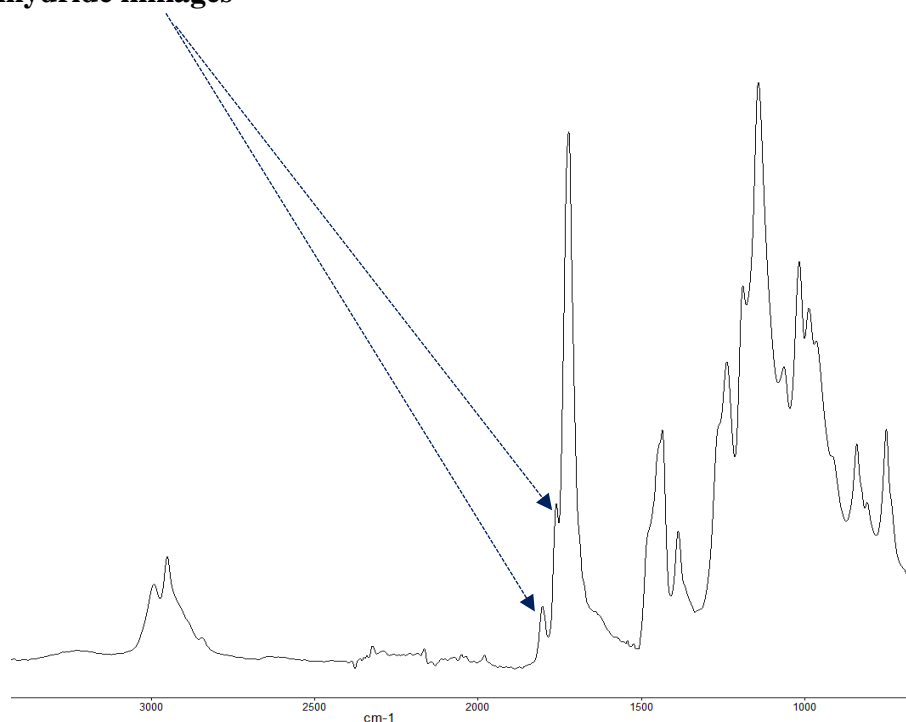


Figure 3.67 FT-IR spectrum of PMMA+DE-1-AEP (partially burnt sample)

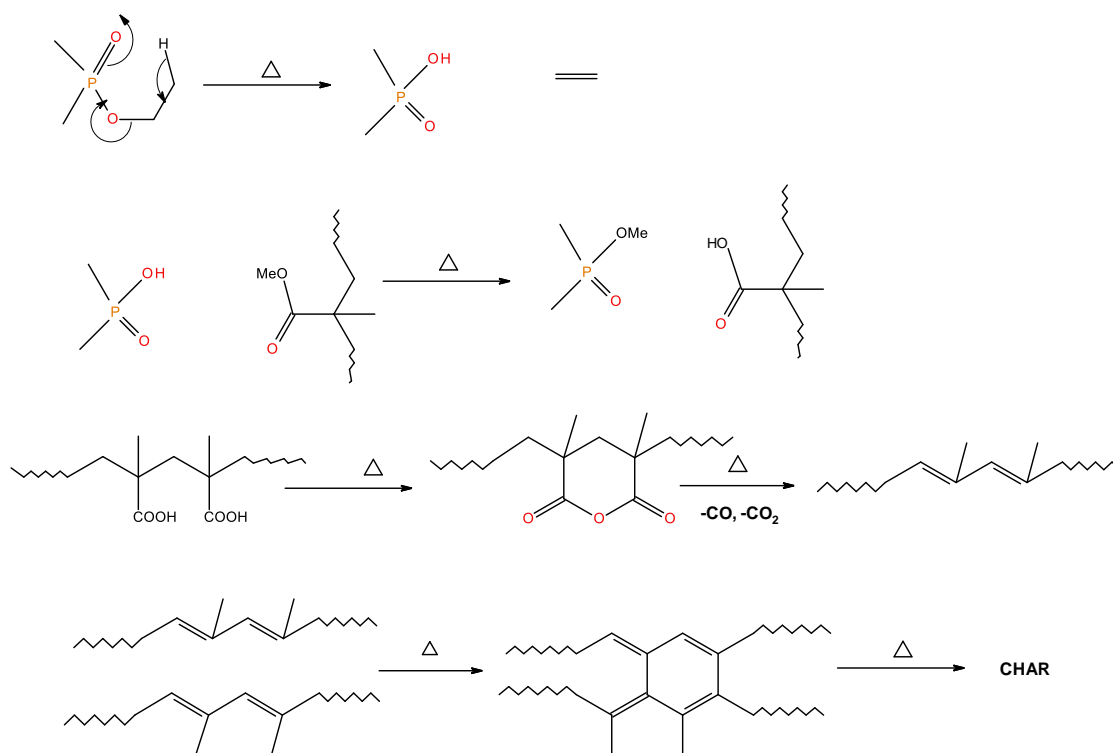


Figure 3.68 A schematic representation of the formation of char residues in the PMMA-based polymers upon flaming combustion (J. R. Ebdon, *et al.*, 2000)

3.5.7.2 PSt-based materials

a. Phosphorus contents of char residues (ICP/OES)

The ratio of the phosphorus content in the unburnt material and the corresponding retention in the char residue can be considered as an indication of the extent of condensed phase activity of the modifying agent. Enhanced degrees of P-retention were observed for several PSt-based systems, such as PSt with TPP, TPPO, ADEPMAE, DEAEPa and DEpVBP. As in the case of the PMMA-based systems, the maximum phosphorus retention was observed for PSt+ADEPMAE. Here also, the conditions under which the char residues were obtained varied in each case in terms of the duration of the pilot applied. Hence any such general inferences that can be drawn in this context, judging by the P-loadings alone, need to be treated with caution.

Table 3.19 Phosphorus contents of the unburned samples and char residues of PSt-based materials

Sl. No.	Samples	wt.% of P in the system	wt.% of P in char	Ratio of P in char to P in sample
1	PSt	0	0.00	0.00
2	PSt+TPP	2	7.56	3.78
3	PSt+TPPO	2	6.19	3.10
4	PSt+DOPO	2	1.62	0.81
5	PSt+DEHPi	2	2.28	1.14
6	PSt+TEPi	2	4.64	2.32
7	PSt+TEPa	2	2.32	1.16
8	PSt+DEPP	2	0.34	0.17
9	PSt+DEBP	2	2.17	1.09
10	PSt+DE-1-AEP	2	3.15	1.58
11	PSt+ADEPMAE	2	15.0	7.48
12	PSt+DEAEPa	2	9.96	4.98
13	PSt+DEpVBP	2	5.48	2.74

b. Solid-state NMR

As in the case of the ^{31}P NMR spectra of char residues from PMMA-based systems, the appearance of signals around 1 ppm cannot be explained easily in the corresponding spectra for char residues from PSt-based systems containing solid additives (TPP and TPPO). It is highly unlikely that these signals arise due to the presence of ‘phosphorus’ acid species from the additives, as the breakage of C-P bonds will yield resonance-stabilised phenyl species. This will, in turn, facilitate the release of P^\cdot and PO^\cdot radicals into the vapour space. Corroborative evidence of this type of bond cleavage can be drawn from the pyrolysis-GC/MS studies of the solid additives (see Figure 3.95). However, thermal cracking of the ethyl groups (in phosphites, phosphates, and phosphonate/phosphoraminoester) is quite feasible in producing the corresponding ‘phosphorus’ acid species with $\delta \sim 0.0$ ppm (Ebdon, *et al.*, 2000). The ‘phosphorus’ acid species, once formed, can then proceed to phosphorylate the phenyl rings of PSt, and can subsequently result in the cross-linking of the polymeric chains through the condensation of the phosphorylated rings (Figure 3.78).

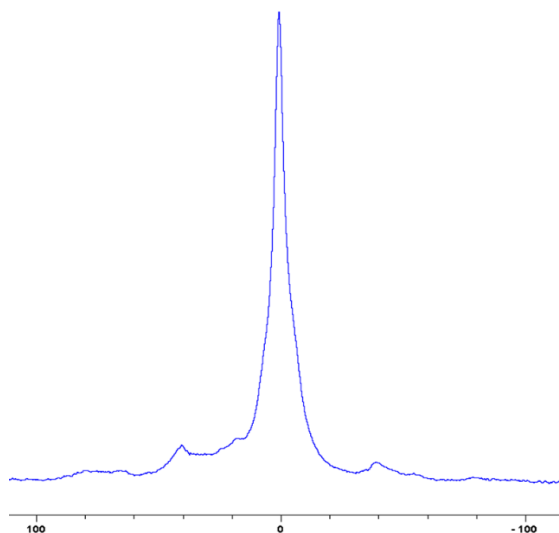


Figure 3.69 Solid-state ^{31}P -NMR spectrum of char obtained from PSt+TPP (the abscissa denotes the chemical shift values, δ , in ppm and the ordinate corresponds to the signal intensity in arbitrary units)

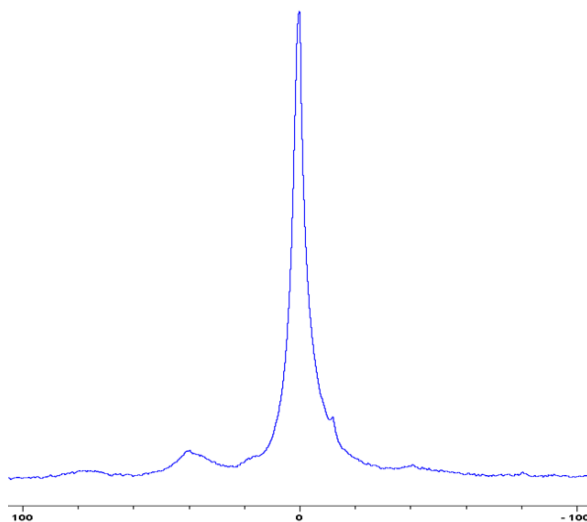


Figure 3.70 Solid-state ^{31}P -NMR spectrum of char obtained from PSt+TPPO (the abscissa denotes the chemical shift values, δ , in ppm and the ordinate corresponds to the signal intensity in arbitrary units)

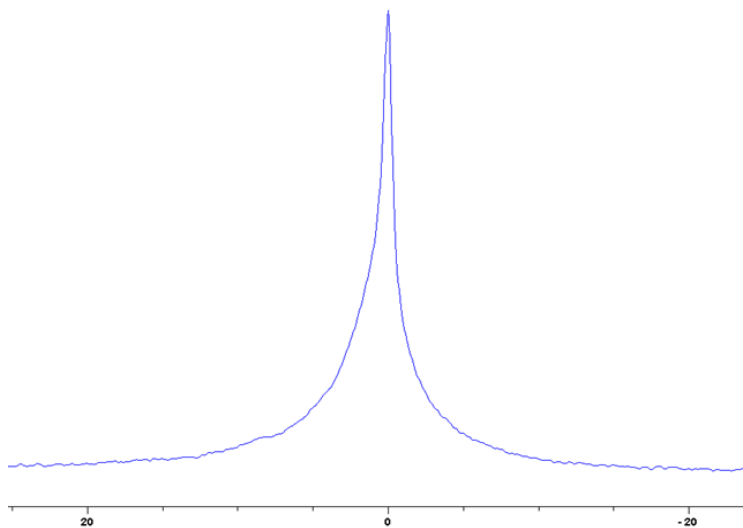


Figure 3.71 Solid-state ^{31}P -NMR spectrum of char obtained from PSt+DEHPi (the abscissa denotes the chemical shift values, δ , in ppm and the ordinate corresponds to the signal intensity in arbitrary units)

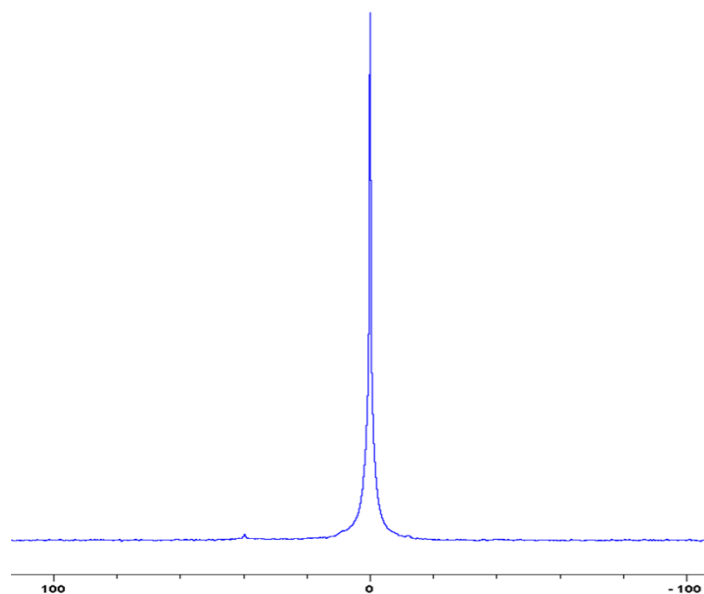


Figure 3.72 Solid-state ^{31}P -NMR spectrum of char obtained from PSt+TEPa (the abscissa denotes the chemical shift values, δ , in ppm and the ordinate corresponds to the signal intensity in arbitrary units)

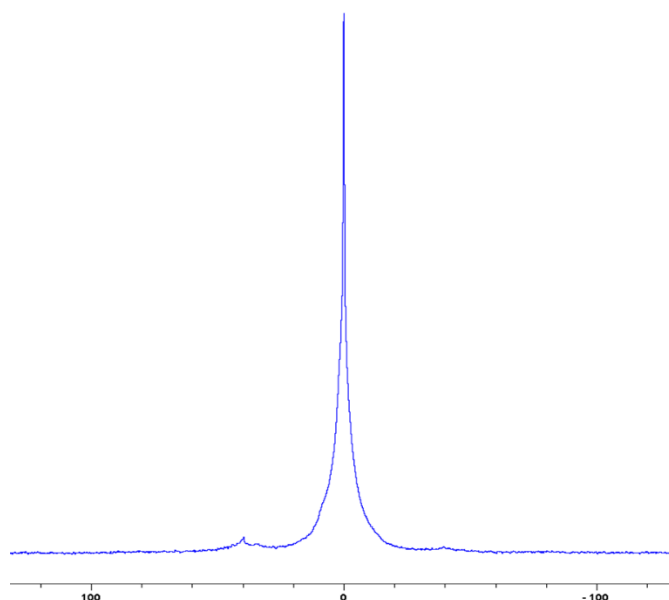


Figure 3.73 Solid-state ^{31}P -NMR spectrum of char obtained from PSt+TEPi (the abscissa denotes the chemical shift values, δ , in ppm and the ordinate corresponds to the signal intensity in arbitrary units)

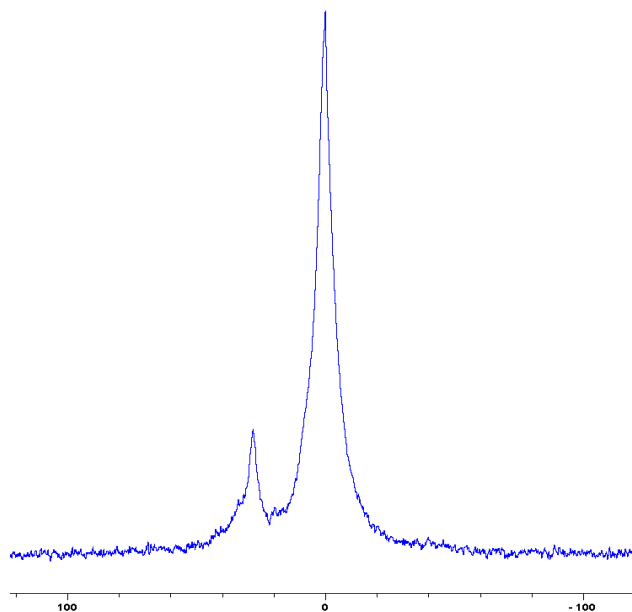


Figure 3.74 Solid-state ^{31}P -NMR spectrum of char obtained from PSt+DEBP (the abscissa denotes the chemical shift values, δ , in ppm and the ordinate corresponds to the signal intensity in arbitrary units)

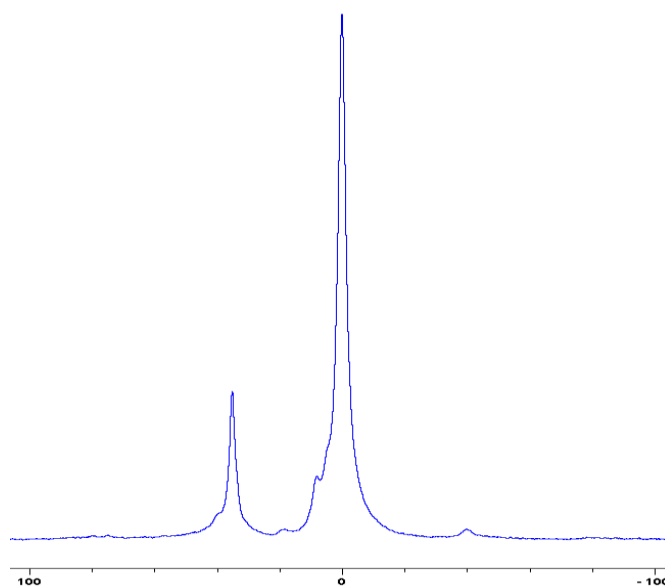


Figure 3.75 Solid-state ^{31}P -NMR spectrum of char obtained from PSt+DE-1-AEP (the abscissa denotes the chemical shift values, δ , in ppm and the ordinate corresponds to the signal intensity in arbitrary units)

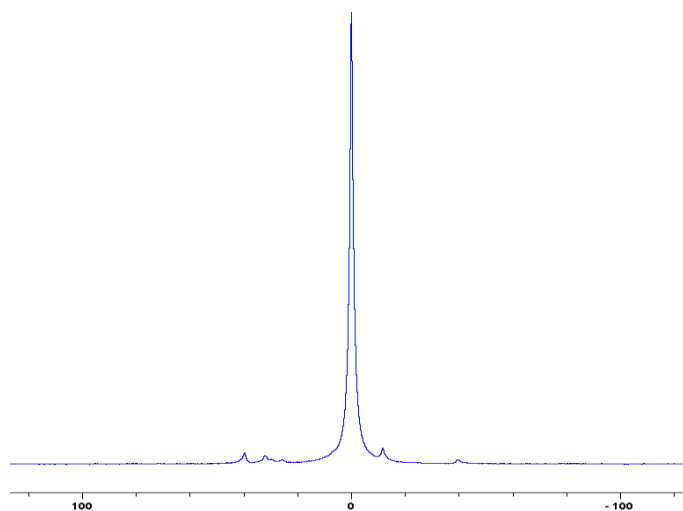


Figure 3.76 Solid-state ^{31}P -NMR spectrum of char obtained from PSt+ADEPMAE (the abscissa denotes the chemical shift values, δ , in ppm and the ordinate corresponds to the signal intensity in arbitrary units)

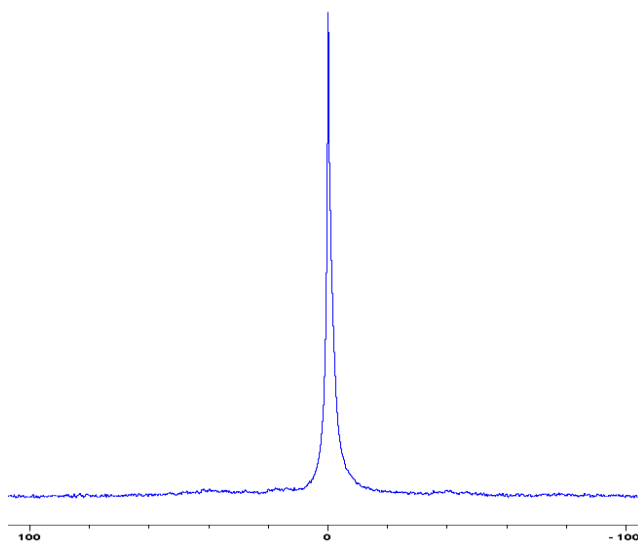


Figure 3.77 Solid-state ^{31}P -NMR spectrum of char obtained from PSt+DEpVBP (the abscissa denotes the chemical shift values, δ , in ppm and the ordinate corresponds to the signal intensity in arbitrary units)

Table 3.20 Chemical shift values (δ in ppm) of P nucleus in the additives/reactives and in the char residue obtained from PSt-based systems

Sl. No.	Additive/reactive	δ value for ^{31}P of the additives [#] (solution-state)	δ value for ^{31}P of the char residue-prominent signal (solid-state)
1	TPP	-7.10	1.00
2	TPPO	27.6	0.30
3	DOPO	16.7	*---
4	DEHPi	7.30	0.30
5	TEPi	7.30	0.00
6	TEPa	-1.00	0.00
7	DEPP	32.2	*---
8	DEBP	26.4	0.70
9	DE-1-AEP	21.4	0.00
10	ADEPMAE	10.4	0.70
11	DEAEPa	0.50	*---
12	DEpVBP	26.6	-0.30

#recorded with broad-band proton decoupling

*not recorded

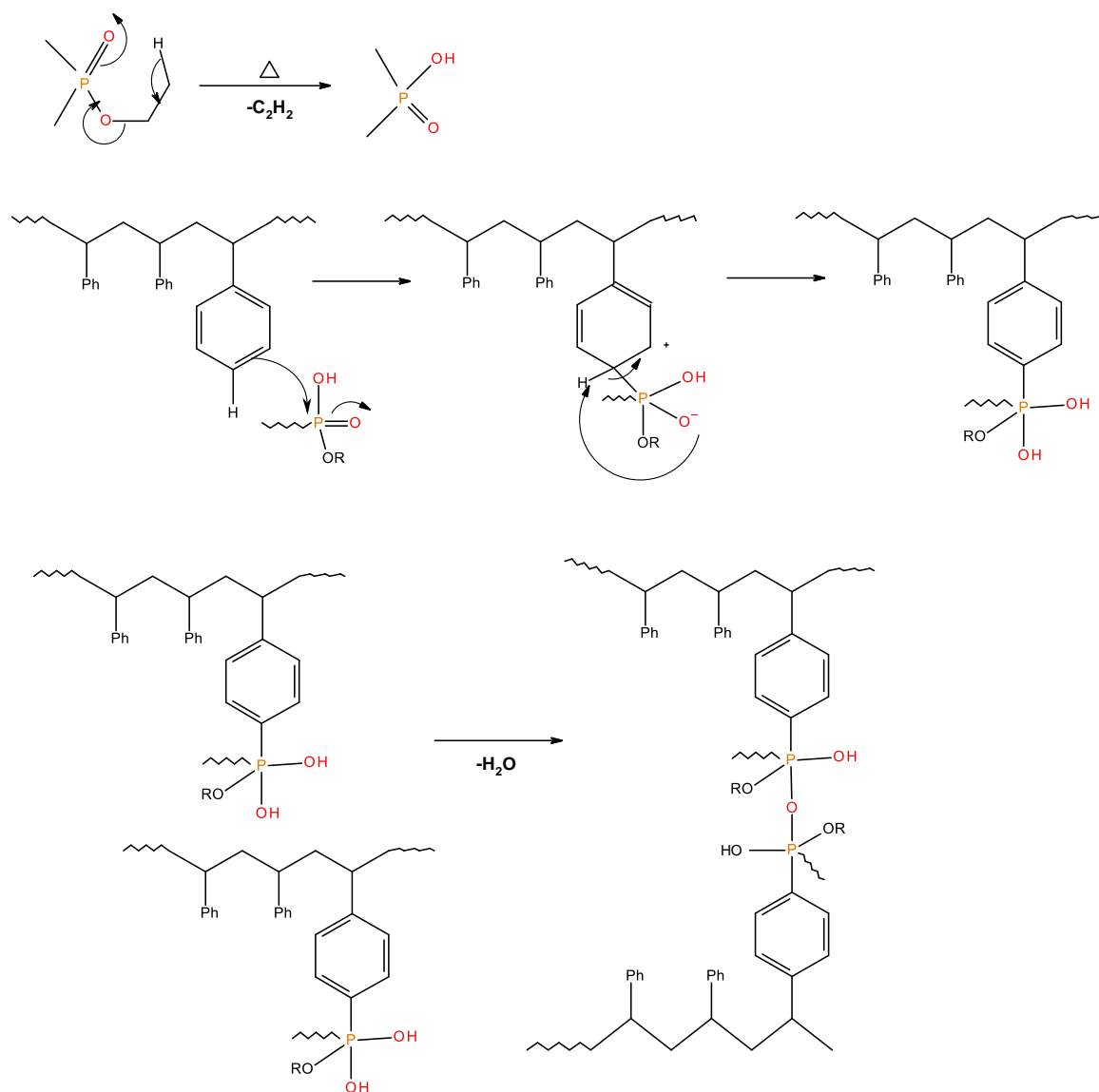


Figure 3.78 A schematic representation of the possible pathway leading to cross-linking and formation of polyphosphate linkages in modified PSt-based materials

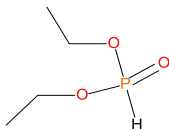
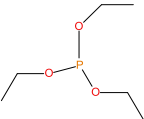
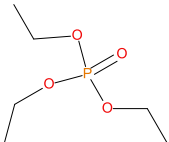
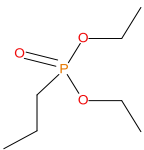
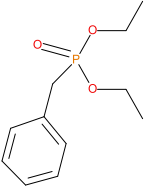
3.5.7.3 Mechanisms of flame retardance – gaseous phase

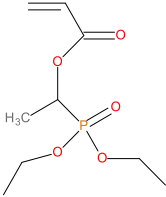
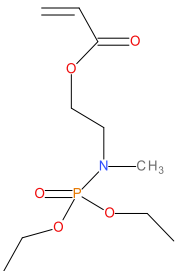
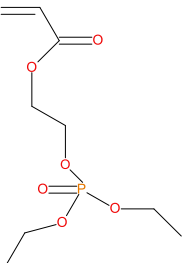
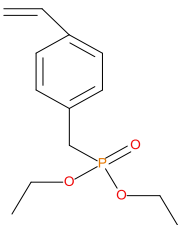
With a view to identifying the volatile fragments emanating from the liquid additives/reactives, the GC/MS data of these compounds were recorded. It should be noted that the ionization of the liquid additives was affected in the MS through an electron impact, whereas in the actual polymeric systems the modifying compounds/groups undergo pyrolysis. However, it can be assumed with a fair degree of confidence that in both cases weaker bonds are preferentially cleaved; therefore, the fragments observed in a spectrum should be similar to those formed under thermal cracking.

a. GC/MS of the liquid additives/reactives

The following table shows the chemical structures, retention times and possible fragmentation products from the various liquid additives/reactives.

Table 3.21 Retention times and fragmentation features of the various liquid additives

Sample (chemical name)	Chemical structures	Retention time (min)	Molar mass	[M] ⁺	[M±1] ⁺	[M] ⁺ (100 %)	Other predominant species/remarks
DEHPi		4.65	138	---	139	83.0	111
TEPi		3.91	166	166	---	65.0	139
TEPa		5.20	182	---	183	99.0	127
DEPP		5.01	180	---	---	125	43.0
DEBP		8.01	228	---	---	91.0	118

DE-1-AEP		5.67	236	---	---	111	45.0
ADEPMAE		7.11	265	---	266	124	55.0
DEAEPa		7.77	252	---	---	55.0	155
DEpVBP		9.07	254	254	---	117	91.0

From the presence of the $[M]^+$, or $[M\pm 1]^+$, and/or nature of $[M]^+$ (100%) and other major species, the following possible fragmentation pathways in the case of the liquid additives/reactives, can be proposed:

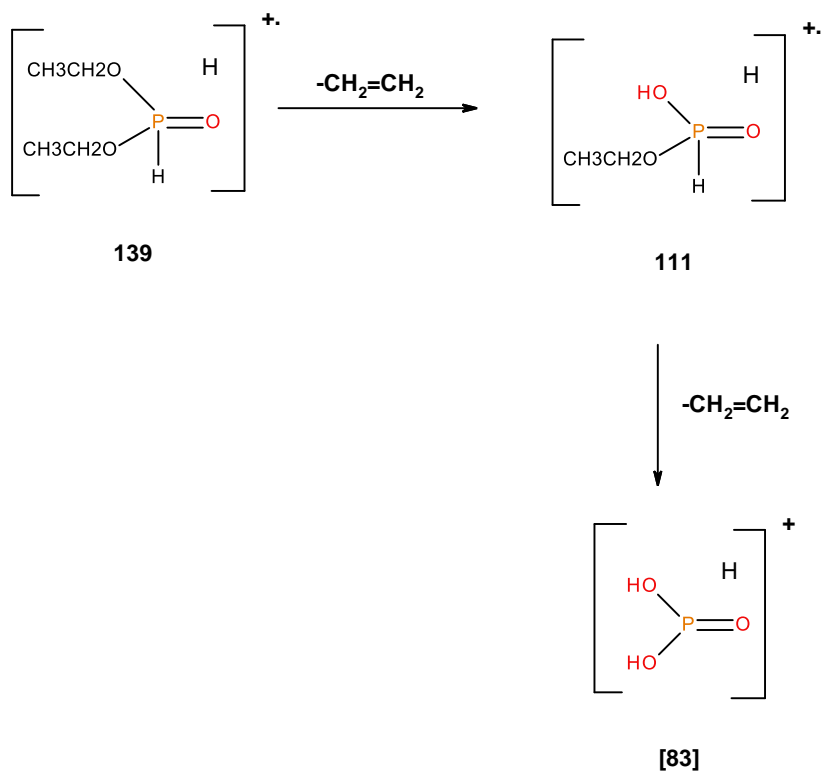


Figure 3.79 A schematic representation of possible fragmentation pattern of DEHPi

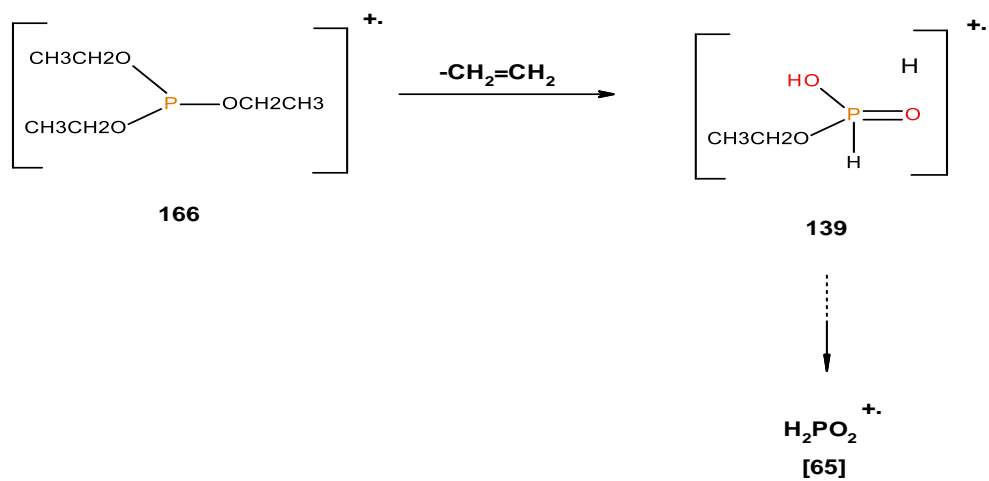


Figure 3.80 A schematic representation of possible fragmentation pattern of TEPI

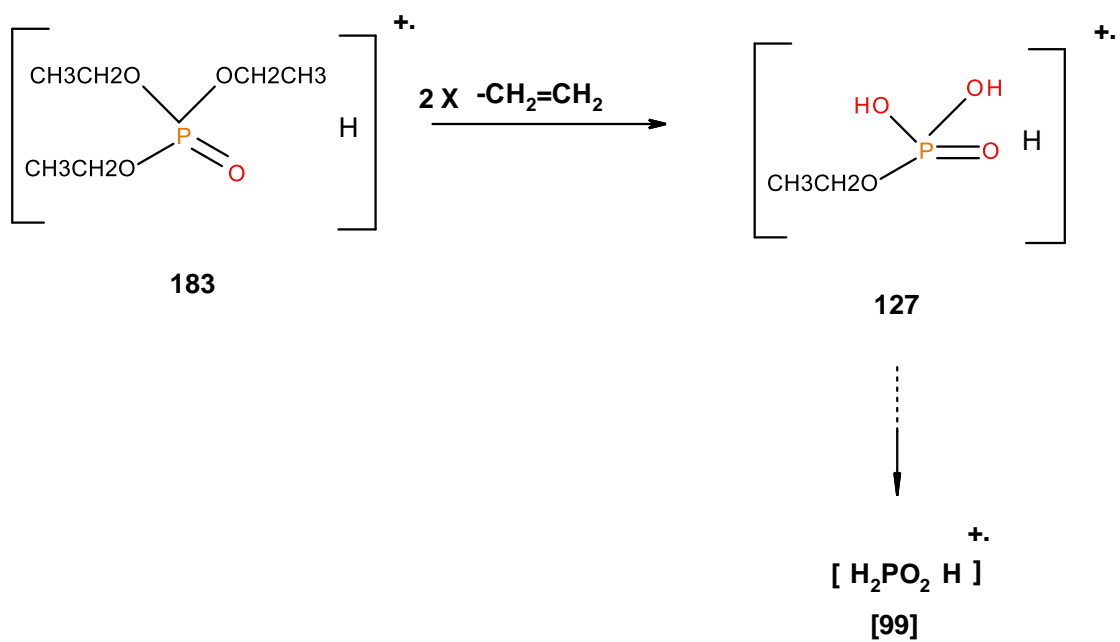


Figure 3.81 A schematic representation of possible fragmentation pattern of TEPA

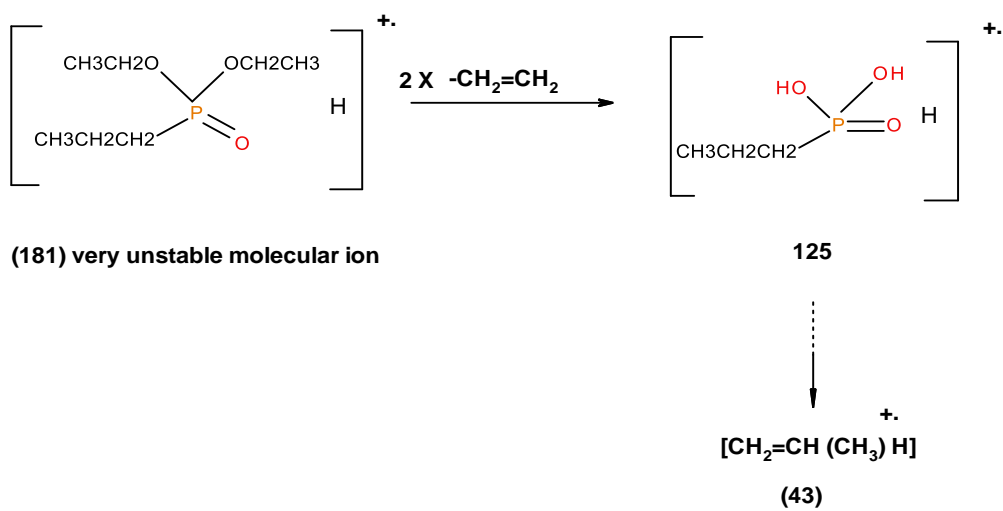


Figure 3.82 A schematic representation of possible fragmentation pattern of DEPP

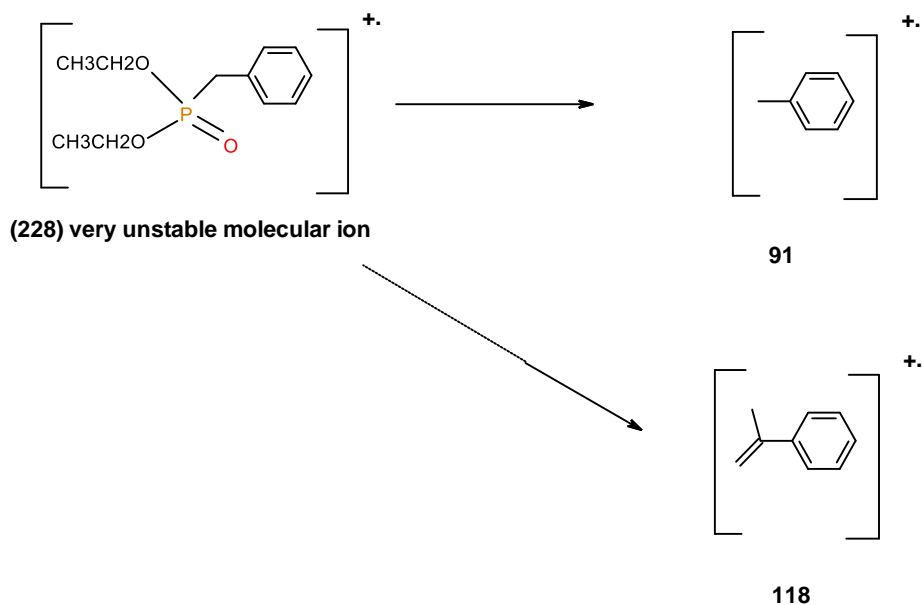


Figure 3.83 A schematic representation of possible fragmentation pattern of DEBP

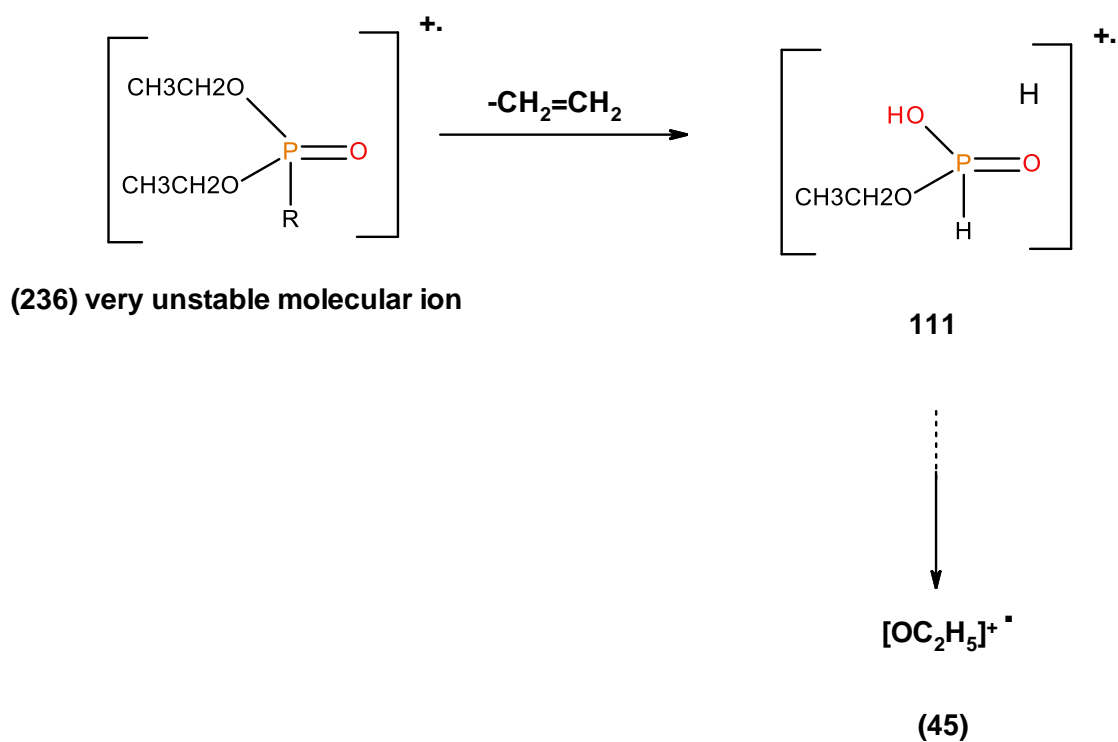


Figure 3.84 A schematic representation of possible fragmentation pattern of DE-1-AEP

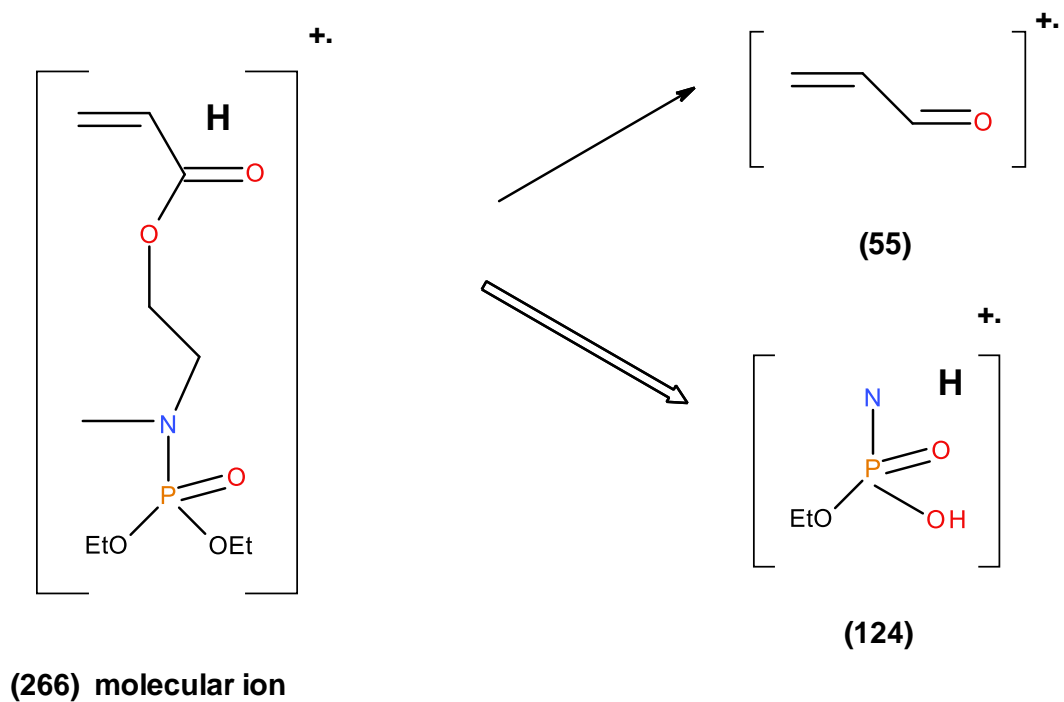


Figure 3.85 A schematic representation of possible fragmentation pattern of ADEPMAE

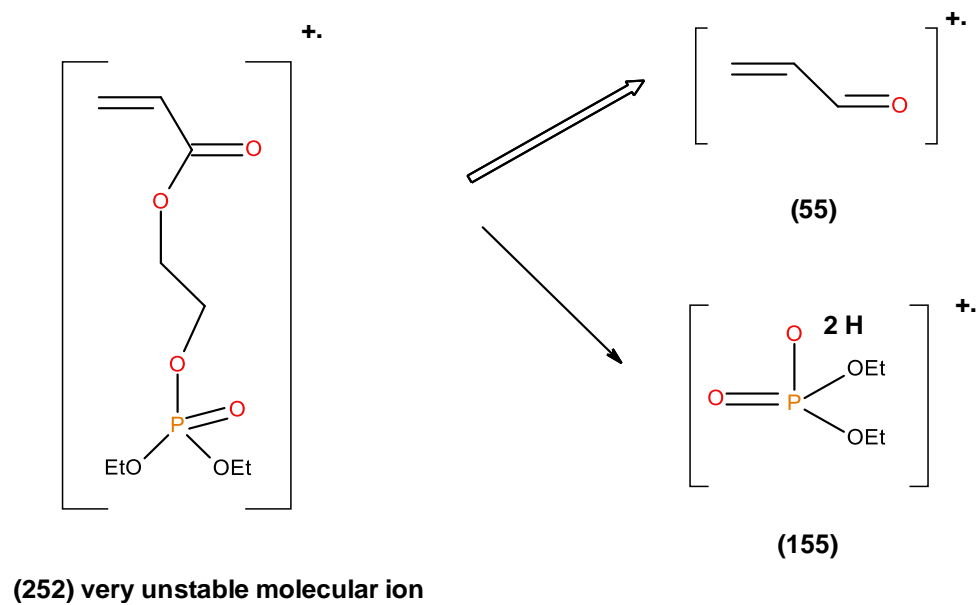


Figure 3.86 A schematic representation of possible fragmentation pattern of DEAEPA

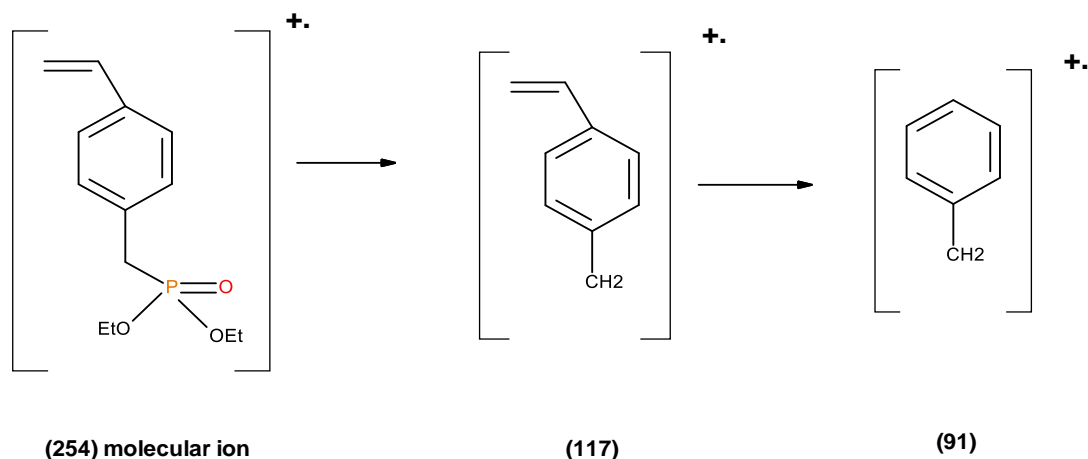


Figure 3.87 A schematic representation of possible fragmentation pattern of DEpVBP

b. Pyrolysis-GC/MS of the solid additives and polymeric systems

The temperatures for pyrolysis of the solid organophosphorus compounds, PMMA, PSt, and their modified versions with the solid additives were selected on the basis of the first derivatives of their thermograms (TGA in nitrogen at heating rate of $10^{\circ}\text{C min}^{-1}$, and from 30 to 900°C and the first derivative)- see in Figures 3.88, 3.90 and 3.92.

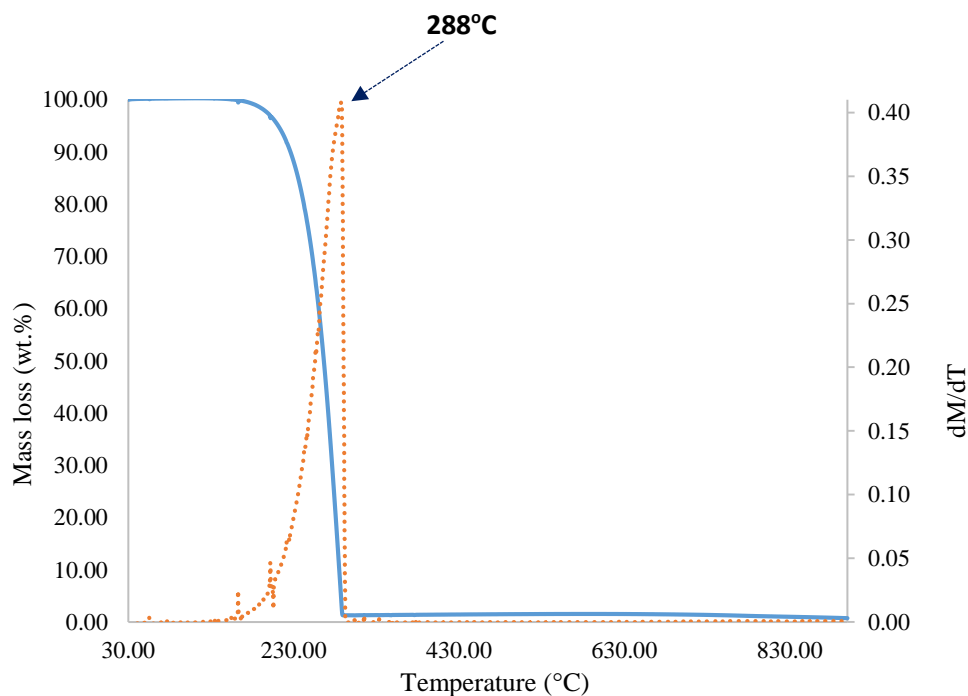


Figure 3.88 Thermogram and the corresponding first derivative of TPP in nitrogen under a heating rate of $10^{\circ}\text{C min}^{-1}$

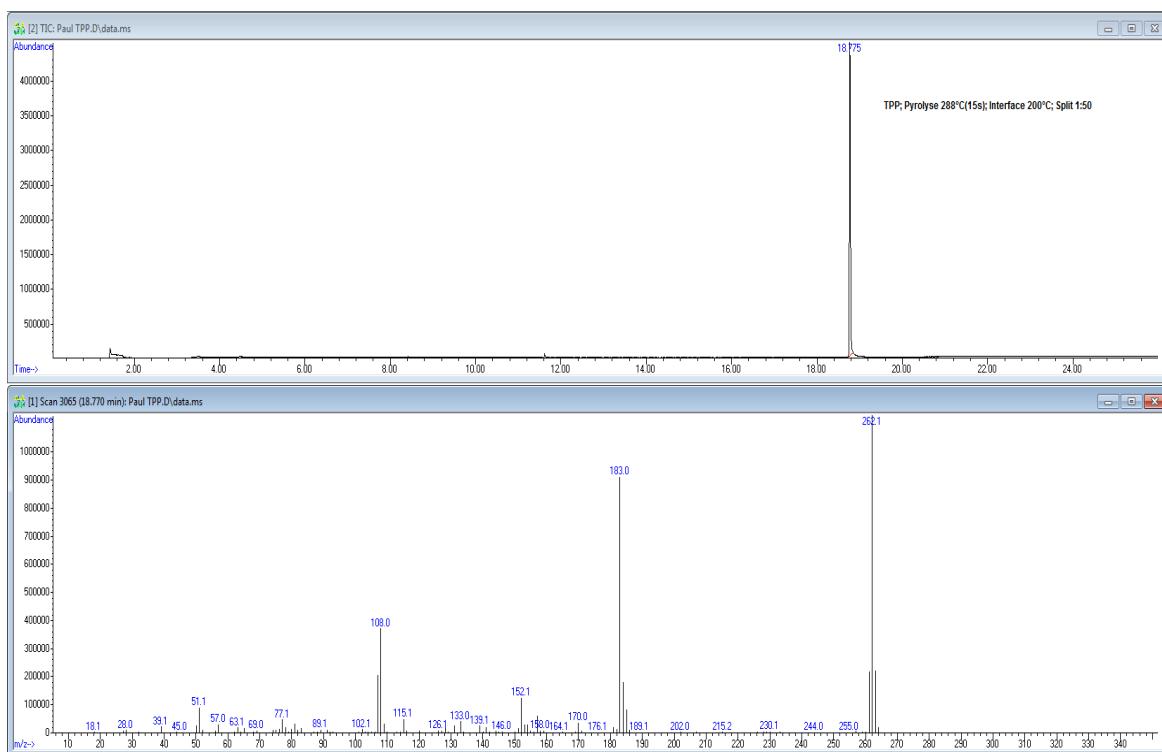


Figure 3.89 GC/MS of TPP (pyrolysis temperature, 288°C) ordinate represents the intensity of the signal (arbitrary units- top section) and abscissa the corresponding mass values (amu- bottom section)

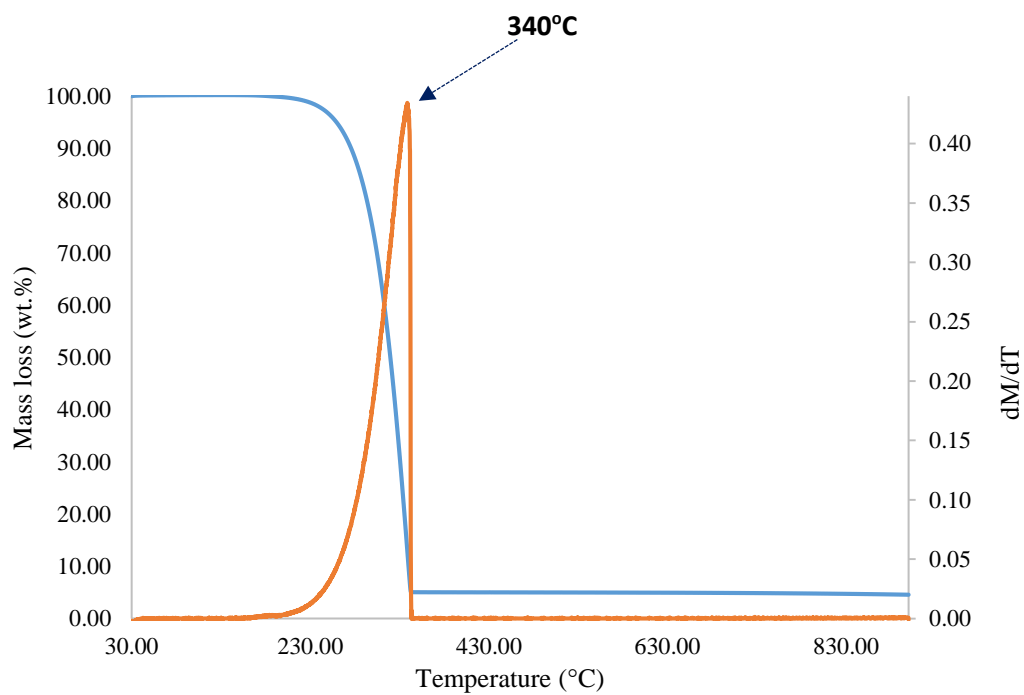


Figure 3.90 Thermogram and the corresponding first derivative of TPPO in nitrogen under a heating rate of 10°C min⁻¹

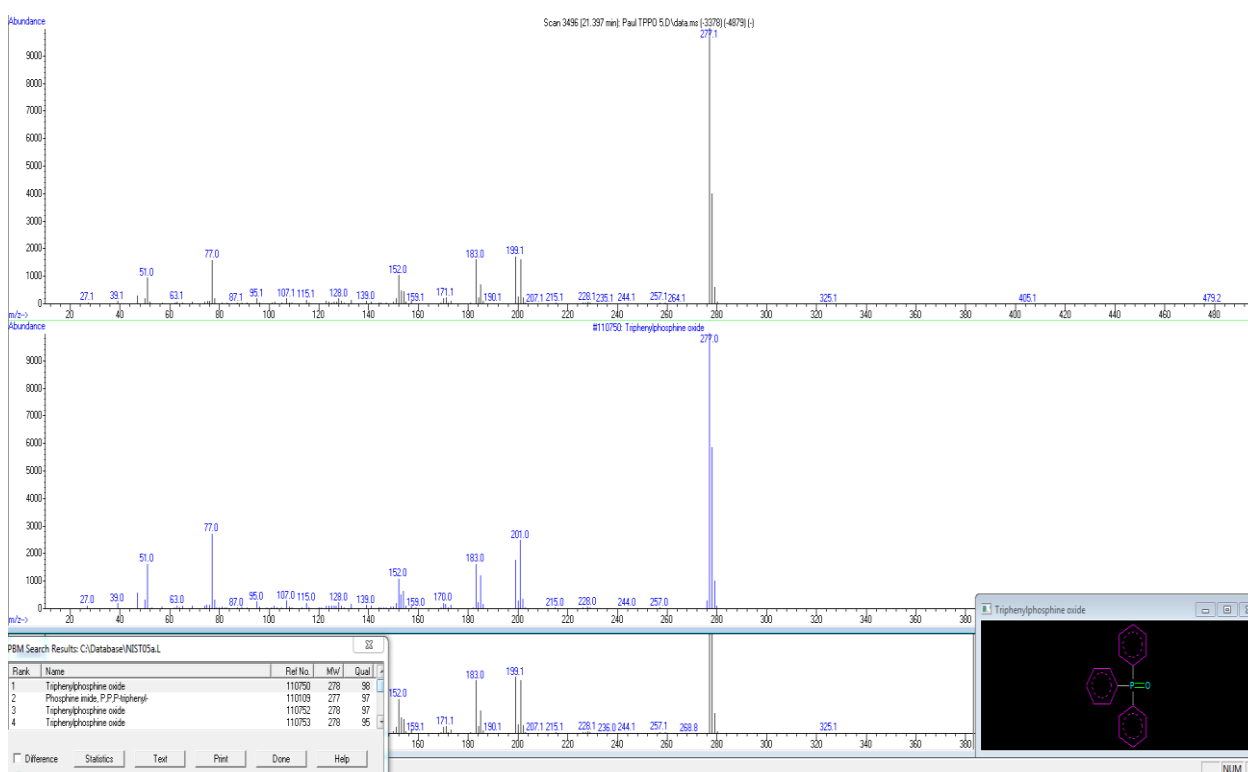
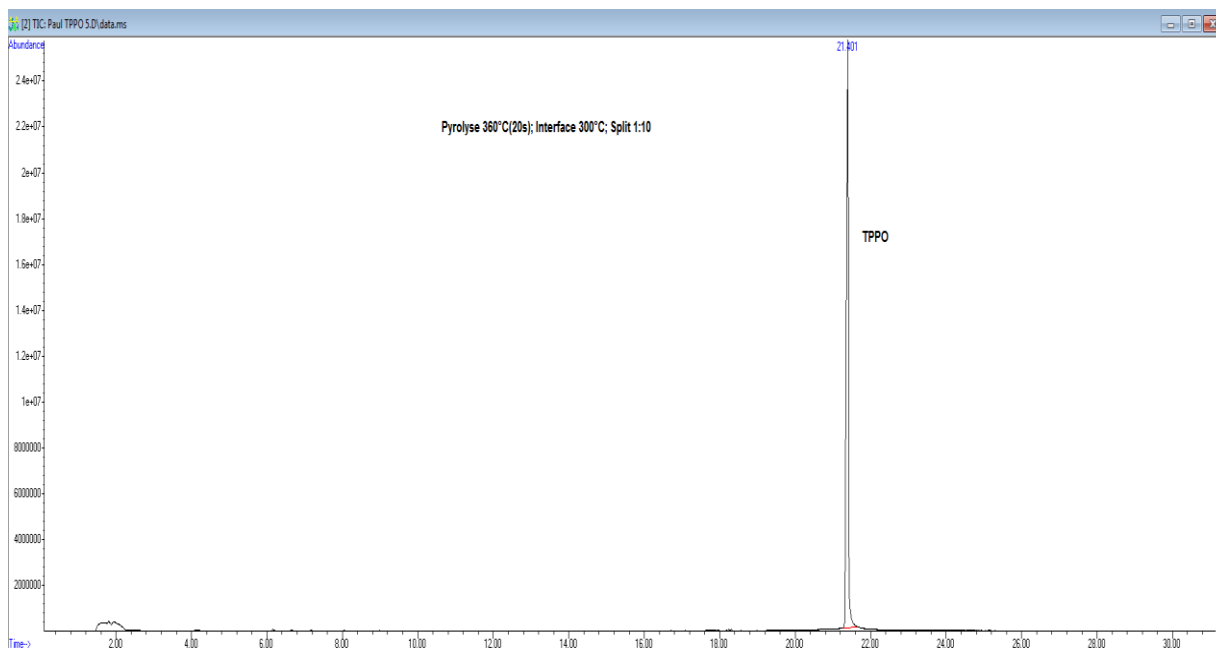


Figure 3.91 GC/MS of TPPO (pyrolysis temperature: 340°C) ordinate represents the intensity of the signal (arbitrary units- top part of the figure) and abscissa the corresponding mass values (amu- an overlay in the bottom section of the figure)

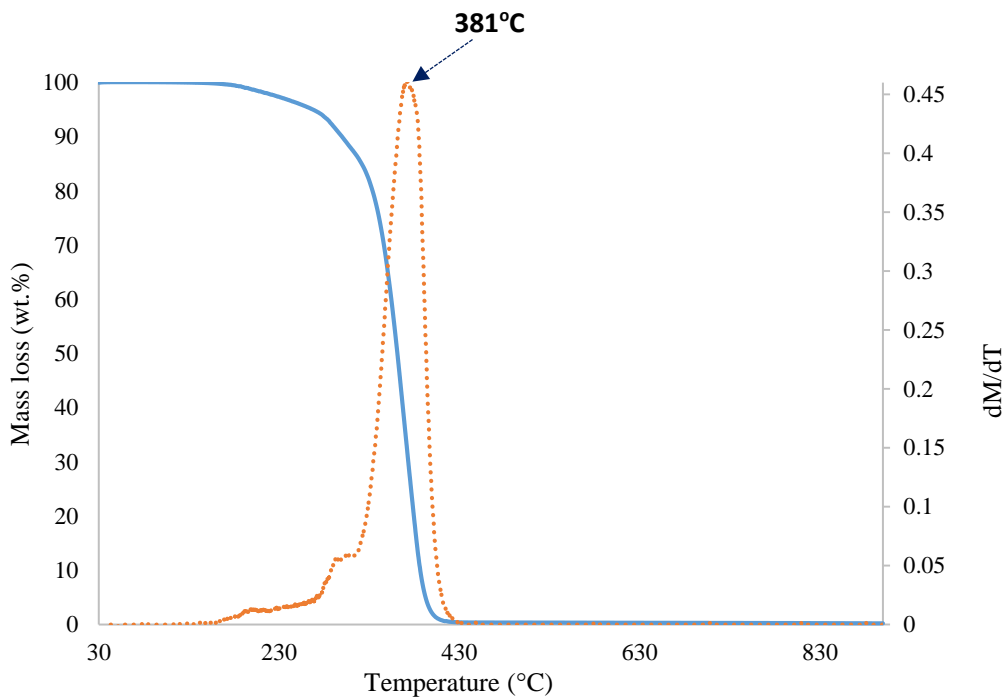


Figure 3.92 Thermogram and the corresponding first derivative of DOPO in nitrogen under a heating rate of $10^{\circ}\text{C min}^{-1}$

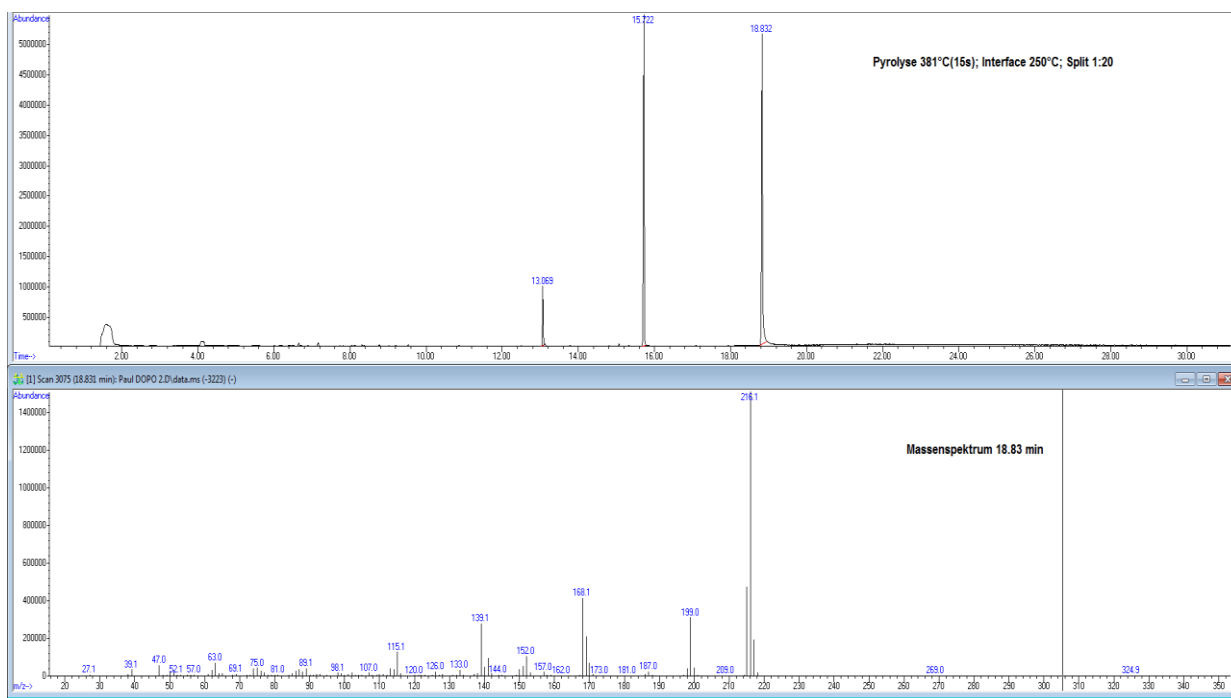
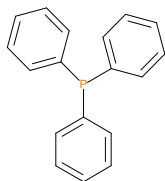
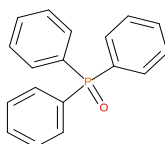
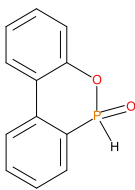


Figure 3.93 GC/MS of DOPO (pyrolysis temperature (381°C)) ordinate represents the intensity of the signal (arbitrary units- top section) and abscissa the corresponding mass values (amu- bottom section)

As can be seen from the data in Table 3.22, the GC/MS runs of TPP and TPPO, the molecular ion initially produced showed the typical fragmentation patterns of aromatic phosphine and phosphine oxide, respectively. However, in the case of DOPO, three distinct peaks were obtained in the chromatogram, and the corresponding mass spectra were indicative of DOPO (retention time = 18.83 min); decomposition product of DOPO (retention time = 15.72 min, with fragments from DOPO with m/z values of: 152, 170, 199 and 200); *o*-hydroxybiphenyl (retention time = 13.07 min) – see in Table 3.22 below for details.

Table 3.22 Retention times and fragmentation features of the various solid additives

Sample	Chemical structures	mp/bp (°C)	Pyrolysis temp. (°C)	Retention time (min)	Molar mass	[M±1] ⁺
TPP		80/377	288	18.8	263	262
TPPO		154-158/360	340	21.4	278	277
DOPO		116-120/200 (at 1mm Hg)	381	18.8	216	216

Judging primarily from the results of the pyrolysis studies (i.e. GC/MS runs) of the solid organophosphorus additives (TPP, TPPO and DOPO), and the corresponding outcomes from GC/MS for the liquid additives, we envisage the following decomposition pathways of these compounds (Figure 3.94).

In the case of the solid additives such as TPP and TPPO, initially the cleavage of the P-C (aromatic) bonds is affected to form aromatics, either phenyl or biphenyl compounds, or results in the release of elemental P and oxygenated phosphorus moieties into the gaseous phase. Elemental phosphorus and/or oxides are reported to be active in the vapour phase (Joseph & Tretsiakova-Mcnally, 2011). Here it should be noted that the presence of phosphorus (as confirmed through ICP/OES) and the chemical environment of phosphorus-bearing moieties in the condensed phase (from the respective ^{31}P NMR spectrum of the char residues) clearly indicate that the phosphine, or phosphine oxide as the case may be, is retained as such without undergoing thermal degradation.

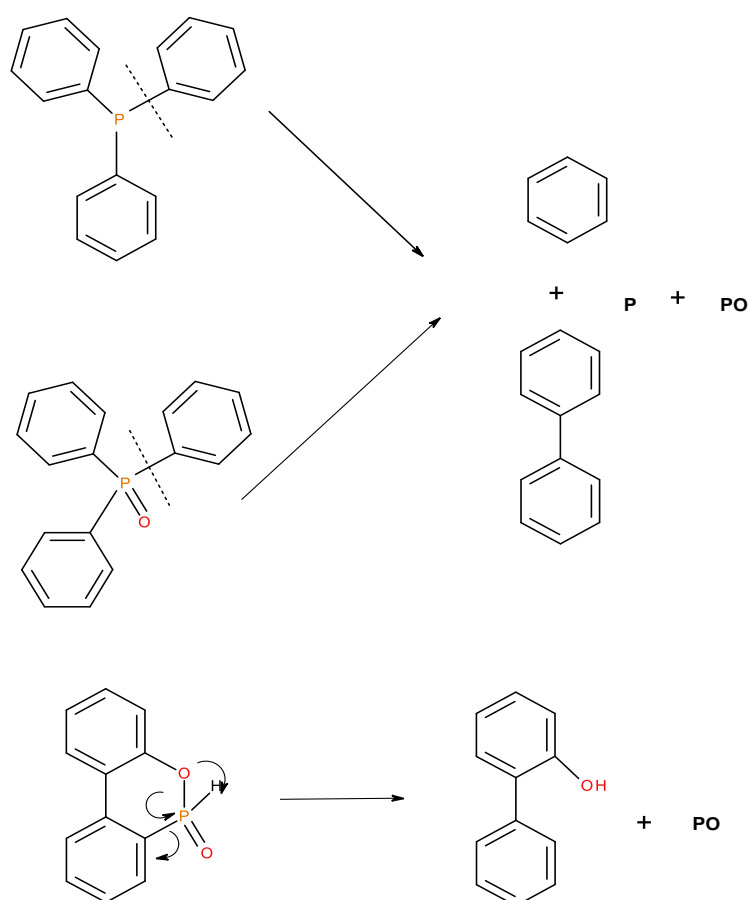


Figure 3.94 A schematic diagram of production of phosphorus-centred species in the gaseous phase in the case of solid organophosphorus additives

In the case of the liquid additives, such as DEHPi, TEPi, TEPa, DEPP and DEBP, it appears that the thermal cracking of the side phosphate, or phosphonate, group is favoured through a preferred cyclic intermediate liberating ethene (Figure 3.95), and the latter can

be considered as entropically favourable (Cinausero, *et al.*, 2008; Tretsiakova-McNally & Joseph, 2015). In the case of the liquid additives, especially with the P-atom in the oxidation state of P(V), elimination can be considered to be very feasible through the six-membered ring intermediate, whereas in the case of the phosphite (where the P-atom is in the oxidation state of P(III)) it has to go through a five-membered ring intermediate, or through a six-membered analogue if prior oxidation of P(III) to P(V) is assumed. It is relevant to note here that there is unequivocal evidence for the presence of ‘phosphorus’ acid species in the char residues from the corresponding ^{31}P solid-state NMR (signals centred around, $\delta = 0.0$ ppm).

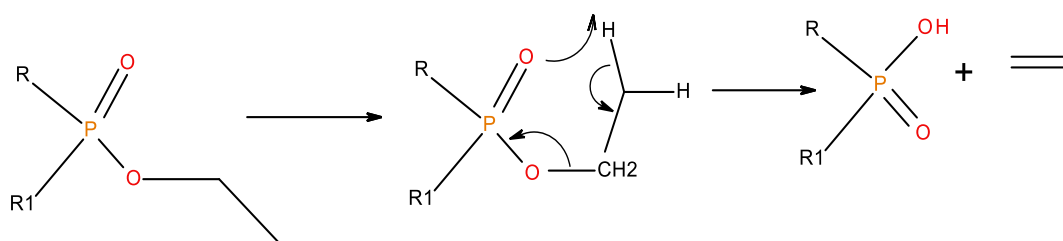


Figure 3.95 A general schematic diagram of the production of phosphorus acidic species, in the condensed phase through the elimination of ethene from the ester side groups of the liquid additives

c. Pyrolysis-GC/MS of PMMA-based materials

In the following sections, the pyrolysis-GC/MS of the unmodified PMMA and the modified versions containing the solid additives are given. Here the temperature for pyrolysis was selected from the first derivative of the TGA run obtained at a heating rate of $10^{\circ}\text{C min}^{-1}$ (Figure 3.39).

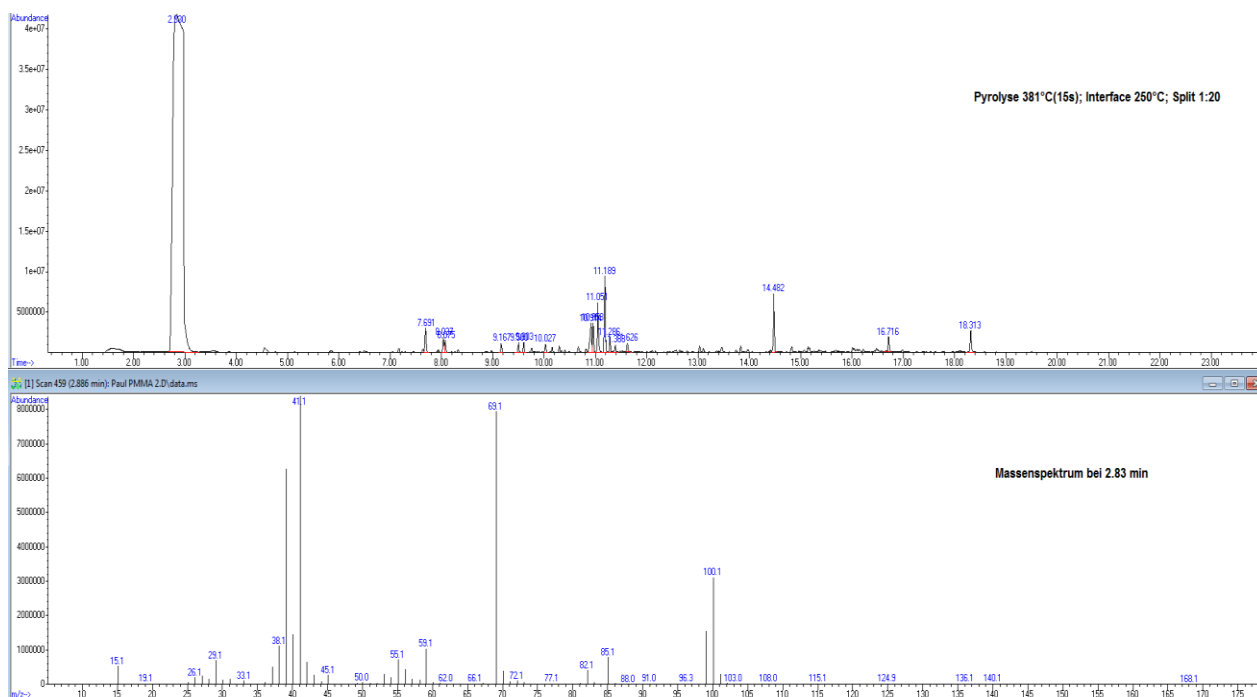


Figure 3.96 GC and MS of PMMA (pyrolysis temperature (381°C): ordinate represents the intensity of the signal (arbitrary units- top section) and abscissa the corresponding mass values (amu- bottom section)

The major component (i.e. MMA monomer) appeared with a retention time of 2.83 min, and other minor components originating from the initiators (BPO and DCP) in varying amounts can be observed as follows: 7.69 min (acetophenone); 8.04 (methylcumyl ether); 14.48 min (phenylbenzoic acid); 16.72 min (methylhexadecanoate); 18.31 min (methyloctadecanoate); etc.

In the case of PMMA+TPP system (Figure 3.97), apart from the major components (MMA monomer from the homopolymer at 2.99 min and the additive, TPP, at 18.77 min), several smaller fragments from the initiator species were also observed: 6.52 min (methyl styrene); 7.71 min (acetophenone); 7.95 (α -cumyl alcohol); 8.10 min (methylbenzoate). It appears that during the pyrolysis at 246°C, the base matrix and additive degrade independently without any noticeable interaction. The same type of behavior was observed in the case of the other two modified PMMA systems (PMMA+TPPO and PMMA+DOPO), as shown in Figures 3.98 and 3.99. Generally, some corroborative evidence regarding the mode of action of the modifying groups can be also drawn from the corresponding TGA, DSC and PCFC tests.

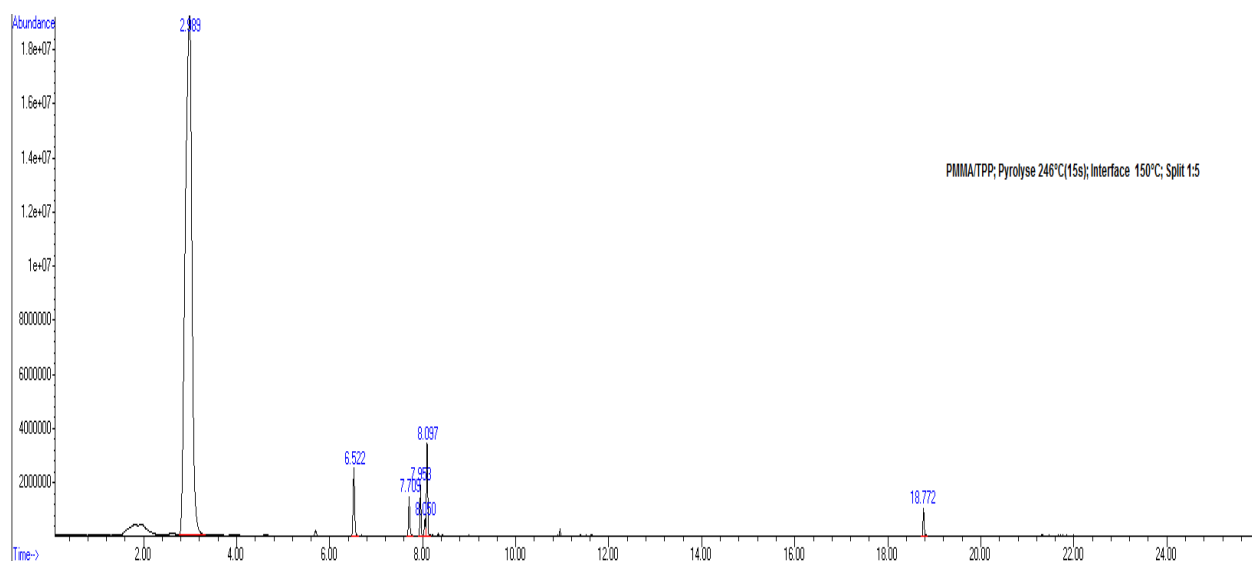


Figure 3.97 Gas chromatogram of PMMA+TPP (pyrolysis temperature: 246°C): ordinate represents the intensity of the signal (arbitrary units) and abscissa the corresponding retention times (min)

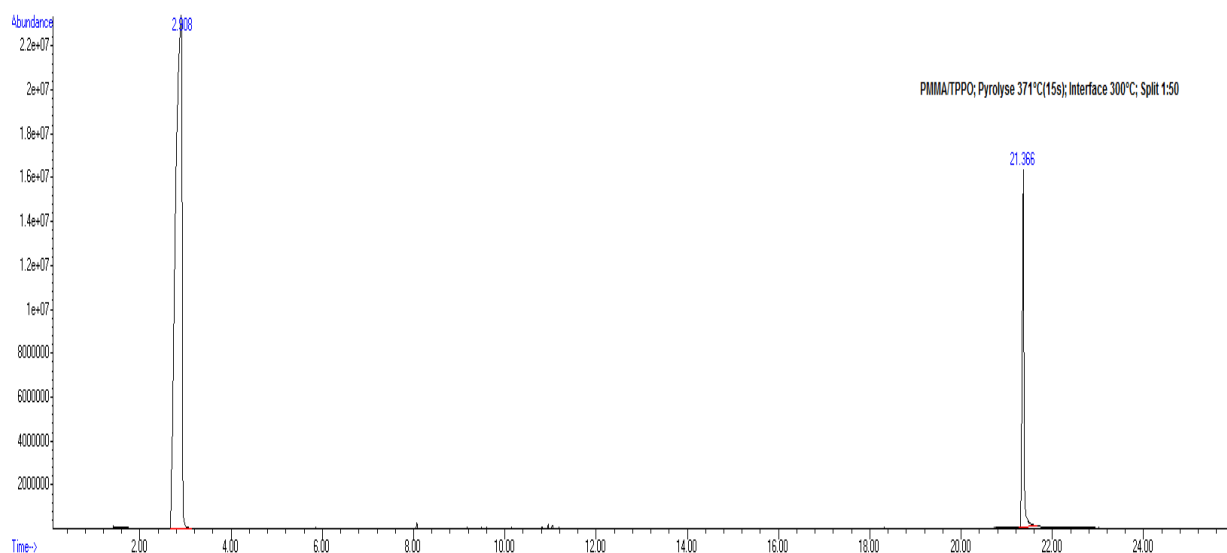


Figure 3.98 Gas chromatogram of PMMA+TPPO (pyrolysis temperature: 371°C): 2.91 min (MMA monomer) and 21.37 min (TPPO) as the major fragments; ordinate represents the intensity of the signal (arbitrary units) and abscissa the corresponding retention times (min)

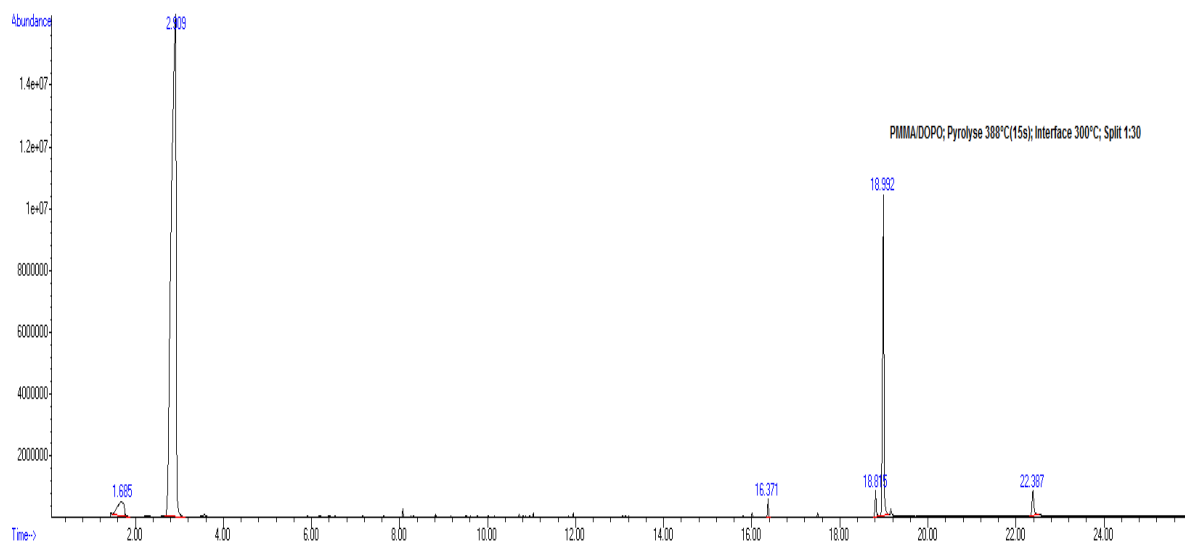


Figure 3.99 Gas chromatogram of PMMA+DOPO (pyrolysis temperature: 388°C): 2.91 min (MMA monomer) and 18.99 min (DOPO) as the major fragments; ordinate represents the intensity of the signal (arbitrary units) and abscissa the corresponding retention times (min)

d. Pyrolysis-GC/MS of PSt-based materials

Here again the temperature for pyrolysis was selected from the first derivative of the TGA run obtained at a heating rate of $10^{\circ}\text{C min}^{-1}$ (Figure 3.45). As expected, apart from the monomeric units, there were varying amounts of decomposition products from the other main chain scissions, or from side groups, from PSt. Furthermore, a small number of minor components emanating from the pyrolysis of initiator species can also be seen in the chromatogram/mass spectrum (see also Table 3.23). In the modified versions (PSt+TPP, PSt+TPPO and PSt+DOPO), in addition to the abovementioned fragments, the corresponding additive compounds were found: TPP (18.85 min); TPPO (21.34 min); DOPO (18.81 min). Here again, no co-operative interaction can be noticed for these solid additives, and therefore it is to be assumed that the homopolymer matrix and the additive compound underwent decomposition independently.

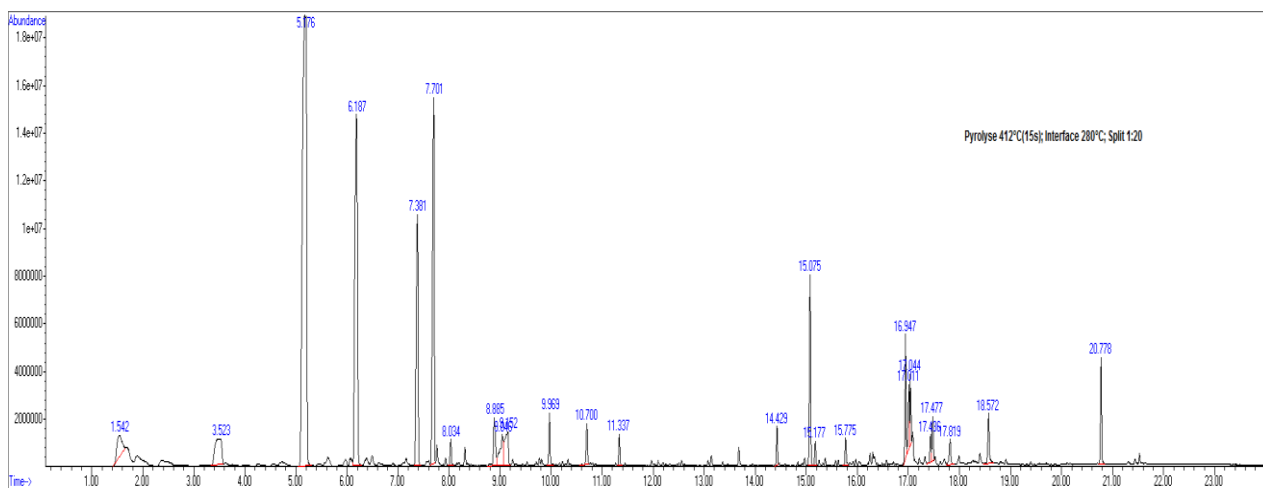


Figure 3.100 Gas chromatogram of PSt (pyrolysis temperature: 412°C): ordinate represents the intensity of the signal (arbitrary units) and abscissa the corresponding to retention time (min)

Table 3.23 The retention times and corresponding masses of the major fragments for PSt

Sl. No.	Retention time (min)	m/z	Species
1	5.18	104	Styrene
2	6.19	106	Benzaldehyde
3	7.70	120	Acetophenone
4	15.1	208	Styrene dimer

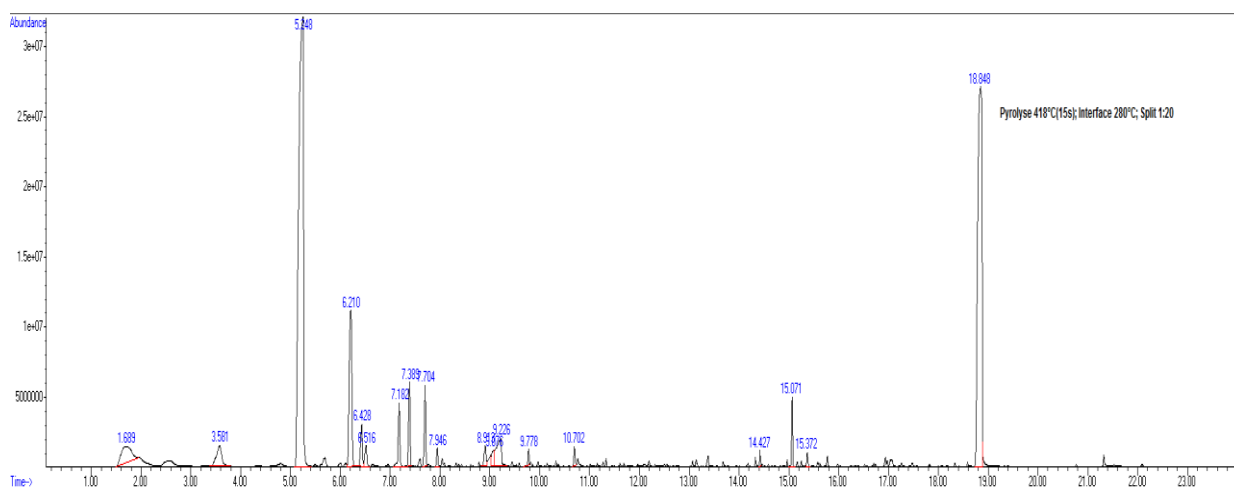


Figure 3.101 Gas chromatogram of PSt+TPP (pyrolysis temperature: 418°C): ordinate represents the intensity of the signal (arbitrary units) and abscissa the corresponding retention times (min)

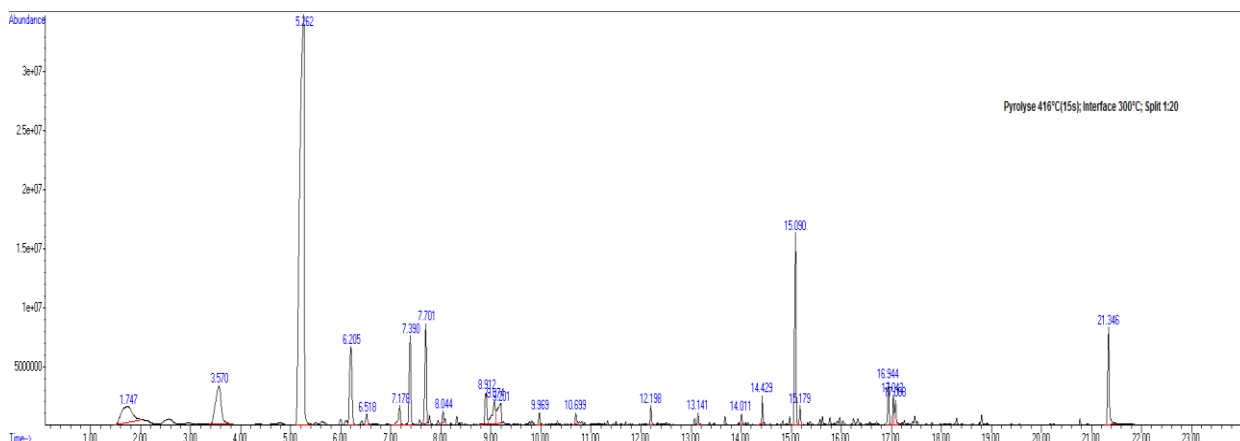


Figure 3.102 Gas chromatogram of PS+TPPO (pyrolysis temperature: 416°C): ordinate represents the intensity of the signal (arbitrary units) and abscissa the corresponding retention times (min)

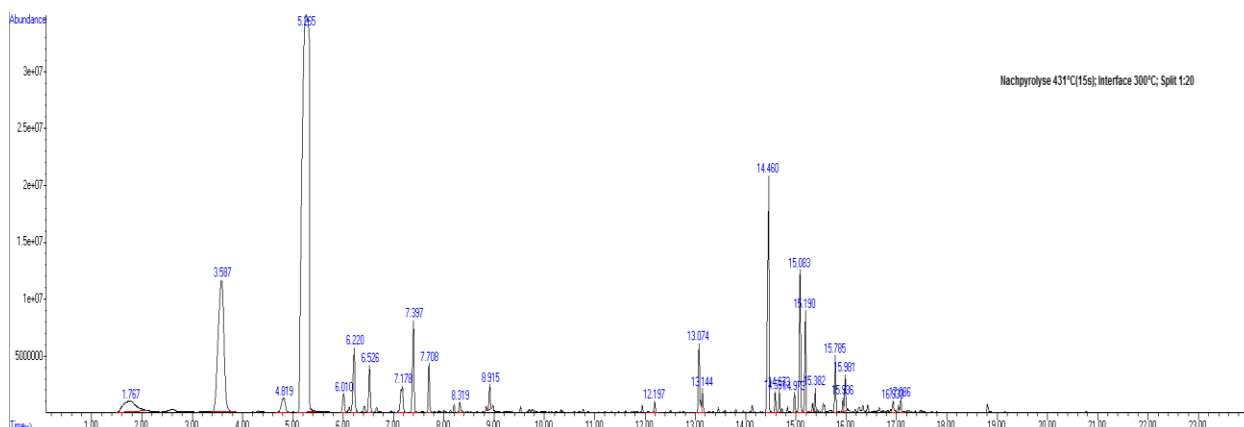


Figure 3.103 Gas chromatogram of PS+DOPO (pyrolysis temperature: 431°C): ordinate represents the intensity of the signal (arbitrary units) and abscissa the corresponding retention times (min)

3.6 Corrosion studies

There are reports in the literature regarding the resistance of some phosphorus-containing acrylic materials towards bio-fouling and corrosion of ferrous metals (Pospiech, *et al.*, 2017; Pospiech, *et al.*, 2013). This can be considered as an advantageous attribute given that bio-fouling can lead to an enhanced degree of corrosion, and *vice versa*. Therefore,

there is a potential application for some of the phosphorus-modified systems obtained through the current project as protective coatings for ferrous metals when they are exposed to aqueous media. Hence, a preliminary investigation into the efficacy of some chosen phosphorus-modified acrylic systems as protective agents for mild steel substrates were performed. For this purpose, the substrate of interest (i.e. mild, thin steel specimens, having dimensions of 1 cm × 1 cm × 1 mm), both uncoated (US) and coated (CS) with PMMA, and two coated of the phosphorus-modified acrylic systems (PMMA+DE-1-AEP and PMMA+DEAEPa), were chosen. It is relevant to note here that the modified systems showed enhanced adhesion to the base substrate, owing to their increased polar character imparted by the pendent phosphonate, or phosphate, group. In this context two different types of aqueous phases, i.e. deionized water (DIW) and sea water (SW) were selected, the latter was sourced locally from a beach situated in the South-sea shore of Victoria, Australia. The pertinent properties of the two media were measured. The corresponding values of tap water is also included for the purpose of comparison (see in Table 3.24).

Table 3.24 Different parameters relating to the aqueous media

Sample	Temp (°C)	pH	*ORP (mV)	Conductivity (mS cm ⁻¹)	Turbidity #(NTU)	^{\$} TDS (g L ⁻¹)	[‡] Salinity (ppt)	[^] Density (σ t)	Depth (m)
DI water	19.36	5.67	233	0.019	0.0	0.012	0.00	0.0	0.10
Sea water	16.74	7.85	250	55.80	0.0	33.50	36.7	27	0.10
Tap water	16.34	5.43	580	0.081	3.0	0.520	0.00	0.0	0.10

The relevant parameters were measured using a proprietary kit (Horiba Water Quality Meter). The probe was immersed in the medium, and allowed to equilibrate for ca. 5 min, and then the readings were taken

*ORP oxidation-reduction potential

#NTU turbidity (nephelometric turbidity unit)

^{\$}TDS total dissolved solids

[‡]ppt salinity (parts per thousand)

[^]σt density (kg L⁻¹)

The sea water was found to be slightly alkaline and, as expected, it exhibited substantial degrees of conductivity, salinity and also contained the maximum amount of dissolved

solid contents. The details of the two laboratory-scale methods that were developed through the present work to study the corrosion behavior are given in Chapter 2, Sections 2.3.5 and 2.4.4.2 (pages 45-50 and 60). Here it was also found that the modification of PMMA- and PSt-based polymers resulted in increased polarity and this, in turn, facilitated a better degree of adhesion of the materials onto mild steel specimens. The Fe(III) ion contents in the aqueous extracts of each sample were quantitatively measured through ICP/OES. The results obtained are given in the tables below (Table 3.25 and 3.26).

Table 3.25 Fe(III) in the aqueous extracts of blank and uncoated substrates

Sl. No	Samples	Medium	Time (d)	Fe(III) content (ppm)
1	*Blank 1	DIW	0	00.00
2	*Blank 2	SW	0	00.00
3	US 1	DIW	8	21.10
4	US 1	SW	8	15.75
5	US 2	DIW	22	44.80
6	US 2	SW	22	49.80

*here no specimens were taken, and therefore the measured Fe(III) contents denotes the values for the media

The phosphorus content of DIW was found to be zero, whereas SW showed a residual phosphorus value, averaged over several measurements, to be *ca.* 13.0 ppm. It can be also noticed from the above table that the aqueous extracts obtained from the tests with the uncoated, mild steel substrates showed increases in the Fe(III) contents with the duration of the experiments. Therefore, the technique showed sufficient sensitivity in gauging the extents of corrosion by quantitatively measuring the iron contents (Malel & Shalev, 2013). Furthermore, the induction periods for the physio-chemical processes resulting in a measurable degree of corrosion is below a week or so, where such effects were also visible in the materials under study. Table 3.26 below shows the results obtained for the coated substrates, in comparison with the second set of uncoated substrates in both DIW and SW, after a time period of 22 days.

Table 3.26 Fe(III) and P contents in the aqueous extracts of uncoated and coated substrates after 22 days

Sl. No	Samples	Medium	Fe(III) content (ppm) \pm 1%	P content (ppm) \pm 1%
1	US 2	DIW	44.8	0.00
2	US 2	SW	49.8	13.9
3	CS (PMMA) 1	DIW	10.0	0.00
4	CS (PMMA) 2	SW	3.02	13.4
5	CS (PMMA+DE-1-AEP) 1	DIW	17.2	67.0
6	CS (PMMA+DE-1-AEP) 2	SW	2.90	89.0
7	CS (PMMA+DEAEPa) 1	DIW	3.98	406
8	CS (PMMA+DEAEPa) 2	SW	0.00	299

Here, it can be clearly observed that all of the polymer-coated substrates showed a significant reduction in the values of the Fe(III) content in both media. The substrate coated with PMMA+DEAEPa, immersed in seawater had an undetectable Fe(III) content thus illustrating that it has the maximum efficiency amongst the materials tested in preventing the corrosion of the underlying substrate. It can be also noticed that the modified systems release varying amounts of phosphorus-bearing moieties that were subsequently converted to soluble phosphates during the ICP/OES run. Furthermore, as expected, the pendent phosphate groups (i.e. in PMMA+DEAEPa) are subjected to an increased degree of hydrolysis than the more stable phosphonate linkages (in PMMA+DE-1-AEP). It is likely that the phosphorus-modified coatings not only are efficient in controlling the extents of corrosion, but also can be considered to be potential barriers for mitigating bio-fouling, resulting from the release of phosphorus-bearing species into the surrounding medium (Pospiech, *et al.*, 2017; Pospiech, *et al.*, 2013).

3.6.1 Imaging software for analyzing the extent of surface corrosion on mild steel

In the following section, the utility of an in-house developed software for gauging the extent of corrosion of a thin, mild steel specimen (10 cm \times 10 cm \times 1 mm) over a two months' period is discussed. The digital photographs of the surface that underwent corrosion were analyzed by utilizing the software, and the degree of corrosion in terms of

the percentage of the black pixels obtained through the runs with time (in days) were plotted, as shown below in Figure 3.104. The corresponding contrasts in the digital colour frames along with the images generated by the software are also given in Figure 3.105.

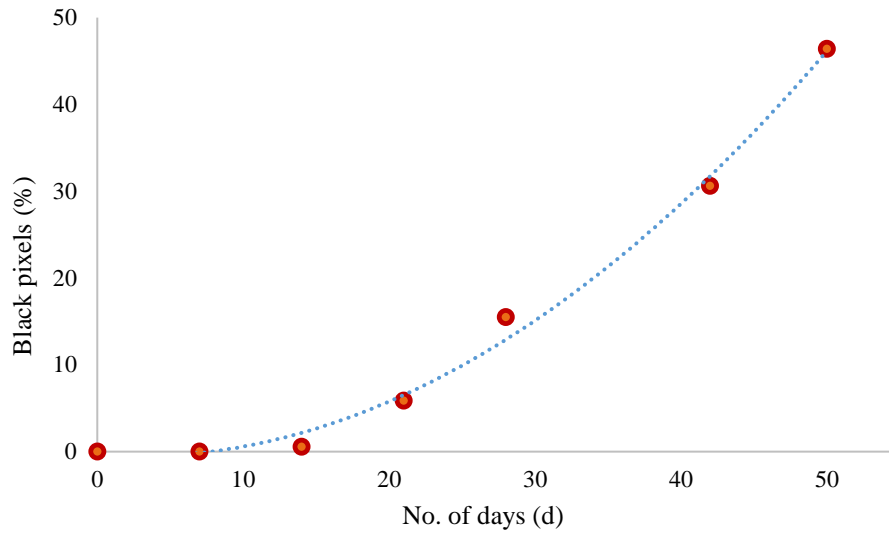


Figure 3.104 A plot of black pixels (in percentage) vs. time (in days)

2 Jan 2020 modified.jpg (296 x 300)

R 255
G 255
B 204
Range 31

Clear Image

Process Image

Progress

Calc Status OK

# black pixels	0	total # pixels	88800
# white pixels	88800	% black pixels	0.00

(A): day 1



9th Jan 2020 modified.jpg (296 x 303)

R 113
G 49
B 5
Range 47

Clear Image

Process Image

Progress

Calc Status OK

# black pixels	0	total # pixels	89688
# white pixels	89688	% black pixels	0.00

(B): after 7 days



16 Jan 2020 modified.jpg (294 x 300)

R 255
G 255
B 255
Range 20

Clear Image

Process Image

Progress

Calc Status OK

# black pixels	456	total # pixels	88200
# white pixels	87744	% black pixels	0.52

(C): after 14 days





23 Jan 2020 modified.jpg (289 x 300)

R	<input type="range" value="143"/>	
G	<input type="range" value="73"/>	
B	<input type="range" value="22"/>	
Range	<input type="range" value="55"/>	



Process Image

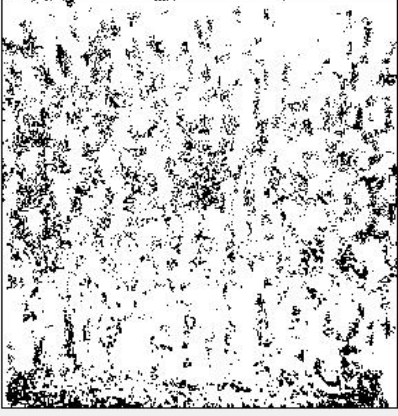
Progress

Calc Status OK

# black pixels	5057	total # pixels	86700
# white pixels	81643	% black pixels	5.83

(D): after 21 days





30 Jan 2020 modified.jpg (290 x 300)

R	<input type="range" value="174"/>	
G	<input type="range" value="83"/>	
B	<input type="range" value="46"/>	
Range	<input type="range" value="35"/>	



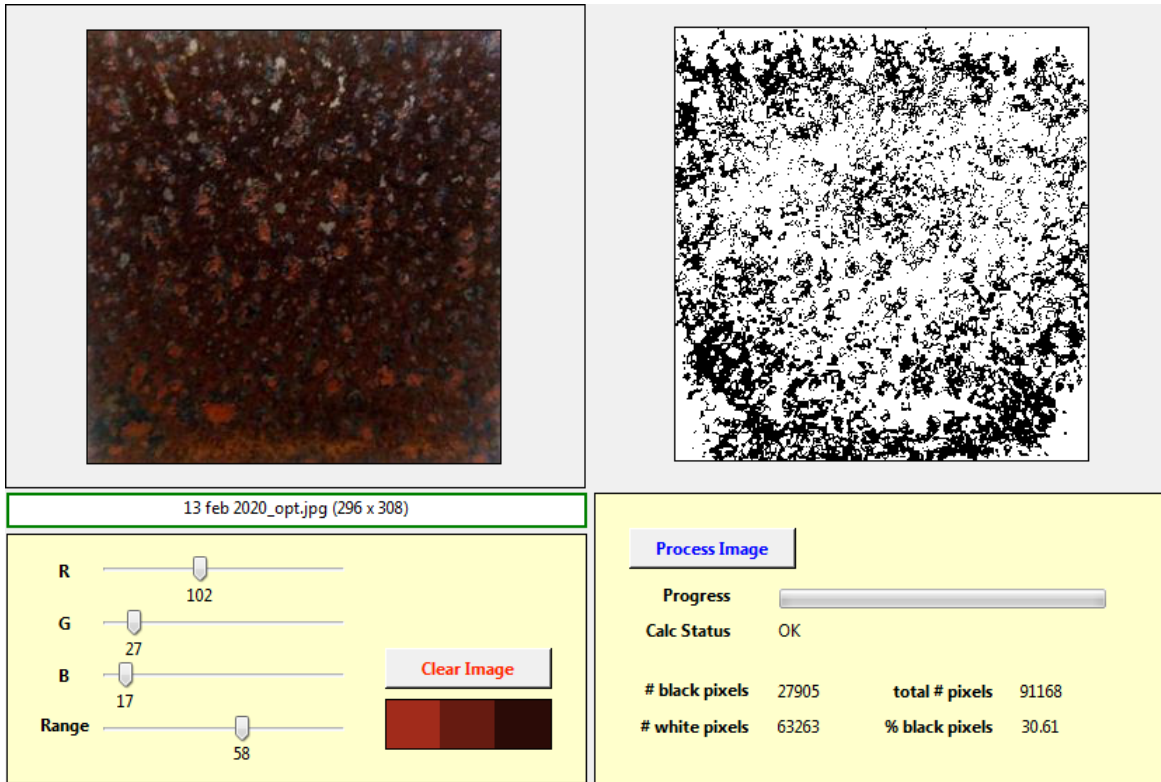
Process Image

Progress

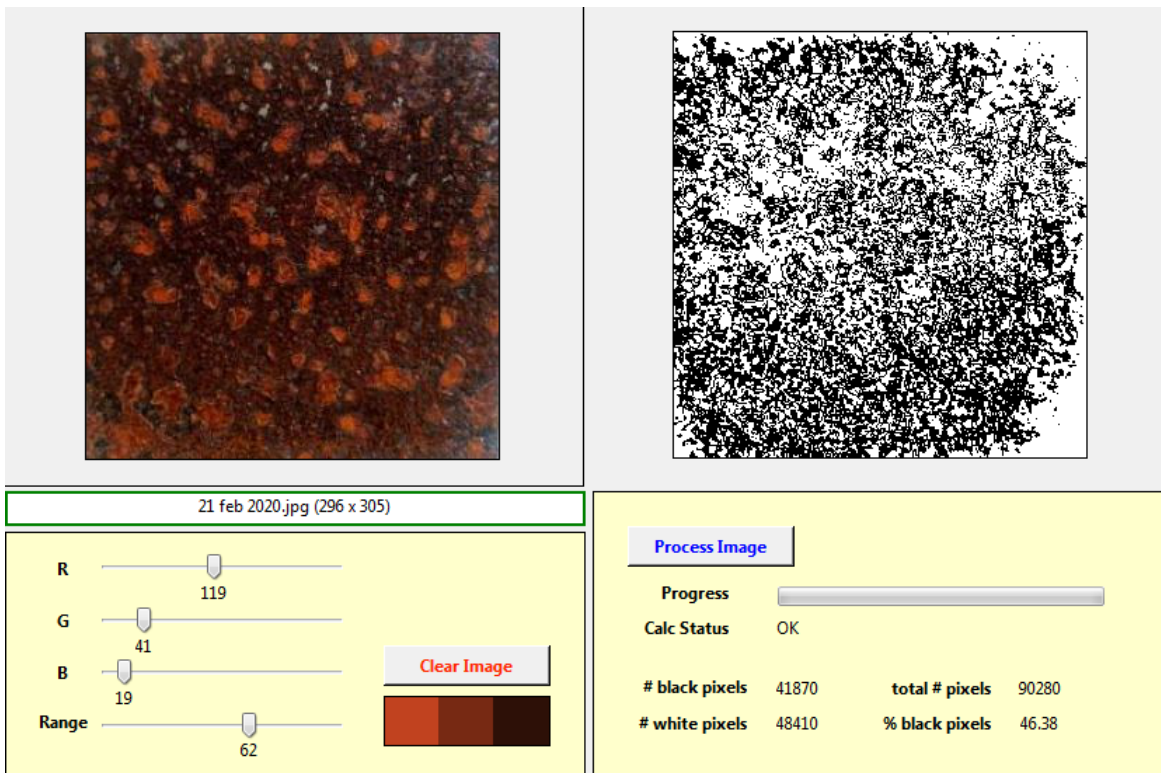
Calc Status OK

# black pixels	13452	total # pixels	87000
# white pixels	73548	% black pixels	15.46

(E): after 28 days



(F): after 42 days



(G): after 50 days

Figure 3.105 Digital photographs and corresponding software outputs of the exposed surface of the test specimen at different time intervals (in days): (A) 0; (B) 7; (C) 14; (D) 21; (E) 28; (F) 42; (G) 50

It can be clearly seen from the graph (Figure 3.104) and the associated pictures (Figure 3.105) that the proposed methodology constitutes a simple, time-bound and semi-quantitative laboratory-scale technique that can lead to reliable results. In addition, it is superior to many of the conventional electro-analytical techniques to follow corrosion in that it completely eliminates the necessity to set up often tedious and bespoke galvanic cells, such as in a Tafel extrapolation test (Amin, *et al.*, 2010). For more quantitative results it is desirable to carry out the analyses of Fe(III) contents, as given in the current work (ICP/OES technique), in conjunction with the proposed method.

CHAPTER 4: MAIN CONCLUSIONS AND SUGGESTIONS FOR FUTURE WORK

4.1 Main conclusions

As initially set out in the introductory part of the thesis, the thermal degradation and combustion behaviours of a number of polymers, produced through both step-growth and chain-growth polymerization techniques, were studied. The step-growth polymers included, polyaniline, polypyrrole and polydopamine. In the case of chain-growth polymers, polymethyl methacrylate and polystyrene were chosen as the base substrates. The modifying agents in the latter case included both additive and reactives, incorporating phosphorus-, and optionally phosphorus-/nitrogen-containing compounds, where the chemical environment/oxidation state of the P atom also differed. The activities of such modifying groups on the thermal degradation behaviours and combustion attributes of the parent polymeric substrates were evaluated, and the underpinning mechanisms were elucidated. The following main conclusions can be drawn from the current study.

The oxidative polymerization of the monomers, aniline hydrochloride, pyrrole and dopamine hydrochloride, for preparing the step-growth polymers were found to be successful, resulting in the desired products with varying yields. In addition, the thermal and calorimetric measurements of the step-growth polymers showed that they are endowed with good thermal stability and combustion resistance, thus making them ideal candidates for the use as fire resistant coatings. However, it was found that a uniform coating of the step-growth polymers cannot be achieved using the two methods that was tried on a laboratory scale.

All synthetic procedures that were used to prepare the additive, precursors for monomers and functional monomers for chain-growth polymers were found to be quite facile, furnishing the desired products in appreciable yields and with an acceptable level of purity. The chemical structures of these compounds were inferred from ^1H and ^{31}P NMR spectra, and through GC/MS analyses. The various laboratory-scale methods for chain-growth polymerizations were also utilized for producing homopolymers of MMA and St (i.e., through solution, bulk, aqueous-slurry, suspension and emulsion). These procedures resulted in the desired products except for PMMA through the suspension route. Regardless of the nature of the initiating

radicals and/or the media, predominantly syndiotactic PMMA and atactic PSt were obtained through the above methods.

The solution polymerizations were mainly conducted in order to gauge the polymerizability of the synthesized functional co-monomers, with MMA and St. On the other hand, the aqueous-slurry, bulk, suspension and emulsion routes were used to explore the feasibility of the preparative routes at a laboratory-scale, as these are frequently practiced in the industry sector. All copolymerization reactions were found to be feasible, forming copolymers in different yields and with varying compositions. The products obtained through the bulk polymerization route were chosen for further and detailed investigations in terms of their thermal (TGA), calorimetric (DSC) properties, and combustion (PCFC and ‘bomb’ calorimetry) characteristics. It is relevant to note that the bulk technique is often adopted for polymerization of acrylic-based monomer, in the absence of solvent(s), at a commercial scale.

From the results obtained through the investigations, the following inferences can be drawn in the case of PMMA-based bulk systems: 1) TGA: Generally, the products obtained through the reactive strategy exhibited improved thermal stabilities and, in particular, the copolymer containing the P/N-monomer, ADEPMAE, was found to be the most effective. On the other hand, such effects greatly varied among the modified polymers containing the additives; 2) DSC: The values of the heats of pyrolysis obtained from the DSC measurements were found to be spread out, where some systems showed higher values whilst the rest exhibited lower values, when compared to virgin PMMA; 3) PCFC: The relevant parameters, such as, pHRR, HRC, THR and EHC of the modified samples also varied to different extents, where some modified versions showed higher values than the unmodified PMMA, whereas others exhibited lower values; 4) ‘Bomb’ calorimetry: The heats of combustion values obtained through this method also varied among the test samples, some of which showed higher values compared to PMMA, whereas the corresponding values were lower in the case of others. This essentially points to the fact that the different modifying groups exerted varying nature and degree of combustion behaviours, in some cases an additive, and even antagonistic, effect.

The following inferences can be drawn in the case of PSt-based bulk systems from the thermal (TGA) and calorimetric measurements (DSC, PCFC and ‘bomb’ calorimetry): 1) TGA: Generally, in the case of PSt-based systems, the presence of additives/reactives was found to enhance the thermal stability; 2) DSC: Here, a gradual decrease in the values of ΔH_{pyro} in the case of all modified materials can be observed, with the PSt+DEAEPa system showing the lowest value; 3) PCFC: All the modified versions showed lower values for the relevant parameters, such as, pHRR, THR, HRC and EHC, when compared to the unmodified polystyrene sample. The material modified with the P/N-monomer, ADEPMAE, showed the lowest values; 4) ‘Bomb’ calorimetry: Again, the modified PSt-based samples showed a definite decrease in the ΔH_{comb} values as compared to the unmodified version, which clearly demonstrated the gaseous phase inhibitory effect(s) of the modifying groups. Such an effect was found to be particularly pronounced in the case of PSt modified with ADEPMAE, the P/N-containing monomer, where it can be also assumed that there is some degree of P-N synergism.

In the case of PMMA- and PSt-based bulk systems, the utility of an in-house developed software, in deducing the Arrhenius parameters, from the TGA runs was also explored and successfully applied. However, given that such values were deduced by considering only a thermogram obtained through a single heating rate, the extended validity of these values should be treated with caution, and that such values can only be treated as ‘apparent’ values at best.

Some probable elements of mechanism(s) operating in the condensed- and gaseous-phases of the PMMA- and PSt-based systems were formulated. These were inferred from the results obtained through a combination of analytical techniques (ICP/OES and solid-state NMR) and, optionally, some hyphenated methods (GC/MS and pyrolysis-GC/MS), where the latter was primarily used for gaseous-phase analyses.

In the case of PMMA-based systems, there is evidence that P-bearing compounds/groups, except TPP, TPPO and DOPO, upon thermal cracking during the early stages of *flaming* combustion, produce ‘phosphorus’ acid species. These acidic species can subsequently initiate the chemical pathway for producing char precursors. In the case of TPP, TPPO and DOPO, it is more likely that they produce phosphorus-

and/or oxygenated phosphorus-containing volatiles that can act in the gaseous-phase. However, in the case of programmed heating under controlled environments, such as in TGA, DSC, PCFC and ‘bomb’ calorimetry, where a flaming mode of combustion is not attained, any such cooperative interaction between the parent polymer matrix and the modifying compound/groups can be assumed to be absent.

On the other hand, with PSt-based systems, the modifying moieties seem to exert some degree of cooperative interactions even in the controlled decomposition tests (i.e. TGA and DSC), and definitely in measurements where combustion occurs (PCFC and ‘bomb’ calorimetry). Here, a probable mechanism involving the phosphorylation of the phenyl rings leading to crosslinking and char formation is proposed.

Some preliminary studies on the efficacy of selected acrylic polymeric systems in mitigating corrosion on mild steel specimens were conducted. In this context, the method of estimation of Fe(III) in aqueous extracts was successfully developed using ICP/OES. The extent of corrosion occurring on the surface of a mild steel specimen was also successfully followed by employing an imaging technique using a proprietary software that was developed in house.

4.2 Some suggestions for future work

The present project opens up a number of worthwhile avenues for further study, which are include: 1) Specialized techniques, such as spray coating, electrospinning, etc., need to be explored in the case of step-growth polymers with a view to obtaining uniform and coherent coatings onto substrates of interest; 2) Phosphorus-containing additives/reactives that incorporate different structural features/chemical environments could be included in an investigation similar to the current one, such as: phosphoramides, phosphoramidates, phosphinates, ‘caged’ phosphates, and polymerizable versions of phosphine/phosphine oxides; 3) Relevant morphological features (e.g., molecular weight and its distribution), physical properties, such as glass transition temperature and rheological parameters and optical properties (e.g. refractive index), etc., need to be ideally evaluated for all modified systems; 4) It would be highly interesting to study the

thermal and calorimetric properties of PMMA- and PSt-based plaques with varying amounts of the P/N-containing monomer (ADEPMAE) with a view to optimizing the P and N loadings.

It is also essential to scale-up the synthesis of the most promising systems to achieve an overall combustion profiles through cone calorimetric tests. Finally, it is desirable to explore the commercial viability of making PSt-based insulating materials and acrylic-based emulsion paints, through copolymerization reactions involving the most promising functional monomers, at a pilot-plant level.

LIST OF REFERENCES

References

- Akovali, G. (2005). *Polymers in construction*: iSmithers Rapra Publishing.
- Amin, M. A., Khaled, K., & Fadel-Allah, S. A. (2010). Testing validity of the Tafel extrapolation method for monitoring corrosion of cold rolled steel in HCl solutions—experimental and theoretical studies. *Corrosion Science*, 52(1), 140-151.
- Bakos, D., Kosik, M., Antos, K., Karolyov, M., & Vyskocil, I. (1982). The role of nitrogen in nitrogen-phosphorus synergism. *Fire and Materials*, 6(1), 10-12.
- Banks, M., Ebdon, J. R., & Johnson, M. (1993). Influence of covalently bound phosphorus-containing groups on the flammability of poly (vinyl alcohol), poly (ethylene-co-vinyl alcohol) and low-density polyethylene. *Polymer*, 34(21), 4547-4556.
- Banks, M., Ebdon, J. R., & Johnson, M. (1994). The flame-retardant effect of diethyl vinyl phosphonate in copolymers with styrene, methyl methacrylate, acrylonitrile and acrylamide. *Polymer*, 35(16), 3470-3473.
- Benin, V., Cui, X., Morgan, A. B., & Seiwert, K. (2015). Synthesis and flammability testing of epoxy functionalized phosphorous-based flame retardants. *Journal of Applied Polymer Science*, 132(30).
- Bhattacharya, A. K., & Thyagarajan, G. (1981). Michaelis-arbuzov rearrangement. *Chemical Reviews*, 81(4), 415-430.
- Bigger, S. W., Cran, M. J., & Bohn, M. A. (2015). Novel theoretical and computer-assisted modeling of isothermal and non-isothermal depolymerization kinetics. *Polymer Testing*, 44, 1-7.
- Bigger, S. W., Cran, M. J., & Tawakkal, I. S. (2015). Two novel algorithms for the thermogravimetric assessment of polymer degradation under non-isothermal conditions. *Polymer Testing*, 43, 139-146.
- Bigger, S. W., Ngeh, L. N., Dann, P., & Orbell, J. D. (2017). Towards a quantitative indicator of feather disruption following the cleansing of oiled birds. *Marine Pollution Bulletin*, 120(1-2), 268-273.
- Boeva, Z. A., & Sergeev, V. (2014). Polyaniline: Synthesis, properties, and application. *Polymer Science Series C*, 56(1), 144-153.
- Boomi, P., Prabu, H. G., & Mathiyarasu, J. (2014). Synthesis, characterization and antibacterial activity of polyaniline/Pt–Pd nanocomposite. *European Journal of Medicinal Chemistry*, 72, 18-25.
- Braun, D., Cherdron, H., Rehahn, M., Ritter, H., & Voit, B. (2012). *Polymer synthesis: theory and practice: fundamentals, methods, experiments*: Springer Science & Business Media.
- Brezoi, D. V. (2010). Polypyrrole films prepared by chemical oxidation of pyrrole in aqueous FeCl₃ solution. *J. Sci. Arts*, 1(12), 53-58.
- Byard, B., Wang, K., Morgan, A., & Benin, V. (2018). New polyether diols as flame retardants for polyurethane: Derivatives of epoxy-functionalized phosphonates and phosphates. *Fire and Materials*, 42(1), 3-17.
- Cai, W., Wang, J., Quan, X., Zhao, S., & Wang, Z. (2018). Antifouling and anticorrosion properties of one-pot synthesized dedoped bromo-substituted polyaniline and its composite coatings. *Surface and Coatings Technology*, 334, 7-18.
- Camino, G. (1998). Flame retardants: intumescent systems. In *Plastics Additives*: Springer.
- Camino, G., & Costa, L. (1986). Mechanism of intumescence in fire retardant polymers. *Reviews in Inorganic Chemistry*, 8(1-2), 69-100.
- Cao, J.-P., Zhao, X., Zhao, J., Zha, J.-W., Hu, G.-H., & Dang, Z.-M. (2013). Improved thermal conductivity and flame retardancy in polystyrene/poly (vinylidene fluoride) blends by

- controlling selective localization and surface modification of SiC nanoparticles. *ACS Applied Materials & Interfaces*, 5(15), 6915-6924.
- Carraher, C. E., Swift, G., & Society, D. o. P. M. A. C. (2002). *Functional condensation polymers*: Springer.
- Carty, P., Price, D., & John Milnes, G. (2002). Chlorinated poly (vinyl chloride) and plasticized chlorinated poly (vinyl chloride)—thermal decomposition studies. *Journal of Vinyl and Additive Technology*, 8(4), 227-237.
- Cheng, H., & Lee, G. (1996). NMR studies of polystyrene tacticity. *International Journal of Polymer Analysis and Characterization*, 2(4), 439-455.
- Cheremisinoff, P. (1997). *Handbook of engineering polymeric materials*: CRC Press.
- Cho, J. H., Vasagar, V., Shanmuganathan, K., Jones, A. R., Nazarenko, S., & Ellison, C. J. (2015). Bioinspired catecholic flame retardant nanocoating for flexible polyurethane foams. *Chemistry of Materials*, 27(19), 6784-6790.
- Cinausero, N., Howell, B., Schmaucks, G., Marosi, G., Brzozowski, Z., Cuesta, J. L., Fina, A. (2008). Strained organophosphorus compounds as reactive flame retardants for polymeric materials. In *Fire retardancy of polymers: new strategies and mechanisms*: Royal Society of Chemistry.
- Cogen, J. M., Lin, T. S., & Lyon, R. E. (2009). Correlations between pyrolysis combustion flow calorimetry and conventional flammability tests with halogen-free flame retardant polyolefin compounds. *Fire and Materials*, 33(1), 33-50.
- Coleman, M. M. (2019). *Fundamentals of Polymer science: An introductory text*: Routledge.
- Covaci, A., Harrad, S., Abdallah, M. A.-E., Ali, N., Law, R. J., Herzke, D., & de Wit, C. A. (2011). Novel brominated flame retardants: a review of their analysis, environmental fate and behaviour. *Environment International*, 37(2), 532-556.
- Cowie, J. M. G., & Arrighi, V. (2007). *Polymers: chemistry and physics of modern materials*: CRC press.
- Crook, V., Ebdon, J., Hunt, B., Joseph, P., & Wyman, P. (2010). The influence of comonomers on the degradation and flammability of polyacrylonitrile: Design input for a new generation of flame retardants. *Polymer Degradation and Stability*, 95(12), 2260-2268.
- Cullis, C. F., & Hirschler, M. (1981). *The combustion of organic polymers* (Vol. 5): Oxford University Press
- David, G., Negrell-Guirao, C., Iftene, F., Boutevin, B., & Chougrani, K. (2012). Recent progress on phosphonate vinyl monomers and polymers therefore obtained by radical (co) polymerization. *Polymer Chemistry*, 3(2), 265-274.
- Denecker, C., Liggat, J., & Snape, C. (2006). Relationship between the thermal degradation chemistry and flammability of commercial flexible polyurethane foams. *Journal of Applied Polymer Science*, 100(4), 3024-3033.
- Dick, C., Dominguez-Rosado, E., Eling, B., Liggat, J., Lindsay, C., Martin, S., Snape, C. (2001). The flammability of urethane-modified polyisocyanurates and its relationship to thermal degradation chemistry. *Polymer*, 42(3), 913-923.
- Dollimore, D., Lerdkanchanaporn, S., & Alexander, K. S. (1997). The use of the Harcourt and Esson relationship in interpreting the kinetics of rising temperature solid state decompositions and its application to pharmaceutical formulations. *Thermochimica Acta*, 290(1), 73-83.
- Drysdale, D. (2011). *An introduction to fire dynamics*: John Wiley & Sons.
- Dumitrascu, A., & Howell, B. A. (2011). Flame-retarding vinyl polymers using phosphorus-functionalized styrene monomers. *Polymer Degradation and Stability*, 96(3), 342-349.

- Dumitrascu, A., & Howell, B. A. (2012). Flame retardant polymeric materials achieved by incorporation of styrene monomers containing both nitrogen and phosphorus. *Polymer Degradation and Stability*, 97(12), 2611-2618.
- Ebdam, A., Jameh-Bozorgi, S., Yousefi, M., & Niazi, A. (2017). Enhanced fire retardancy of poly methyl methacrylate by combination with aluminium hydroxide and magnesium hydroxide. *Bioscience Biotechnology Research Communications, Special Issue* (1), 54-59.
- Ebdon, J., Hunt, B., Joseph, P., & Konkel, C. (2001). Flame-retarding Thermoplastics: Additive versus Reactive Approach. In *Speciality polymer additives: Principles and applications*: Blackwell publishers
- Ebdon, J., Huckerby, T., & Hunter, T. (1994). Free-radical aqueous slurry polymerizations of acrylonitrile: 1. End-groups and other minor structures in polyacrylonitriles initiated by ammonium persulfate/sodium metabisulfite. *Polymer*, 35(2), 250-256.
- Ebdon, J. R., Huckerby, T. N., & Hunter, T. C. (1994a). Free-radical aqueous slurry polymerizations of acrylonitrile: 2. End-groups and other minor structures in polyacrylonitriles initiated by potassium persulfate/sodium bisulfite. *Polymer*, 35(21), 4659-4664.
- Ebdon, J. R., Hunt, B. J., Joseph, P., Konkel, C. S., Price, D., Pyrah, K., Lindsay, C. I. (2000). Thermal degradation and flame retardance in copolymers of methyl methacrylate with diethyl (methacryloyloxymethyl) phosphonate. *Polymer Degradation and Stability*, 70(3), 425-436.
- Ebdon, J. R., Hunt, B. J., Joseph, P., & Wilkie, T. K. (2008). Flame retardance of polyacrylonitriles covalently modified with phosphorus-and nitrogen containing groups. In *Fire Retardancy of Polymers: New Strategies and Mechanisms*: Royal Society of Chemistry.
- Ebdon, J. R., Price, D., Hunt, B. J., Joseph, P., Gao, F., Milnes, G. J., & Cunliffe, L. K. (2000). Flame retardance in some polystyrenes and poly (methyl methacrylate) s with covalently bound phosphorus-containing groups: initial screening experiments and some laser pyrolysis mechanistic studies. *Polymer Degradation and Stability*, 69(3), 267-277.
- Edenharter, A., Feicht, P., Diar-Bakerly, B., Beyer, G., & Breu, J. (2016). Superior flame retardant by combining high aspect ratio layered double hydroxide and graphene oxide. *Polymer*, 91, 41-49.
- Ezechiáš, M., Covino, S., & Cajthaml, T. (2014). Ecotoxicity and biodegradability of new brominated flame retardants: a review. *Ecotoxicology and Environmental Safety*, 110, 153-167.
- Fang, J., Xu, K., Zhu, L., Zhou, Z., & Tang, H. (2007). A study on mechanism of corrosion protection of polyaniline coating and its failure. *Corrosion Science*, 49(11), 4232-4242.
- Fateh, T., Richard, F., Rogaume, T., & Joseph, P. (2016). Experimental and modelling studies on the kinetics and mechanisms of thermal degradation of polymethyl methacrylate in nitrogen and air. *Journal of Analytical and Applied Pyrolysis*, 120, 423-433.
- Friedman, H. L. (1964). *Kinetics of thermal degradation of char-forming plastics from thermogravimetry. Application to a phenolic plastic*. Paper presented at the Journal of polymer science part C: polymer symposia.
- Fu, Y., Su, Y.-S., & Manthiram, A. (2012). Sulfur-polypyrrole composite cathodes for lithium-sulfur batteries. *Journal of the Electrochemical Society*, 159(9), A1420.
- Grand, A. F., & Wilkie, C. A. (2010). *Fire retardancy of polymeric materials*: CRC Press.

- Holland, B., & Hay, J. N. (2001). The kinetics and mechanisms of the thermal degradation of poly (methyl methacrylate) studied by thermal analysis-Fourier transform infrared spectroscopy. *Polymer*, 42(11), 4825-4835.
- Horrocks, A. R., & Price, D. (2001). *Fire retardant materials*: Woodhead Publishing.
- Huggett, C. (1980). Estimation of rate of heat release by means of oxygen consumption measurements. *Fire and Materials*, 4(2), 61-65.
- Jakab, E., Mészáros, E., & Omastová, M. (2007). Thermal decomposition of polypyrroles. *Journal of Thermal Analysis and Calorimetry*, 88(2), 515-521.
- Jankowski, P., & Kedzierski, M. (2011). Synthesis of polystyrene of reduced flammability by suspension polymerization in the presence of halogen-free additives. *Polimery*, 56(1), 20-26.
- Jiang, S., Yu, B., Zhou, K., Yang, H., Shi, Y., Lo, S., . . . Gui, Z. (2014). Sol-gel synthesis and enhanced properties of a novel transparent PMMA based organic-inorganic hybrid containing phosphorus, nitrogen and silicon. *Journal of Sol-gel Science and Technology*, 69(2), 418-428.
- Joseph, P., & Ebdon, J. R. (2000). Recent developments in flame-retarding thermoplastics and thermosets. In *Fire Retardant Materials*: Woodhead publishing
- Joseph, P., & Tretsiakova-McNally, S. (2012a). Chemical modification of polyacrylonitrile (PAN) with phosphate groups: Effects on flame retardance. *Polymeric Materials: Science and Engineering*, 106, 22-23.
- Joseph, P., & Tretsiakova-McNally, S. (2012b). Combustion behaviours of chemically modified polyacrylonitrile polymers containing phosphorylamino groups. *Polymer Degradation and Stability*, 97(12), 2531-2535.
- Joseph, P., & Tretsiakova-McNally, S. (2015). Melt-flow behaviours of thermoplastic materials under fire conditions: Recent experimental studies and some theoretical approaches. *Materials*, 8(12), 8793-8803.
- Joseph, P., & Tretsiakova-McNally, S. (2011). Reactive modifications of some chain-and step-growth polymers with phosphorus-containing compounds: effects on flame retardance—a review. *Polymers for Advanced Technologies*, 22(4), 395-406.
- Joseph, P., Tretsiakova-McNally, S., & Zhang, R. (2016). Techniques for assessing the combustion behaviour of polymeric materials: some current perspectives and future directions. *Macromolecular Symposia*, 362(1), 105-118.
- Kausar, A., Haider, S., & Muhammad, B. (2017). Nanocomposite based on polystyrene/polyamide blend and bentonite: morphology, thermal, and nonflammability properties. *Nanomaterials and Nanotechnology*, 7, 1847980417702785.
- Kepler, J. L., Darwin, D., & Locke Jr, C. E. (2000). *Evaluation of corrosion protection methods for reinforced concrete highway structures*. A Research Report. University of Kansas Center for Research.
- Koenig, J. L. (1999). *Spectroscopy of polymers*: Elsevier.
- Kricheldorf, H. R. (1991). *Handbook of polymer synthesis* (Vol. 24): CRC Press.
- Kulkarni, V. G., Campbell, L. D., & Mathew, W. R. (1989). Thermal stability of polyaniline. *Synthetic Metals*, 30(3), 321-325.
- Kumar, S. A., Balakrishnan, T., Alagar, M., & Denchev, Z. (2006). Development and characterization of silicone/phosphorus modified epoxy materials and their application as anticorrosion and antifouling coatings. *Progress in Organic Coatings*, 55(3), 207-217.
- Liebscher, J. r., Mrówczyński, R., Scheidt, H. A., Filip, C., Hädade, N. D., Turcu, R., Beck, S. (2013). Structure of polydopamine: a never-ending story? *Langmuir*, 29(33), 10539-10548.

- Liepins, R., Surles, J., Morosoff, N., Stannett, V., Duffy, J., & Day, F. (1978). Localized radiation grafting of flame retardants to polyethylene terephthalate. II. Vinyl phosphonates. *Journal of Applied Polymer Science*, 22(9), 2403-2414.
- Lin, T. S., Cogen, J. M., & Lyon, R. E. (2007). Correlations between microscale combustion calorimetry and conventional flammability tests for flame retardant wire and cable compounds. *Proceedings of the 56th IWCS*.
- Liu, A. S., & Oliveira, M. A. S. (2007). Corrosion control of aluminum surfaces by polypyrrole films: influence of electrolyte. *Materials Research*, 10(2), 205-209.
- Liu, Y., Ai, K., & Lu, L. (2014). Polydopamine and its derivative materials: synthesis and promising applications in energy, environmental, and biomedical fields. *Chemical Reviews*, 114(9), 5057-5115.
- Lovell, P. A., El-Aasser, M. S., & Lovell, P. (1997). *Emulsion Polymerization and Emulsion Polymers*: Wiley New York.
- Luo, H., Gu, C., Zheng, W., Dai, F., Wang, X., & Zheng, Z. (2015). Facile synthesis of novel size-controlled antibacterial hybrid spheres using silver nanoparticles loaded with polydopamine spheres. *RSC Advances*, 5(18), 13470-13477.
- Lynwood, C. (2014). *Polystyrene: synthesis, characteristics, and applications*: Nova Science Publishers.
- Lyon, R. E., & Walters, R. N. (2004). Pyrolysis combustion flow calorimetry. *Journal of Analytical and Applied Pyrolysis*, 71(1), 27-46.
- Malel, E., & Shalev, D. E. (2013). Determining the effect of environmental conditions on iron corrosion by atomic absorption. *Journal of Chemical Education*, 90(4), 490-494.
- Matoetoe, M., Okumu, F., Maphale, C., & Fatoki, O. S. (2014). Thermal and spectroscopic dynamics of titanium oxide functionalized polyaniline coated sawdust. *Asian Journal of Chemistry*, 27(4), 1411-1416.
- McNeill, I. C. (1970). Polymer degradation and characterization by thermal volatilization analysis with differential condensation of products. *European Polymer Journal*, 6(2), 373-395.
- McNeill, I., Zulfiqar, M., & Kousar, T. (1990). A detailed investigation of the products of the thermal degradation of polystyrene. *Polymer Degradation and Stability*, 28(2), 131-151.
- Menczel, J. D., Judovits, L., Prime, R. B., Bair, H. E., Reading, M., & Swier, S. (2009). Differential scanning calorimetry (DSC). *Thermal analysis of polymers: Fundamentals and applications*: Wiley.
- Moad, G., & Solomon, D. H. (2006). *The chemistry of radical polymerization*: Elsevier.
- Mohammadi, M., & Davoodi, J. (2018). The effect of alumina nanoparticles on the thermal properties of PMMA: a molecular dynamics simulation. *Molecular Simulation*, 44(16), 1304-1311.
- Morgan, A. B. (2019). The future of flame retardant polymers—unmet needs and likely new approaches. *Polymer Reviews*, 59(1), 25-54.
- Morgan, A. B., & Galaska, M. (2008). Microcombustion calorimetry as a tool for screening flame retardancy in epoxy. *Polymers for Advanced Technologies*, 19(6), 530-546.
- Morgan, A. B., Wilkie, C. A., & Nelson, G. L. (2012). *Fire and polymers VI: New advances in flame retardant chemistry and science*: ACS Publications.
- Morgan, A. B., Worku, A. Z. (2015). Flame Retardants: Overview. *Kirk Othmer Encyclopedia of Chemical Technology John Wiley & Sons*.
- Mostafaei, A., & Zolriasatein, A. (2012). Synthesis and characterization of conducting polyaniline nanocomposites containing ZnO nanorods. *Progress in Natural Science: Materials International*, 22(4), 273-280.

- Nair, C. R., Clouet, G., & Brossas, J. (1988). Copolymerization of diethyl 2-(methacryloyloxy) ethyl phosphate with alkyl acrylates: Reactivity ratios and glass transition temperatures. *Journal of Polymer Science Part A: Polymer Chemistry*, 26(7), 1791-1807.
- Nanishi, K., & Nakayama, H. (1990). Antifouling coating. US Patent 4,908,061.
- Nautiyal, A., Qiao, M., Cook, J. E., Zhang, X., & Huang, T.-S. (2018). High performance polypyrrole coating for corrosion protection and biocidal applications. *Applied Surface Science*, 427, 922-930.
- Novozhilov, V., Joseph, P., Ishiko, K., Shimada, T., Wang, H., & Liu, J. (2011). Polymer combustion as a basis for hybrid propulsion: A comprehensive review and new numerical approaches. *Energies*, 4(10), 1779-1839.
- Odian, G. (2004). *Principles of polymerization*: John Wiley & Sons.
- Olesik, J. W. (1991). Elemental analysis using ICP-OES and ICP/MS. *Analytical Chemistry*, 63(1), 12A-21A.
- Ou, J., Wang, J., Zhou, J., Liu, S., Yu, Y., Pang, X., & Yang, S. (2010). Construction and study on corrosion protective property of polydopamine-based 3-layer organic coatings on aluminum substrate. *Progress in Organic Coatings*, 68(3), 244-247.
- Ozawa, T. (1965). A new method of analyzing thermogravimetric data. *Bulletin of the Chemical Society of Japan*, 38(11), 1881-1886.
- Peikertová, P., Matějka, V., Kulhánková, L., Neuwirthová, L., Tokarský, J., & Capková, P. (2011). Thin Polyaniline Films: Study of the Thermal Degradation. *Nanocon*, 3, 516-520.
- Pospiech, D., Jehnichen, D., Starke, S., Müller, F., Bünker, T., Wollenberg, A., Oertel, U. (2017). Multifunctional methacrylate-based coatings for glass and metal surfaces. *Applied Surface Science*, 399, 205-214.
- Pospiech, D., Starke, S., Bünker, T., Müller, F., Frenzel, R., Simon, F., Kruspe, R. (2013). Methacrylate copolymers for anti-biofouling coatings: a chemical approach. *Proceedings of International Conference on Heat Exchanger Fouling and Cleaning*, Budapest, Hungary.
- Poth, U., Baumstark, R., Schwartz, M., & Schwalm, R. (2011). *Acrylic Resins*: Vincentz Network.
- Price, D., Bullett, K., Cunliffe, L. K., Hull, T. R., Milnes, G. J., Ebdon, J. R., Joseph, P. (2005). Cone calorimetry studies of polymer systems flame retarded by chemically bonded phosphorus. *Polymer Degradation and Stability*, 88(1), 74-79.
- Price, D., Cunliffe, L., Bullett, K., Hull, T. R., Milnes, G., Ebdon, J., . . . Joseph, P. (2008). Thermal behavior of covalently bonded phosphonate flame-retarded poly (methyl methacrylate) systems. *Polymers for Advanced Technologies*, 19(6), 710-723.
- Price, D., Cunliffe, L. K., Bullett, K., Hull, T. R., Milnes, G. J., Ebdon, J. R., . . . Joseph, P. (2007). Thermal behaviour of covalently bonded phosphate and phosphonate flame retardant polystyrene systems. *Polymer Degradation and Stability*, 92(6), 1101-1114.
- Price, D., Gao, F., Milnes, G. J., Eling, B., Lindsay, C. I., & McGrail, P. (1999). Laser pyrolysis/time-of-flight mass spectrometry studies pertinent to the behaviour of flame-retarded polymers in real fire situations. *Polymer Degradation and Stability*, 64(3), 403-410.
- Price, D., Pyrah, K., Hull, T. R., Milnes, G. J., Ebdon, J. R., Hunt, B. J., Konkol, C. S. (2001). Flame retarding poly (methyl methacrylate) with phosphorus-containing compounds: comparison of an additive with a reactive approach. *Polymer Degradation and Stability*, 74(3), 441-447.
- Prime, R. B., Bair, H. E., Vyazovkin, S., Gallagher, P. K., & Riga, A. (2009). Thermogravimetric analysis (TGA). In *Thermal analysis of polymers: Fundamentals and applications*, Wiley.

- Röchow, E. T., Häußler, L., Korwitz, A., & Pospiech, D. (2018). Thermal decomposition of phosphonate-containing methacrylate-based copolymers. *Polymer Degradation and Stability*, *152*, 235-243.
- Salmeia, K. A., & Gaan, S. (2015). An overview of some recent advances in DOPO-derivatives: Chemistry and flame retardant applications. *Polymer Degradation and Stability*, *113*, 119-134.
- Saunders, K. (1988). *Organic Chemistry of Polymers*: Chapman and Hall Publishers.
- Sayadi, A. A., Tapia, J. V., Neitzert, T. R., & Clifton, G. C. (2016). Effects of expanded polystyrene (EPS) particles on fire resistance, thermal conductivity and compressive strength of foamed concrete. *Construction and Building Materials*, *112*, 716-724.
- Schartel, B., Pawlowski, K. H., & Lyon, R. E. (2007). Pyrolysis combustion flow calorimeter: a tool to assess flame retarded PC/ABS materials? *Thermochimica Acta*, *462*(1-2), 1-14.
- Schartel, B., Wilkie, C. A., Camino, G. (2016). Recommendations on the scientific approach to polymer flame retardancy: Part 1 – Scientific terms and methods. *Journal of Fire Sciences*, *34*, 447-467.
- Schartel, B., Wilkie, C. A., Camino, G. (2017). Recommendations on the scientific approach to polymer flame retardancy: Part 2 – Concepts. *Journal of Fire Sciences*, *35*, 3-20.
- Solorzano, J. A. P., Moinuddin, K. A. M., Tretsiakova-McNally, S., & Joseph, P. (2019). A Study of the Thermal Degradation and Combustion Characteristics of Some Materials Commonly Used in the Construction Sector. *Polymers*, *11*(11), 1833.
- Sonnier, R., Otazaghine, B., Ferry, L., & Lopez-Cuesta, J.-M. (2013). Study of the combustion efficiency of polymers using a pyrolysis–combustion flow calorimeter. *Combustion and Flame*, *160*(10), 2182-2193.
- Sonnier, R., Vahabi, H., Ferry, L., & Lopez-Cuesta, J.-M. (2012). Pyrolysis-combustion flow calorimetry: A powerful tool to evaluate the flame retardancy of polymers. In *Fire and polymers VI: New advances in flame retardant chemistry and science*: ACS Publications.
- Stempel Jr, G. H., Cross, R. P., & Mariella, R. P. (1950). The preparation of acrylyl chloride. *Journal of the American Chemical Society*, *72*(5), 2299-2300.
- Tawakkal, I. S., Cran, M. J., & Bigger, S. W. (2017). Effect of poly (lactic acid)/kenaf composites incorporated with thymol on the antimicrobial activity of processed meat. *Journal of Food Processing and Preservation*, *41*(5), e13145.
- Tretniakova-McNally, S., & Joseph, P. (2015). Pyrolysis combustion flow calorimetry studies on some reactively modified polymers. *Polymers*, *7*(3), 453-467.
- Vahabi, H., Ferry, L., Longuet, C., Sonnier, R., Negrell-Guirao, C., David, G., & Lopez-Cuesta, J.-M. (2012). Theoretical and empirical approaches to understanding the effect of phosphonate groups on the thermal degradation for two chemically modified PMMA. *European Polymer Journal*, *48*(3), 604-612.
- Vahabi, H., Longuet, C., Ferry, L., David, G., Robin, J. J., & Lopez-Cuesta, J. M. (2012). Effect of aminobisphosphonated copolymer on the thermal stability and flammability of poly (methyl methacrylate). *Polymer International*, *61*(1), 129-134.
- Valença, D. P., Alves, K. G. B., Melo, C. P. d., & Bouchonneau, N. (2015). Study of the Efficiency of Polypyrrole/ZnO Nanocomposites as Additives in Anticorrosion Coatings. *Materials Research*, *18*, 273-278.
- Van Krevelen, D. W., & Te Nijenhuis, K. (2009). *Properties of polymers: their correlation with chemical structure; their numerical estimation and prediction from additive group contributions*: Elsevier.

- Varesano, A., Vineis, C., Aluigi, A., Rombaldoni, F., Tonetti, C., & Mazzuchetti, G. (2013). Antibacterial efficacy of polypyrrole in textile applications. *Fibers and Polymers*, 14(1), 36.
- Vyazovkin, S., Burnham, A. K., Criado, J. M., Pérez-Maqueda, L. A., Popescu, C., & Sbirrazzuoli, N. (2011). ICTAC Kinetics Committee recommendations for performing kinetic computations on thermal analysis data. *Thermochimica Acta*, 520(1-2), 1-19.
- Vyazovkin, S., & Wight, C. A. (1998). Isothermal and non-isothermal kinetics of thermally stimulated reactions of solids. *International Reviews in Physical Chemistry*, 17(3), 407-433.
- Wang, K., Morgan, A. B., & Benin, V. (2017). Preparation and studies of new phosphorus-containing diols as potential flame retardants. *Fire and Materials*, 41(8), 973-982.
- White, A. J., & Filisko, F. E. (1982). Tacticity determination of poly(methyl methacrylate) (PMMA) by high-resolution NMR. *Journal of Polymer Science: Polymer Letters Edn.*, 20(10), 525-529.
- Wilkie, C. A., Morgan A. B. (2010). Fire Retardancy of Polymeric Materials, 2nd Edition. *Taylor and Francis. Boca Raton.*
- Wyman, P., Crook, V., Ebdon, J., Hunt, B., & Joseph, P. (2006). Flame-retarding effects of dialkyl-p-vinylbenzyl phosphonates in copolymers with acrylonitrile. *Polymer International*, 55(7), 764-771.
- Wyman, P., Crook, V. L., Hunt, B. J., & Ebdon, J. R. (2004). Improved synthesis of phosphorus-containing styrenic monomers. *Designed Monomers and Polymers*, 7(3), 301-309.
- Zhu, L., Su, S., & Hossenlopp, J. M. (2012). Thermal stability and fire retardancy of PMMA (nano) composites with layered metal hydroxides containing dodecyl sulfate anions. *Polymers for Advanced Technologies*, 23(2), 171-181.